Determination of Unknown Coefficients in the Heat Equation

Mousa Jaar M Huntul

Submitted in accordance with the requirements for the degree of
Doctor of Philosophy

The University of Leeds
Department of Applied Mathematics

October 2018

The candidate confirms that the work submitted is his own, except where work which has formed part of jointly authored publications has been included. The contribution of the candidate and the other authors to this work has been explicitly indicated below. The candidate confirms that appropriate credit has been given within the thesis where reference has been made to the work of others.

Joint Publications

Some material of this thesis is based on several publications detailed as follows:

▶ Some of the material of Chapter 2 is included in:

1. Huntul, M.J. and Lesnic, D. (2017) An inverse problem of finding the time-dependent thermal conductivity from boundary data, *International Communications in Heat and Mass Transfer*, **85**, 147–154.

▶ Some of the material of Chapter 3 is included in:

1. Huntul, M.J., Lesnic, D. and Hussein, M.S. (2017) Reconstruction of time-dependent coefficients from heat moments, *Applied Mathematics and Computation*, **301**, 233–253.

▶ Some of the material of Chapter 4 is included in:

1. Huntul, M.J. and Lesnic, D. (2018) Time-dependent reaction coefficient identification problems with a free boundary, *International Journal for Computational Methods in Engineering Science and Mechanics*, accepted.

▶ Some of the material of Chapter 5 is included in:

1. Huntul, M.J. and Lesnic, D. (2017) Determination of time-dependent coefficients and multiple free boundaries, *Eurasian Journal of Mathematical and Computer Applications*, **5**, 15–43.

▶ Some of the material of Chapter 6 is included in:

1. Huntul, M.J. and Lesnic, D. (2018) Determination of time-dependent coefficients for a weakly degenerate heat equation, *Siberian Journal of Numerical Mathematics*, submitted.

▶ Some of the material of Chapter 7 is included in:

1. Huntul, M.J., Lesnic, D. and Johansson, B.T. (2018) Determination of an additive time- and space-dependent coefficient in the heat equation, *International Journal of Numerical Methods for Heat and Fluid Flow*, 28(6), 1352–1373.

▶ Some of the material of Chapter 8 is included in:

1. Huntul, M.J. and Lesnic, D. (2018) Determination of a time-dependent free boundary in a two-dimensional parabolic problem, *International Journal of Applied and Computational Mathematics*, submitted.

Acknowledgments

Foremost, I would like to express my deepest gratitude and appreciation to my supervisor Professor Daniel Lesnic for his patience, motivation, enthusiasm, insightful comments, helpful conversations, continuous support and expert guidance throughout my PhD study. He has made himself available and offered assistance even with his busy schedule. His help has been greatly acknowledged. I could not have thought to have a better supervisor and mentor for my study. I would also like to thank Dr O.G. Harlen and Dr O. Chalykh for their constructive comments and advices during my annual reviews.

I would like to express my thanks to all staff in the School of Mathematics for their help, cooperation and constant encouragement during my studies. My deepest appreciation to all my postgraduate colleagues for their company and friendship during my time in Leeds.

My deepest gratitude and thanks extend to Dr B.T. Johansson and Dr M.S. Hussein for their, valuable advice, helpful discussions, company and friendship during their visits to the University of Leeds in November 2017. Fruitful discussion with Professor M.I. Ivanchov is gratefully acknowledged.

I would like to express my deepest gratitude and special thanks to my parents, for their continuous love, tolerance, support, praying and the sacrifices they made for me in order to receive my higher education. I am very much thankful to my dear wife, Aisha Hassani and my daughter Janna, for their continuous love, patience, understanding, praying and continuing support that always kept me going. Also, I express my thanks to my brothers and sisters for their assistance and valuable prayers. I dedicate this thesis to them.

Lastly, but by no means in the least, I would like to thank Jazan University in Saudi Arabia and Saudi Arabian Cultural Bureau (SACB) in London for their financially supporting my postgraduate studies.

Mousa Jaar M Huntul

Abstract

The purpose of this thesis is to find the numerical solutions of one or multiple unknown coefficient identification problems in the governing heat transfer parabolic equations. These inverse problems are numerically solved subject to various types of overdetermination conditions such as the heat flux, nonlocal observation, mass/energy specification, additional temperature measurement, Cauchy data, general integral type over-determination, Stefan condition and heat momentum of the first, second and third order.

The main difficulty associated with solving these inverse problems is that they are ill-posed since small changes in the input data can result in enormous changes in the output solution, therefore traditional techniques fail to provide accurate and stable solutions.

Throughout this thesis, the finite-difference method (FDM) with the Crank-Nicolson (C-N) scheme is mainly used as a direct solver except in Chapters 8 and 9 where an alternating direction explicit (ADE) method is employed in order to deal with the two-dimensional heat equation. An explicit forward time central space (FTCS) method is also employed in Chapter 2 for the extension to higher dimensions. The treatment for solving a degenerate parabolic equation, which vanishes at the initial moment of time is discussed in Chapter 6.

The inverse problems investigated are discretised using FDM or ADE and recast as nonlinear least-squares minimization problems with lower and upper simple bounds on the unknown coefficients. The resulting optimization problems are numerically solved using the *lsqnonlin* routine from MATLAB optimization toolbox. The stability of the numerical solutions is investigated by introducing random noise into the input data which yields unstable results if no regularization is employed. The regularization method is included (where necessary) in order to reduce the influence of measurement errors on the numerical results. The choice of the regularization parameter(s) is based on the L-curve method, on the discrepancy principle criterion or on trial and error.

Nomenclature

Some of these symbols are used more than once to represent different quantities from chapter to chapter due to the considerable amount of notation present in this thesis. In some cases, the use of a symbol not listed below is local to a short portion of the text and in such happenstance, it is defined where it is introduced.

Latin symbols

a	time-dependent thermal conductivity in (Chapters 2 and 3), time-dependent thermal diffusivity in (Chapter 6), and space, time-dependent function in (Chapters 4 and 5) and an orthotropic thermal conductivity in (Chapter 9)
$\mathcal{A}$	operator (Chapter 2)
$\mathcal{A}_\alpha$	non-uniformly class for parabolic degenerate PDEs (Chapter 6)
A_j, $A_{i,j}$	vector components of difference equation in (Chapters 2, 3, 5 and 6)
b	time-dependent convection (or advection) in (Chapters 3 and 6)
b_1, b_2	time-dependent coefficients (Chapter 5) and space, time-dependent function (Chapters 4 and 8)
$\mathbf{b^j}$, $\tilde{\mathbf{b^j}}$	vector components of difference equation in (Chapters 2 and 3)
B_j, $B_{i,j}$	vector components of difference equation in (Chapters 2, 3, 5, 6 and 7)
c	time-dependent absorbtion (Chapter 3) and space, time-dependent function (Chapter 8)
c_1, c_2	time-dependent coefficients (Chapter 4)
C_j, $C_{i,j}$	vector components of difference equation in (Chapters 3, 5 and 6)
$C[a,b]$	the space of continuous functions in $[a,b]$
$C^1[a,b]$	the space of functions once time continuously differentiable in $[a,b]$
$C^3[a,b]$	the space of functions three times continuously differentiable in $[a,b]$

$C^{2,1}(Q)$	the space of functions twice continuously differentiable in first variable and once continuously differentiable in the second variable in Q
$C^{k+\alpha}$	the space of k continuously differentiable functions with the k-order derivative being Hölder continuous with exponent $\alpha \in (0, 1)$
D	diagonal scaling matrix (Chapter 1)
D, $\tilde{D}$, E, $\tilde{E}$	matrix given by expressions (2.13), (3.13) (Chapters 2 and 3)
$\mathcal{D}(\mathcal{A})$	the domain of $\mathcal{A}$ (Chapter 2)
f	heat sources (Chapters 2–6 and 8), and time-dependent coefficient (Chapter 7)
F	nonlinear objective least-squares function (Chapters 2, 3, 4 and 8)
F_λ	nonlinear objective least-squares function with penalty term in (Chapters 2 and 8)
F_1, F_2, F_3	nonlinear objective least-squares functions (Chapters 5 and 6)
$\mathbb{F}$	nonlinear objective least-squares functions (Chapter 7)
g	time-dependent free boundary (Chapter 8)
G	the right hand side of equations (2.5) and (7.13), and matrix given by equation (6.16)
h	length for y_1-axis (Chapter 8) and the time-dependent free boundary (Chapter 4)
h_1, h_2, h_3	time-dependent free boundaries (Chapter 5)
H	Hessian matrix of a function (Chapter 1) and matrix given by expression (5.22) (Chapter 5)
H_0, H_1	heat moment functions of order zero and one (Chapter 3)
i, j, n	indices
$\mathbf{k}$	vector of difference equation in (Chapter 6)
L	matrix given by equation (7.19) and length of the conductor (Chapters 2, 3 and 7)

l	length of the finite slab (Chapter 6)
$L^2[a,b]$	the space of square integrable functions in $[a,b]$
$lsqnonlin$	MATLAB optimization routine
M	number of finite differences in x-coordinate (all chapters except Chapters 8 and 9)
M_1	number of finite differences in x_1 or x-coordinate (Chapters 8 and 9)
M_2	number of finite differences in x_2 or y coordinate (Chapters 8 and 9)
N	number of finite differences in t-coordinate
$\mathcal{N}$	the neighborhood (trust-region) (Chapter 1)
$normrnd$	MATLAB function generating Gaussian random numbers
p	percentage of noise (Chapters 3–8)
Q_T	fixed domain $(0,L)\times(0,T)$ (Chapters 2,3 and 7), $(0,l)\times(0,T)$ (Chapter 6) and $(0,h)\times(0,l)\times(0,T)$ (Chapter 9)
$\overline{Q_T}$	closure of the solution domain Q_T
$\mathcal{R}(\mathcal{A})$	range of the operator $\mathcal{A}$ (Chapter 1)
R_k	regularization derivative operator of order k (Chapter 1)
$rand$	MATLAB function generating uniformly distributed random numbers and arrays (Chapter 2)
$\mathbf{r}$	vector components of difference equation in (Chapter 5)
t	time variable
t_j	time node
T	final time
u	solution/temperature
u_0	initial condition function (Chapter 1)
u_1	Stefan interface conditions on the moving boundary (Chapter 1)
u_2	Neumann heat flux boundary condition (Chapter 1)
$u_{i,j}$	values of u at the node (i,j)
$u^n_{i,j}$	values of u at the node (i,j,n) (Chapter 8)
v	the transformed solution (Chapters 4,5 and 8)
$v_{i,j}$	components of transformed solution v (Chapters 4 and 5)
$v^n_{i,j}$	components of transformed solution v (Chapter 8)
x	space variable
x_i	space nodes
X, Y	vector space, Hilbert spaces (Chapter 1)
y, y_1, y_2	space variables (Chapters 4, 5 and 8)
y^ϵ	perturbed data (Chapter 1)

Greek symbols

α	degree of weakly power law degeneration (Chapter 6)
β	regularization parameter (Chapters 1, 3 and 6) and additional temperature measurement (Chapter 7)
β_i	regularization parameter (Chapters 4, 5 and 7)
λ	regularization parameter (Chapters 2 and 8)
∇	gradient of function (Chapter 1)
Δ	trust-region size (Chapter 1)
Δt, Δx, Δy	sizes of time and space steps
Δx_1, Δx_2	sizes of space steps (Chapter 8)
ϵ	total amount of noise
ϵk	Gaussian random variables
σ_k	standard deviation
$\mathcal{E}$	solution domain (Chapter 6)
ϕ	initial condition function (Chapters 2–4 and 7)
φ	initial condition function (Chapters 5, 6, 8 and 9) and additional temperature measurement (Chapter 7) function (Chapter 8)
Ω_T	moving solution domain (Chapters 4, 5 and 8)

Superscripts

T	Transpose of a matrix
$' = \frac{\partial}{\partial n}$	normal derivative

Abbreviations

BEM	boundary element method
FDM	finite difference method
FEM	finite element method
FVM	finite volume method
FTCS	forward time central space
IP	inverse problem
LB	lower bound
O	order of
PDEs	partial differential equations
$rmse$	root mean square error

SLAE	system of linear algebraic equations
TTR	trust-region-reflective
UB	upper bound

Contents

List of Figures

List of Tables

Chapter 1

General introduction

1.1 Introduction

With the current advancement and reliance on science and engineering, inverse problems are becoming a core component in these fields. Some of the applications include the use of heat equation which has been widely applied in scientific processes such as melting, freezing, manufacturing, and in microwave heating applications. Many of the applications are modelled using partial differential equations (PDE's). If the input values or conditions are known, solutions can be obtained to determine the behaviour of the system [38]. Some of the necessary inputs that are required include initial and boundary conditions, solution domain's geometry, coefficients and forcing terms. If some of this information is missing or unknown, in general it will not be possible to determine the behaviour of the physical system. However, certain outputs can be experimentally measured and this information, in addition to the input data can be used to restore the missing input data. This is what is called an inverse problem.

Inverse problems are in general ill-posed. In most cases, this means that a small change in the input data can bring about a substantial change in the output solution.

The scope of inverse problems has been present in several branches of mathematics, engineering, and physics for a long period. Over the past decade, the theory of inverse problems has been considerably developed given partly its significance in applications. However, the numerical solutions to these problems require considerable computations. For example, deconvolution in parameter identification, image reconstruction, and seismic exploration all require high performance computers to do the computation in a timely fashion, or to solve the problem more precisely within a specific duration [135]. Such a consideration is mostly associated with commercial and economy production. For instance, problems in

oil and gas detection, problems in data assimilation, and problems in numerical weather prediction are needed to be solved to couple atmosphere, hydrosphere, and biosphere.

Most of the time, the coefficient entries in a PDE model are linked to the physical properties of the system under consideration. In cases where the model is quite simple, these physical properties can be identified through experimentation and the outcomes used to reduce the model to a particular physical system. In cases where the model is sophisticated, it may be difficult or even impossible to measure the physical properties linked to a coefficient in a model equation. In such a case, it may be important to move forward indirectly because of inadequate information, that is, to design and solve the inverse problem for the missing data.

Parameter identification problems tend to involve the use of actual observation or indirect measurement contaminated by noise, to deduce the values of the parameters making up the system under consideration. In most cases, these inverse problems are ill-posed in line with the Hadamard postulate, which is, if the solution does not exist or, is not unique or, if it is in violation of the continuous dependence on input data [46].

Over the past few years, many scholars have shown a significant interest in inverse coefficient identification problems. The primary motivation for this study is to determine the unknown properties of a given region by considering only the data on its boundary. There is also a specific attention to such coefficients that describe physical quantities as the conductivity of a medium. The methods applied rely mostly on the type of equation and the variables on which the unknown coefficient is anticipated a priori to depend. The equation can be linear, semilinear, or nonlinear. However, there is somewhat a unique instance when the unknown conductivity, for example, depends on the dependent variable [15]. For a heat flow problem, for example, this has a physical interpretation of a conductivity that is temperature-dependent. Regardless if the medium or material is uniform, then it is expected that the unknown coefficient will be independent of the spatial variable. In other words, if the spatial change in the problem is negligible considering the change in time, then a rational approximation to this state of affairs can be considered whereby the coefficient is to be a function of the time variable only. If, additionally, the characteristic properties fail to change with time when the dependent variables are held constant, then it is expected that the coefficients are also independent of time [109]. Many studies as well as some practical applications seek to determine the leading coefficient or the coefficient of the high-order derivative in the parabolic heat equation. For instance, there

is a study of identification in the problem of space-dependent diffusivity in [50]. Also, there is an investigation of the time-dependent case in [93], while there are references to the temperature-dependent case in [18, 136].

1.2 Direct problems

Direct problems have been extensively studied over the last two centuries, resulting in a wealth of literature of procedures relating to their solution. A direct problem or forward problem, according to the discipline of mathematical physics, is a problem which involves physical fields, processes, or phenomena such as audio, or electromagnetic, acoustic, seismic, heat, etc. The aim of solving a direct problem is to find a function that describes a physical field or process at any point of a given domain at any instant of time if the field is non-stationary. When forming a direct problem, the following are included, the initial condition when the process is not-stationary, the domain for the process being calculated, the function which expresses the process and the boundary conditions. Most of all, direct problems are in general well-posed. According to Hadamard's (1923) definition, a problem is called well-posed if it satisfies the following properties:

- the solution exists for all data (existence).
- the solution is unique for all data (uniqueness).
- the solution depends continuously on the data (stability), such that when there is a small error in the input data it results in a relatively small error in the output solution.

1.3 Ill-posed problems

A problem that violates one or more of the above properties of well-posedness is called an ill-posed problem.

Suppose that $\mathcal{A} : X \to Y$ is an operator from a vector space X to another vector space Y such that

$$\mathcal{A}x = y, \tag{1.1}$$

where $x \in X$ and $y \in Y$. Then the operator equation (1.1) is well-posed if $\mathcal{A}$ is bijective (one-to-one and onto) and the inverse operator $\mathcal{A}^{-1} : Y \to X$ is continuous; otherwise the equation (1.1) is ill-posed. Therefore, three types of ill-posedness can be classified according to this definition as follows:

1. If $\mathcal{A}$ is not surjective (onto) this means that the equation (1.1) is not solvable for all $y \in Y$ (non-existence).

2. If $\mathcal{A}$ is not injective (one-to-one) this means that the equation (1.1) may have more than one solution (non-uniqueness).

3. If $\mathcal{A}^{-1}$ exists but is not continuous this means that the equation (1.1) does not continuously depend on the data y (instability).

A few simple examples of systems of equations which illustrate ill-posed problems, are given below.

Example 1. Consider the following over-determined system of linear algebraic equations (SLAE) (Sizikov, 2005):

$$\begin{cases} 2x_1 - 3x_2 = -4, \\ -x_1 + 2x_2 = 3, \\ x_1 + 4x_2 = 15. \end{cases} \tag{1.2}$$

This SLAE has no solution because the rank of the extended matrix $rank(\mathcal{A}|\underline{y}) = 3$ and the rank of $\mathcal{A}$ is $rank(\mathcal{A}) = 2$ are not equal. The fact that this SLAE has no solution x_1, x_2 can be proved immediately. Indeed, from the first two equations we obtain the solution $x_1 = 1$, $x_2 = 2$. Introducing this into the third equation we get $9 = 15$ which is absurd. Hence, the first condition (existence) for well-posedness is violated.

Example 2. Consider the following under-determined system of linear algebraic equations (SLAE) (Sizikov, 2005):

$$2x_1 - 3x_2 = -4. \tag{1.3}$$

For this SLAE, $rank(\mathcal{A}) = rank(\mathcal{A}|\underline{y}) = 1 < 2$; this SLAE is therefore an under-determined system that has many solutions. For instance, (1) $x_1 = 1$, $x_2 = 2$; (2) $x_1 = 2$, $x_2 = 8/3$; (3) $x_1 = 0$, $x_2 = 4/3$, etc. are all solutions of the system (1.3). Thus, the solution of the SLAE is non-unique, and the second condition (uniqueness) for well-posedness is violated.

Example 3. Consider the determined system (SLAE) (Sizikov, 2005):

$$\begin{cases} 2x_1 - 3x_2 = 3, \\ -1.33x_1 + 2x_2 = -1.99. \end{cases} \tag{1.4}$$

For this SLAE, $rank(\mathcal{A}) = rank(\mathcal{A}|\underline{y}) = 2$; this SLAE is therefore a determined system. The solution of (1.4) exists and is unique, $x_1 = 3$, $x_2 = 1$. Yet this solution is unstable. Indeed, for the perturbed SLAE

$$\begin{cases} 2x_1 - 3x_2 = 3.01, \\ -1.33x_1 + 2x_2 = -2, \end{cases}$$

i.e., with introduced relative errors $||\underline{y} - \underline{y}^{\epsilon}||/||\underline{y}|| \approx 0.5\%$, where

$$\underline{y} = \begin{pmatrix} 3 \\ -1.99 \end{pmatrix}, \ \underline{y}^{\epsilon} = \begin{pmatrix} 3.01 \\ -2 \end{pmatrix}, \ ||\underline{y} - \underline{y}^{\epsilon}|| = \epsilon \approx 0.01,$$

we obtain a new, different solution: $x_1 = 2$ (relative error $||\underline{x_1} - \underline{x_1}^{\epsilon}||/||\underline{x_1}|| \approx 33\%$), $x_2 = 0.33$ (relative error $||\underline{x_2} - \underline{x_2}^{\epsilon}||/||\underline{x_2}|| \approx 67\%$), i.e. the small error in the input data has caused large errors in the output solution. Hence the third condition (stability) for well-posedness is violated. These estimates can also be made considering the condition number $cond(\mathcal{A})$, for more details see [108].

1.4 Inverse problems

Mathematical problems are considered inverse if the model has some unknown parameters. Solving such problems requires using additional information to restore these parameters. These are known as the over determination conditions. The application is important in that they resolve problems whose measurement of the required parameters is not possible.

Most inverse problems are ill-posed or rather they are termed as problems that are unstable. This usually means that in such problems a small modification in the input data can lead to bigger impact on the ultimate result in the output solution. Earlier in 1920s it was believed that these problems do not have any practical significance. This opinion was so strong that it was not until 1943, that the issue of ill-posedness was revisited in the pioneering paper by Tikhonov [125].

The application of inverse problems is of unique importance in the case when the immediate measurement of suitable parameters is impossible. For example, an inaccessibility of either material or environment and also the rapidity of the process, see [74].

Inverse problems can be classified, as follows:

- Coefficient identification problems, that means problems in which the coefficient(s) of equation(s) is(are) not known(s), see Chapters 2–9.

- Retrospective, which means problems which have reverse direction of time, such as the backward heat conduction problem.
- Boundary values includes problems that are related to determining unknown boundary conditions.
- Source or force problems are those that require the determination of the source or force.
- Geometrical aspect focuses on problems that concern the determination of unknown areas of the solution domain or even portions of the boundary, see Chapters 4, 5 and 8.

All of the above classifications of inverse problems are ill-posed in the Hadamard concept. Therefore, they are unstable and hence a sort of regularization must be employed in order to recover the loss of stability. Also, these classifications are incomplete. In some cases, the initial and boundary conditions are unknown whereas in other cases either the domain or part of its boundary is unknown. An over specified condition is helpful when determining the unknown conditions. When the overspecified condition is provided by use of experimental data, noise becomes an important concern.

As mentioned before, the problems investigated in Chapters 4, 5 and 8 possess an unknown moving boundary part which needs to be identified. More generally, these are Stefan-type problems which are described in the next section.

1.5 Stefan problems

A Stefan problem is a moving boundary value problem that concerns the distribution of heat in a period of transforming medium. For instance, during heat diffusion in melting ice, the melting of the ice happens as the boundary of the ice keeps on shifting, [69]. Some authors have denoted the problem as a free boundary value problem because of the domain boundary which is a priori unknown. Authors have also referred to it as a moving boundary problem because the interface between two phases changes with time.

Stefan problems have natural occurrences that are associated with solidification and melting problems. Nonetheless, there are some problems that are almost similar to Stefan problems. An example is the fluid flow in a permeable medium or shock waves in gas dynamics.

1.5.1 Physical background

The melting of ice and water solidification are significant examples of the phase transformation. Phase transformation is the discontinuous modification of properties within a substance. Aggregation has different states which in transition are referred to as phases. The states share similar physical properties. As a result, a phase is more particular than a state of matter. During the occurrence of phase transition, a latent heat appears. The latent heat is absorbed or released by the thermodynamic system without a change in temperature, [25]. Phase transformations take place in an appropriate process in natural sciences, physics, and engineering. Most industrial products involve solidification at some stages. For instance, steel annealing and thermal welding are some of the processes. Two fundamental phenomena characterize these processes: diffusion of heat and exchange of latent heat. Stefan problems are a model that accounts for this behavior.

The first paper on Stefan problem by Gabriel Lamé and Benoît Paul Clapeyron in 1831 [89], was to cool a liquid that filled the halfspace $x > 0$ and establish the thickness of the solid crust that was generated using a constant boundary at $x = 0$. The authors established that the crust thickness was the square root of the time. However, there was no attached determination of the coefficient of proportionally. After several years, Joseph Stefan described mathematical models of the actual physical problems within a changing phase state, [19, 20].

In 1890, Joseph Stefan modelled the melting of arctic ice in the summer by a simple one-dimensional model, [85]. Consider a homogeneous block of ice filling the region $x \geq l = h(0)$ at the time $t = 0$. The ice starts to melt by heating the block at the left end. Thus, at $t \geq 0$ the region between $x = 0$ and $x = h(t) > 0$ is filled with water and the region $x \geq h(t)$ is filled with ice. The system of equations that model this problem with the temperature $u(x, t)$ over the domain $(0, h(t)) \times (0, T]$ at time t, where T is a given arbitrary final time of interest is

$$\frac{\partial u}{\partial t}(x,t) = \frac{\partial^2 u}{\partial x^2}(x,t), \quad (x,t) \in (0,h(t)) \times (0,T], \tag{1.5}$$

$$u(x,0) = u_0(x), \quad x \in (0,h(t)), \tag{1.6}$$

the Stefan interface conditions on the moving boundary $x = h(t)$,

$$u(h(t),t) = u_1(t), \quad t \in [0,T], \tag{1.7}$$

$$h'(t) = -\frac{\partial u}{\partial x}(h(t), t), \quad t \in [0, T]. \tag{1.8}$$

Equation (1.8) is a heat balance condition, which states that the rate of change of the moving boundary (denoted by $h'(t)$) is equal to the amount of heat entering through the boundary interface. In (1.7), u_1 is the melting temperature (often constant) at the interface $h(t)$ (and (1.7) is natural to impose since it represents a change of phase at $h(t)$). The Neumann heat flux boundary condition at $x = 0$ is

$$\frac{\partial u}{\partial x}(0, t) = u_2(t), \quad t \in [0, T], \tag{1.9}$$

which is introduced to generate the melting process. When $u_0 \equiv 0$ the problem represents, for example, the heating of an ice block via a heat flux $u_2(t)$ on the fixed boundary. The representation of the two-phase direct Stefan problem, with specification of the initial and boundary conditions (1.6)–(1.9) is shown in Figure 1.1.

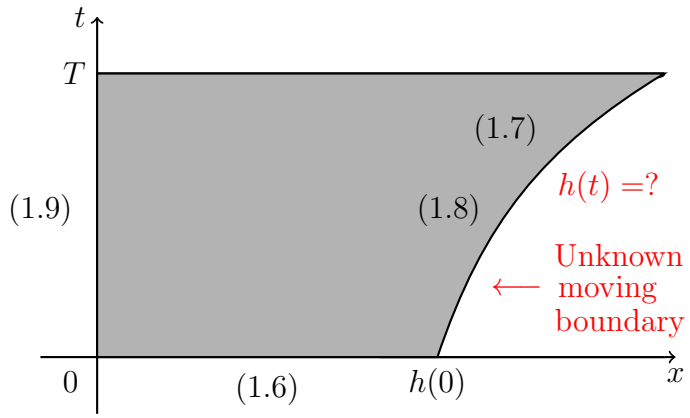

Figure 1.1: Representation of the two-phase direct Stefan problem, with specification of the initial and boundary conditions (1.6)–(1.9).

We mention that in Chapters 4 and 5 we focus on inverse Stefan problems which have the task of determining the temperature $u(x, t)$ and the unknown(s) boundary(ies) function in addition to the unknown(s) coefficients in a parabolic partial differential equation.

1.6 Stability analysis of inverse problems

Identification of coefficients in inverse problems are generally nonlinear in nature. These nonlinear problems can be represented in a nonlinear operator form (1.1),

where $\mathcal{A}$ acts between two Hilbert spaces X and Y. The solution of (1.1) is said to be unstable if it does not depend continuously on the data $y \in Y$. For example, if $\mathcal{A}$ is compact, i.e. the image of any bounded set in X is pre-compact (a subset whose closure is compact) in Y, with infinite dimensional range, hence non-closed, it follows that $\mathcal{A}^{-1}$, if it exists, is unbounded [40]. To restore stability regularization needs to be employed, as described next.

1.6.1 Regularisation

The solution of inverse and ill-posed problems are well-known to generate instability. To deal with this difficulty the inverse problem is solved as the minimization of an appropriate regularization functional in order to achieve the stability of the solution, as described in the subsection below.

1.6.2 The Tikhonov regularisation method

The Tikhonov regularization is one of the most popular methods for computing an approximate solution of ill-posed problems with error-contaminated data. The method is applied to obtain a stable solution to the nonlinear operator equation (1.1). In practice, the right-hand side of the equation (1.1) is perturbed as y^ϵ with $||y - y^\epsilon|| \approx \epsilon$, where ϵ represents the level of noise. Then, instead of (1.1) one has to solve

$$\mathcal{A}x = y^\epsilon. \tag{1.10}$$

But of course equation (1.10) may have no solution if $y^\epsilon \notin \mathcal{R}(\mathcal{A})$, where $\mathcal{R}(\mathcal{A}) \subset Y$ denotes the range of the operator $\mathcal{A}$. In this situation, one has to define a quasi-solution given by the minimization of the least-squares gap $||\mathcal{A}x - y^\epsilon||^2$. Moreover, if the inverse problems are ill-posed (a small modification in the input data can lead to bigger impact on the ultimate result in the output solution) we employ the Tikhonov regularization method based on minimizing

$$||\mathcal{A}x - y^\epsilon||^2 + \beta||R_k x||^2 \rightarrow \min, \quad x \in \mathcal{D}(\mathcal{A}), \tag{1.11}$$

where $\mathcal{D}(\mathcal{A})$ represents the domain of $\mathcal{A}$, R_k is the regularization (derivative) operator of order $k = 0, 1, ...$, and $\beta > 0$ is a positive regularization parameter. A minimizer to (1.11) always exists under certain conditions but it may not be unique, [39]. The order k of the regularization operator R_k is related to the C^k-smoothness of the solution which may (or may not) be a *priori* known or assumed, [131]. Thus, the order k penalises the kth-order derivative, i.e. continuity class

C^0 for $k = 0$ and first-order smoothness class C^1 for $k = 1$, etc.

1.6.3 The choice of the regularisation parameters

Over the last four decades many different methods for selecting regularisation parameters have been proposed. Their appropriate choice plays an important role in equation (1.11) for achieving accurate and stable numerical results of inverse problems. The choice of regularization parameters can be made according to certain criteria as follows:

- The L-curve criterion, see [48]. The L-curve method is one of the most convenient tools for the analysis of discrete ill-posed problems and it will be used quite a lot in this thesis. This technique is actually a plot for many positive regularization parameters of the norm of the regularised solution $||x_\beta||$ versus the corresponding residual norm $||\mathcal{A}x - y^\epsilon||$. The L-curve displays the compromise between minimisation of these two quantities, [47]. If such a curve has an L-shape then one can choose the regularization parameter at the 'corner' of it. It is also worth mentioning that there are counterexamples for which the L-curve fails to provide a clearly defined corner or no corner at all, see [134].

- The discrepancy principle is a widely used technique for choosing the regularisation parameter, see Morozov (1966) and Tikhonov and Arsenin (1977). According to this principle, the regularisation parameter β is chosen such as $||\mathcal{A}x_{\beta(\varepsilon)} - y^\varepsilon|| \approx \varepsilon$, where $x_{\beta(\varepsilon)}$ is the minimizer to (1.11).

- Trial and error. As mentioned in [35], the regularization parameter β can be selected based on experience by first choosing a small positive value, and gradually increasing it until any numerical oscillations in the unknown solution disappear.

1.7 Numerical methods for discretising partial differential equations

There are several numerical methods which can be used to solve partial differential equations (PDEs) for example, finite difference, finite element, finite volume and boundary element. These methods will be briefly described in the subsections below.

1.7.1 Finite difference method

The finite difference method (FDM) is one of the most historic methods that can be used for solving PDEs by use of finite difference equations to approximate derivatives, see [126].

The advantage of FDM with a Crank-Nicolson scheme, [123], is that it is unconditionally stable and second-order accurate in space and time. Also, the alternating direction explicit (ADE) or the alternating direction implicit (ADI) methods can be employed, with significant advantages, especially in higher dimensions [106]. One possible drawback of the FDM is that it becomes quite complicated when solving PDEs in irregular domains and the other is that it is difficult to carry out the mathematical analysis of stability and convergence for nonlinear PDEs.

1.7.2 Finite element method

The finite element method (FEM) is a numerical method that can solve differential or integral equations. The method is such that it consists of assuming piecewise continuous approximating functions for the solution. It works by rewriting the governing equation into an equivalent variational weak form, meshing the domain into small finite elements and looking for appropriate solutions at the mesh nodes using appropriate basis functions over each elements [111].

1.7.3 Finite volume method

The finite volume method (FVM), also known as the box method, is one that is mainly used for the numerical solution of problems in fluid dynamics. The idea of FVM is to integrate the differential equation over a finite size control volume surrounding each node point on a mesh, and then changing the volume integrals to surface integrals, see [94] for more details.

1.7.4 Boundary element method

The boundary element method (BEM) is used to solve those PDEs which possess a fundamental solution available explicitly. The main idea of the BEM, which is based on using the Green's identity and the fundamental solution, is to find the solution inside the domain by using the solution to the PDE on the boundary only. The BEM reduces the dimensionality of the problem by one and produces a fully populated matrix (different from FDM which is tridiagonal). A limitation

of the BEM is that it can only be used in problems for which the fundamental solution of the governing equation is available explicitly [97].

1.8 Optimization

Optimization concerns the minimization (or maximization) of functions. The optimization toolbox consists of functions that perform minimization on general nonlinear functions. Throughout the thesis we apply the nonlinear Tikhonov regularization method which minimizes the least-squares functional penalized by some extra terms to stabilise the solution, see equation (1.11). In this thesis, the *lsqnonlin* MATLAB toolbox optimization technique will be used. Simple bounds on the variables are allowed and the explicit calculation (analytical or numerical) of the gradient is not required to be supplied by the user.

1.8.1 *lsqnonlin* routine

The *lsqnonlin* routine is a nonlinear least-squares solver available from the MATLAB optimization toolbox which is used to find the minimum of a sum of squares specified by

$$\min_{\underline{x}} ||\underline{F}(\underline{x})||_2^2 = \min_{\underline{x}} \Big(F_1^2(\underline{x}) + F_2^2(\underline{x}) + ... + F_n^2(\underline{x}) \Big),$$

subject to a set of upper and lower bounds defined on the components of $\underline{x}$. The solution is therefore, in this range. Rather than computing the norm $||\underline{F}(\underline{x})||_2^2 =: F(\underline{x})$ (the sum of squares), *lsqnonlin* requires user-defined functions (does not compute the sum of squares) to compute the vector-valued function in the form of $\underline{F} = (F_1, ..., F_n)$. This routine is recalled on the MATLAB syntax as follows:
`>> lsqnonlin(fun,x0,LB,UB,options)`, where
`fun`: the least-squares function $F(\underline{x})$ to be minimized;
`x0`: the initial guess vector $\underline{x}_0$ to start the minimization process;
`LB,UB`: vectors containing the lower and upper simple bounds on the solution.
The `options` are passed to the routine as follows:

```
% Default options
options = optimset;
% Modify options setting
options = optimset(options,'Display','iter');
options = optimset(options,'MaxIter',MaxIter_Data);
options = optimset(options,'TolFun',TolFun_Data);
options = optimset(options,'TolX',TolX_Data);
```

```
options = optimset(options,'MaxFunEvals',MaxFunEvals_Data);
options = optimset(options,'Algorithm','trust-region-reflective').
```

The iterate for the unknown coefficient is passed to the FDM forward solver which maps the coefficient into the output that is compared with the experimentally measured or numerically simulated data, after which the *lsqnonlin* updates the iterate based on an optimization embedded algorithm. There are various such algorithms that could be selected, e.g. the trust-region-reflective (TRR) or the Levenberg-Marquardt algorithm. In this thesis, we choose the TRR algorithm, which is a subspace trust-region method based on the interior-reflective Newton method described in [30]. At each iteration it involves the solution of a large linear system of equations using the method of preconditioned conjugate gradients or Cholesky factorization.

1.8.2 Description of the minimization algorithm

In this section, we explain the algorithm that we use to find the minimizer of the nonlinear Tikhonov functional (1.11). Generally, the least-squares problem is the problem of finding a vector $\underline{x}$ that is a local minimizer to a function that is a sum of squared quantities, possibly subjected to some constraints.

There are several algorithms to solve this type of optimization problem. One of them is the TRR, [31, 32], which is based on a simple and powerful concept in optimization, namely, the Trust-Region method. The idea of this approach is to consider an unconstrained minimization problem for the function F. Let $\underline{x}$ be a point in $\mathbb{R}^n$ and we want to move to the next point with lower function value, viz we approximate F with a simpler function q which is usually the quadratic form Taylor expansion at the point $\underline{x}$. Therefore, q reflects the behaviour of F in a neighbourhood $\mathcal{N}$ around $\underline{x}$ which is called Trust-Region. Mathematically, we can express this as the following definition of the Trust-Region subproblem:

$$\min_{\underline{s}}\{q(\underline{s}), \underline{s} \in \mathcal{N}\}. \tag{1.12}$$

After solving (1.12) for $\underline{s}$, if $F(\underline{x}+\underline{s}) < F(\underline{x})$, then $\underline{x}+\underline{s}$ becomes the current point; otherwise, $\underline{x}$ remains the current point, but the Trust Region size is decreased and we resolve (1.12) for $\underline{s}$ once again. The key questions in finding a specific Trust-Region approach to minimizing $F(\underline{x})$ are how to choose and compute q and how to control the neighborhood $\mathcal{N}$. In a typical Trust-Region method, the quadratic approximation to q is defined by taking the first two terms of Taylor's

expansion for F at $\underline{x}$, i.e. the Trust-Region subproblem (1.12) becomes

$$\min\left\{q(\underline{s}) = \frac{1}{2}\underline{s}^T H\underline{s} + \underline{s}^T.\nabla F(\underline{x}) \text{ such that } ||D\underline{s}|| \leq \Delta\right\}, \tag{1.13}$$

where ∇ is the gradient of $F(\underline{x})$ at the current point x, $H = \left(\frac{\partial^2 F}{\partial x_i \partial x_j}\right)_{1\leq i,j\leq n}$ is the Hessian matrix of $F(\underline{x})$, D is a diagonal scaling matrix, Δ is the Trust-Region size, and $||.||$ is the 2-norm. Such algorithms need some computational effort because it involves the computation of a full eigensystem and a Newton process applied to the scalar equation $\frac{1}{\Delta} - \frac{1}{\|\underline{s}\|} = 0$, for more details, see [102]. The approximation approach followed in Optimization Toolbox solvers is to restrict the Trust-Region subproblem (1.12) to a two-dimensional subspace S, see [8]. Once the subspace S has been computed, then the solution to solve (1.13) is trivial even if full eigenvalue/eigenvector information is needed (since in the subspace, the problem is only two-dimensional). The two-dimensional subspace S is determined with the aid of a preconditioned conjugate gradient process described below. The toolbox assigns $S = \{\underline{s}_1, \underline{s}_2\}$, where $\underline{s}_1$ is in the direction of the gradient ∇F, and $\underline{s}_2$ is either an approximate Newton direction, i.e., a solution to

$$H\underline{s}_2 = -\nabla F, \tag{1.14}$$

or a direction of negative curvature

$$\underline{s}_2^T H\underline{s}_2 < 0. \tag{1.15}$$

The fundamental idea behind this choice of S is to force global convergence (via the steepest descent direction or negative curvature direction) and achieve fast local convergence (via the Newton step, when it exists). In the MATLAB optimization toolbox we use the *lsqnonlin* routine with TRR algorithm and we choose Cholesky factorization[1] to solve the subproblem (1.13). The mechanism of TRR algorithm can be summarized as follows:

1. Formulate the Trust-Region subproblem (1.12).
2. Solve equation (1.13) to determine the initial (trial) step $\underline{s}$.
3. If $F(\underline{x} + \underline{s}) < F(\underline{x})$ then $\underline{x} \mapsto \underline{x} + \underline{s}$.
4. The quantity Δ is adjusted according to the value of $F(\underline{x}+\underline{s})$; if it is greater than $F(\underline{x})$ then the value of Δ will be decreased, for more details, see [32].

[1]Cholesky Factorization Theorem: Given a symmetric positive definite matrix A there exists a lower triangular matrix L such that $A = LL^T$. The lower triangular matrix L is known as the Cholesky factor and LL^T is known as the Cholesky factorization of A.

As mentioned in [31], the essential idea behind the Trust-Region method is to adjust the Trust-Region size Δ for each subproblem (1.12) so as to ensure a sufficient decrease of the objective function.

These steps are repeated until convergence is achieved.

1.8.3 Limitations of the routine

- One of the limitations of this routine is that it only handles real values. If the function is comprised of complex variables, it has to be split into real and imaginary components, then a solution can be sought.
- Another limitation is that it is a requirement for the function being minimized to be continuous. In general, depending on the initial guess, only local solutions may be achieved [33]. Finding a global minimizer to these nonlinear optimization problems is not an easy task. Since the inverse problems under investigation are nonlinear the least-squares functional is not convex and could have many local minima in which, depending on the initial guess, a descent-based method tends to get stuck if the underlying problems are ill-posed. A possible way to deal with this difficulty could be to develop a global convergent method, [112], whose convergence to a good approximation of the true solution is independent of the initial guess, but this challenging task is deferred to a future work.
- The algorithm does not allow for equal lower and upper simple bounds.
- The Levenberg-Marquardt algorithm does not handle linear or nonlinear bound constraints.
- The TRR algorithm, [31], which is used in *lsqnonlin*, assumes that n must be greater or equal than the length of $\underline{x}$.

1.9 Purpose and outline of the thesis

Coefficient identification problems, some with an unknown moving boundary, have been investigated theoretically for reconstructing a single coefficient in the parabolic heat equation assuming that it is constant [17], or time-dependent [73, 77], or space-dependent [1], or temperature-dependent [103, 104]. In these research articles, the authors investigated the existence and uniqueness of solutions to the inverse problems, but no numerical method/solution has been attempted. Some numerical technique has been attempted in [122], based on space

decomposition in a reproducing kernel space. Also, in [11], the author considered determining the time-dependent coefficients using the method of suboptimal stage-by-stage optimization.

The simultaneous reconstruction of two time-dependent coefficients has been investigated theoretically in the monographs [74, 110]. The case of identification of multiple time-dependent coefficients together with an unknown free boundary (Stefan) problem such as a solid/liquid phase change has been investigated in [117–121], but no numerical solution/method has been attempted to solve such inverse problems.

Based on the above literature research, this thesis aims to fill in the gaps on the numerical solution for multiple (mainly time-dependent) coefficient identification problems in one and two-dimensions in a fixed or moving domain. The technique used in this thesis is based on the minimization of the least-squares objective functional which naturally represents the gap between the measured and computed data. This optimization problem is solved effectively using a MATLAB optimization toolbox routine. The Tikhonov regularization method is employed for noisy input data in order to obtain stable and accurate solutions. Numerical results have been presented, discussed and compared with the analytical solutions, where available. The generation of input data were obtained either from the analytical solution, if available, or numerically simulated by solving first the direct problem and with care not to commit an inverse crime in the inversion [84].

Throughout the thesis, the mathematical essence of having a time-dependent conductivity/diffusivity multiplying the second-order derivative u_{xx} in the heat equation enables the transformation $\theta(t) = \int_0^t a(\tau)d\tau$ to be performed and the resulting PDE becomes the classical heat equation with constant coefficients. Then, for this latter PDE one can employ a classical analysis based on employing Green's functions. For the existence of a solution the Schauder fixed point theorem[2] is applied, whilst for the uniqueness the theory of Volterra integral equations of the second kind[3] is applied. More general details can be found in [74].

The purpose of this thesis is to find the numerical solution for various coefficient identification problems and extend the possibility of simultaneous reconstruction of physical properties of interest. Most of the inverse problems investigated in this thesis model real phenomena like heat conduction, melting of ice or water, steel annealing and freezing food, solidification, etc. Initially, we

[2]Schauder fixed point theorem: Let C be a closed convex subset of a normed linear space and let $f : C \to C$ be a compact map, then f has a fixed point, [10].

[3]Theorem. The Volterra integral equation of the second kind $\varphi(x) - \int_a^x K(x,y)\varphi(y)dy = f(x)$, $x \in [a,b]$, with continuous kernel K for each right hand side $f \in [a,b]$ has a unique solution $\varphi \in C[a,b]$, [88].

investigate numerically the determination of one unknown coefficient (thermal conductivity) in Chapter 2 and develop the numerical procedure to be extended to the case of multi-coefficients (parameters), i.e. two coefficient or more, in the subsequent chapters.

The structure of the thesis is based upon the type of domain, fixed or moving, and we arrange the chapters according to the number of unknown coefficients as follows. Chapters 2, 3, 6, 7 and 9 are fixed domain problems with one or two coefficients to be identified, whilst Chapters 4, 5 and 8 are moving domains problems with one, three, and four coefficients to be identified. Finally, Chapters 8 and 9 present extensions to two-dimensions. The FDM with a Crank-Nicolson scheme is mainly used in this thesis as a direct solver except in Chapters 8 and 9 where the ADE scheme is employed in two-dimensions. An explicit forward time central space (FTCS) method is also employed in Chapter 2 for the extension to higher dimensions. The optimization routine *lsqnonlin* is used in order to find the numerical solution of these nonlinear inverse and ill-posed problems.

In Chapter 2, we investigate an identification of the time-dependent thermal conductivity from heat flux overspecification in the one-dimensional parabolic heat equation. An extension to a two-dimensional coefficient identification problem, which is a variant of the one-dimensional problem, is investigated. Three numerical examples are illustrated and discussed for one- and two-dimensional inverse problems.

In Chapter 3, we investigate a couple of inverse problems of simultaneous determination of time-dependent thermal conductivity and convection, or absorption coefficients from the measurements of the heat moments in the one-dimensional parabolic heat equation. These problems are ill-posed and need to be stabilised through the Tikhonov regularization method.

The simultaneous determination of several time-dependent reaction coefficients in free boundary heat transfer problems is investigated in Chapter 4. Whilst, in Chapter 5, a novel inverse problem consisting of determining the multiple time-dependent coefficients and multiple free boundaries, together with the temperature in the heat equation with Stefan condition and several-orders heat moment conditions, is investigated.

In Chapter 6, we consider an inverse problem of determining the time-dependent thermal diffusivity coefficient the convection coefficient and the temperature for a weakly degenerate heat equation, which vanishes at the initial moment of time, from heat flux and/or mass/energy measurement/specification/overdetermination.

In Chapter 7, we investigate the determination of an additive time and space-dependent perfusion coefficient from additional temperature measurements in the

one-dimensional parabolic heat equation.

In Chapter 8, a nonlinear problem concerning the identification of a time-dependent free boundary in a two-dimensional parabolic equation is investigated. An ADE scheme is used to discretise the governing equation and the unknown coefficient is computed via the solution to a nonlinear least-squares minimization problem.

In Chapter 9, the inverse problem concerning the reconstruction of an orthotropic thermal conductivity and the temperature in the two-dimensional parabolic heat equation in a rectangular domain from the heat flux overspecification is investigated. The ADE-FDM is developed as a direct solver, whilst the inverse solver is based on a nonlinear least-squares minimization using the MATLAB optimization toolbox routine *lsqnonlin*.

Finally, in Chapter 10, general conclusions and suggestions for possible future work are highlighted.

Chapter 2

Determination of the time-dependent thermal conductivity from boundary data

2.1 Introduction

In inverse identification problems, the unknown coefficients involved in the governing PDEs or in the boundary conditions are sought from additional information on the main dependent variable solution of the original direct initial boundary value problem, [124]. In particular, the inverse problem of identifying the thermal diffusivity/conductivity from boundary data (temperature and partial heat flux) has been investigated widely by many researchers in the past, see [12, 15, 66, 72, 82, 83, 138] to mention only a few. In this chapter, the novelty consists in the development of a numerical optimization method for solving this nonlinear inverse coefficient problem for the heat equation. Numerically, the implementation is realised using the MATLAB toolbox routine *lsqnonlin*.

The chapter is organized as follows. In Section 2.2, the mathematical formulation of the inverse problem is presented. In Section 2.3, the numerical solution of the direct problem is based on the FDM with the Crank-Nicolson scheme. In Section 2.4, the minimization algorithm to solve the inverse problem is presented. The numerical results are discussed in Section 2.5. The extension to higher dimensions is discussed in Section 2.6. Finally, conclusions are highlighted in Section 2.7.

2.2 Mathematical formulation

In the domain $Q_T = \{(x,t)|\ 0 < x < L, 0 < t < T\} = (0,L) \times (0,T)$ we consider the inverse problem given by the parabolic heat equation

$$\frac{\partial u}{\partial t}(x,t) = a(t)\frac{\partial^2 u}{\partial x^2}(x,t) + f(x,t), \quad (x,t) \in Q_T, \tag{2.1}$$

with known heat source $f(x,t)$, unknown temperature $u(x,t)$ and unknown thermal conductivity $a(t) > 0$, $t \in [0,T]$, subject to the initial condition

$$u(x,0) = \phi(x), \quad x \in [0,L], \tag{2.2}$$

the Dirichlet temperature boundary conditions

$$u(0,t) = \mu_1(t), \quad u(L,t) = \mu_2(t), \quad t \in [0,T], \tag{2.3}$$

and the heat flux overdetermination condition

$$a(t)u_x(0,t) = q_0(t), \quad t \in [0,T]. \tag{2.4}$$

For simplicity, we have assumed that the heat capacity is constant and taken to be unity. The sketch of the inverse problem under investigation is shown in Figure 2.1. Physical problems where a time-dependent conductivity/diffusivity $a(t)$ appears occur in radioactive decay or damage applications, [13, p.187].

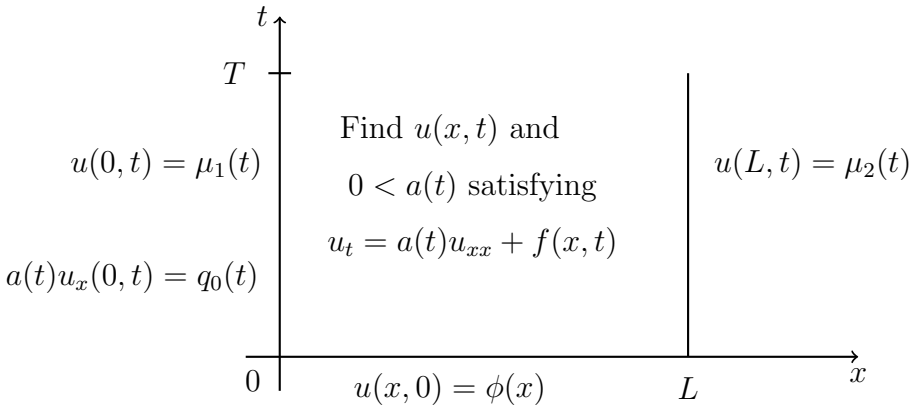

Figure 2.1: Sketch of the inverse problem under investigation.

The uniqueness of the solution of the inverse problem (2.1)–(2.4) has been established in [72] and reads as follows.

Theorem 2.2.1. (Uniqueness of the solution). *If* $0 < q_0 \in C[0,T]$, *then a solu-*

tion $(a(t), u(x,t)) \in C^{1+\alpha/2}[0,T] \times C^{2+\alpha,1+\alpha/2}(\overline{Q_T})$ *for some* $\alpha \in (0,1)$, *with* $a(t) > 0$ *for* $t \in [0,T]$, *to the problem (2.1)–(2.4) is unique.*

In this theorem, the Hölder space $C^{1+\alpha/2}[0,T]$ denotes the space of continuously differentiable functions on $[0,T]$ with the derivative being Hölder continuous[1] with exponent $\alpha/2$. Also, $C^{2+\alpha,1+\alpha/2}(\overline{Q_T})$ denotes the space of continuous functions u along with their partial derivatives u_x, u_{xx}, u_t in $\overline{Q_T}$, with u_{xx} being Hölder continuous with exponent α in $x \in [0,L]$ uniformly with respect to $t \in [0,T]$, and with u_t being Hölder continuous with exponent $\alpha/2$ in $t \in [0,T]$ uniformly with respect to $x \in [0,L]$. Lower-order terms $b(x,t)\frac{\partial u}{\partial x}(x,t) + c(x,t)u(x,t)$, with b and c known functions, can also be added to the right-hand side of equation (2.1), with no qualitative change in both analytical and numerical analyses, [72].

2.3 Numerical solution of direct problem

In this section, we consider the direct initial boundary value problem given by equations (2.1)–(2.3). We use FDM with the Crank-Nicholson scheme, [123], which is unconditionally stable and second-order accurate in space and time. We denote $u(x_i, t_j) = u_{i,j}$, where $x_i = i\Delta x$, $t_j = j\Delta t$ for $i = \overline{0, M}$, $j = \overline{0, N}$, and $\Delta x = L/M$, $\Delta t = T/N$.

Considering the general time-dependent PDE

$$u_t = G(x, t, u, u_x, u_{xx}), \tag{2.5}$$

the Crank-Nicolson method, [123], discretises (2.5), (2.2) and (2.3) as

$$\frac{u_{i,j+1} - u_{i,j}}{\Delta t} = \frac{1}{2}(G_{i,j} + G_{i,j+1}), \quad i = \overline{1, (M-1)}, \quad j = \overline{0, (N-1)}, \tag{2.6}$$

$$u_{i,0} = \phi(x_i), \quad i = \overline{0, M}, \tag{2.7}$$

$$u_{0,j} = \mu_1(t_j), \quad u_{M,j} = \mu_2(t_j), \quad j = \overline{0, N}, \tag{2.8}$$

where

$$G_{i,j} = G\Big(x_i, t_j, u_{i,j}, \frac{u_{i+1,j} - u_{i-1,j}}{2(\Delta x)}, \frac{u_{i+1,j} - 2u_{i,j} + u_{i-1,j}}{(\Delta x)^2}\Big),$$

$$G_{i,j+1} = G\Big(x_i, t_{j+1}, u_{i,j+1}, \frac{u_{i+1,j+1} - u_{i-1,j+1}}{2(\Delta x)}, \frac{u_{i+1,j+1} - 2u_{i,j+1} + u_{i-1,j+1}}{(\Delta x)^2}\Big),$$

$$i = \overline{1, (M-1)}, \quad j = \overline{0, (N-1)}. \tag{2.9}$$

[1] A function f is called Hölder continuous with exponent $\alpha \in (0,1)$ if there exists $M > 0$ such that $|f(x) - f(x')| \leq M|x - x'|^\alpha$, $\forall x, x'$.

For our problem (2.1)–(2.3), the FDM discretisation reads as

$$\begin{aligned} &-A_{j+1}u_{i-1,j+1} + (1+B_{j+1})u_{i,j+1} - A_{j+1}u_{i+1,j+1} \\ &= A_j u_{i-1,j} + (1-B_j)u_{i,j} + A_j u_{i+1,j} + \frac{\Delta t}{2}(f_{i,j} + f_{i,j+1}), \\ &\qquad i = \overline{1,(M-1)}, \quad j = \overline{0,(N-1)}, \end{aligned} \tag{2.10}$$

$$u_{i,0} = \phi(x_i), \quad i = \overline{0,M}, \tag{2.11}$$

$$u_{0,j} = \mu_1(t_j), \quad u_{M,j} = \mu_2(t_j), \quad j = \overline{0,N}, \tag{2.12}$$

where

$$a_j = a(t_j), \quad f_{i,j} = f(x_i, t_j), \quad A_j = \frac{(\Delta t)a_j}{2(\Delta x)^2}, \quad B_j = \frac{(\Delta t)a_j}{(\Delta x)^2}.$$

Starting from the initial time $t = 0$ where the initial temperature is prescribed in (2.11), we march forward in time. At each time step t_{j+1} for $j = \overline{0,(N-1)}$, using the Dirichlet boundary conditions (2.12), the above difference equation can be reformulated as a $(M-1) \times (M-1)$ system of linear equations of the form,

$$D\mathbf{u_{j+1}} = E\mathbf{u_j} + \mathbf{b^j}, \tag{2.13}$$

where $\mathbf{u_{j+1}} = (u_{1,j+1}, u_{2,j+1}, ..., u_{M-2,j+1}, u_{M-1,j+1})^{\mathrm{T}}$,

$$D = \begin{pmatrix} 1+B_{j+1} & -A_{j+1} & 0 & ... & 0 & 0 & 0 \\ -A_{j+1} & 1+B_{j+1} & -A_{j+1} & ... & 0 & 0 & 0 \\ \vdots & \vdots & \vdots & \ddots & \vdots & \vdots & \vdots \\ 0 & 0 & 0 & ... & -A_{j+1} & 1+B_{j+1} & -A_{j+1} \\ 0 & 0 & 0 & ... & 0 & -A_{j+1} & 1+B_{j+1} \end{pmatrix},$$

$$E = \begin{pmatrix} 1-B_j & A_j & 0 & ... & 0 & 0 & 0 \\ A_j & 1-B_j & A_j & ... & 0 & 0 & 0 \\ \vdots & \vdots & \vdots & \ddots & \vdots & \vdots & \vdots \\ 0 & 0 & 0 & ... & A_j & 1-B_j & A_j \\ 0 & 0 & 0 & ... & 0 & A_j & 1-B_j \end{pmatrix},$$

and

$$\mathbf{b^j} = \begin{pmatrix} \frac{\Delta t}{2}(f_{1,j} + f_{1,j+1}) + A_j\mu_1(t_j) + A_{j+1}\mu_1(t_{j+1}) \\ \frac{\Delta t}{2}(f_{2,j} + f_{2,j+1}) \\ \vdots \\ \frac{\Delta t}{2}(f_{M-2,j} + f_{M-2,j+1}) \\ \frac{\Delta t}{2}(f_{M-1,j} + f_{M-1,j+1}) + A_j\mu_2(t_j) + A_{j+1}\mu_2(t_{j+1}) \end{pmatrix}.$$

The discretisation of the heat flux (2.4) is given by

$$q_0(t_j) = a(t_j)u_x(0,t_j) = \frac{(4u_{1,j} - u_{2,j} - 3\mu_1(t_j))a_j}{2\Delta x}, \quad j = \overline{1,N}. \tag{2.14}$$

2.4 Numerical approach for the inverse problem

The nonlinear inverse problem (2.1)–(2.4) can be formulated as a nonlinear minimization of the least-squares objective function

$$F(a) := \|a(t)u_x(0,t) - q_0(t)\|^2, \tag{2.15}$$

the discretization of which is

$$F(\mathbf{a}) = \sum_{j=1}^{N} \Big[a_j u_x(0,t_j) - q_0(t_j)\Big]^2, \tag{2.16}$$

where $\mathbf{a} = (a_j)_{j=\overline{1,N}} \in \mathbb{R}_+^N$. It is worth mentioning that in (2.16) at the first time step, i.e. $j = 0$, the derivative $u_x(0,0)$ is obtained from the initial condition (2.2), via (2.14), as

$$u_x(0,0) = \frac{4\phi_1 - \phi_2 - 3\phi_0}{2(\Delta x)}, \tag{2.17}$$

where $\phi_i = \phi(x_i)$ for $i = \overline{0,M}$. The minimization of (2.16) is performed using the MATLAB toolbox routine *lsqnonlin*, which does not require supplying by the user of the gradient of the objective function, [99]. This routine attempts to find the minimum of a sum of squares by starting from the arbitrary initial guesses $\mathbf{a}^{(0)}$ for $\mathbf{a}$. Furthermore, within *lsqnonlin*, we use the TRR algorithm [31], which is based on the interior-reflective Newton method. We have compiled this routine with the following specifications :

- Number of variables $M = N$.

- Maximum number of iterations, (MaxIter) = 400.
- Maximum number of objective function evaluations, (MaxFunEvals) = $10^2\times$(number of variables).
- Termination tolerance on the function value, (TolFun) = 10^{-20}.
- x Tolerance, (xTol)=10^{-20}.
- The lower and upper bounds for $\mathbf{a}$ are 10^{-10} and 10^3. These bounds allow a wide search range for the vector of unknowns.

2.5 Numerical results and discussion

For all the numerical results produced in this thesis, we have used a TOSHIBA laptop with the processor Inter(R) Core(TM) i7-5500 CPU, 64-bit operating system and installed memory (RAM) 8.00 GB.

In this section, we present a few examples in order to test the accuracy and stability of the numerical method introduced in Section 2.4. The root mean square error (rmse)

$$rmse(a(t)) = \sqrt{\frac{1}{N}\sum_{j=1}^{N}\Big(a^{numerical}(t_j) - a^{exact}(t_j)\Big)^2} \tag{2.18}$$

is used to evaluate the accuracy of the numerical results.

In all the numerical results presented below we take $L = T = 1$. We also take the initial guess for the unknown thermal diffusivity $a(t)$ equal to the constant $a(0)$, which from the compatibility of the conditions (2.2) and (2.4) at $t = 0$ is known and given by $a(0) = q_0(0)/\phi'(0)$.

2.5.1 Example 1

We consider recovering a non-smooth thermal conductivity, as given by equation (2.24) below. We take input data given by

$$\phi(x) = u(x,0) = 2x - x^2\Big(x + \frac{1}{2}\Big)^2, \tag{2.19}$$

$$\mu_1(t) = u(0,t) = 2t - \frac{t^2}{4}, \quad \mu_2(t) = u(1,t) = 2 + 2t - \frac{9}{4}(1+t)^2, \tag{2.20}$$

$$f(x,t) = 2 - 2\Big(x+\frac{1}{2}\Big)^2(x+t) - \Big(\Big|t-\frac{1}{2}\Big| + \frac{1}{2}\Big)\Big(-2\Big(x+\frac{1}{2}\Big)^2 - 8\Big(x+\frac{1}{2}\Big)(x+t) - 2(x+t)^2\Big), \tag{2.21}$$

and

$$q_0(t) = a(t)u_x(0,t) = \Big(2 - \frac{1}{2}t - t^2\Big)\Big(\Big|t-\frac{1}{2}\Big| + \frac{1}{2}\Big). \tag{2.22}$$

Then, the analytical solution of the inverse problem (2.1)–(2.4) is given by

$$u(x,t) = 2t + 2x - \Big(x+\frac{1}{2}\Big)^2(x+t)^2, \tag{2.23}$$

and

$$a(t) = \Big|t-\frac{1}{2}\Big| + \frac{1}{2}. \tag{2.24}$$

Figure 2.2 shows the numerical heat flux in equation (2.4) in comparison with the exact solution (2.22) obtained by solving the direct problem (2.1)–(2.3) with the input data (2.19)–(2.21) and (2.24) using the FDM, described in Section 2.3, with $M = N \in \{10, 20, 40\}$. From this figure it can be seen that the good agreement between the exact solution (2.22) and the numerical solutions.

We now fix $M = N = 40$ and try to recover the thermal conductivity $a(t)$ and the temperature $u(x,t)$ for exact input data, i.e. $p = 0$, as well as for $p \in \{1\%, 3\%\}$ additive noisy data numerically simulated as

$$q_0^\epsilon(t_j) = q_0(t_j) + \epsilon_j, \quad j = \overline{1,N}, \tag{2.25}$$

where ϵ_j are random variables generated from a Gaussian normal distribution with mean zero and standard deviation σ given by

$$\sigma = p \times \max_{t\in[0,T]} |q_0(t)|, \tag{2.26}$$

where p represents the percentage of noise. We use the MATLAB function *normrnd* to generate the random variables $\boldsymbol{\epsilon} = (\epsilon_j)_{j=\overline{1,N}}$ as follows:

$$\boldsymbol{\epsilon} = normrnd(0, \sigma, N). \tag{2.27}$$

The objective function (2.16) is plotted, as a function of the number of iterations, in Figure 2.3. From this figure, it can be seen that a very fast convergence is achieved in about 7 to 11 iterations to reach to a very low value of $O(10^{-27})$. The related numerical results for $a(t)$ and $u(x,t)$ are presented in Figures 2.4 and 2.5, respectively. From these figures it can be seen clearly that there is good

agreement between the numerical results and the analytical solutions for exact data, i.e. $p = 0$, and is proportional with the errors in the input data for $p > 0$. The numerical solutions for $a(t)$ and $u(x,t)$ converge to their corresponding exact solutions in equations (2.24) and (2.23), as the percentage of noise p decreases from 3% to 1% and then to zero.

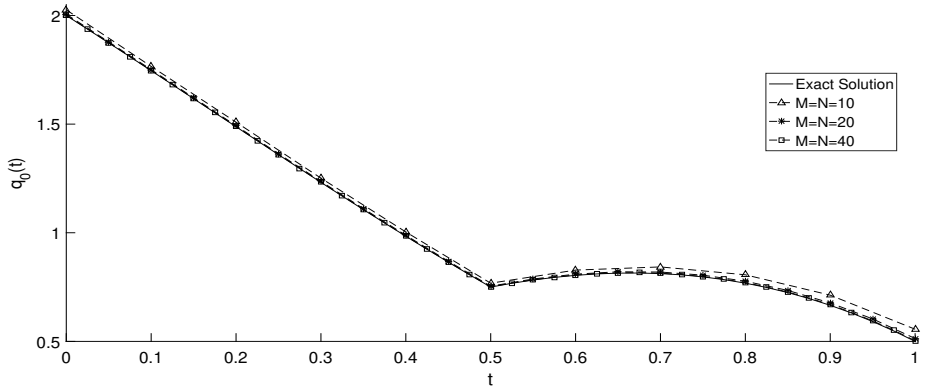

Figure 2.2: The exact (equation (2.22)) and numerical solutions for the heat flux (2.4), for Example 1 with $M = N \in \{10, 20, 40\}$, for the direct problem.

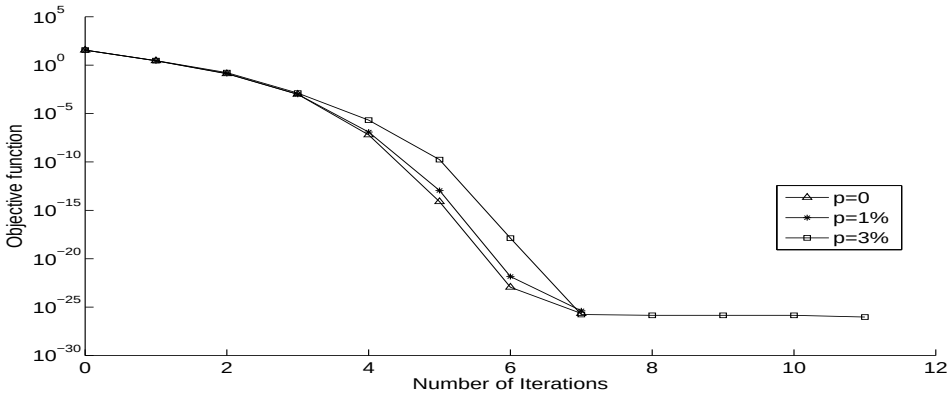

Figure 2.3: Objective function (2.16), for Example 1 with $p \in \{0, 1\%, 3\%\}$ noise.

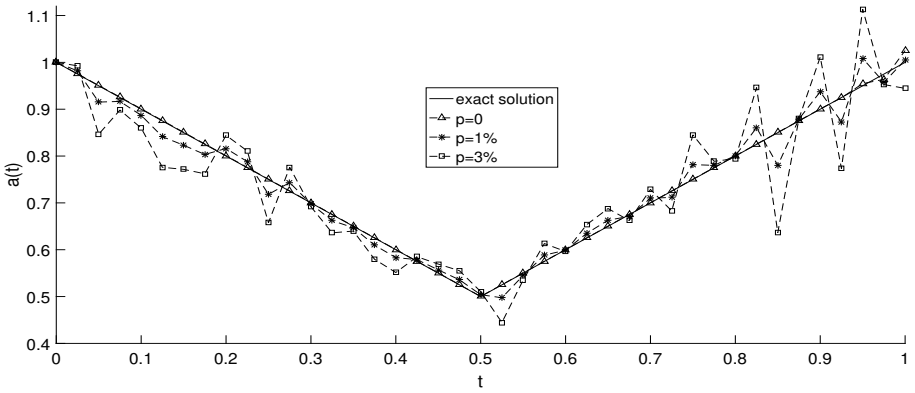

Figure 2.4: The exact (equation (2.24)) and numerical solutions for the thermal conductivity $a(t)$, for Example 1 with $p \in \{0, 1\%, 3\%\}$ noise.

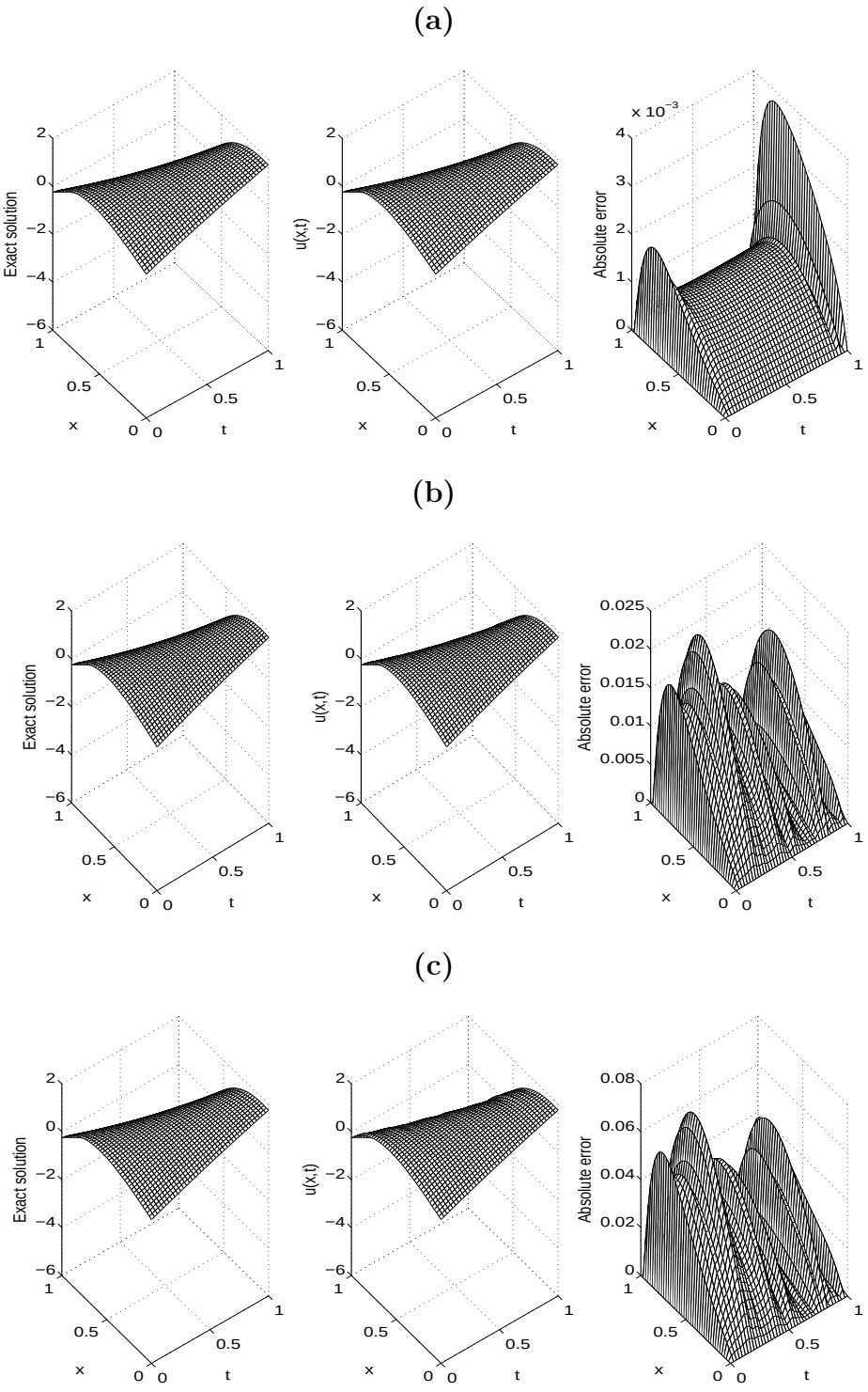

Figure 2.5: The exact (equation (2.23)) and numerical solutions for the temperature $u(x,t)$, for Example 1, with (a) no noise, (b) $p = 1\%$ noise, and (c) $p = 3\%$ noise. The absolute error between them is also included.

Table 2.1: Number of iterations, number of function evaluations, value of the objective function (2.16) at final iteration, $rmse(a)$ and the computational time, for Example 1.

Numerical outputs	$p = 0$	$p = 1\%$	$p = 3\%$
Number of iterations	7	7	11
Number of function evaluations	336	336	504
Value of objective function (2.16) at final iteration	2.2E-26	4.2E-26	9.4E-27
$rmse(a)$	0.0325	0.2123	0.6643
Computational time	4 mins	4 mins	6 mins

Other details about number of iterations, the number of function evaluations, the value of the objective function (2.16) at final iteration, the $rmse$ in (2.18) and the computational time are given in Table 2.1. From this table it can be seen that accurate and stable numerical results are rapidly achieved by the iterative MATLAB toolbox routine *lsqnonlin*.

2.5.2 Example 2

Consider the inverse problem (2.1)–(2.4) with the input data

$$\phi(x) = u(x,0) = \sin(\pi x), \quad \mu_1(t) = \mu_2(t) = 0, \quad f(x,t) = 0, \tag{2.28}$$

$$q_0(t) = \pi(1.01 + \sin(3\pi t)) \exp\Big[- \pi^2 \Big(1.01t + \frac{1 - \cos(3\pi t)}{3\pi}\Big)\Big]. \tag{2.29}$$

The exact solution for the temperature $u(x,t)$ is

$$u(x,t) = \sin(\pi x) \exp\Big[- \pi^2 \Big(1.01t + \frac{1 - \cos(3\pi t)}{3\pi}\Big)\Big], \tag{2.30}$$

and for the thermal conductivity $a(t)$ is

$$a(t) = 1.01 + \sin(3\pi t). \tag{2.31}$$

This example was considered in [138] and we generate the noisy heat flux measurement (2.4), as multiplicative (rather than additive as in (2.25)), namely,

$$q_0^{\tilde{\epsilon}}(t_j) = q_0(t_j)(1 + p\tilde{\epsilon}_j), \quad j = \overline{1, N}, \tag{2.32}$$

where p represents the percentage of noise and $\tilde{\underline{\epsilon}} = (\tilde{\epsilon}_j)_{j=\overline{1,N}}$, is a random real number between $[-1, 1]$ generated from a uniform distribution using the MAT-

LAB function *rand* as

$$\underline{\tilde{\epsilon}} = 2 \times rand(1, N) - 1. \tag{2.33}$$

The objective function (2.16), as a function of the number of iterations is shown in Figure 2.6 with no noise and with various mesh sizes. From this figure it can be seen that very low converging values of the monotonically decreasing objective function F in (2.16) are achieved. The corresponding numerical results for $a(t)$ are compared with the analytical solution (2.31) in Figure 2.7, with the numerical details included in Table 2.2. From this figure and table it can be seen that the numerical solution for $a(t)$ converges to exact solution (2.31), as the mesh size decreases.

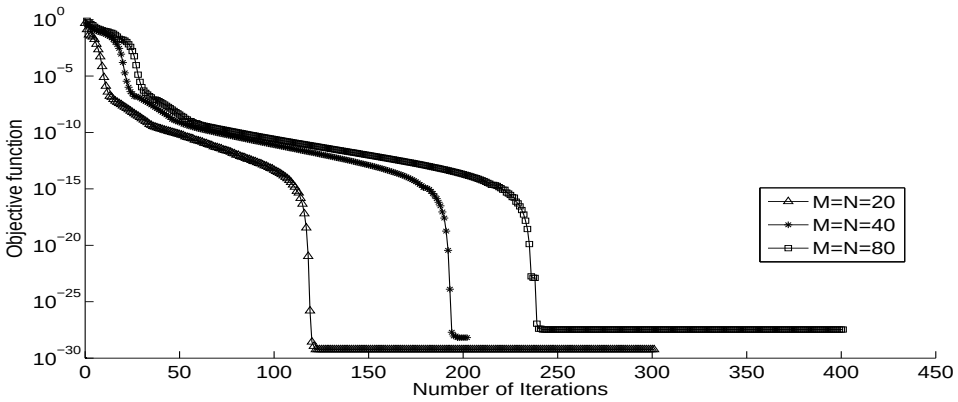

Figure 2.6: Objective function (2.16), for Example 2 with no noise and with $M = N \in \{20, 40, 80\}$.

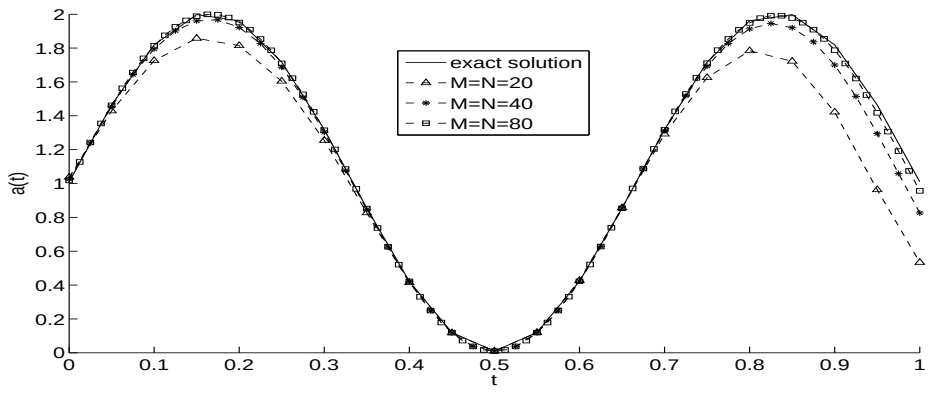

Figure 2.7: The exact (equation (2.31)) and numerical solutions for the thermal conductivity $a(t)$, for Example 2 with no noise and with various mesh size $M = N \in \{20, 40, 80\}$.

Table 2.2: Number of iterations, number of function evaluations, value of the objective function (2.16) at final iteration, $rmse(a)$ and the computational time, for Example 2 with various mesh size $M = N \in \{20, 40, 80\}$ and with no noise.

Numerical outputs	$M = N = 20$	$M = N = 40$	$M = N = 80$
Number of iterations	301	201	401
Number of function evaluations	6644	16884	32964
Value of objective function (2.16) at final iteration	5.7E-30	6.4E-29	3.4E-28
$rmse(a)$	0.1977	0.0634	0.0170
Computational time	6 mins	478 mins	600 mins

When we include various levels of noise $p \in \{1, 3, 5\}\%$ as in (2.32) to the heat flux measurement (2.4) we obtain stable results for the $a(t)$ as thermal conductivity shown in Figure 2.8. Furthermore, the results become more accurate as the amount of noise p decreases. Numerical results are also comparable in terms of stability and accuracy with those in [138] obtained using a totally different method.

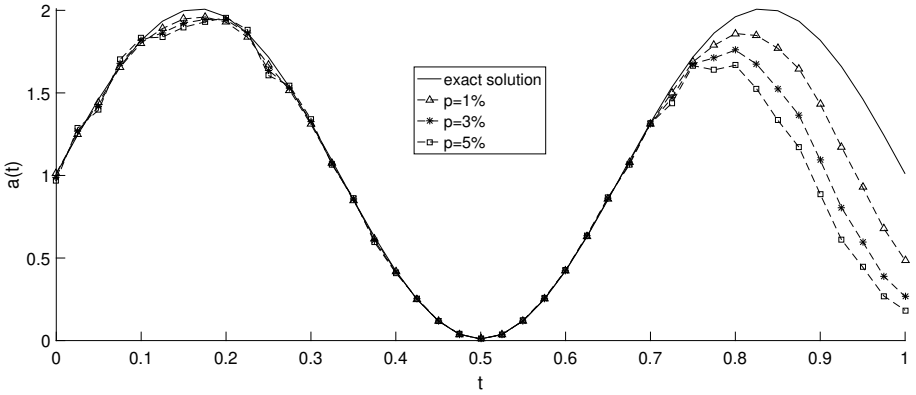

Figure 2.8: The exact (equation (2.31)) and numerical solutions for the thermal conductivity $a(t)$, for Example 2 with $p \in \{1\%, 3\%, 5\%\}$ noise and no regularization with $M = N = 40$.

2.6 Extension to higher dimensions

The extension to two-dimensions case is straightforward. In the rectangular domain $Q_T = \{(x, y, t) : 0 < x < h, 0 < y < l, 0 < t < T\}$, we consider the inverse problem of reconstructing the time-dependent thermal conductivity $a(t) > 0$ in the two-dimensional parabolic heat equation

$$u_t = a(t)\Delta u + f(x, y, t), \quad (x, y, t) \in Q_T, \tag{2.34}$$

where f is a given heat source, with unknown temperature $u(x, y, t)$, subject to the initial condition

$$u(x, y, 0) = \varphi(x, y), \quad (x, y) \in [0, h] \times [0, l], \tag{2.35}$$

the Dirichlet boundary conditions

$$u(0, y, t) = \mu_{11}(y, t), \quad u(h, y, t) = \mu_{12}(y, t), \quad (y, t) \in [0, l] \times [0, T], \tag{2.36}$$

$$u(x, 0, t) = \mu_{21}(x, t), \quad u(x, l, t) = \mu_{22}(x, t), \quad (x, t) \in [0, h] \times [0, T], \tag{2.37}$$

and the nonlocal observation

$$v_1(t)u_x(0, Y_0, t) + v_2(t)u_x(h, Y_0, t) = \chi(t), \quad t \in [0, T], \tag{2.38}$$

where Y_0 is a fixed point within the interval $(0, l)$, and v_1 and v_2 are given functions.

This is the mathematical formulation of the inverse problem analysed in [86], though one can remark that, physically, the observation (2.38) (compare with (2.4)) is missing a conductivity factor $a(t)$ in its left-hand side. We defer this more physical observation for future investigations and instead concentrate on (2.38) for which a solid mathematical analysis already exists [86]. In particular, the local existence and uniqueness of solution of the inverse problem (2.34)–(2.38) was established in [86] and read as stated in the following two theorems.

Theorem 2.6.1. *Suppose that the following assumptions are satisfied:*

(A1) $f \in C(\overline{Q_T})$, $\varphi \in C^2([0, h] \times [0, l])$, $\Psi \in C^{2,1}(\overline{Q_T})$, $\tilde{\chi}, v_1, v_2 \in C^1([0, T])$, *and the functions* $f, \Delta\varphi, \Delta\Psi$ *and* Ψ_t *satisfy the Hölder condition with exponent* α *in the space variables, where*

$$\begin{aligned}
\tilde{\chi}(t) &:= \chi(t) - v_1(t)(\varphi_x(0, Y_0) + \Psi_x(0, Y_0, t)) - v_2(t)(\varphi_x(h, Y_0) + \Psi_x(h, Y_0, t)), \\
t \in [0, T], \Psi(x, y, t) &:= \mu_{11}(y, t) - \mu_{11}(y, 0) + \frac{x}{h}\Big(\mu_{12}(y, t) - \mu_{12}(y, 0) - \mu_{11}(y, t) \\
&\quad + \mu_{11}(y, 0)\Big) + \mu_{21}(x, t) - \mu_{21}(x, 0) - \Big[\mu_{11}(0, t) - \mu_{11}(0, 0) + \frac{x}{h}\Big(\mu_{12}(0, t) \\
&\quad - \mu_{12}(0, 0) - \mu_{11}(0, t) + \mu_{11}(0, 0)\Big)\Big] + \frac{y}{l}\Big[\mu_{22}(x, t) - \mu_{22}(x, 0) - \mu_{11}(l, t) \\
&\quad + \mu_{11}(l, 0) - \frac{x}{h}\Big(\mu_{12}(l, t) - \mu_{12}(l, 0) - \mu_{11}(l, t) + \mu_{11}(l, 0)\Big) - \mu_{21}(x, t) \\
&\quad + \mu_{21}(x, 0) + \mu_{11}(0, t) - \mu_{11}(0, 0) + \frac{x}{h}\Big(\mu_{12}(0, t) - \mu_{12}(0, 0) - \mu_{11}(0, t) \\
&\quad + \mu_{11}(0, 0)\Big)\Big];
\end{aligned}$$

(A2) $-v_1(t)(\Delta\varphi(0,Y_0)+\Delta\Psi(0,Y_0,t))+v_2(t)(\Delta\varphi(h,Y_0)+\Delta\Psi(h,Y_0,t))>0,$
$-v_2(t)(f(h,Y_0,t)-\Psi_t(h,Y_0,t))+v_1(t)(f(0,Y_0,t)-\Psi_t(0,Y_0,t))>0,\ t\in[0,T];$

(A3) $v_1(0)\varphi'(0,Y_0)+v_2(0)\varphi'(h,Y_0)=\tilde{\chi}(0),\ \varphi(0,y)=\mu_{11}(y,0),$
$\varphi(h,y)=\mu_{12}(y,0),\ \varphi(x,0)=\mu_{21}(x,0),\ \varphi(x,l)=\mu_{22}(x,0),$
$\mu_{11}(0,t)=\mu_{21}(0,t),\ \mu_{11}(l,t)=\mu_{22}(0,t),\ \mu_{12}(0,t)=\mu_{21}(h,t),$
$\mu_{12}(l,t)=\mu_{22}(h,t).$

Then, there exists $T_0\in(0,T]$, which is determined by the input data, such that the problem (2.34)–(2.38) has a solution $(a(t),u(x,y,t))\in C([0,T_0])\times C^{2,1}(\overline{Q_{T_0}})$, with $a(t)>0$ for $t\in[0,T_0]$.

Theorem 2.6.2. *Let assumption* ***(A1)*** *and the condition*

$$U(t):=v_2(t)(\Delta\varphi(h,Y_0)+\Delta\Psi(h,Y_0,t))-v_1(t)(\Delta\varphi(0,Y_0)+\Delta\Psi(0,Y_0,t))\neq 0,\quad t\in[0,T], \tag{2.39}$$

be satisfied. Then, the inverse problem (2.34)–(2.38) cannot have more than one solution in the class $(a(t),u(x,y,t))\in C([0,T])\times C^{2,1}(\overline{Q_T})$, with $a(t)>0$ for $t\in[0,T]$.

2.6.1 Numerical solution of the direct 2D problem

In this section, we consider the direct initial boundary value problem (2.34)–(2.38), where $a(t)$, $v_1(t)$, $v_2(t)$, $f(x,y,t)$, $\varphi(x,y)$, $\mu_{1i}(y,t)$, $i=1,2$ and $\mu_{2i}(x,t)$, $i=1,2$, are known and the solution $u(x,y,t)$ is to be determined. To achieve this, we use the forward time central space (FTCS) FDM, which is conditionally stable, as described in the next subsection.

We subdivide the solution domain Q_T into M_1, M_2 and N subintervals of equal step lengths Δx, Δy, and uniform time step Δt, where $\Delta x=h/M_1$, $\Delta y=l/M_2$, and $\Delta t=T/N$, respectively. At the node (i,j,n), we denote $u^n_{i,j}:=u(x_i,y_j,t_n)$, where $x_i=i\Delta x$, $y_j=j\Delta y$, $t_n=n\Delta t$, $a_n:=a(t_n)$, $v_{1_n}:=v_1(t_n)$, $v_{2_n}:=v_2(t_n)$ and $f^n_{i,j}:=f(x_i,y_j,t_n)$ for $i=\overline{0,M_1}$, $j=\overline{0,M_2}$ and $n=\overline{0,N}$.

2.6.2 Forward time central space (FTCS) method

In this method, the first-order time derivative term in the two-dimensional parabolic equation (2.34) is approximated by forward finite differences, whilst the space par-

tial derivatives are approximated by second-order central finite differences. This gives

$$\frac{u_{i,j}^{n+1}-u_{i,j}^{n}}{\Delta t}=a_n\Big(\frac{u_{i-1,j}^{n}-2u_{i,j}^{n}+u_{i+1,j}^{n}}{(\Delta x)^2}+\frac{u_{i,j-1}^{n}-2u_{i,j}^{n}+u_{i,j+1}^{n}}{(\Delta y)^2}\Big)+f_{i,j}^{n},$$
$$i=\overline{1,M_1-1},\quad j=\overline{1,M_2-1},\quad n=\overline{0,N}. \tag{2.40}$$

Equation (2.40) can be rearranged into an explicit expression as

$$u_{i,j}^{n+1}=u_{i,j}^{n}+a_nr_1(u_{i-1,j}^{n}-2u_{i,j}^{n}+u_{i+1,j}^{n})+a_nr_2(u_{i,j-1}^{n}-2u_{i,j}^{n}+u_{i,j+1}^{n})$$
$$+(\Delta t)f_{i,j}^{n},\quad i=\overline{1,M_1-1},\quad j=\overline{1,M_2-1},\quad n=\overline{0,N}, \tag{2.41}$$

where $r_1=\frac{\Delta t}{(\Delta x)^2}$ and $r_2=\frac{\Delta t}{(\Delta y)^2}$.

Let $\tilde{a}$ be the maximum value of $a(t)$ for $t\in[0,T]$, then, the stability condition for the explicit FTCS (2.41), is [101],

$$\tilde{a}\,(r_1+r_2)\leq\frac{1}{2}. \tag{2.42}$$

The initial (2.35) and boundary conditions (2.36) and (2.37) discretise as

$$u_{i,j}^{0}=\varphi_{i,j},\quad i=\overline{0,M_1},\quad j=\overline{0,M_2}, \tag{2.43}$$

$$u_{0,j}^{n}=\mu_{11}(y_j,t_n),\quad u_{M_1,j}^{n}=\mu_{12}(y_j,t_n),\quad j=\overline{0,M_2},\quad n=\overline{1,N}, \tag{2.44}$$

$$u_{i,0}^{n}=\mu_{21}(x_i,t_n),\quad u_{i,M_2}^{n}=\mu_{22}(x_i,t_n),\quad i=\overline{0,M_1},\quad n=\overline{1,N}. \tag{2.45}$$

The function (2.38) can be calculated using the FDM as follows:

$$\chi(t_n)=v_{1_n}\left(\frac{4u(1,Y_0,t_n)-u(2,Y_0,t_n)-3u(0,Y_0,t_n)}{2\Delta x}\right)$$
$$+v_{2_n}\left(\frac{4u(h,Y_0,t_n)-u(h,Y_0,t_n)-3u(h,Y_0,t_n)}{-2\Delta x}\right),\quad n=\overline{1,N}. \tag{2.46}$$

2.6.3 Numerical solution of the 2D inverse problem

In this section, our goal is to obtain stable reconstruction for the time-dependent thermal conductivity $a(t)>0$ together with the temperature $u(x,y,t)$, satisfing equations (2.34)–(2.38). The inverse problem can be formulated as a nonlinear

minimization of the Tikhonov regularization function given by

$$F_\lambda(a) = \|v_1(t)u_x(0, Y_0, t) + v_2(t)u_x(h, Y_0, t) - \chi(t)\|^2 + \lambda\|a(t)\|^2, \tag{2.47}$$

or, in discretized form

$$F_\lambda(\mathbf{a}) = \sum_{n=1}^{N} \Big[v_{1_n}u_x(0, Y_0, t_n) + v_{2_n}u_x(h, Y_0, t_n) - \chi(t_n)\Big]^2 + \lambda \sum_{n=1}^{N} a_n^2, \tag{2.48}$$

where $u(x, y, t)$ solves (2.34)–(2.37) for given $\mathbf{a}$, and $\lambda \geq 0$ is regularization parameter to be prescribed. The minimization of the objective function (2.48) is performed using the MATLAB toolbox routine *lsqnonlin*.

We employ the root mean square errors ($rmse$), in order to assess the accuracy of the numerical results, defined by (2.18). For simplicity, we take $h = l = T = 1$.

The inverse problem given by (2.34)–(2.38) is solved subject to both exact and noisy measurement (2.38). The noisy data are numerically simulated as

$$\chi^\epsilon(t_n) = \chi(t_n) + \epsilon_n, \quad n = \overline{1, N}, \tag{2.49}$$

where ϵ_n is random variable generated from a Gaussian normal distribution with mean zero and standard deviation σ

$$\sigma = p \times \max_{t\in[0,T]} |\chi(t)|, \tag{2.50}$$

and p represents the percentage of noise. We use the MATLAB function *normrnd* to generate the random variables $\underline{\boldsymbol{\epsilon}} = (\epsilon_n)_{n=\overline{1,N}}$ as in (2.27). In the case of noisy data (2.49), we replace $\chi(t_n)$ by $\chi^\epsilon(t_n)$ in (2.48).

2.6.4 Example 3

Consider the inverse problem (2.34)–(2.38) with unknown time-dependent thermal conductivity $a(t)$ and with the input data φ, μ_{1i} and μ_{2i}, $i = 1, 2$, as follows:

$$\begin{aligned}
\varphi(y, x) = \frac{1}{3}\cos(x + \pi y), \quad v_1(t) = 1,\ v_2(t) = 1,\ Y_0 = \frac{1}{2},\\
\mu_{11}(y, t) = \frac{1}{3}(1 + t)\cos(\pi y),\ \mu_{12}(y, t) = \frac{1}{3}(1 + t)\cos(1 + \pi y),\\
\mu_{21}(x, t) = \frac{1}{3}(1 + t)\cos(x),\ \mu_{22}(x, t) = -\frac{1}{3}(1 + t)\cos(1 + x),\\
f(x, y, t) = \frac{1}{3}\cos(x + \pi y) - \frac{1}{50}(1.1 + \cos(2\pi t))(-\frac{1}{3}(1 + t)\cos(x + \pi y)\\
-\frac{1}{3}\pi^2(1 + t)\cos(x + \pi y)),
\end{aligned} \tag{2.51}$$

$$\chi(t) = v_1(t)u_x(0, Y_0, t) + v_2(t)u_x(1, Y_0, t) = -\frac{(1+t)(1+\cos(1))}{3}. \qquad (2.52)$$

First, it can easily be checked that with this data, the conditions (**A1**)–(**A3**) of Theorem 2.6.1 are satisfied. Also, the graph of the function $U(t)$ given by equation (2.39) is shown in Figure 2.9. From this figure it can be seen that this function never vanishes over the time interval $t \in [0, 1]$ and hence condition (2.39) is satisfied. Then, according to Theorems 2.6.1 and 2.6.2 the local existence and uniqueness of the solution are guaranteed. In fact, it can easily be checked by direct substitution that the exact solutions for the temperature $u(x, y, t)$ and conductivity $a(t)$ are given by

$$u(x, y, t) = \frac{(1+t)\cos(x+\pi y)}{3}, \quad (x, y, t) \in \overline{Q_T}, \qquad (2.53)$$

$$a(t) = \frac{1.1 + \cos(2\pi t)}{50}, \quad t \in [0, 1]. \qquad (2.54)$$

First, we solve the direct problem (2.34)–(2.37), when $a(t)$ is known and given by (2.54), using the FTCS described in Subsection 2.6.2 with the mesh size $M_1 = M_2 = 10$ and $N = 20$, i.e. $\Delta x = \Delta y = 1/10 = 0.1$ and $\Delta t = 1/20 = 0.05$. The exact solutions (2.53) and (2.52) for the temperature $u(x, y, t)$ and the nonlocal heat flux $\chi(t)$ are compared with the numerical solutions in Figure 2.10 and Table 2.3, respectively, and one can observe that an excellent agreement is obtained.

Next, we solve the inverse problem (2.34)–(2.38) using the *lsqnonlin* minimization of the functional (2.48) with the initial guess for the vector $\mathbf{a} = (a(t_n))_{n=\overline{1,N}}$ given by

$$a^0(t_n) = a(0) = 0.042, \quad n = \overline{1, N}. \qquad (2.55)$$

We take the same mesh size as in the direct problem above. We choose the upper bound $UB = 0.05$ for a such that the stability condition (2.42) is always satisfied in the iterative process. Also, since a represents a positive physical quantity we take the lower bound for a to be a small positive number such as $LB = 10^{-3}$.

We start the investigation for determining the unknown time-dependent thermal conductivity $a(t)$ and the temperature $u(x, y, t)$ in the case of exact input data, i.e. $p = 0$ in (2.50). The unregularized objective function (2.48), i.e. with $\lambda = 0$, as a function of the number of iterations, is shown in Figure 2.11(a). From this figure, it can be seen that the objective function (2.48) is rapidly decreasing

to a very low value of $O(10^{-29})$ in about 25 iterations (in about 5 minutes CPU time). The related numerical results for the thermal conductivity $a(t)$, with no regularization, are presented in Figure 2.11(b). From this figure, it can be seen that, as expected, there is good agreement between the numerical results and the exact solution (2.54) for exact data.

Next, we investigate the stability of the numerical solution with respect to various levels of $p \in \{1\%, 3\%\}$ noise in (2.50) included in the input data $\chi(t)$. Although not illustrated, it is reported that a rapid monotonic decreasing convergence of the objective function (2.48), without and with regularization is achieved in about 11 to 25 iterations. The related numerical results for the thermal conductivity $a(t)$ are presented in Figure 2.13(a) for $p = 1\%$ noise and in Figure 2.14(a) for $p = 3\%$ noise. From these figures, it can be seen that the numerical results are unstable (oscillating), if no regularization, i.e. $\lambda = 0$, is employed. We expect that regularization is needed in order to obtain stable and accurate solutions because the inverse problem is ill-posed. The L-curve, [47], for the choice of the regularization parameter is shown in Figure 2.12, by plotting the solution norm $||\mathbf{a}|| = \sqrt{\sum_{n=1}^{N} a_n^2}$ versus the residual norm given by

$$\text{Residual norm} = \sqrt{\sum_{n=1}^{N} \Big[v_1(t_n) u_x(0, Y_0, t_n) + v_2(t_n) u_x(h, Y_0, t_n) - \chi(t_n) \Big]^2}. \quad (2.56)$$

The corner of the L-curve occurs around $\lambda \in \{3, 4\}$ for $p = 1\%$ noise, and $\lambda \in \{6, 7\}$ for $p = 3\%$ noise, and is taken as a good choice for the regularization parameter λ balancing the fit of data (residual norm in (2.56)) with the stability of solution (solution norm). From Figures 2.13(b) and 2.14(b), and Table 2.4, it can be seen that stable and reasonable accurate numerical results for the thermal conductivity $a(t)$ are obtain for $\lambda = 3$ or 4 (suggested by the L-curve in Figure 2.12(a)), for $p = 1\%$ noise, and with $\lambda = 6$ or 7 (suggested by the L-curve in Figure 2.12(b)), for $p = 3\%$ noise.

Finally, details about the number of iterations, the $rmse(a)$ in (2.18), and the computational time are given in Table 2.4, for various levels of noise and with and without regularization.

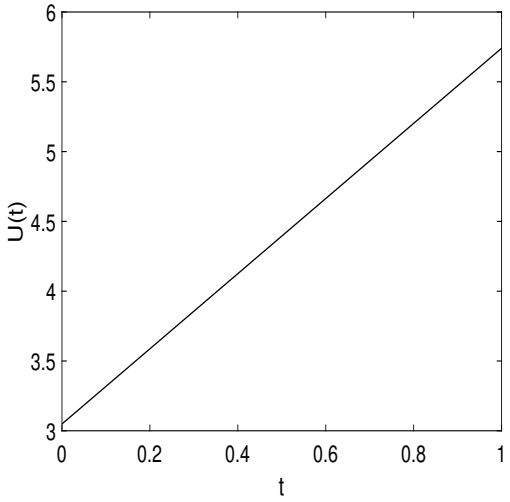

Figure 2.9: The graph of the function $U(t)$, as a function of t.

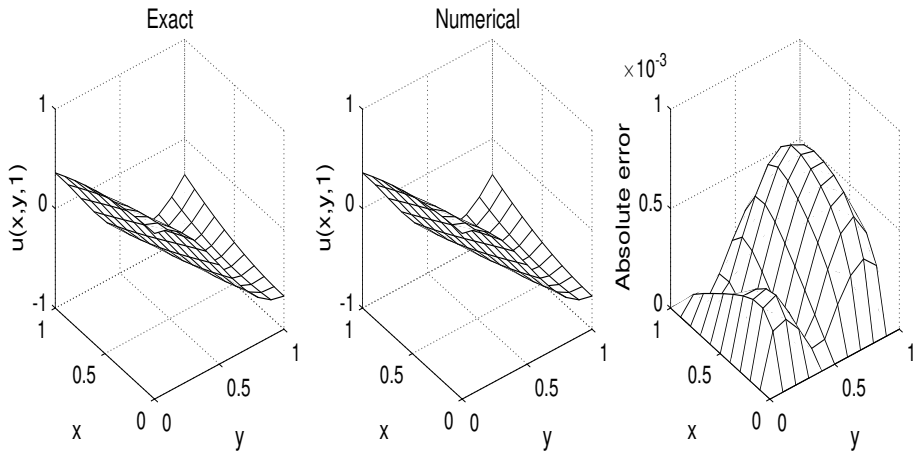

Figure 2.10: The exact (2.53) and numerical solutions for the temperature $u(x, y, 1)$, for Example 3, for the direct problem.

Table 2.3: The exact (2.52) and numerical solutions for $\chi(t)$, for Example 3, for the direct problem.

t	0.1	0.2	0.3	0.4	...	0.8	0.9	$rmse$
$\chi(t)$	-0.5657	-0.6166	-0.6678	-0.7191	...	-0.9245	-0.9755	6.5E-4
Exact	-0.5648	-0.6161	-0.6675	-0.7188	...	-0.9242	-0.9755	0

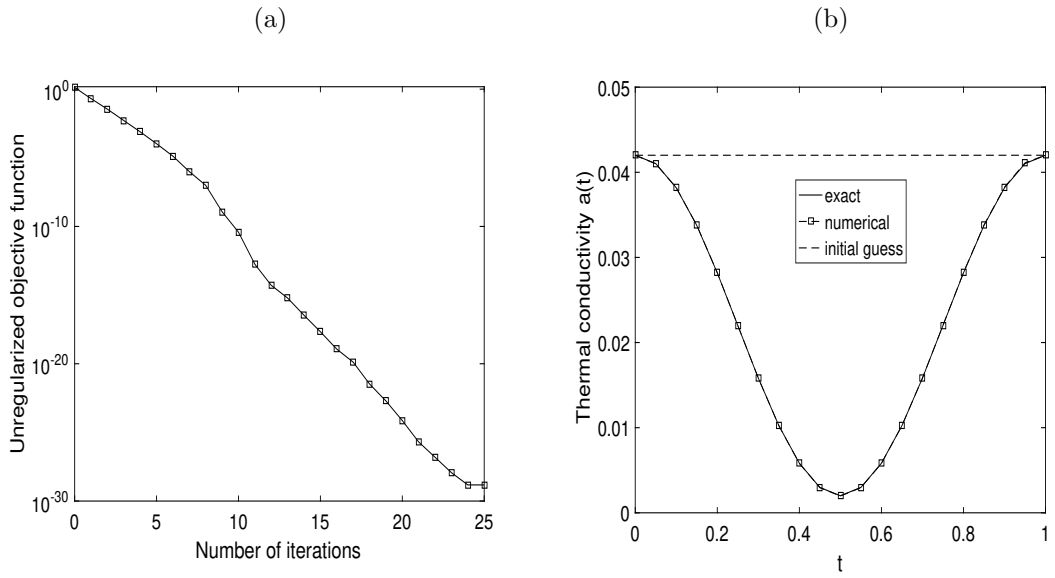

Figure 2.11: (a) The unregularized objective function (2.48), as a function of the number of iterations, and (b) the solution for the thermal conductivity $a(t)$, with no noise and no regularization, for Example 3.

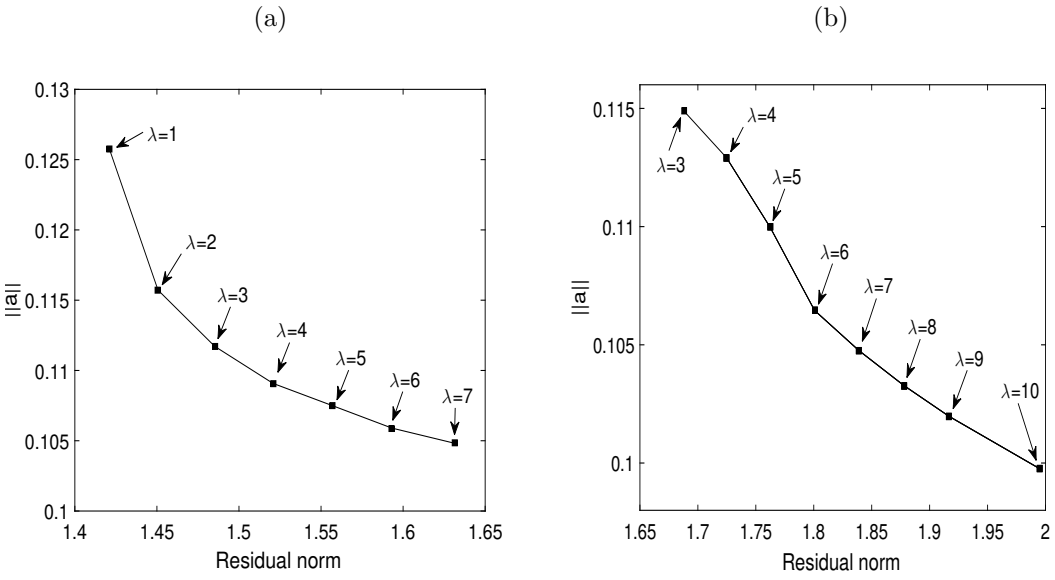

Figure 2.12: The residual norm versus the solution norm for various regularization parameters, for Example 3, with (a) $p = 1\%$ and (b) $p = 3\%$ noise.

(a) (b)

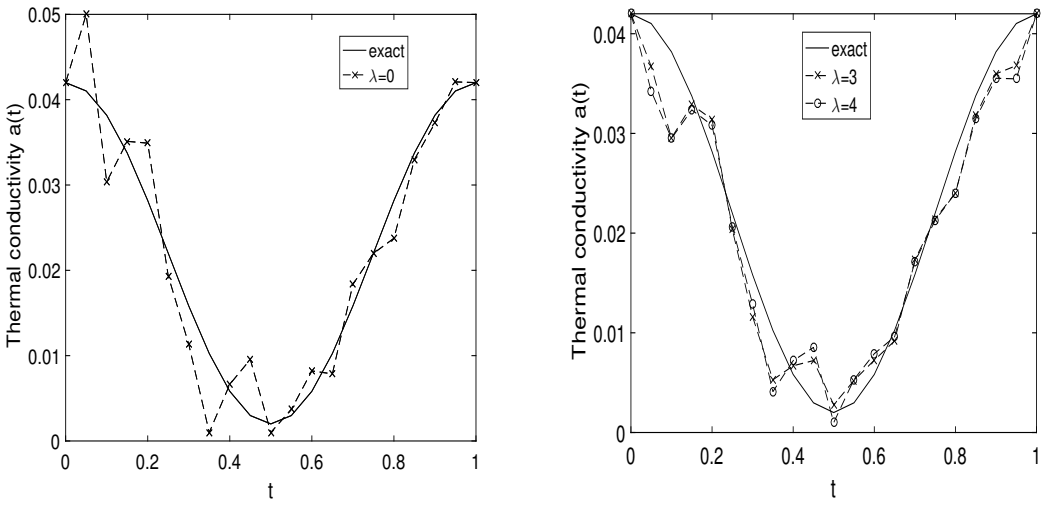

Figure 2.13: The exact (2.54) and numerical solutions, for the thermal conductivity $a(t)$, for $p = 1\%$ noise, with (a) no regularization and (b) with regularization, for Example 3.

(a) (b)

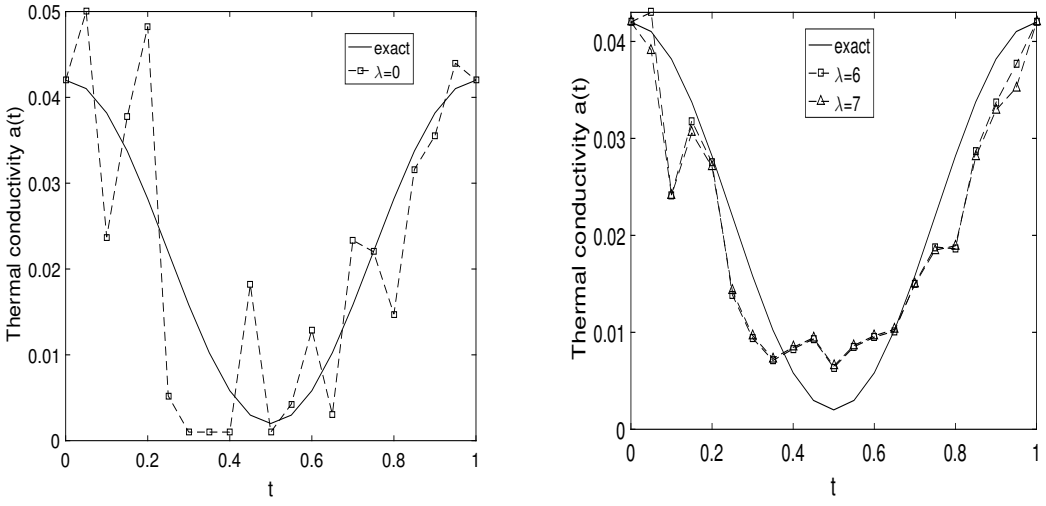

Figure 2.14: The exact (2.54) and numerical solutions, for the thermal conductivity $a(t)$, for $p = 3\%$ noise, with (a) no regularization and (b) with regularization, for Example 3.

Table 2.4: The $rmse(a)$ values, number of iterations and computational time for $p \in \{0, 1\%, 3\%\}$ noise, with and without regularization, for Example 3.

p	Regul	$rmse(a)$	Iter	Time
0	$\lambda = 0$	3.3E-5	25	5 mins
1%	$\lambda = 0$	0.0044	21	4 mins
	$\lambda = 1$	0.0041	11	2 mins
	$\lambda = 2$	0.0036	11	2 mins
	$\lambda = 3$	0.0033	11	2 mins
	$\lambda = 4$	0.0037	11	2 mins
	$\lambda = 5$	0.0040	11	2 mins
3%	$\lambda = 0$	0.0098	21	4 mins
	$\lambda = 5$	0.0070	11	2 mins
	$\lambda = 6$	0.0066	11	2 mins
	$\lambda = 7$	0.0067	11	2 mins
	$\lambda = 8$	0.0069	11	2 mins

2.7 Conclusions

This chapter has initially presented (Sections 2.2–2.5) the determination of the time-dependent thermal conductivity from heat flux measurements in the one-dimensional parabolic heat equation. The resulting inverse problem has been reformulated as a nonlinear least-squares optimization problem, which has been solved using the MATLAB toolbox routine *lsqnonlin*. Accurate and reasonably stable (with no regularization necessary to be employed) numerical results have been obtained. An extension to a two-dimensional coefficient identification problem, which is a variant of the one-dimensional problem, has been presented in Section 2.6. For this newly formulated problem the use of regularization is necessary in order to ensure that a numerically stable solution is obtained. Nevertheless, future work (both theoretical and numerical) could concern replacing the additional observation (2.38) by the more physical heat flux combination $a(t)(v_1(t)u_x(0, Y_0, t) + v_2(t)u_x(h, Y_0, t)) = \overline{\chi}(t)$ for $t \in [0, T]$.

Chapter 3

Reconstruction of time-dependent coefficients from heat moments

3.1 Introduction

In the previous chapter, the reconstruction of a single time-dependent coefficient from heat flux measurement has been performed. In this chapter, the identification of multiple coefficients is analysed.

Simultaneous determination of several unknown physical property coefficients in heat transfer which dependent on time, space or temperature has been investigated in various studies, see e.g. [62, 65, 78, 79, 104]. In particular, in [62], the authors investigated the inverse problems of simultaneous numerical reconstruction of time-dependent thermal conductivity and convection coefficients in a one-dimensional parabolic equation from Cauchy boundary data measurements represented by the boundary temperature and heat flux. In this chapter, we investigate the reconstruction of the same coefficients, as well as of the absorption coefficient, using the measurement of the heat moments instead of the heat flux.

The chapter is organized as follows: In Section 3.2, the mathematical of formulation of the inverse problems are reformulated and uniqueness results are stated. In Section 3.3, the numerical solution of the direct problem based on the FDM is presented. In Section 3.4, the numerical approach to solve the minimization of the nonlinear Tikhonov regularization functional is presented. The numerical results for various examples are presented and discussed in Section 3.5. The choice of multiple regularization parameters is also addressed. Finally, conclusions are presented in Section 3.6.

3.2 Mathematical formulation

We consider an extended version of (2.1) given by

$$\frac{\partial u}{\partial t}(x,t) = a(t)\frac{\partial^2 u}{\partial x^2}(x,t) + b(t)\frac{\partial u}{\partial x}(x,t) + c(t)u(x,t) + f(x,t),\ (x,t) \in Q_T,\ (3.1)$$

where b and c are coefficients representing convection and absorption. Equation (3.1) has to be solved subject to the initial condition

$$u(x,0) = \phi(x), \quad x \in [0,L], \tag{3.2}$$

and the Dirichlet boundary conditions

$$u(0,t) = \mu_1(t), \quad u(L,t) = \mu_2(t), \quad t \in [0,T]. \tag{3.3}$$

If a, b, c and f are given then (3.1)–(3.3) constitute a direct Dirichlet problem for the temperature $u(x,t)$. Other outputs of interest are the heat fluxes

$$a(t)u_x(0,t) = q_0(t), \quad a(t)u_x(L,t) = q_L(t), \quad t \in [0,T], \tag{3.4}$$

and the heat moments of order $k = 0$ and $k = 1$, namely,

$$H_k(t) = \int_0^L x^k u(x,t)dx, \quad k = 0,1, \quad t \in [0,T]. \tag{3.5}$$

However, if any of the coefficients a, b, c and/or f are not known then we are dealing with inverse coefficient identification problems.

Prior to this study, the simultaneous identification of the coefficients $a(t)$ and $b(t)$ in the problem (3.1)–(3.3) with the additional flux data (3.4) has been considered in [62]. In this chapter, we consider the simultaneous reconstruction of the same time-dependent coefficients, as well as $c(t)$, but from the heat moments (3.5) instead of the heat fluxes (3.4). The heat moment of order $k = 0$, i.e. $H_0(t) = \int_0^L u(x,t)dx$, is also called the mass (or energy) of the heat conducting system, [22, 92], whilst the heat moment of order $k = 1$, i.e. $H_1(t) = \int_0^L xu(x,t)dx$ represents the barycenter (the center of mass of two or more bodies that are orbiting each other, which is the point around which they both orbit) of the system, [105]. The uniqueness of solution of these inverse problems is stated in the next two subsections.

3.2.1 Inverse Problem 1

Assuming that $c(t) = 0$, the inverse problem 1 (IP1) requires the simultaneous determination of the time-dependent thermal conductivity $a(t) > 0$ and the convection (or advection) coefficient $b(t)$, together with the temperature $u(x,t)$ satisfying

$$\frac{\partial u}{\partial t}(x,t) = a(t)\frac{\partial^2 u}{\partial x^2}(x,t) + b(t)\frac{\partial u}{\partial x}(x,t) + f(x,t), \quad (x,t) \in Q_T, \tag{3.6}$$

subject to (3.2), (3.3) and (3.5). The sketch of the IP1 is shown in Figure 3.1(a).

The uniqueness of solution $(a(t), b(t), u(x,t))$ of this inverse problem was established in [107] and reads as follows.

Theorem 3.2.1. *Let $\phi \in C^1[0,L]$, $\mu_k \in C^1[0,T]$, $H_k \in C^1[0,T]$ for $k = 0,1$, and $f \in C(\overline{Q_T})$.*
Suppose that the following condition is satisfied:

$$U_1(t) := \Big(\mu_2(t) - \mu_1(t)\Big)\int_0^L xf(x,t)dx$$
$$-\Big(L\mu_2(t) - H_0(t)\Big)\int_0^L f(x,t)dx \neq 0, \quad \forall t \in [0,T]. \tag{3.7}$$

Then a solution $(a(t), b(t), u(x,t)) \in C[0,T] \times C[0,T] \times \Big(C^{2,1}(Q_T) \cap C(\overline{Q_T})\Big)$ with $a(t) > 0$ for $t \in [0,T]$, to the problem (3.2), (3.3), (3.5) and (3.6) is unique.

Remark 1. Observe that by multiplying equation (3.6) by $x^k, k = 0,1$, integrating with respect to x from 0 to L, and taking into account condition (3.5), we obtain,
$H_0'(t) = a(t)\Big(u_x(L,t) - u_x(0,t)\Big) + b(t)\Big(u(L,t) - u(0,t)\Big) + \int_0^L f(x,t)dx,$
$H_1'(t) = a(t)\Big(Lu_x(L,t) - u(L,t) + u(0,t)\Big) + b(t)\Big(Lu(L,t) - H_0(t)\Big) + \int_0^L xf(x,t)dx.$
Taking $t = 0$ in these equations, using the compatibility conditions $u_x(0,t) = \phi'(0)$, $u_x(L,t) = \phi'(L)$, the Dirichlet boundary conditions (3.3) and solving for $a(0)$ and $b(0)$, we obtain,

$$a(0) = \Big(\Delta(0)\Big)^{-1}\Bigg[\Big(H_0'(0) - \int_0^L f(x,0)dx\Big)\Big(L\mu_2(L) - H_0(0)\Big)$$
$$-\Big(\mu_2(L) - \mu_1(0)\Big)\Big(H_1'(0) - \int_0^L xf(x,0)dx\Big)\Bigg],$$

$$b(0) = \Big(\Delta(0)\Big)^{-1}\Bigg[\Big(\phi'(L) - \phi'(0)\Big)\Big(H_1'(0) - \int_0^L xf(x,0)dx\Big)$$

$$-\Big(H_0'(0) - \int_0^L f(x,0)dx\Big)\Big(L\phi'(L) - \mu_2(L) + \mu_1(0)\Big)\Bigg], \tag{3.8}$$

where
$\Delta(0) = \Big(\mu_2(L)-\mu_1(0)\Big)^2 + L\Big(\phi'(L)\mu_1(0) - \phi'(0)\mu_2(L)\Big) - H_0(0)\Big(\phi'(L) - \phi'(0)\Big) \neq 0.$

(a)

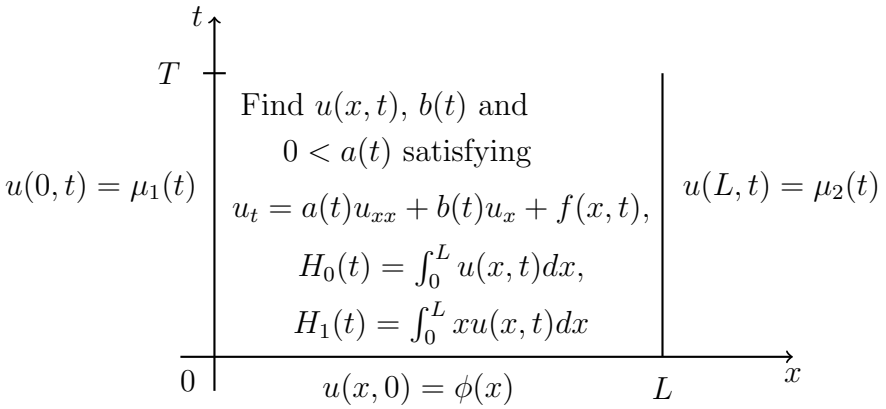

(b)

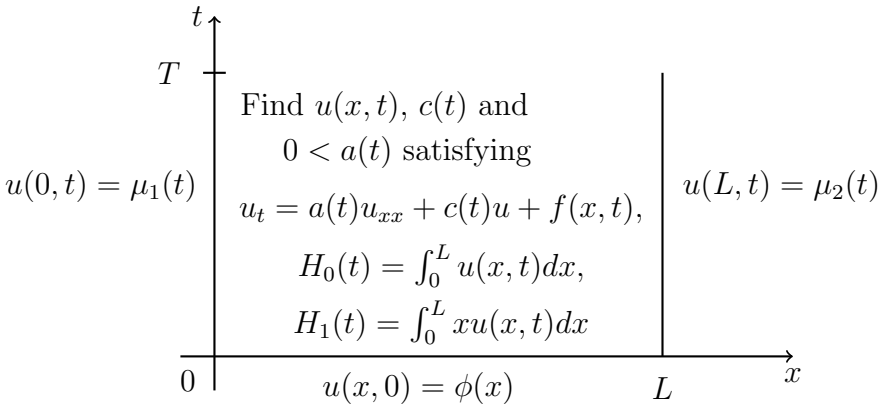

Figure 3.1: Sketch of the inverse problems under investigation (a) IP1 and (b) IP2.

3.2.2 Inverse Problem 2

Assuming that $b(t) = 0$, the inverse problem 2 (IP2) requires the simultaneous determination of the time-dependent thermal conductivity $a(t) > 0$ and the absorption coefficient $c(t)$, together with the temperature $u(x,t)$ satisfying

$$\frac{\partial u}{\partial t}(x,t) = a(t)\frac{\partial^2 u}{\partial x^2}(x,t) + c(t)u(x,t) + f(x,t), \quad (x,t) \in Q_T, \tag{3.9}$$

subject to (3.2), (3.3) and (3.5). The sketch of the IP2 is shown in Figure 4.1(b).

In bio-heat transfer, equation (3.9) is known as the Pennes bio-heat equation and $c(t)$ represents the perfusion coefficient, [127]. In case where the thermal conductivity coefficient $a(t)$ is known, and taken to be unity, the inverse problem (3.2), (3.3), (3.9) with the the integral condition (3.5) for $k = 0$, for recovering the perfusion coefficient $c(t)$ and the temperature $u(x,t)$ was studied both theoretically and numerically in [16] and [127], respectively.

The uniqueness of solution $(a(t), c(t), u(x,t))$ of the IP2 was established in [78] and reads as follows.

Theorem 3.2.2. *Let* $\phi \in C^1[0,L]$, $\mu_k \in C[0,T]$, $H_k \in C^1[0,T]$ *for* $k = 0, 1$, *and* $f \in C(\overline{Q_T})$.
Suppose that the following condition is satisfied:

$$U_2(t) := H_0(t)H_1'(t) - H_0'(t)H_1(t) + \int_0^L \Big(H_1(t) - xH_0(t)\Big) f(x,t)dx \neq 0, \quad \forall t \in [0,T]. \tag{3.10}$$

Then a solution $(a(t), c(t), u(x,t)) \in C[0,T] \times C[0,T] \times \Big(C^{2,1}(Q_T) \cap C^{1,0}(\overline{Q_T})\Big)$ *with* $a(t) > 0$ *for* $t \in [0,T]$, *to the problem (3.2), (3.3), (3.5) and (3.9) is unique.*

Remark 2. Observe that by multiplying equation (3.8) by $x^k, k = 0, 1$, integrating with respect to x from 0 to L, and taking into account condition (3.5), we obtain, [78],
$H_0'(t) = a(t)\Big(u_x(L,t) - u_x(0,t)\Big) + c(t)H_0(t) + \int_0^L f(x,t)dx$,
$H_1'(t) = a(t)\Big(Lu_x(L,t) - u(L,t) + u(0,t)\Big) + c(t)H_1(t) + \int_0^L xf(x,t)dx$.
As before in Remark 1, taking $t = 0$ in these equations and solving for $a(0)$ and $c(0)$, we obtain,

$$a(0) = \frac{1}{\Theta(0)}\left[H_1(0)\Big(H_0'(0) - \int_0^L f(x,0)dx\Big) - H_0(0)\Big(H_1'(0) - \int_0^L xf(x,0)dx\Big)\right],$$

$$c(0) = \frac{1}{\Theta(0)}\left[\Big(H_1'(0) - \int_0^L xf(x,0)dx\Big)\Big(\phi'(L) - \phi'(0)\Big)\right.$$

$$-\Big(H_0'(0) - \int_0^L f(x,0)dx\Big)\Big(L\phi'(L) - \mu_2(L) + \mu_1(0)\Big)\Big], \tag{3.11}$$

where
$\Theta(0) = H_1(0)\Big(\phi'(L) - \phi'(0)\Big) - H_0(0)\Big(L\phi'(L) - \mu_2(L) + \mu_1(0)\Big) \neq 0.$

3.3 Numerical solution of direct problem

Equation (3.1) can be discretised in the form of (2.6) as

$$\begin{aligned} -A_{j+1}u_{i-1,j+1} + (1+B_{j+1})u_{i,j+1} - C_{j+1}u_{i+1,j+1} \\ = A_j u_{i-1,j} + (1-B_j)u_{i,j} + C_j u_{i+1,j} + \frac{\Delta t}{2}(f_{i,j} + f_{i,j+1}), \\ i = \overline{1,(M-1)},\ j = \overline{0,(N-1)}, \end{aligned} \tag{3.12}$$

where

$$b_j = b(t_j),\ c_j = c(t_j),\ A_j = \frac{(\Delta t)a_j}{2(\Delta x)^2} - \frac{(\Delta t)b_j}{4(\Delta x)},\ B_j = \frac{(\Delta t)a_j}{(\Delta x)^2} - \frac{(\Delta t)c_j}{2},$$
$$C_j = \frac{(\Delta t)a_j}{2(\Delta x)^2} + \frac{(\Delta t)b_j}{4(\Delta x)}.$$

At each time step t_{j+1}, for $j = \overline{0,(N-1)}$, using the Dirichlet boundary conditions (2.8), the above difference equation can be reformulated as a $(M-1)\times(M-1)$ system of linear equations of the form

$$\tilde{D}\mathbf{u_{j+1}} = \tilde{E}\mathbf{u_j} + \tilde{\mathbf{b}}^{\mathbf{j}}, \tag{3.13}$$

where $\mathbf{u_{j+1}} = (u_{1,j+1}, u_{2,j+1}, ..., u_{M-2,j+1}, u_{M-1,j+1})^{\mathrm{T}}$,

$$\tilde{D} = \begin{pmatrix} 1+B_{j+1} & -C_{j+1} & 0 & ... & 0 & 0 & 0 \\ -A_{j+1} & 1+B_{j+1} & -C_{j+1} & ... & 0 & 0 & 0 \\ \vdots & \vdots & \vdots & \ddots & \vdots & \vdots & \vdots \\ 0 & 0 & 0 & ... & -A_{j+1} & 1+B_{j+1} & -C_{j+1} \\ 0 & 0 & 0 & ... & 0 & -A_{j+1} & 1+B_{j+1} \end{pmatrix},$$

$$\tilde{E} = \begin{pmatrix} 1-B_j & C_j & 0 & ... & 0 & 0 & 0 \\ A_j & 1-B_j & C_j & ... & 0 & 0 & 0 \\ \vdots & \vdots & \vdots & \ddots & \vdots & \vdots & \vdots \\ 0 & 0 & 0 & ... & A_j & 1-B_j & C_j \\ 0 & 0 & 0 & ... & 0 & A_j & 1-B_j \end{pmatrix},$$

and

$$\tilde{\mathbf{b}}^{\mathbf{j}} = \begin{pmatrix} \frac{\Delta t}{2}(f_{1,j} + f_{1,j+1}) + A_j\mu_1(t_j) + A_{j+1}\mu_1(t_{j+1}) \\ \frac{\Delta t}{2}(f_{2,j} + f_{2,j+1}) \\ \vdots \\ \frac{\Delta t}{2}(f_{M-2,j} + f_{M-2,j+1}) \\ \frac{\Delta t}{2}(f_{M-1,j} + f_{M-1,j+1}) + C_j\mu_2(t_j) + C_{j+1}\mu_2(t_{j+1}) \end{pmatrix}.$$

As an example, consider the direct problem (3.1)–(3.3) with $T = L = 1$,

$$c(t) = 0, \quad \phi(x) = u(x,0) = e^{-x} + x^2, \quad \mu_1(t) = u(0,t) = e^t,$$
$$\mu_2(t) = u(1,t) = (e^{-1}+1)e^t, \; f(x,t) = e^t\Big((1+t)e^{-x} + x^2 - 2(1+t) - 2x(1+2t)\Big), \quad (3.14)$$

and

$$a(t) = 1 + t, \quad b(t) = 1 + 2t. \quad (3.15)$$

The exact solution is given by

$$u(x,t) = (e^{-x} + x^2)e^t. \quad (3.16)$$

The numerical results for the interior temperature $u(x,t)$ have been obtained and are in excellent agreement with the exact solution (3.16) and therefore they are not presented.

Apart from the interior temperature $u(x,t)$, other outputs of interest are the heat moments in equation (3.5) over the time interval $[0,T]$, which analytically are given by

$$H_0(t) = \int_0^1 e^t(e^{-x} + x^2)dx = e^t\Big(-e^{-1} + \frac{4}{3}\Big), \quad t \in [0,1], \quad (3.17)$$

$$H_1(t) = \int_0^1 xe^t(e^{-x} + x^2)dx = e^t\Big(- 2e^{-1} + \frac{5}{4}\Big), \quad t \in [0, 1]. \tag{3.18}$$

Figure 3.2 shows that the exact and numerical solutions for the heat moments (3.5) are indistinguishable. The exact solutions are given in equations (3.17) and (3.18), whilst the numerical solutions have been calculated using the trapezoidal rule formula:

$$H_k(t_j) = \int_0^1 x^k u(x, t_j)dx = \frac{1}{2N}\Big(x_0^k u_{0,j} + x_M^k u_{M,j} + 2\sum_{i=1}^{M-1} x_i^k u_{i,j}\Big),$$
$$k = 0, 1, \quad j = \overline{0, N}, \tag{3.19}$$

with the convention that $x_0^0 = 1$. Note that for $j = 0$ in (3.17) and (3.18), using (3.2) and (3.5), we obtain,

$$H_k(0) = \int_0^1 x^k u(x, 0)dx = \frac{1}{2N}\Big(x_0^k \phi(x_0) + x_M^k \phi(x_M) + 2\sum_{i=1}^{M-1} x_i^k \phi(x_i)\Big),$$
$$k = 0, 1. \tag{3.20}$$

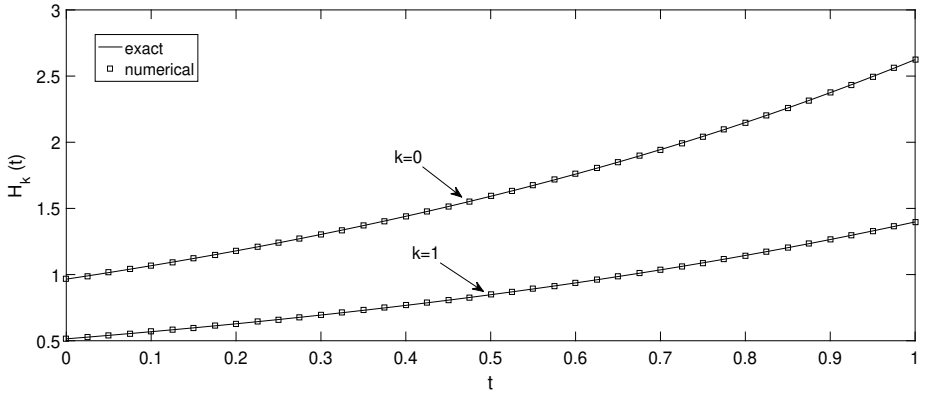

Figure 3.2: The exact and the numerical heat moments $H_k(t)$, $k = 0, 1$, for $M = N = 40$, for the direct problem.

The root means square errors ($rmse$) between the numerical and exact solutions heat moments (3.5) are shown in Table 3.1. These have been calculated using the formula

$$rmse(H_k) := \sqrt{\frac{1}{N}\sum_{j=1}^{N}\Big(H_k^{numerical}(t_j) - H_k^{exact}(t_j)\Big)^2}, \quad k = 0, 1. \tag{3.21}$$

From Table 3.1 it can be seen that the $rmse$ (3.21) decreases, as $M = N$ increases.

Table 3.1: The ($rmse$) given by eqution (3.21) between the exact and numerical solutions for the heat moments, for $M = N \in \{10, 20, 40\}$, for the direct problem.

$M = N$	10	20	40
$rmse(H_0)$	0.0041	0.0009	0.0002
$rmse(H_1)$	0.0031	0.0007	0.0001

3.4 Numerical solution of inverse problem

Here we assume that the coefficients $a(t)$, $b(t)$ or $c(t)$ are unknown. Usually, nonlinear inverse problems can be formulated as a nonlinear minimization. The regularized objective function which is minimized is given by

$$F(a,b) = \Big\| \int_0^1 u(x,t)dx - H_0(t) \Big\|^2 + \Big\| \int_0^1 xu(x,t)dx - H_1(t) \Big\|^2 + \beta_1 \|a(t)\|^2 + \beta_2 \|b(t)\|^2, \tag{3.22}$$

or

$$F(a,c) = \Big\| \int_0^1 u(x,t)dx - H_0(t) \Big\|^2 + \Big\| \int_0^1 xu(x,t)dx - H_1(t) \Big\|^2 + \beta_1 \|a(t)\|^2 + \beta_2 \|c(t)\|^2, \tag{3.23}$$

where u solves (3.2), (3.3) and (3.6) or (3.9) for given (a,b) or (a,c), respectively, $\beta_1, \beta_2 \geq 0$ are regularization parameters and the norm is usually the $L^2[0,T]$-norm. The discretizations of (3.22) and (3.23) are:

$$F(\mathbf{a},\mathbf{b}) = \sum_{j=1}^{N} \Big[\int_0^1 u(x,t_j)dx - H_0(t_j) \Big]^2 + \sum_{j=1}^{N} \Big[\int_0^1 xu(x,t_j)dx - H_1(t_j) \Big]^2 + \beta_1 \sum_{j=1}^{N} a_j^2 + \beta_2 \sum_{j=1}^{N} b_j^2 \tag{3.24}$$

and

$$F(\mathbf{a},\mathbf{c}) = \sum_{j=1}^{N} \Big[\int_0^1 u(x,t_j)dx - H_0(t_j) \Big]^2 + \sum_{j=1}^{N} \Big[\int_0^1 xu(x,t_j)dx - H_1(t_j) \Big]^2 + \beta_1 \sum_{j=1}^{N} a_j^2 + \beta_2 \sum_{j=1}^{N} c_j^2. \tag{3.25}$$

The case $\beta_1 = \beta_2 = 0$ yields the ordinary nonlinear least-squares method which is usually unstable. The minimization of F subject to the physical con-

straints $\mathbf{a} > \mathbf{0}$ is accomplished using the MATLAB toolbox routine *lsqnonlin*.

We take the parameters of the routine as follows:

- Number of variables $M = N = 40$.
- xTolerance (xTol) = 10^{-30}.
- Function Tolerance (FunTol) = 10^{-30}.
- Initial guess $(\mathbf{a}^{(0)}, \mathbf{b}^{(0)}) = (\mathbf{a}(0), \mathbf{b}(0))$ for IP1 and $(\mathbf{a}^{(0)}, \mathbf{c}^{(0)}) = (\mathbf{a}(0), \mathbf{c}(0))$ for IP2. The values of $a(0)$, $b(0)$ and $c(0)$ are calculated from equations (8) and (11).
- The lower and upper simple bounds are 10^{-10} and 10^3 for a, and -10^3 and 10^3 for b and c.

3.5 Numerical results and discussion

In this section, we discuss a few test examples to illustrate the accuracy and stability of the numerical solutions. We take $T = L = 1$. We investigate the cases when the coefficients $a(t)$, $b(t)$ or $c(t)$ are smooth and non-smooth. In addition, we add noise to the measured heat moments input data (3.5) as

$$H_k^{\epsilon}(t_j) = H_k(t_j) + \epsilon_k^j, \quad k = 0, 1, \quad j = \overline{1, N}, \tag{3.26}$$

where ϵ_k^j are random variables generated from a Gaussian normal distribution with mean zero and standard deviations σ_k, given by

$$\sigma_k = p \times \max_{t \in [0,T]} |H_k(t)|, \quad k = 0, 1, \tag{3.27}$$

where p represents the percentage of noise. We use the MATLAB function *normrnd* to generate the random variables as

$$\boldsymbol{\epsilon}_k = normrnd(0, \sigma, N), \quad k = 0, 1. \tag{3.28}$$

The root mean square error ($rmse$) to analyse the error between the exact and estimated coefficients, is defined by (2.18) and similar expressions exist for $b(t)$ and $c(t)$.

3.5.1 Example 1 (for IP1)

Consider the IP1 given by equations (3.2), (3.3), (3.5) and (3.6) with unknown coefficients $a(t)$, $b(t)$ and solve this inverse problem with the input data (3.14), (3.17) and (3.18). The graph of the function $U_1(t)$ given by equation (3.7) is shown in Figure 3.3. From this figure it can be seen that this function never vanishes over the time interval $t \in [0, 1]$ and hence condition (3.7) is satisfied. Consequently, according to Theorem 3.2.1, a solution to the IP1 given by equations (3.3), (3.4), (3.6) and (3.7) with data (3.14), (3.17) and (3.18) is unique. In fact, it can easily be verified by direct substitution that the solution $(a(t), b(t), u(x, t))$ is given by equations (3.15) and (3.16). Note also that the direct problem (3.1)–(3.3) associated to this example has been previously solved numerically using the FDM in Section 3.3.

First, we consider that there is no noise in the input data (3.6). The unregularized objective function (3.24), i.e. with $\beta_1 = \beta_2 = 0$, as a function of the number of iterations, is shown in Figure 3.4. From this figure it can be seen that it decreases rapidly to a very low value of $O(10^{-28})$ in 20 iterations. The numerical results for the corresponding coefficients $a(t)$ and $b(t)$ are presented in Figure 3.5. From this figure it can be seen that the retrieved coefficients are in very good agreement with the exact solution (3.15).

Next, we add $p = 1\%$ noise to the heat moments $H_0(t)$ and $H_1(t)$, as given by equation (3.26). Taking first $\beta_1 = \beta_2$, the L-curve, [48], for the choice of the regularization parameter is shown in Figure 3.6, where the

$$\text{Residual norm} = \sqrt{\sum_{k=0}^{1} \left\| \int_0^1 x^k u(x, \cdot) dx - H_k^{noise}(\cdot) \right\|^2}. \tag{3.29}$$

From this figure it can be seen that the three regularization parameters near the "corner" of the L-curve are $\beta_1 = \beta_2 \in \{10^{-4}, 10^{-3}, 10^{-2}\}$. Second, allowing for independent values of β_1 and β_2 we obtain the numerical results summarised in Table 3.2. In this table, we have highlighted some representative choices for β_1 and β_2 with the corresponding numerical solutions for a and b plotted in Figure 3.7 and the absolute errors between numerical and exact solutions for u plotted in Figure 3.8.

We note that for the choice of the two-parameter family of regularization parameters (β_1, β_2) we have initially tried to apply the heuristic L-surface method, [7], but without obtaining a clear graphical indication of an L-shaped surface. Next, we investigate the application of the discrepancy domain principle, [41],

which selects the regularization parameters (β_1, β_2) belonging to the domain

$$D(\varepsilon) = \Big\{ (\beta_1, \beta_2) \in \mathbb{R}^2_+ \Big| \quad \varepsilon < \text{Residual norm} \leq \tau\varepsilon \Big\}, \tag{3.30}$$

for some constant $\tau > 1$ independent on β_1, β_2 and ε, where

$$\varepsilon = \varepsilon(p) = \sqrt{\sum_{k=0}^{1} \sum_{j=1}^{N} (\epsilon_k^j)^2} \tag{3.31}$$

represents the total amount of noise which is input in (3.26). For $p = 1\%$, from (3.31) we report $\varepsilon(1\%) = 0.2459$. By inspecting Table 3.2 and invoking criterion (3.30) one can discard choices with $\beta_1 \leq 10^{-3}$ as producing unstable solutions. Also, one can observe that the choices $\beta_1 = 10^{-2}$, $\beta_2 = 10^{-3}$ and $\beta_1 = 10^{-2}$, $\beta_2 = 10^{-2}$ satisfy criterion (3.30) for some $\tau > 1$, but the choice $\beta_1 = 10^{-3}$, $\beta_2 = 10^{-4}$ does not. This is consistent with the numerical results presented in Figure 3.7 where the numerical solution obtained with the under-regularization parameters $\beta_1 = 10^{-3}$, $\beta_2 = 10^{-4}$ is rather unstable, whilst the choice $\beta_1 = 10^{-2}$, $\beta_2 = 10^{-3}$ seems optimal.

From the above discussion and related solution [7, 41, 95] one can realise that the choice of multiple regularization parameters is a difficult and open topic and more research needs to be undertaken in the future. In what follows, in Examples 2–4, for simplicity, we present results obtained with some trial-and-error typical values of β_1 and β_2 which ensure that stable solutions are obtained.

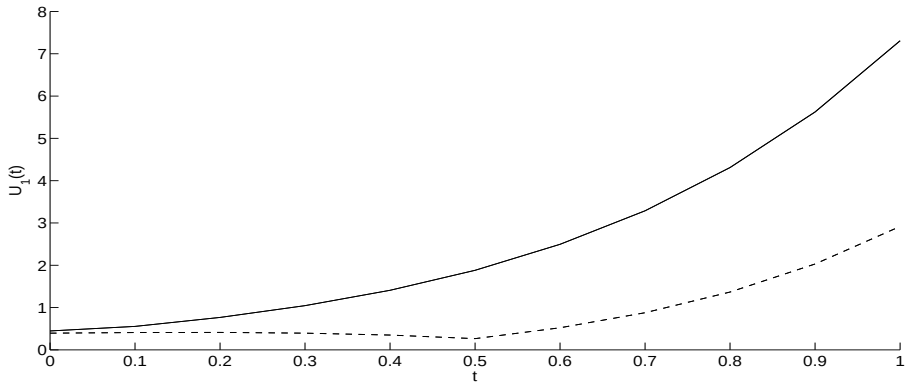

Figure 3.3: The graph of the function $U_1(t)$, as a function of t, given by (3.7) for Example 1 (——) and Example 2 (− − −).

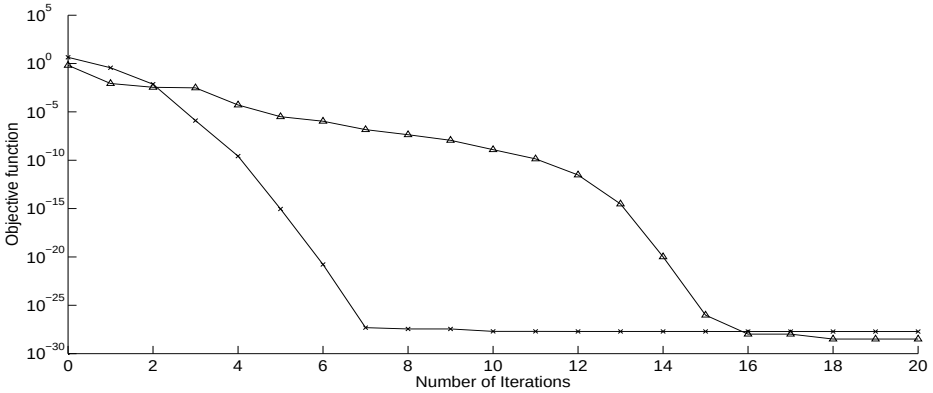

Figure 3.4: Objective function (3.24), for Example 1 ($-$x$-$) and Example 2 ($-\triangle-$), with no noise and no regularization.

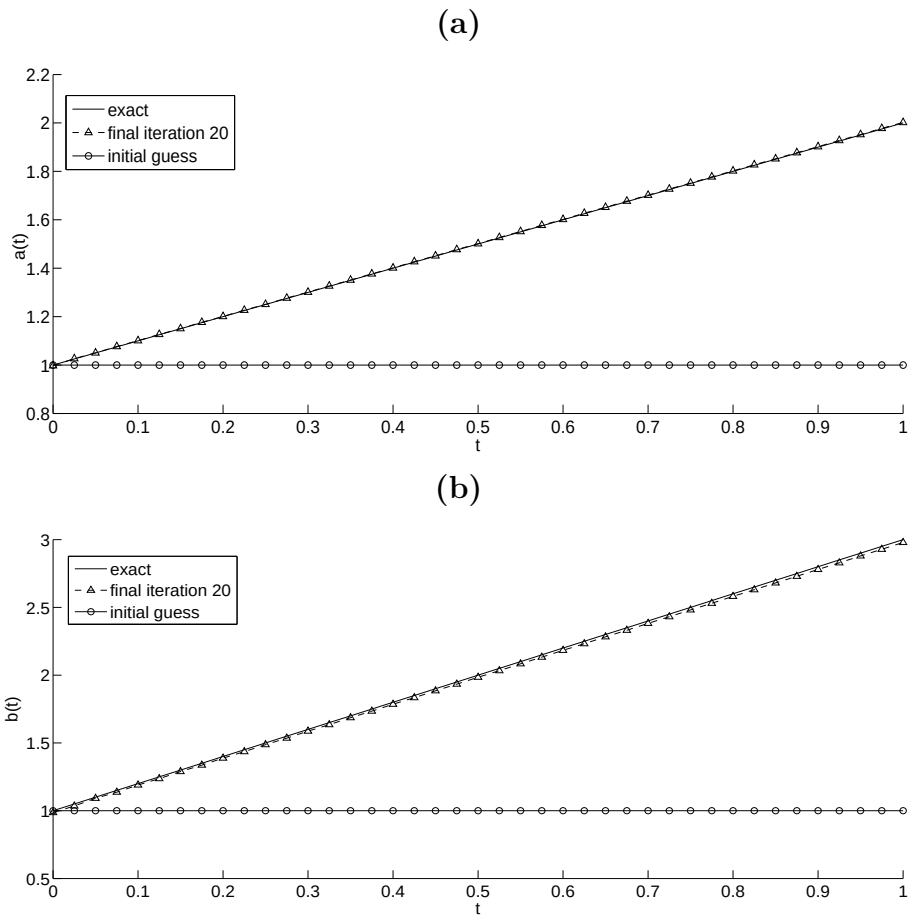

Figure 3.5: (a) Coefficient $a(t)$ and (b) Coefficient $b(t)$, for Example 1 with no noise and no regularization.

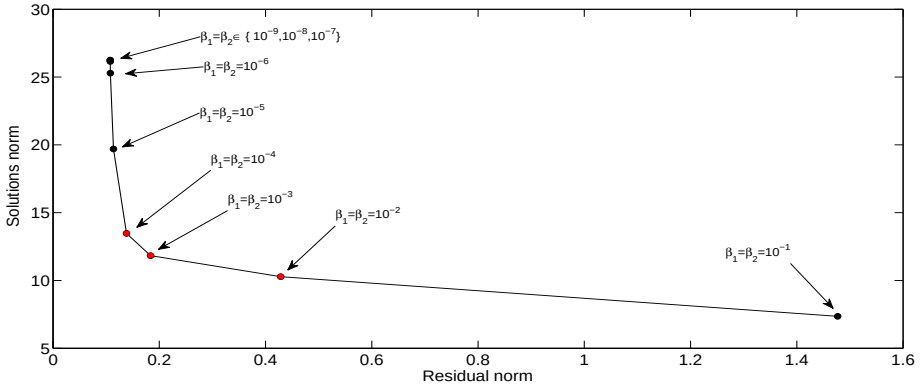

Figure 3.6: The residual norm (3.29) versus the solution norm $\sqrt{||a||^2+||b||^2}$ for the L-curve with various regularization parameters, for Example 1 with $p = 1\%$ noise.

Table 3.2: The objective function (3.24), $rmse$, residual and norms for estimated coefficients for IP1 of Example 1 with $p = 1\%$ noise and various regularization parameters.

$\beta_1 \backslash \beta_2$		10^{-9}	10^{-8}	10^{-7}	10^{-6}	10^{-5}	10^{-4}	10^{-3}	10^{-2}	10^{-1}
10^{-9}	Obj.function	0.0116	0.0116	0.0117	0.0121	0.0152	0.0193	0.0200	0.0201	0.0201
	$rmse(a)$	1.1252	1.1252	1.1253	1.1254	1.1235	1.2054	1.1365	1.1261	1.1252
	$rmse(b)$	2.8876	2.8862	2.8717	2.7267	1.7860	1.8301	2.0577	2.0829	2.0854
	Residual	0.1078	0.1078	0.1078	0.1079	0.1144	0.1359	0.1411	0.1416	0.1416
	$\|\|a\|\|$	12.199	12.201	12.211	12.303	12.941	14.207	14.087	14.062	14.060
	$\|\|b\|\|$	23.242	23.231	23.122	22.063	14.508	2.8511	0.2680	0.0265	0.0027
10^{-8}	Obj.function	0.0116	0.0116	0.0117	0.0121	0.0152	0.0193	0.0200	0.0201	0.0201
	$rmse(a)$	1.1251	1.1251	1.1253	1.1253	1.1235	1.2054	1.1364	1.1261	1.1252
	$rmse(b)$	2.8876	2.8862	2.8717	2.7268	1.7860	1.8301	2.0577	2.0829	2.0854
	Residual	0.1078	0.1078	0.1078	0.1079	0.1144	0.1359	0.1411	0.1416	0.1416
	$\|\|a\|\|$	12.199	12.200	12.211	12.302	12.941	14.207	14.087	14.062	14.060
	$\|\|b\|\|$	23.243	23.232	23.123	22.064	14.509	2.8513	0.2679	0.0265	0.0027
10^{-7}	Obj.function	0.0116	0.0116	0.0117	0.0122	0.0152	0.0193	0.0200	0.0201	0.0201
	$rmse(a)$	1.1246	1.1246	1.1248	1.1249	1.1231	1.2050	1.1354	1.1251	1.1242
	$rmse(b)$	2.8876	2.8861	2.8717	2.7265	1.7860	1.8299	2.0577	2.0829	2.0854
	Residual	0.1078	0.1078	0.1078	0.1079	0.1144	0.1359	0.1411	0.1416	0.1416
	$\|\|a\|\|$	12.196	12.197	12.208	12.299	12.939	14.205	14.083	14.058	14.056
	$\|\|b\|\|$	23.249	23.238	23.129	22.068	14.5135	2.8518	0.2678	0.0265	0.0026
10^{-6}	Obj.function	0.0118	0.0118	0.0118	0.0123	0.0154	0.0195	0.0202	0.0202	0.0203
	$rmse(a)$	1.1200	1.1201	1.1203	1.1207	1.1198	1.2016	1.1254	1.1165	1.1158
	$rmse(b)$	2.8884	2.8869	2.8723	2.7245	1.7860	1.8282	2.0576	2.0828	2.0854
	Residual	0.1078	0.1078	0.1078	0.1079	0.1143	0.1359	0.1411	0.1416	0.1416
	$\|\|a\|\|$	12.163	12.164	12.175	12.270	12.919	14.190	14.045	14.026	14.024
	$\|\|b\|\|$	23.309	23.298	23.187	22.111	14.559	2.8544	0.2665	0.0264	0.0026
10^{-5}	Obj.function	0.0131	0.0131	0.0131	0.0136	0.0168	0.0213	0.0219	0.0220	0.0220
	$rmse(a)$	1.0854	1.0854	1.0856	1.0882	1.0938	1.1446	1.0713	1.0692	1.0691
	$rmse(b)$	2.9189	2.9171	2.8995	2.7385	1.7776	1.8147	2.0565	2.0827	2.0854
	Residual	0.0856	0.1080	0.1080	0.1080	0.1139	0.1361	0.0219	0.1417	0.1417
	$\|\|a\|\|$	11.884	11.885	11.899	12.021	12.742	13.960	13.840	13.846	13.847
	$\|\|b\|\|$	23.965	23.952	23.820	22.634	15.023	2.8359	0.2641	0.0263	0.0026
10^{-4}	Obj.function	0.0236	0.0236	0.0237	0.0245	0.0297	0.0373	0.0385	0.0386	0.0386
	$rmse(a)$	0.9040	0.9039	0.9022	0.8995	0.9146	0.9100	0.9353	0.9371	0.9372
	$rmse(b)$	3.7526	3.7494	3.7169	3.3481	1.9023	1.6453	2.0384	2.0809	2.0852
	Residual	0.1175	0.1175	0.1173	0.1162	0.0297	0.1383	0.1437	0.1442	0.1442
	$\|\|a\|\|$	9.8774	9.8789	9.8940	10.067	11.154	12.972	13.322	13.353	13.356
	$\|\|b\|\|$	31.558	31.538	31.333	29.148	19.9816	3.6333	0.3591	0.0359	0.0036
10^{-3}	Obj.function	0.0581	0.0581	0.0583	0.0604	0.0756	0.1464	0.1737	0.1763	0.1766
	$rmse(a)$	0.9978	0.9977	0.9968	0.9723	0.8990	0.3452	0.4391	0.4597	0.4618
	$rmse(b)$	6.1800	6.1775	6.1525	5.4835	4.1854	0.8470	1.8259	2.0598	2.0831
	Residual	0.1996	0.1996	0.1995	0.1983	0.1929	0.1694	0.1837	0.1855	0.1857
	$\|\|a\|\|$	4.2682	4.2687	4.2743	4.3567	4.8573	9.3536	11.707	11.901	11.919
	$\|\|b\|\|$	49.073	49.059	48.924	45.311	38.438	17.384	1.7106	0.1699	0.0170
10^{-2}	Obj.function	0.0868	0.0759	0.0871	0.0931	0.1141	0.2812	1.0709	1.2397	1.2535
	$rmse(a)$	1.4304	1.4446	1.4302	1.4166	1.4087	1.3140	0.2534	0.1848	0.1923
	$rmse(b)$	7.4462	8.2955	7.4317	6.7808	5.3679	4.4335	0.4258	1.8922	2.0666
	Residual	0.2815	0.2616	0.2814	0.2865	0.2898	0.2942	0.3578	0.4285	0.4348
	$\|\|a\|\|$	0.8702	0.8629	0.8709	0.8974	0.9301	1.5236	8.4957	10.199	10.310
	$\|\|b\|\|$	57.551	62.8293	57.469	53.806	46.3387	41.400	14.869	1.2524	0.1231
10^{-1}	Obj.function	0.0586	0.0738	0.0722	0.0719	0.0863	0.3054	1.8226	7.0848	7.5868
	$rmse(a)$	1.5163	1.5173	1.5159	1.5123	1.5217	1.5044	1.4064	0.5129	0.4327
	$rmse(b)$	9.9355	9.0484	8.8824	8.8319	7.5404	4.7963	4.0608	0.8014	1.9854
	Residual	0.2328	0.2670	0.2619	0.2467	0.2190	0.3327	0.4810	1.3505	1.4769
	$\|\|a\|\|$	0.2103	0.1573	0.1788	0.2560	0.1255	0.1879	0.8083	6.7276	7.3235
	$\|\|b\|\|$	73.594	68.030	67.018	67.370	60.633	43.724	39.062	8.5725	0.6492

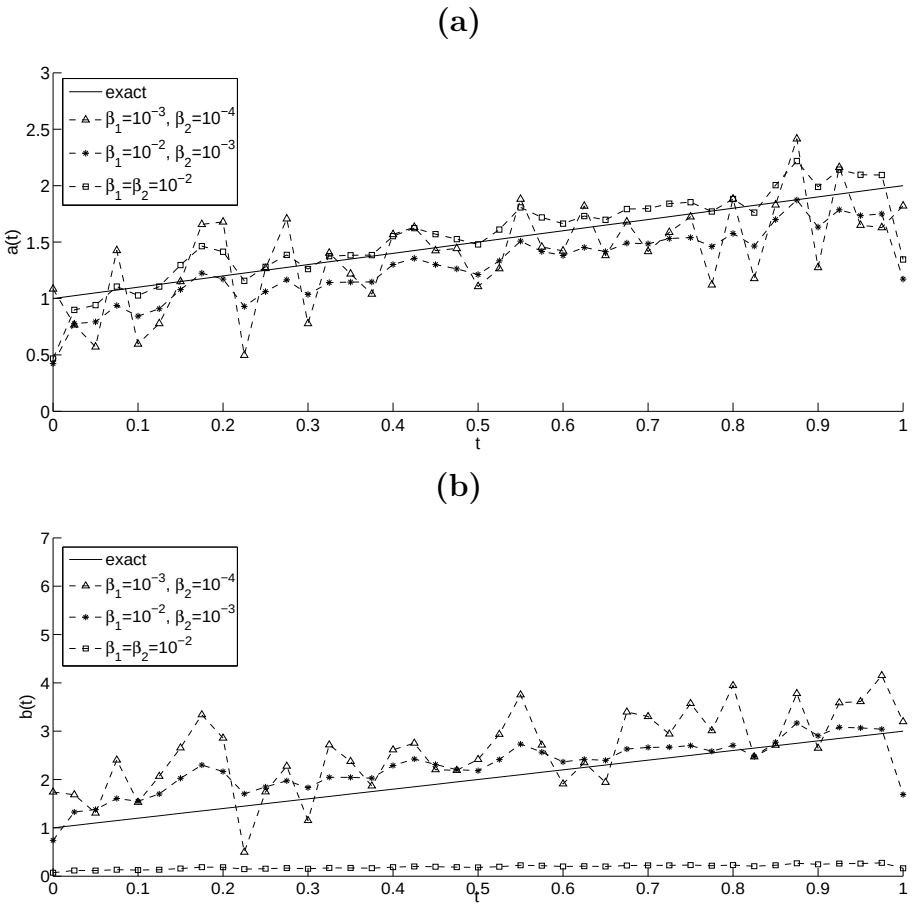

Figure 3.7: (a) Coefficient $a(t)$ and (b) Coefficient $b(t)$, for Example 1 with $p = 1\%$ noise and regularization.

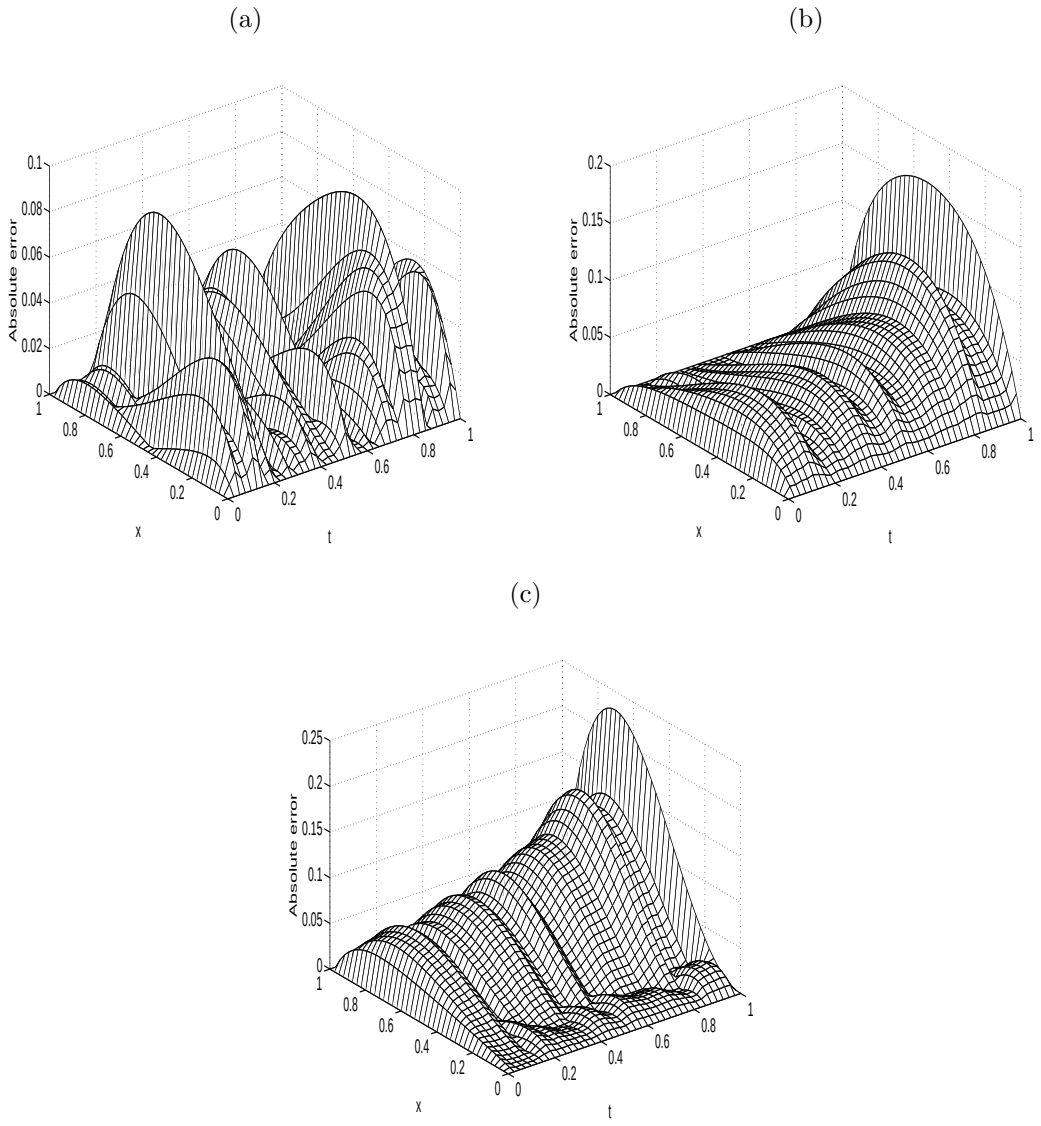

Figure 3.8: The absolute error between the exact and numerical temperatures $u(x,t)$, for Example 1, with (a) $\beta_1 = 10^{-3}$, $\beta_2 = 10^{-4}$, (b) $\beta_1 = 10^{-2}$, $\beta_2 = 10^{-3}$, (c) $\beta_1 = \beta_2 = 10^{-2}$, for $p = 1\%$ noise.

3.5.2 Example 2 (for IP1)

In this example, we consider the IP1 given by equations (3.2), (3.3), (3.5) and (3.6) with unknown coefficients $a(t)$ and $b(t)$ and we solve this inverse problem with the following input data:

$$\phi(x) = e^{-x} + x^2,\ \mu_1(t) = e^t,\ \mu_2(t) = (e^{-1}+1)e^t,\ H_0(t) = \Big(-e^{-1} + \frac{4}{3}\Big)e^t,$$

$$H_1(t) = \Big(-2e^{-1} + \frac{5}{4}\Big)e^t,\quad T = L = 1,$$

$$f(x,t) = (e^{-x}+x^2)e^t - \left(\left|t-\frac{1}{2}\right| + \frac{1}{2}\right)(e^{-x}+2)e^t - \left|t^2-\frac{1}{2}\right|(-e^{-x}+2x)e^t. \quad (3.32)$$

As for Example 1, the graph of the function $U_1(t)$ given by equation (3.7) is shown in Figure 3.3 and it can be seen that this function never vanishes over the time interval $t \in [0,1]$. Hence, condition (3.7) is satisfied and consequently, according to Theorem 3.2.1, a solution to the IP1 given by equations (3.2), (3.3), (3.5) and (3.6) with the input data (3.32) is unique. In fact, the exact solution to the inverse problem is given by

$$a(t) = \left|t-\frac{1}{2}\right| + \frac{1}{2}, \quad b(t) = \left|t^2-\frac{1}{2}\right|, \quad (3.33)$$

and $u(x,t)$ is given by (3.16).

Considering no noise and no regularization the objective function (3.24) plotted in Figure 3.4 shows a rapid decrease to a low value of $O(10^{-29})$ in 20 iterations. However, this convergence is slower than in Example 1 for the first 15 iterations. This is to be expected because the coefficients (3.15) for Example 1 are smoother than the coefficients (3.33) for Example 2. In Figure 3.9, we obtain a stable and accurate recovery of $a(t)$ but less stable for $b(t)$.

When $p = 0.01\%$ noise is included in the heat moments data (3.26), regularization is even more needed in order to achieve a stable and accurate solution. Table 3.3 shows the $rmse(a)$ and $rmse(b)$ for some values of the regularization parameters β_1 and β_2. Figure 3.10 shows the plots of the recovered coefficients $a(t)$ and $b(t)$. From both Table 3.3 and Figure 3.10 it can be seen that the retrieval of the thermal conductivity coefficient $a(t)$ is more stable and accurate than that of the convective coefficient $b(t)$.

Finally, we mention that a comparison between Figures 3.9 and 3.10, and Figures 22 and 24 of [62], respectively, shows that the IP1 based on measuring the heat moments (3.5) is less stable than when measuring the heat fluxes (3.4). This is to be expected since supplying the bounded normal derivatives (3.4) contains stronger information than prescribing the integral average heat moments (3.5).

In the next two examples we consider solving the IP2 formulated in subsection 3.2.2.

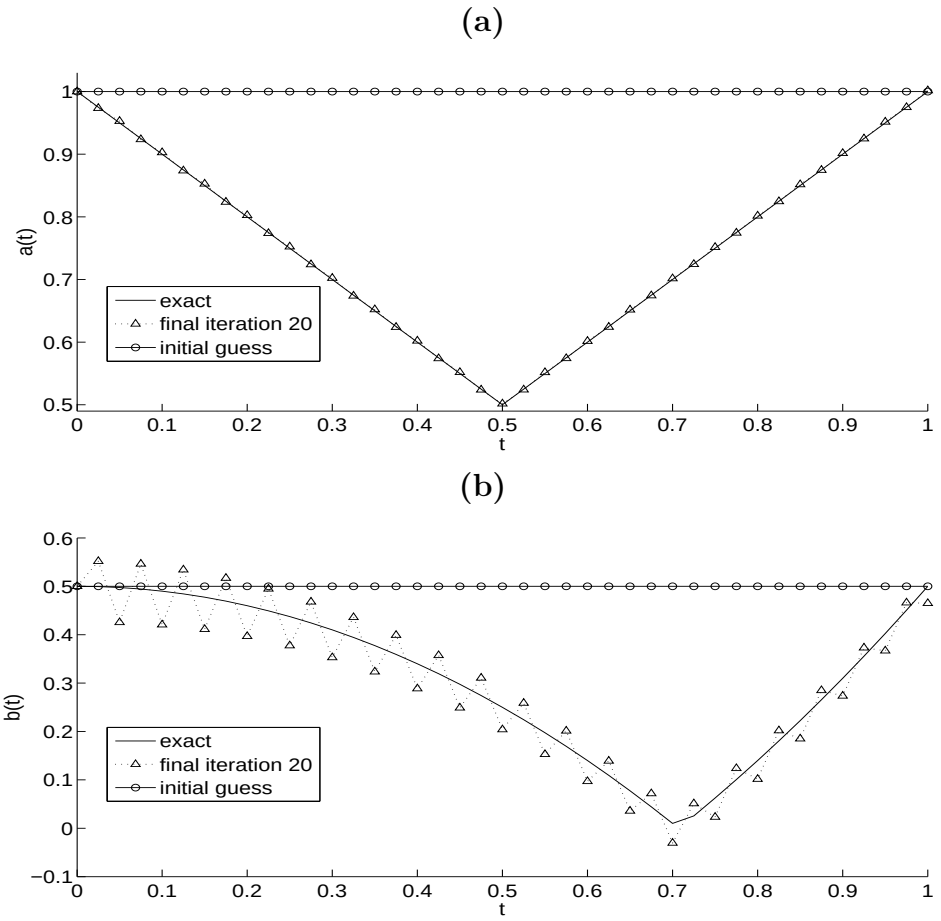

Figure 3.9: (a) Coefficient $a(t)$ and (b) Coefficient $b(t)$, for Example 2 with no noise and no regularization.

Table 3.3: The $rmse$ values for estimated coefficients for Example 2 with and without noise.

$rmse$	$p = 0$ $(\beta_1 = \beta_2 = 0)$	$p = 0.01\%$ $(\beta_1 = \beta_2 = 0)$	$p = 0.01\%$ $(\beta_1 = \beta_2 = 10^{-6})$
$rmse(a)$	0.0016	0.0830	0.0250
$rmse(b)$	0.0434	0.5360	0.0677

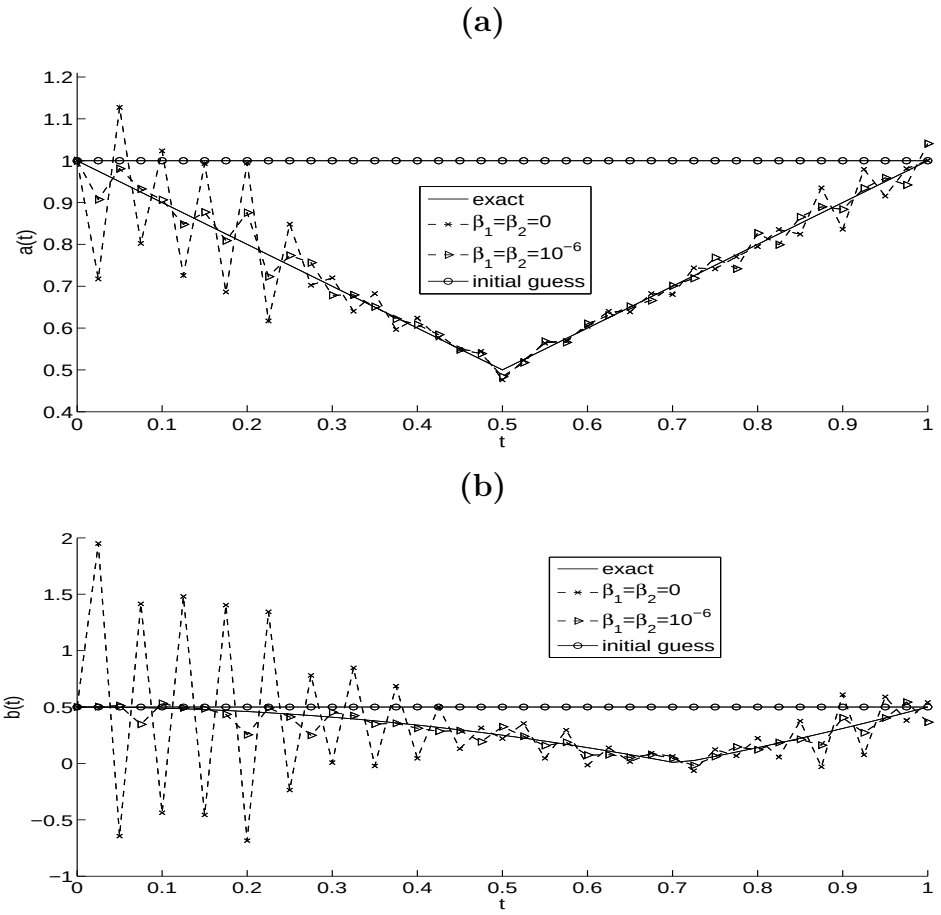

Figure 3.10: (a) Coefficient $a(t)$ and (b) Coefficient $b(t)$, for Example 2 with $p = 0.01\%$ noise, with and without regularization.

3.5.3 Example 3 (for IP2)

In this example, we consider the IP2 given by equations (3.2), (3.3), (3.5) and (3.9) with unknown coefficients $a(t)$ and $c(t)$ and solve this inverse problem with the following input data:

$$\phi(x) = (-2+x)^2,\ \mu_1(t) = (-2+t)^2+t,\ \mu_2(t) = (-1+t)^2+t,\ H_0(t) = t^2-2t+\frac{7}{3},$$

$$H_1(t) = \frac{1}{12}\Big(6t^2 - 10t + 11\Big),\ f(x,t) = 1 - 2(1+t) + 2(-2+x+t)$$
$$-(1+t)\Big(t + (-2+x+t)^2\Big),\quad T = L = 1. \tag{3.34}$$

The graph of the function $U_2(t)$ given by equation (3.10) is shown in Figure 3.11 and it can be seen that this function never vanishes over the time interval $t \in [0, 1]$. Hence, condition (3.10) is satisfied and consequently, according to Theorem 3.2.2, a solution to the IP2 given by equations (3.2), (3.3), (3.5) and

(3.9) with input data (3.34) is unique. In fact, this solution is given by

$$a(t) = 1 + t, \quad c(t) = 1 + t, \tag{3.35}$$

$$u(x,t) = (x + t - 2)^2 + t. \tag{3.36}$$

First, we consider the case that there is no noise in the input data (3.5). The convergence of the objective function (3.25) that is minimized with and without regularization is shown in Figure 3.12 and the corresponding numerical reconstructions of the coefficients $a(t)$ and $c(t)$ are shown in Figure 3.13. We also obtain the $rmse$ values of $rmse(a) \in \{0.0775, 0.1195\}$ and $rmse(c) \in \{0.1007, 0.1522\}$ with regularization $\beta_1 = 10^{-7}, \beta_2 = 10^{-9}$ and without regularization $\beta_1 = \beta_2 = 0$, respectively. Unlike the Example 1 for IP1, where no regularization was needed for exact data, in this Example 3 for IP2 the numerical results shown in Figure 3.13 and the decrease in the $rmse$ values reported above show that including a little regularization in (3.25) improves the accuracy and stability of the solution. It also shows that the IP2 is more ill-posed than the IP1.

To show this ill-posedness more dearly next we perturb the input data (3.5) by $p = 0.01\%$ noise as in equation (3.26). Figures 3.14 and 3.15 for this noisy data are the analogous of Figures 3.12 and 3.13 for exact data. We also report the values of $rmse(a) \in \{0.0719, 0.2489\}$ and $rmse(c) \in \{0.1025, 0.3709\}$ with regularization $\beta_1 = \beta_2 = 10^{-7}$ and without regularization $\beta_1 = \beta_2 = 0$, respectively. From these figures and $rmse$ values one can observe that the IP2 is ill-posed and regularization should be included in order to obtain a stable solution. The results also show that the IP2 is more ill-posed in the absorption coefficient $c(t)$ than in the diffusion coefficient $a(t)$.

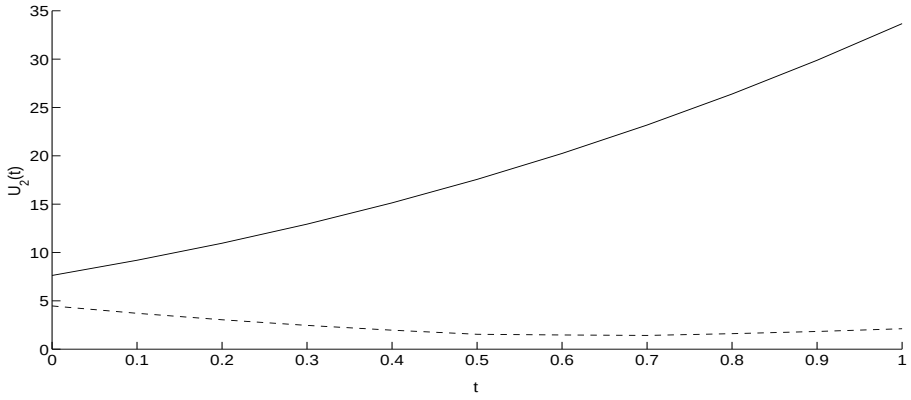

Figure 3.11: The graph of the function $U_2(t)$, as a function of t, given by (3.10) for Example 3 (——) and Example 4 (– – –).

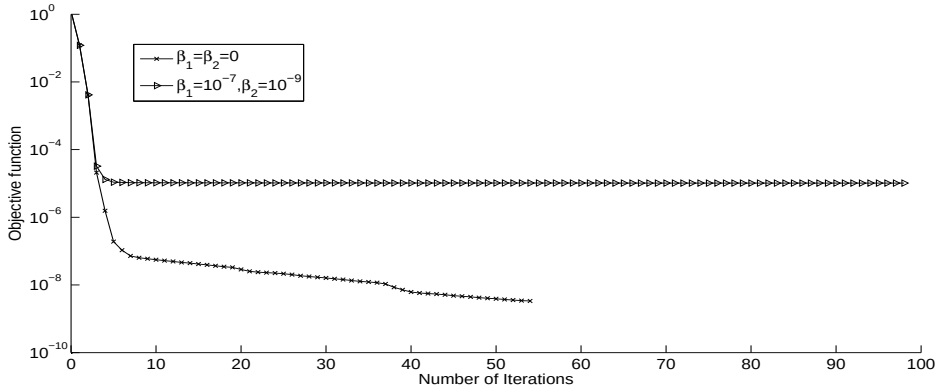

Figure 3.12: Objective function (3.25), for Example 3 with no noise, and with and without regularization.

(a)

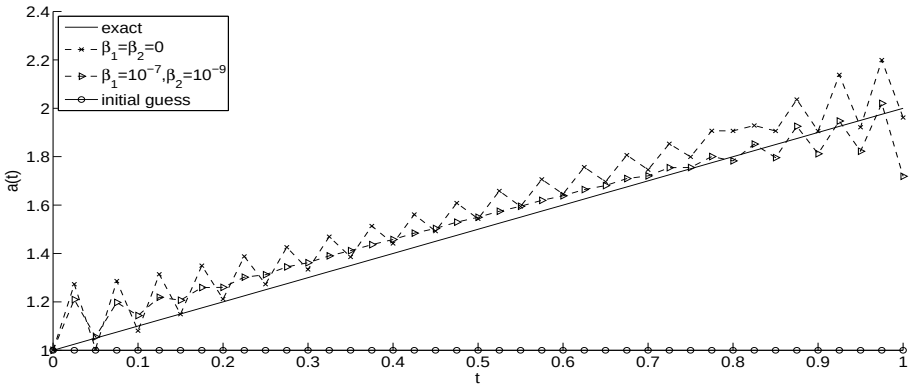

(b)

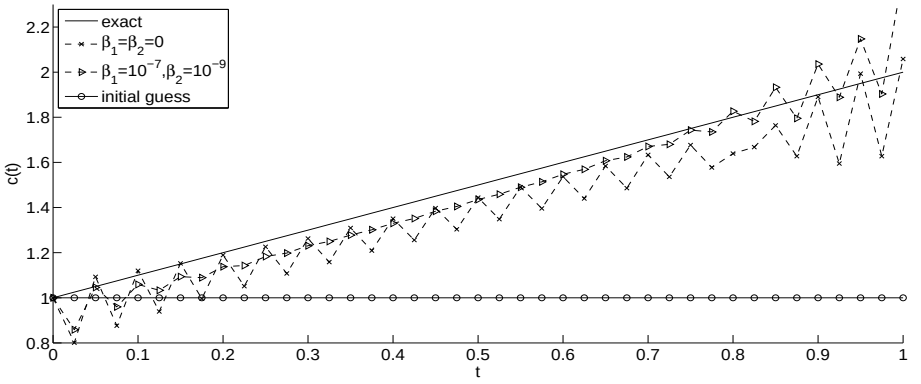

Figure 3.13: (a) Coefficient $a(t)$ and (b) Coefficient $c(t)$, for Example 3 with no noise, and with and without regularization.

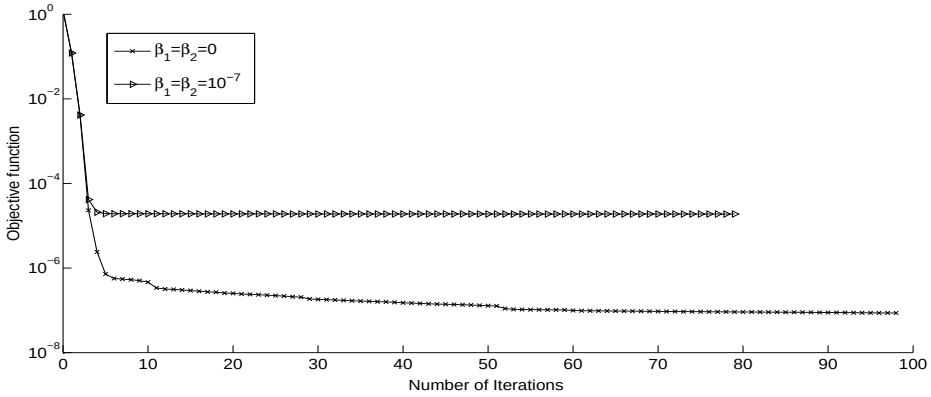

Figure 3.14: Objective function (3.25), for Example 3 with $p = 0.01\%$ noise, with and without regularization.

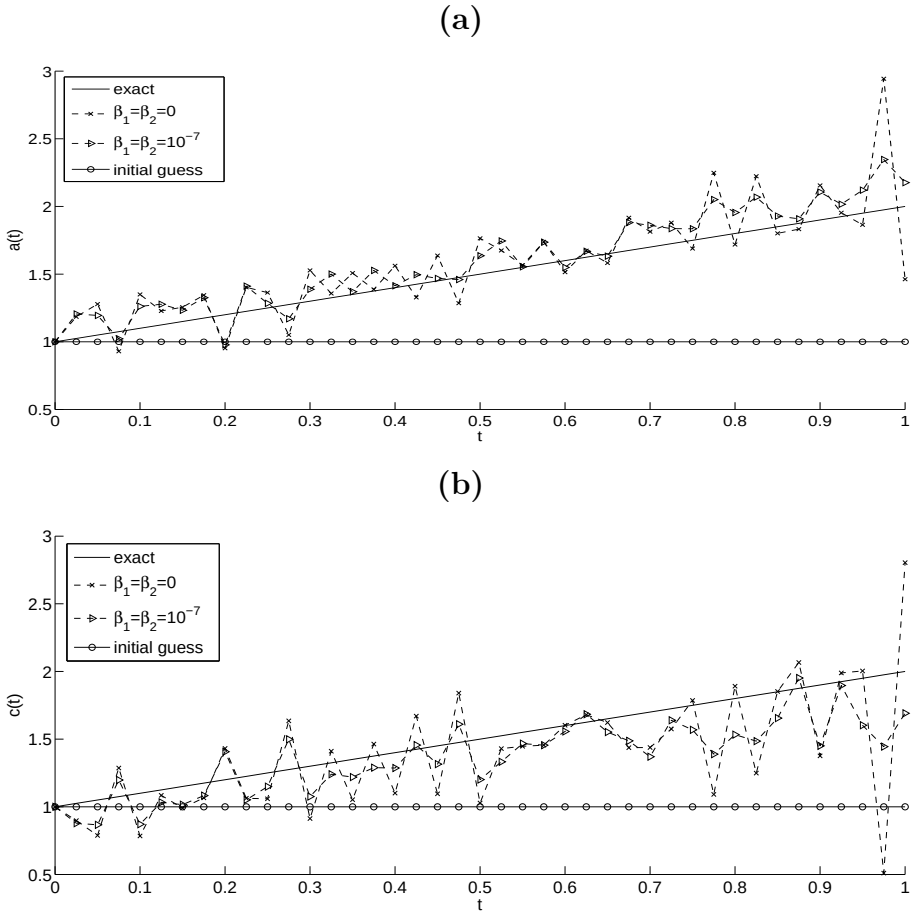

Figure 3.15: (a) Coefficient $a(t)$ and (b) Coefficient $c(t)$, for Example 3 with $p = 0.01\%$ noise, with and without regularization.

3.5.4 Example 4 (for IP2)

In this example, we consider the IP2 given by equations (3.2), (3.3), (3.5) and (3.9) with unknown coefficients $a(t)$ and $c(t)$ and we solve this inverse problem

with the following input data:

$$\phi(x) = (-2+x)^2,\ \mu_1(t) = (-2+t)^2+t,\ \mu_2(t) = (-1+t)^2+t,\ H_0(t) = t^2-2t+\frac{7}{3},$$
$$H_1(t) = \frac{1}{12}\Big(6t^2-10t+11\Big),\ f(x,t) = 1+2(-2+t+x)-2\Big(\Big|t-\frac{1}{2}\Big|+\frac{1}{2}\Big)$$
$$-\Big(t+(-2+x+t)^2\Big)\Big(\Big|t^2-\frac{1}{2}\Big|+\frac{1}{2}\Big),\ \ T=L=1. \tag{3.37}$$

As in Example 3, the function $U_2(t)$, given by equation (3.10) and plotted in Figure 3.11, never vanishes over the time interval $t \in [0,1]$ and consequently, the IP2 given by equations (3.2), (3.3), (3.5) and (3.9) with data (3.37) has at most one solution. In fact, this solution is given by

$$a(t) = \Big|t-\frac{1}{2}\Big|+\frac{1}{2}, \quad c(t) = \Big|t^2-\frac{1}{2}\Big|+\frac{1}{2}, \tag{3.38}$$

and $u(x,t)$ given by (3.36).

Figures 3.16–3.19 for Example 4 are the analogous of Figures 3.12–3.15 for Example 3. For exact data, we also obtain $rmse(a) \in \{0.0579, 0.0756\}$ and $rmse(c) \in \{0.0690, 0.0890\}$ with regurarization $\beta_1 = \beta_2 = 10^{-7}$ and without regularization $\beta_1 = \beta_2 = 0$, respectively.

Similar conclusions to those obtained for Example 3 are also obtained for Example 4.

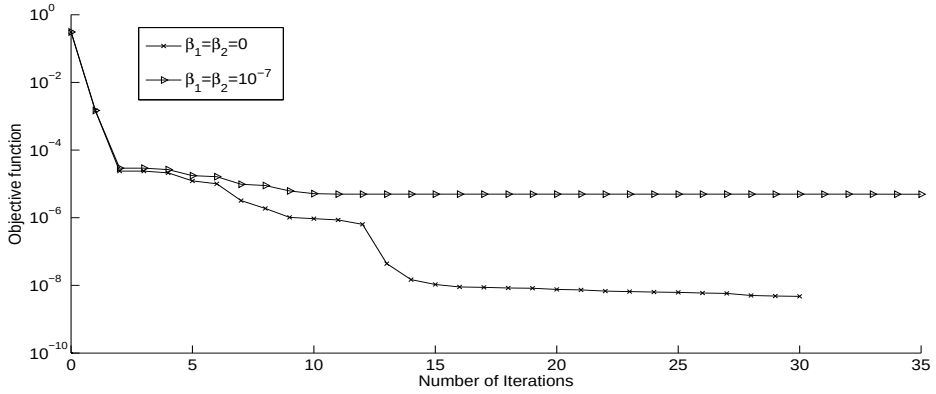

Figure 3.16: Objective function (3.25), for Example 4 with no noise, and with and without regularization.

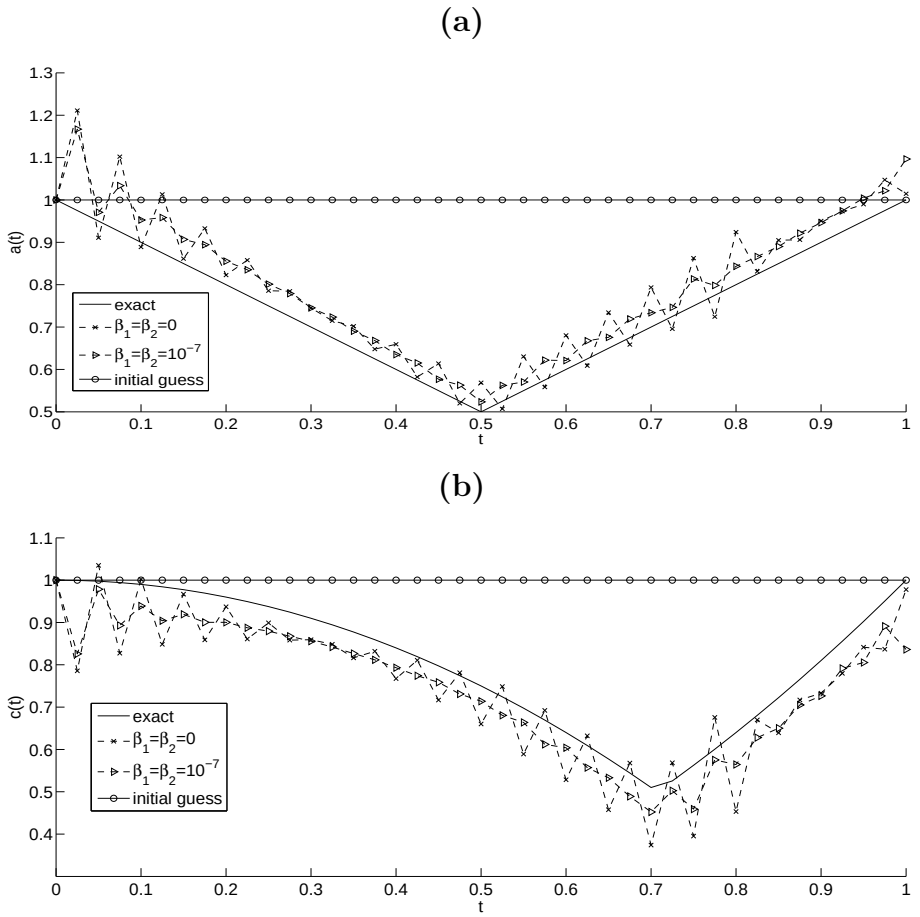

Figure 3.17: (a) Coefficient $a(t)$ and (b) Coefficient $c(t)$, for Example 4 with no noise, and with and without regularization.

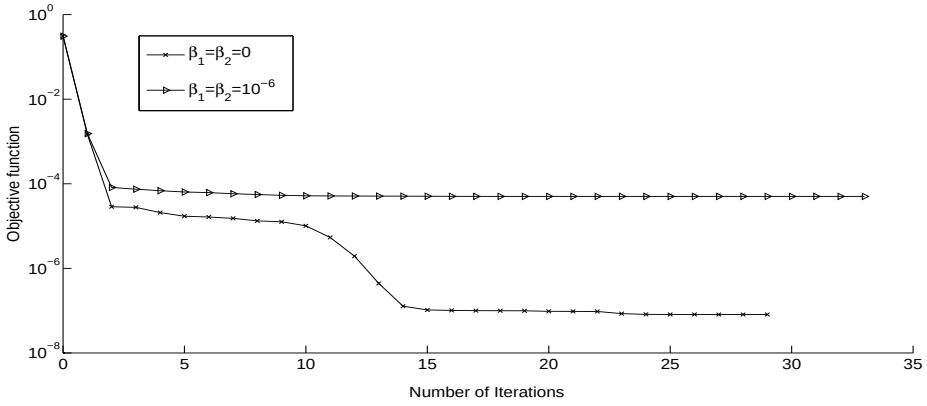

Figure 3.18: Objective function (3.25), for Example 4 with $p = 0.01\%$ noise, with and without regularization.

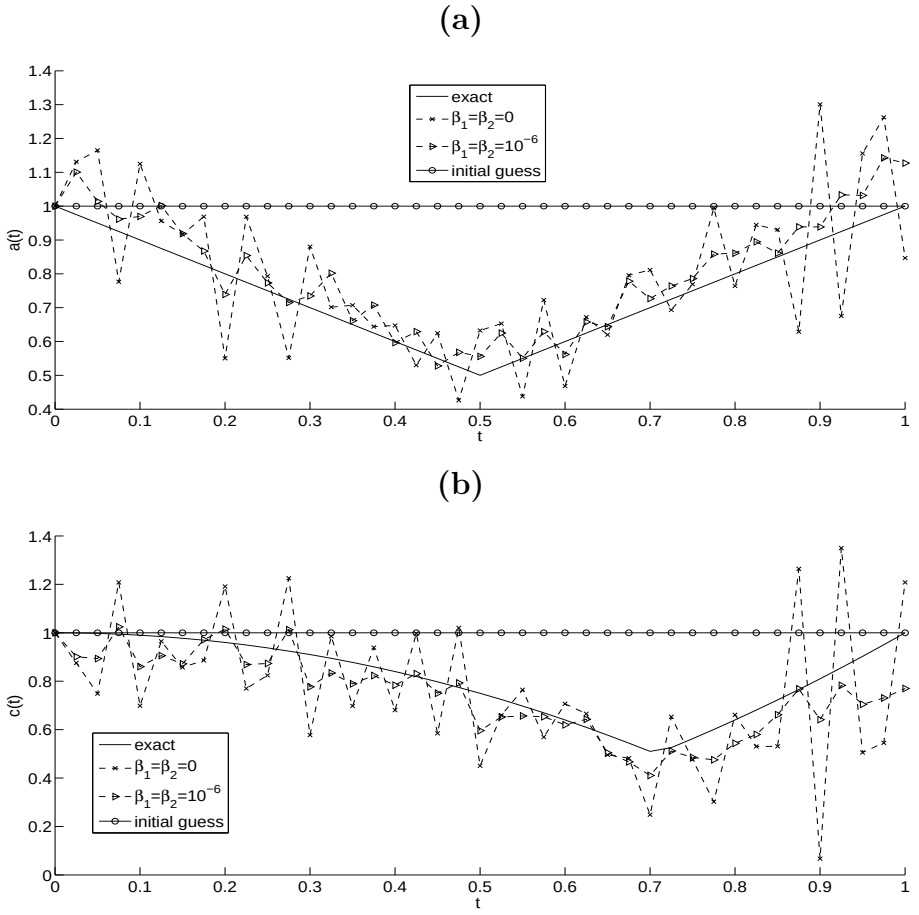

Figure 3.19: (a) Coefficient $a(t)$ and (b) Coefficient $c(t)$, for Example 4 with $p = 0.01\%$ noise, with and without regularization.

3.6 Conclusions

This chapter has presented the simultaneous determination of time-dependent thermal conductivity and convection, or absorption coefficients from the measurements of heat moments in the one-dimensional parabolic heat equation. The resulting inverse problems have been reformulated as constrained regularized minimization problems which have been solved using the MATLAB optimization toolbox routine *lsqnonlin*. The following conclusions can be made:

• the IP2 seems more ill-posed that the IP1

• the retrieval of the diffusivity $a(t)$ is more stable and accurate than the retrieval of the lower-order coefficients $b(t)$ or $c(t)$

• the measurement of the heat moments (3.5) formulates a less stable inverse problem than the measurement of the heat fluxes (3.4)

The determination of three or more unknown coefficients in equation (3.1) will be investigated in a future work.

Chapter 4

Time-dependent reaction coefficient identification problems with a free boundary

4.1 Introduction

Coefficient identification problems involving an unknown free boundary are some of the most complicated and practically important problems, [117, 118, 120], and the Stefan problem is a particular example, [27, 45].

In [9, 68], the authors investigated free boundary problems with nonlinear diffusion. The numerical solution of inverse Stefan problems based on the method of fundamental solutions has been investigated in [51, 81]. The determination of time-dependent thermal coefficients was solved using the method of suboptimal stage-by-stage optimization in [11]. The heat equation with an unknown time-dependent thermal diffusivity or heat source in a domain with a free boundary has been investigated in [67] and [96], respectively. Time-dependent thermal conductivity identifications subject to various kind of overdetermination conditions have been studied in [93].

In recent papers, [61, 69], the authors have investigated the identification of multiple time-dependent coefficients together with an unknown free boundary. Continuing these analyses, in this chapter, we investigate the numerical reconstruction of time-dependent reaction coefficients in the heat equation with a free boundary subject to initial, Dirichlet and Stefan boundary conditions, as well as heat moment measurements. It should be noted that the fundamental contribution of this work is the proposal of a regularization algorithm to solve the identification problem and its numerical realization.

The chapter is structured in the following way. The mathematical formulation

of the inverse problems are formulated in Section 4.2. The numerical solution for the direct problem based on the FDM is briefly mentioned in Section 4.3. In Section 4.4, the numerical approach based on the minimization of the nonlinear Tikhonov regularization functional is introduced. Numerical results are presented and discussed in Section 4.5. Finally, conclusions are presented in Section 4.6.

4.2 Mathematical formulation

Consider the one-dimensional time-dependent parabolic heat equation

$$\frac{\partial u}{\partial t}(x,t) = a(x,t)\frac{\partial^2 u}{\partial x^2}(x,t) + b(x,t)\frac{\partial u}{\partial x}(x,t) + (c_1(t)x + c_2(t))u(x,t) + f(x,t), \quad (x,t) \in \Omega_T, \tag{4.1}$$

for the unknown temperature $u(x,t)$ in the moving domain $\Omega_T = \{(x,t)|0 < x < h(t), 0 < t < T\}$ with unknown free boundary $x = h(t) > 0$ and time-dependent coefficients $c_1(t)$ and $c_2(t)$, subject to the initial condition

$$u(x,0) = \phi(x), \quad 0 \le x \le h(0) =: h_0, \tag{4.2}$$

where $h_0 > 0$ is given, the Dirichlet boundary conditions

$$u(0,t) = \mu_1(t), \quad u(h(t),t) = \mu_2(t), \quad t \in [0,T], \tag{4.3}$$

and the over-determination conditions

$$h'(t) + u_x(h(t),t) = \mu_3(t), \quad t \in [0,T], \tag{4.4}$$

$$\int_0^{h(t)} u(x,t)dx = \mu_4(t), \quad t \in [0,T], \tag{4.5}$$

$$\int_0^{h(t)} xu(x,t)dx = \mu_5(t), \quad t \in [0,T], \tag{4.6}$$

where $\phi(x)$ and $\mu_i(t)$ for $i = \overline{1,5}$ are given functions. We assume that the functions in the above equations are sufficiently regular as required in the sequel and that the input data (4.2)–(4.6) are compatible.

Equation (4.4) represents a Stefan interface moving boundary condition. Also, equations (4.5) and (4.6) represent the specification of the energy (or mass) and heat momentum, respectively. In equation (4.1), the coefficients a and b representing diffusion and convection/advection are assumed to be known, as is the heat source f. Finally, remark that the reaction coefficient in (4.1) is linearly

dependent on the space variable x with two unknown time-dependent coefficients $c_1(t)$ and $c_2(t)$. This can also be seen as a particular case of a space and time-dependent blood perfusion coefficient in bio-heat transfer, [130].

We perform the change of variable $y = x/h(t)$, see [120], to reduce the problem (4.1)–(4.6) to the following inverse problem for the unknowns $h(t)$, $c_1(t)$, $c_2(t)$ and $v(y,t) := u(yh(t),t)$:

$$\frac{\partial v}{\partial t}(y,t) = \frac{a(yh(t),t)}{h^2(t)}\frac{\partial^2 v}{\partial y^2}(y,t) + \frac{b(yh(t),t) + yh'(t)}{h(t)}\frac{\partial v}{\partial y}(y,t) + (yh(t)c_1(t) + c_2(t))v(y,t) + f(yh(t),t),\ (y,t) \in Q_T, \tag{4.7}$$

in the fixed domain $Q_T := \{(x,t)|0 < y < 1, 0 < t < T\} = (0,1) \times (0,T)$,

$$v(y,0) = \phi(yh_0), \quad y \in [0,1], \tag{4.8}$$

$$v(0,t) = \mu_1(t), \quad v(1,t) = \mu_2(t), \quad t \in [0,T], \tag{4.9}$$

$$h'(t) + \frac{1}{h(t)}v_y(1,t) = \mu_3(t), \quad t \in [0,T], \tag{4.10}$$

$$h(t)\int_0^1 v(y,t)dy = \mu_4(t), \quad t \in [0,T], \tag{4.11}$$

$$h^2(t)\int_0^1 yv(y,t)dy = \mu_5(t), \quad t \in [0,T]. \tag{4.12}$$

The sketch of the transformed inverse problem under investigation is shown in Figure 4.1.

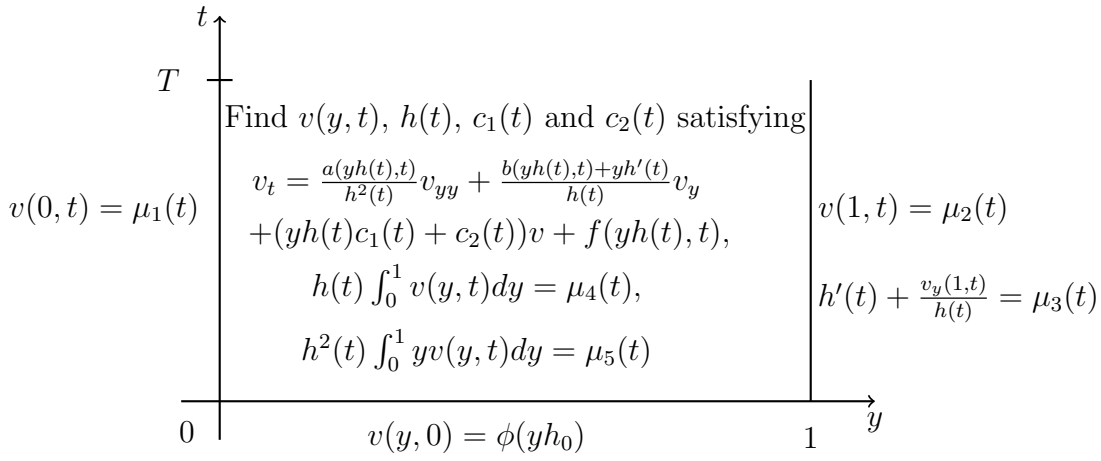

Figure 4.1: Sketch of the transformed inverse problem under investigation.

The uniqueness of a solution of the inverse problem (4.7)–(4.12) was established in [120] and reads as follows.

Theorem 4.2.1. *Assume that*

$$0 < a \in C^{2,0}([0,\infty) \times [0,T]),\ b, f \in C^{1,0}([0,\infty) \times [0,T]),$$
$$\phi(x) \geq \phi_0 > 0,\ x \in [0,\infty),\ \mu_i(t) > 0,\ i = 1,2,4,\ t \in [0,T].$$

Then, a solution $(h, c_1, c_2, v) \in C^1[0,T] \times (C[0,T])^2 \times C^{2,1}(\overline{Q_T})$, $h(t) > 0$ *for* $t \in [0,T]$, *of the inverse problem (4.7)–(4.12) is unique.*

Remark 1.
(*i*) The values of $c_1(0)$ and $c_2(0)$ can be determined using the compatibility of input data in (4.1)–(4.6), see [57, 120].
(*ii*) As remarked in [61, 69, 117], the Stefan condition (4.4) can be replaced by the second-order moment specification

$$\int_0^{h(t)} x^2 u(x,t)dx = \mu_6(t), \quad t \in [0,T], \tag{4.13}$$

or, in terms of the variable v, by

$$h^3(t) \int_0^1 y^2 v(y,t)dy = \mu_6(t), \quad t \in [0,T]. \tag{4.14}$$

4.3 Solution of direct problem

In this section we consider the direct initial boundary value problem given by equations (4.7)–(4.9), where $h(t)$, $c_1(t)$, $c_2(t)$, $a(x,t)$, $b(x,t)$, $f(x,t)$, $\phi(x)$, and $\mu_i(t)$, $i = 1,2$, are known and the solution $v(y,t)$ is to be determined together with the quantities of interest $\mu_i(t)$, $i = \overline{3,6}$. To achieve this, we use the FDM with the Crank-Nicolson scheme, [69], based on subdividing the solution domain $Q_T = (0,1) \times (0,T)$ into M and N subintervals of equal step lengths Δy and Δt, where $\Delta y = 1/M$ and $\Delta t = T/N$, respectively. At the node (i,j) we denote $v(y_i, t_j) = v_{i,j}$, where $y_i = i\Delta y$, $t_j = j\Delta t$, $a(y_i,t_j) = a_{i,j}$, $b(y_i,t_j) = b_{i,j}$, $h(t_j) = h_j$, $c_1(t_j) = c1_j$, $c_2(t_j) = c2_j$, and $f(y_i,t_j) = f_{i,j}$ for $i = \overline{0,M}$ and $j = \overline{0,N}$. The expressions in equations (4.10)–(4.12) and (4.14) are calculated using the following finite difference approximation formula and trapezoidal rule for integrals:

$$\mu_3(t_j) = \frac{h_j - h_{j-1}}{\Delta t} - \frac{4v_{M-1,j} - v_{M-2,j} - 3v_{M,j}}{2(\Delta y)h_j}, \quad j = \overline{1,N}, \tag{4.15}$$

$$\mu_{k+3}(t_j) = \frac{h_j^k}{2N}\Big(y_0^{k-1}v_{0,j} + y_M^{k-1}v_{M,j} + 2\sum_{i=1}^{M-1} y_i^{k-1}v_{i,j}\Big), \quad j = \overline{1,N}, \quad k = 1,2,3. \tag{4.16}$$

4.4 Numerical approach for the inverse problem

In this section, we wish to obtain a simultaneous stable determination of the two unknown coefficients $c_1(t)$ and $c_2(t)$, together with the free boundary $h(t)$ and the transformed temperature $v(y,t)$, satisfing equations (4.7)–(4.12), or (4.7)–(4.9), (4.11), (4.12) and (4.14). The inverse problem can be formulated as a nonlinear minimization of the Tikhonov regularization function

$$F(\mathbf{h},\mathbf{c_1},\mathbf{c_2}) = \sum_{j=1}^{N}\Big[\frac{h_j - h_{j-1}}{\Delta t} + \frac{v_y(1,t_j)}{h_j} - \mu_3(t_j)\Big]^2 + \sum_{j=1}^{N}\Big[h_j\int_0^1 v(y,t_j)dy - \mu_4(t_j)\Big]^2 + \sum_{j=1}^{N}\Big[h_j^2\int_0^1 yv(y,t_j)dy - \mu_5(t_j)\Big]^2 + \beta_1\sum_{j=1}^{N}h_j^2 + \beta_2\sum_{j=1}^{N}c_{1j}^2 + \beta_3\sum_{j=1}^{N}c_{2j}^2, \tag{4.17}$$

or,

$$F(\mathbf{h},\mathbf{c_1},\mathbf{c_2}) = \sum_{j=1}^{N}\Big[h_j\int_0^1 v(y,t_j)dy - \mu_4(t_j)\Big]^2 + \sum_{j=1}^{N}\Big[h_j^2\int_0^1 yv(y,t_j)dy - \mu_5(t_j)\Big]^2 + \sum_{j=1}^{N}\Big[h_j^3\int_0^1 y^2v(y,t_j)dy - \mu_6(t_j)\Big]^2 + \beta_1\sum_{j=1}^{N}h_j^2 + \beta_2\sum_{j=1}^{N}c_{1j}^2 + \beta_3\sum_{j=1}^{N}c_{2j}^2, \tag{4.18}$$

where v solves (4.7)–(4.9) for given (h, c_1, c_2). The minimization of the objective function (4.17), or (4.18), is performed using the MATLAB toolbox routine *lsqnonlin*. This routine attempts to find the minimum of a sum of squares by starting from the initial guesses $\mathbf{h}^{(0)}$, $\mathbf{c_1}^{(0)}$ and $\mathbf{c_2}^{(0)}$ for $\mathbf{h}$, $\mathbf{c_1}$ and $\mathbf{c_2}$, respectively. We have compiled this routine with the following specifications:

- Algorithm is the Trust Region Reflective (TRR) minimization, [31].
- Maximum number of iterations, (MaxIter) = 10×(number of variables).
- Maximum number of objective function evaluations, (MaxFunEvals) = 10^5×(number of variables).

- Termination tolerance on the function value, (TolFun) = 10^{-20}.
- Solution tolerance value, (xTol)=10^{-20}.
- The lower and upper simple bounds are 10^{-10} and 10^{3} for h, and -10^{3} and 10^{3} for c_1 and c_2.

The inverse problems are solved subject to both exact and noisy input data which is numerically simulated as follows:

$$\mu_{k+2}^{\epsilon k}(t_j) = \mu_{k+2}(t_j) + \epsilon k_j, \quad j = \overline{1, N}, \quad k = \overline{1, 4}, \tag{4.19}$$

where ϵk_j are random variables generated from a Gaussian normal distribution with mean zero and standard deviation σ_k given by

$$\sigma_k = p \times \max_{t\in[0,T]} |\mu_{k+2}(t)|, \quad k = \overline{1, 4}, \tag{4.20}$$

where p represents the percentage of noise. We use the MATLAB function $normrnd(0, \sigma_k, N)$ to generate the random variables $(\epsilon k_j)_{j=\overline{1,N}}$ for $k = \overline{1, 4}$.

4.5 Numerical results and discussion

In this section we investigate a couple of examples in order to assess the accuracy and stability of the numerical methods introduced in Section 4.3 for the direct problem based on the FDM with $M = N = 40$, and in Section 4.4 for the numerical approach to solve the inverse problem based on minimizing the nonlinear Tikhonov regularization objective functional (4.17) or (4.18). Furthermore, we add noise to the input data in equations (4.10)–(4.12) and (4.14) to mimic the real situation of measurement errors, by using equations (4.19) and (4.20). We compute the root mean squares error given by

$$rmse(h) = \left[\frac{T}{N}\sum_{j=1}^{N}\left(h^{numerical}(t_j) - h^{exact}(t_j)\right)^2\right]^{1/2}, \tag{4.21}$$

and similar expressions exist for $c_1(t)$ and $c_2(t)$. For simplicity, we take $T = 1$ in all examples.

4.5.1 Example 1

We consider the inverse problem (4.1)–(4.6) with unknown coefficients $h(t)$, $c_1(t)$ and $c_2(t)$, and the input data given by

$$a(x,t)=\frac{1}{2}(1+t)+x,\quad b(x,t)=-1-x-t,\quad \phi(x)=2+x,$$
$$\mu_1(t)=e^t(2+t),\quad \mu_2(t)=e^t(3+2t),\quad \mu_3(t)=1+e^t,$$
$$\mu_4(t)=\frac{1}{2}e^t(1+t)(5+3t),\quad \mu_5(t)=\frac{1}{4}(1+t)^2(3+6t+t^2),\quad h_0=1,$$
$$f(x,t)=e^t(2+t+x)(3+t+x+tx). \quad (4.22)$$

One can observe that the conditions of Theorem 4.2.1 are satisfied and hence, the uniqueness of solution is guaranteed. The analytical solution is given by

$$h(t)=1+t,\quad c_1(t)=-1-t,\quad c_2(t)=-1-t, \quad (4.23)$$

$$u(x,t)=e^t(2+t+x). \quad (4.24)$$

Also, the analytical solution for the transformed temperature $v(y,t)$ satisfying (4.7)–(4.12) is given by

$$v(y,t)=e^t\Big(2+t+y(1+t)\Big). \quad (4.25)$$

The initial guesses for the vectors $\mathbf{h}$, $\mathbf{c_1}$ and $\mathbf{c_2}$ are taken as

$$h^0(t_j)=h(0)=h_0=1,\quad c_1^0(t_j)=c_1(0)=-1,\quad c_2^0(t_j)=c_2(0)=-1,$$
$$j=\overline{1,N}, \quad (4.26)$$

where the values of $c_1(0)$ and $c_2(0)$ have been obtained exactly using the compatibility of (4.1)–(4.6).

We consider first the case when there is no noise in the input data μ_3, μ_4 and μ_5, i.e. $p=0$ in (4.20). The objective function (4.17), as a function of a number of iterations, is plotted in Figure 4.2, with and without regularization. From this figure, it can be seen that a rapid monotonic decreasing convergence is achieved in a few iterations.

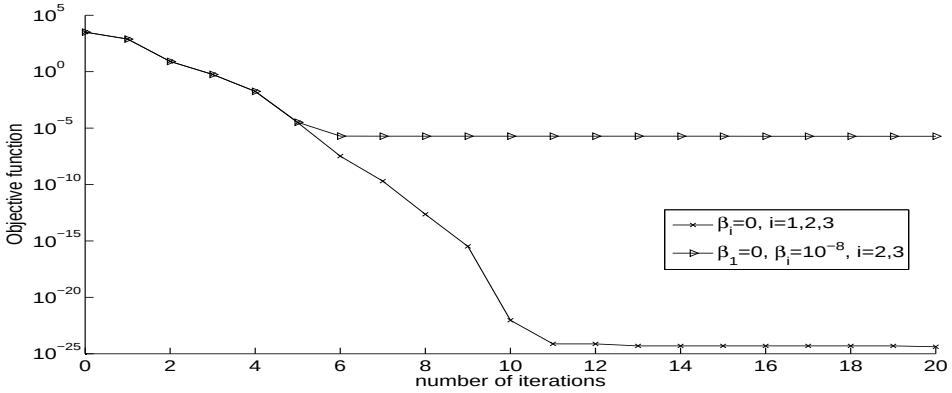

Figure 4.2: The objective function (4.17), as a function of a number of iterations, no noise, with and without regularization, for Example 1.

The *rmse* values for the unknowns coefficients $h(t)$, $c_1(t)$ and $c_2(t)$, obtained with and without regularization are presented, versus the number of iterations, in Figure 4.3. The corresponding numerical solutions obtained after 20 iterations (in 38 minutes computational time) are illustrated in Figure 4.4 (for $h(t)$, $c_1(t)$ and $c_2(t)$) and Figure 4.5 (for $v(y,t)$).

First, from Figure 4.3 it can be observed that $rmse(h)$ values are much lower than the $rmse(c_i)$, $i = 1, 2$, indicating that the free boundary $h(t)$ is retrieved more accurately than the coefficients c_1 and c_2. Second, from Figure 4.3 it can be observed that in the case of no regularization the *rmse* values settle to stationary levels after 6 to 8 iterations. However, the numerical results presented in Figure 4.4 show that whilst the retrieval of $h(t)$, see Figure 4.4(a), is very accurate, instabilities manifest in the unregularized solutions for the coefficients $c_1(t)$ and $c_2(t)$, see Figures 4.4(b) and 4.4(c), respectively. Note that although there is no random noise numerically simulated through (4.19), there still exists some small numerical noise caused by the discrepancy between the FDM direct problem numerical solution with a fixed mesh size and the exact values of the data (4.22). Thus the instabilities for the unregularized solution illustrated in Figures 4.4(b) and 4.4(c) show that the inverse coefficient identification problem is ill-posed in the coefficients $c_1(t)$ and $c_2(t)$. These will be even more amplified when later on we will include noise in the data (4.19). Including a small regularization in (4.17) alleviates this instability, as shown in the regularized numerical results in Figures 4.3 and 4.4. The choice of $\beta_1 = 0$, $\beta_2 = \beta_3 = 10^{-8}$ is of course not optimal and in fact these regularization parameters may still be too small, see for example, the occurence of minima in the *rmse* values after a certain number of iterations. But overall, corroborated with the more stable results achieved in Figures 4.4(b) and 4.4(c), it shows that regularization is required in order to

obtain stable solutions for the coefficients $c_1(t)$ and $c_2(t)$. Finally, by inspecting Figures 4.4(a) and 4.5 it can be seen that the inverse problem seems stable in the components $h(t)$ and $v(y,t)$ of the solution for which regularization is not necessary. Based on this argument we shall take $\beta_1 = 0$, i.e. we do not penalise $\mathbf{h}$ in (4.17) (or (4.18)), in the remaining of the chapter.

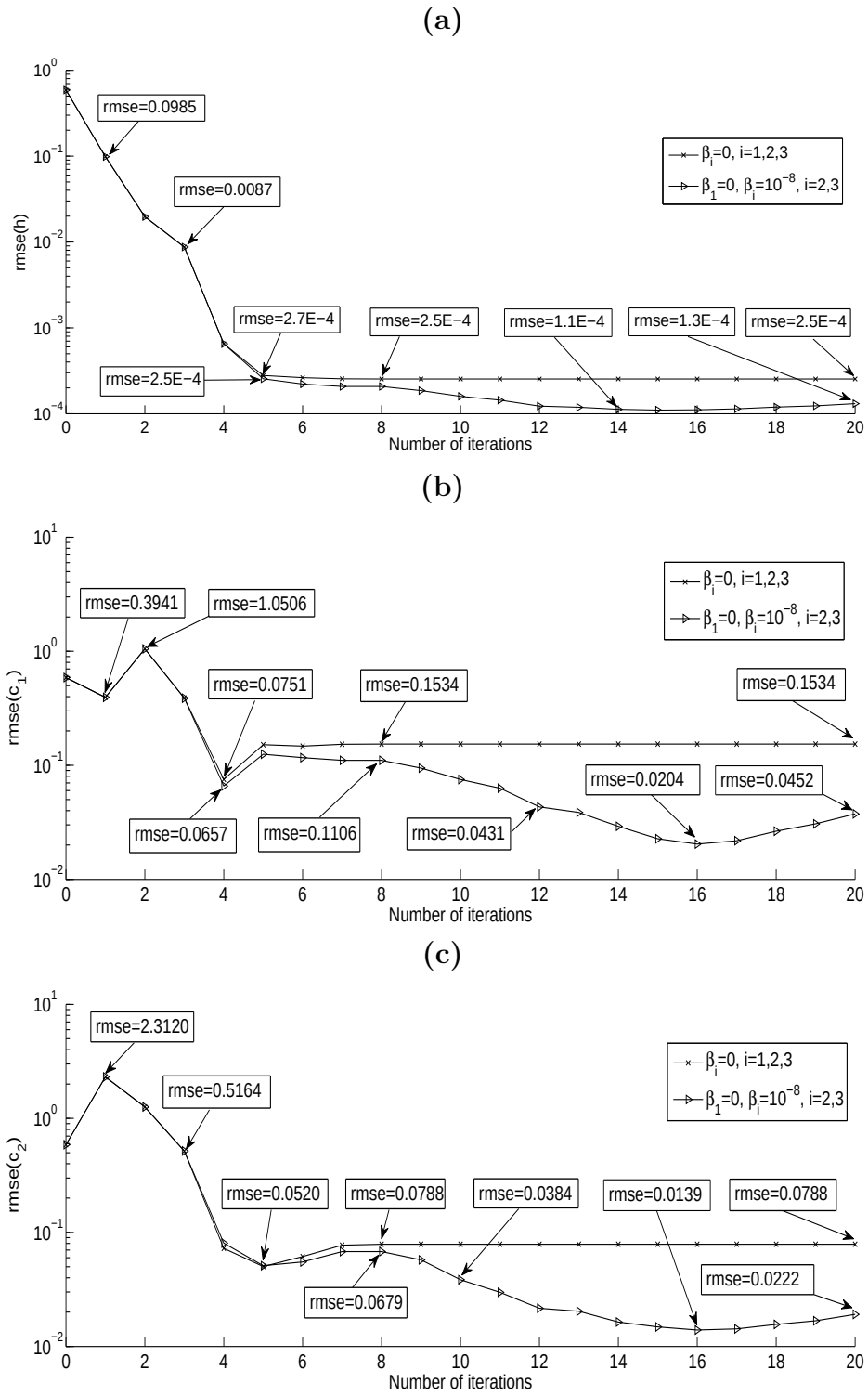

Figure 4.3: The *rmse*: (a) $rmse(h)$, (b) $rmse(c_1)$ and (c) $rmse(c_2)$, as functions of the number of iterations, no noise, with and without regularization, for Example 1.

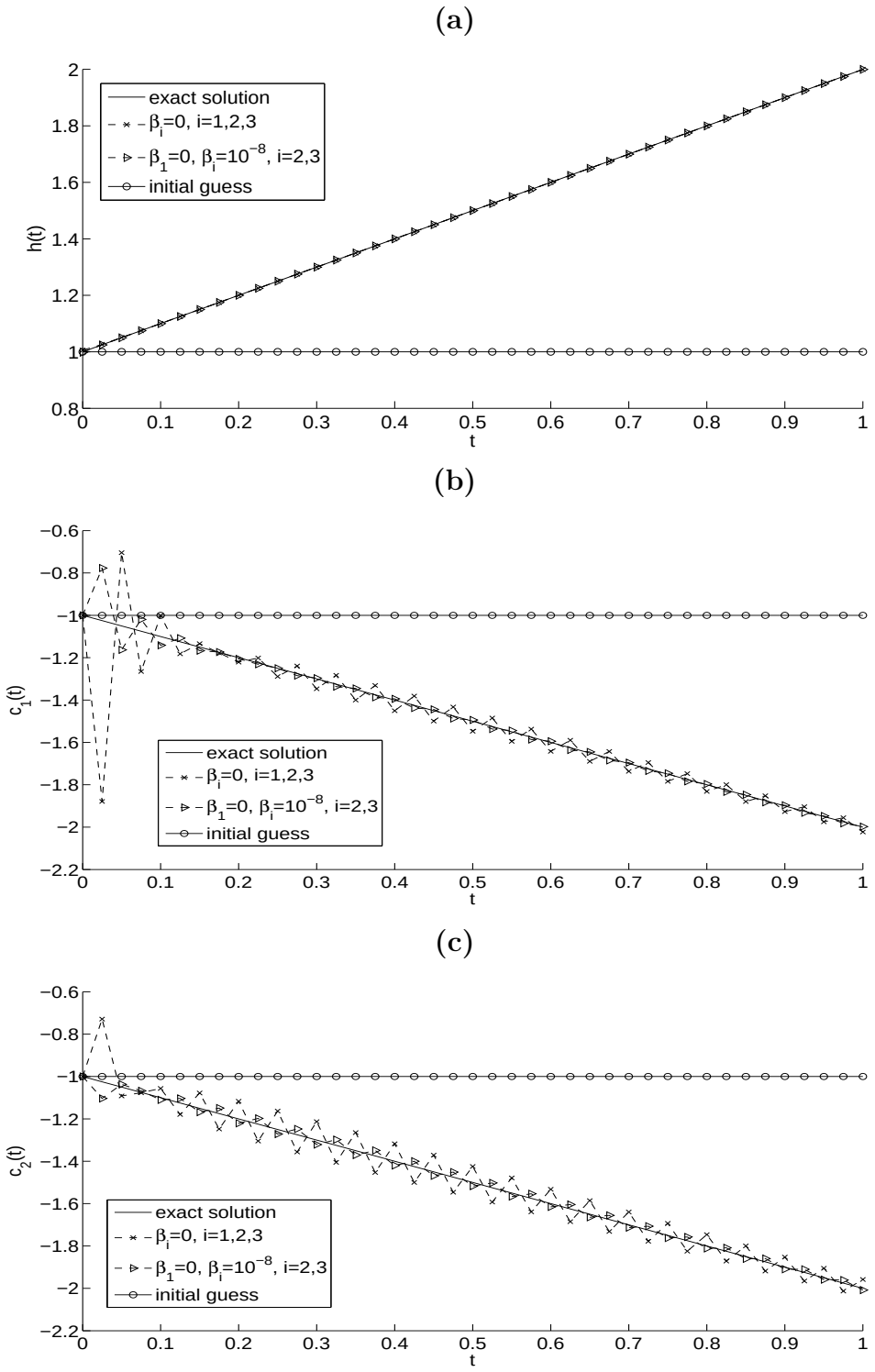

Figure 4.4: The exact (4.23) and numerical solutions for: (a) $h(t)$, (b) $c_1(t)$ and (c) $c_2(t)$, no noise, with and without regularization, for Example 1.

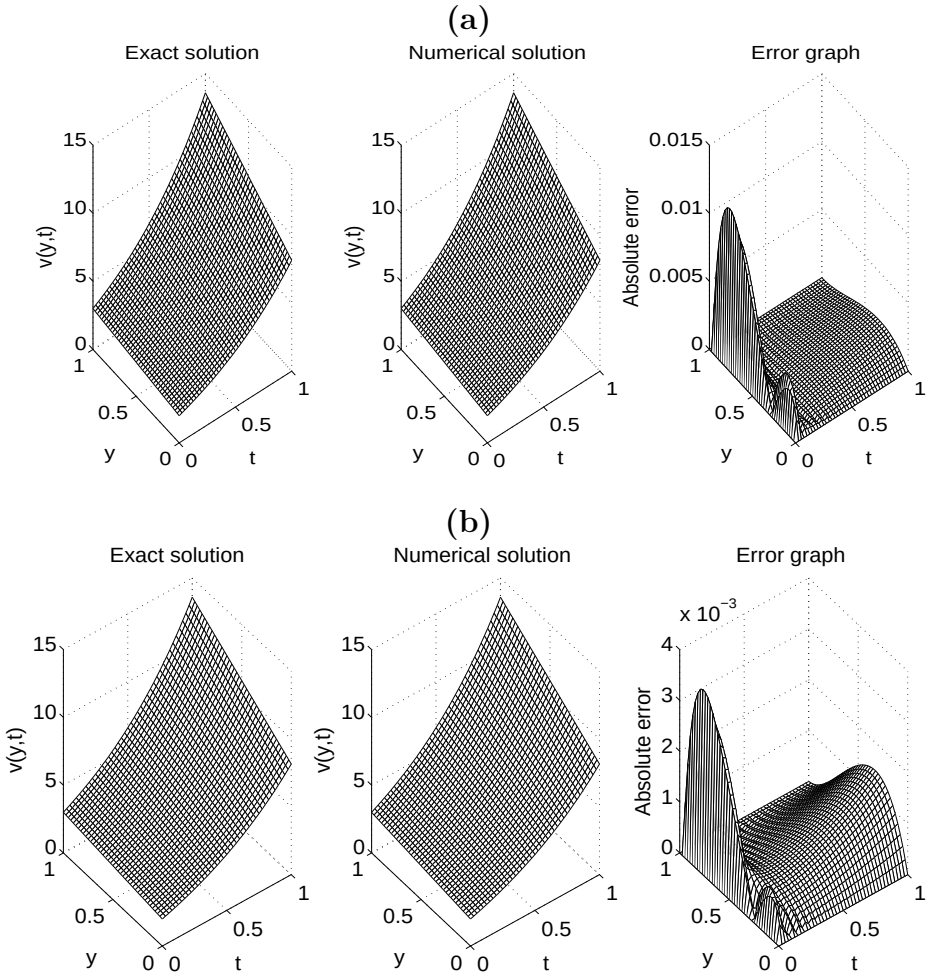

Figure 4.5: The exact (4.25) and numerical solutions for the transformed temperature $v(y,t)$, for Example 1, no noise, with (a) $\beta_i = 0, i = 1,2,3$ and (b) $\beta_1 = 0, \beta_i = 10^{-8}, i = 2,3$. The absolute error between them is also included.

Next, we add a small amount of $p = 0.01\%$ noise to the data $\mu_3(t), \mu_4(t)$ and $\mu_5(t)$, as in (4.19), in order to model the errors which are inherently present in any practical measurement and moreover, to investigate the stability of the numerical results. We have also experimented with higher amounts of noise p in equation (4.20), but the results obtained were less accurate and therefore they are not presented. From the previous analysis, we anticipate that the regularization is needed in order to achieve stable and accurate results because the problem is ill-posed and very sensitive to noise. The decreasing convergence of the objective function (4.17), as a function of the number of iterations, is shown in Figure 4.6 with and without regularization. Notice that the total amount of noise included in the input data when $p = 0.01\%$ is 0.0220.

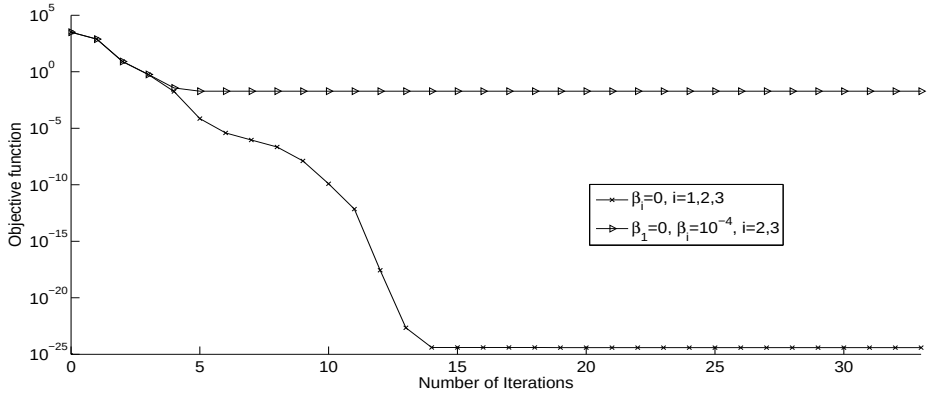

Figure 4.6: The objective function (4.17), as a function of a number of iterations, $p = 0.01\%$ noise, with and without regularization, for Example 1.

As previously argued, since there is no need to regularize the free boundary $h(t)$ we fix $\beta_1 = 0$. Also, taking $\beta_2 = \beta_3$, as positive regularization parameters in (4.17), the L-curve, [47, 48], for the choice of the regularization parameter is shown in Figure 4.7, by plotting the solution norm $\sqrt{||\mathbf{h}||^2+||\mathbf{c_1}||^2+||\mathbf{c_2}||^2}$, as a function of the residual norm given by square root of the sum of first three terms in the right-hand side of (4.17). From this figure, it can be seen that regularization parameters near the "corner" of the L-curve are $\beta_2 = \beta_3 \in \{10^{-6}, 10^{-5}, 10^{-4}\}$.

The exact and numerical solutions for the free boundary $h(t)$, and the coefficients $c_1(t)$ and $c_2(t)$, with and without regularization are shown in Figure 4.8. From this figure, it can be noticed that the accurate and stable results are achieved for the free boundary $h(t)$ both with and without regularisation, but unstable results are obtained for the coefficients $c_1(t)$ and $c_2(t)$, if no regularization is imposed with $rmse(c_1) = 0.5645$ and $rmse(c_2) = 0.5949$. In order to stabilise the coefficients $c_1(t)$ and $c_2(t)$, we employed regularization with $\beta_1 = 0$, $\beta_2 = \beta_3 = 10^{-4}$ (given by the L-curve in Figure 4.7), obtaining $rmse(c_1) = 0.1089$ and $rmse(c_2) = 0.1040$. Finally, the numerical solutions for $v(y, t)$ were obtained stable and accurate and, for brevity, they are not presented.

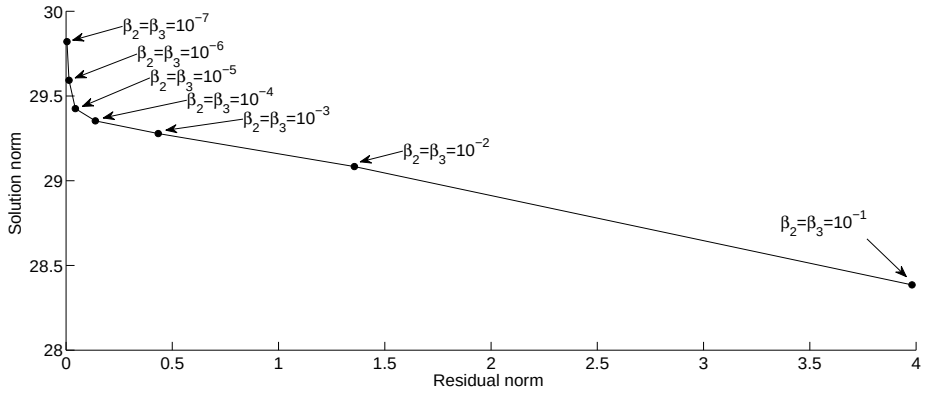

Figure 4.7: The residual norm versus the solution norm for various regularization parameters $\beta_2 = \beta_3 \in \{10^{-i} | i = \overline{1,7}\}$, for Example 1 with $p = 0.01\%$ noise.

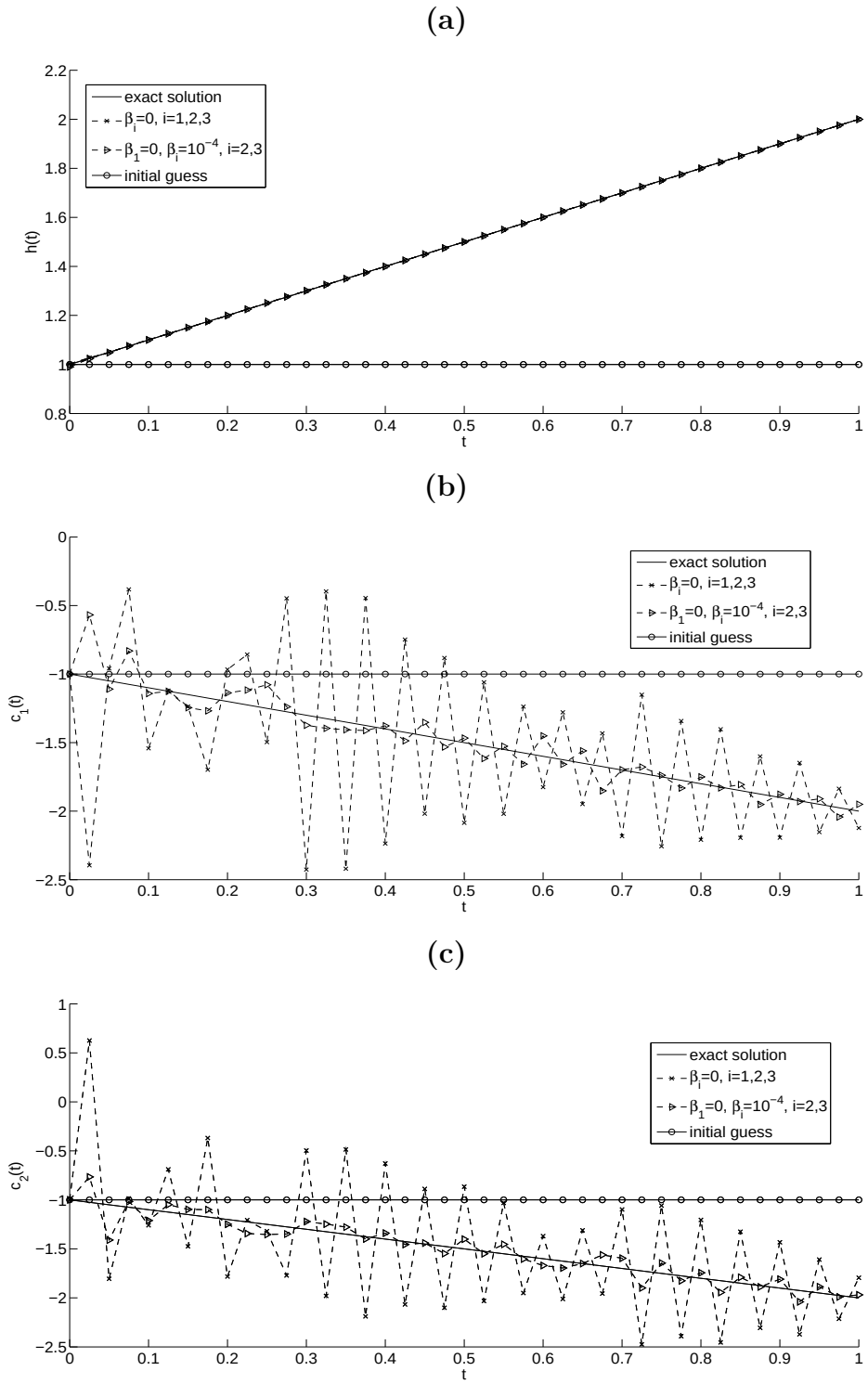

Figure 4.8: The exact (4.23) and numerical solutions for: (a) $h(t)$, (b) $c_1(t)$ and (c) $c_2(t)$, $p = 0.01\%$ noise, with and without regularization, for Example 1.

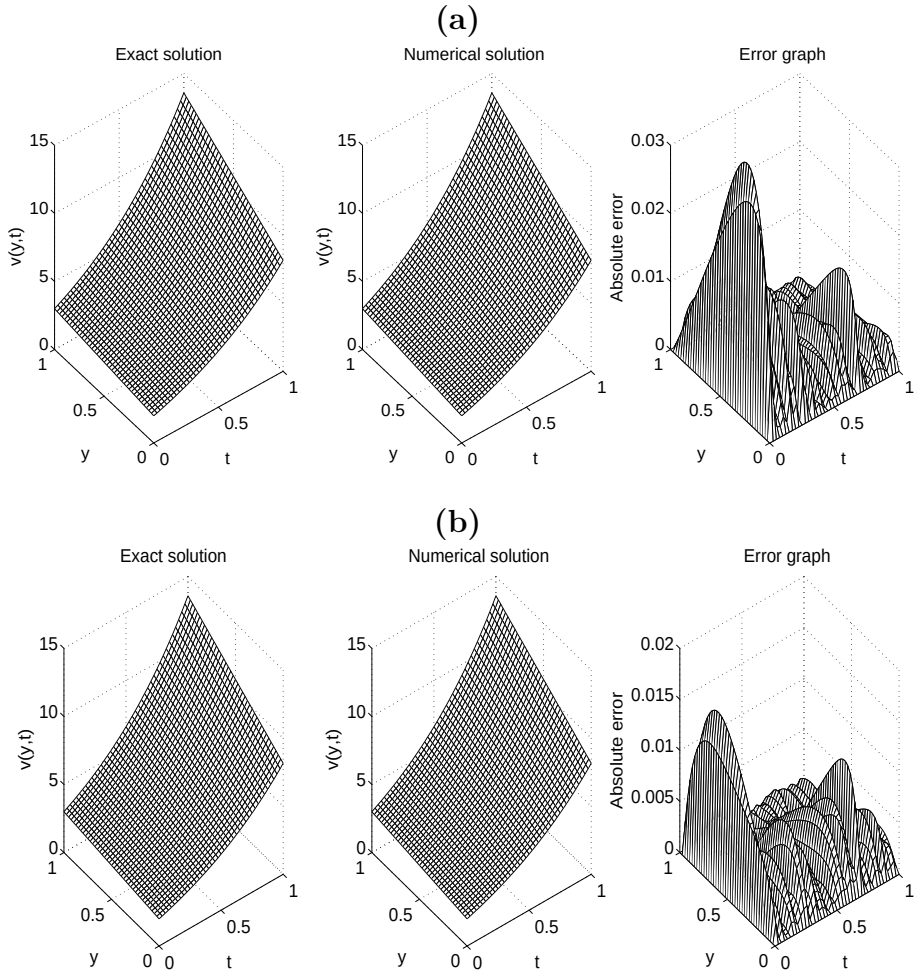

Figure 4.9: The exact (4.25) and numerical solutions for the transformed temperature $v(y,t)$, for Example 1, $p = 0.01\%$ noise, with (a) $\beta_i = 0, i = 1,2,3$ and (b) $\beta_1 = 0, \beta_i = 10^{-4}, i = 2,3$. The absolute error between them is also included.

4.5.2 Example 2

In this example we consider the second inverse problem given by equations (4.1)–(4.3), (4.5), (4.6) and (4.13), with the same input data (4.22) as in Example 1, except that the data $\mu_3(t)$ given by equation (4.4) is replaced by the second-order heat moment $\mu_6(t)$ given by equation (4.14) as

$$\mu_6(t) = \frac{1}{12} e^t (t+1)^3 (7t+11), \quad t \in [0,1]. \tag{4.27}$$

Also, the initial guesses for the vectors $\mathbf{h}$, $\mathbf{c_1}$ and $\mathbf{c_2}$ are given by equation (4.26), the same as in Example 1.

Figures 4.10–4.17 for Example 2 are the corresponding analogues of Figures 4.2–4.9 for Example 1 and, in order to avoid repetition, we shall discuss below only the main similarities and differences between the two examples.

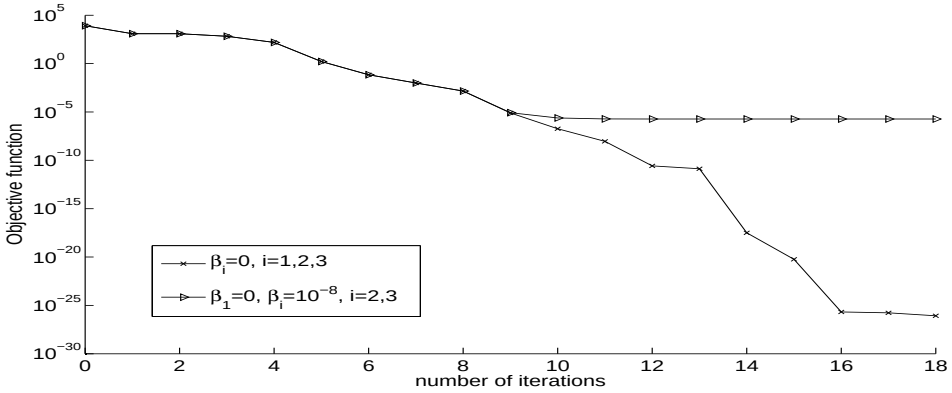

Figure 4.10: The objective function (4.18), as a function of a number of iterations, no noise, with and without regularization, for Example 2.

Whilst all the results of Examples 1 and 2 are consistent in terms of the numerical regularization method employed being accurate and stable, overall one can see that the second inverse problem (Example 2) is more ill-posed than the first inverse problem (Example 1). This can be seen by:
(i) the larger number of iterations required to achieve convergence in the case of no noise (compare Figures 4.2 and 4.10);
(ii) the more enhanced non-monotonic behaviour of the $rmse$ curves (compare Figures 4.3 and 4.11);
(iii) the higher and larger oscillations manifested in retrieving the coefficients $c_1(t)$ and $c_2(t)$ in case of no regularization (compare Figures 4.4, 4.8 and 4.12, 4.16);
(iv) the larger $rmse$ values, as illustrated by the comparison shown in Table 4.1.

Table 4.1: The $rmse$ values for Examples 1 and 2.

Example 1	$rmse(h)$	$rmse(c_1)$	$rmse(c_2)$
$p = 0, \beta_1 = \beta_2 = 0$	2.5E-4	0.1534	0.0788
$p = 0, \beta_1 = \beta_2 = 10^{-8}$	1.3E-4	0.0452	0.0222
$p = 0.01\%, \beta_1 = \beta_2 = 0$	6.1E-4	0.5645	0.5949
$p = 0.01\%, \beta_1 = \beta_2 = 10^{-4}$	4.7E-4	0.1089	0.1040
Example 2	$rmse(h)$	$rmse(c_1)$	$rmse(c_2)$
$p = 0, \beta_1 = \beta_2 = 0$	6.8E-4	0.4892	0.4480
$p = 0, \beta_1 = \beta_2 = 10^{-8}$	6.8E-4	0.1968	0.0504
$p = 0.01\%, \beta_1 = \beta_2 = 0$	3.3E-3	6.6965	3.7308
$p = 0.01\%, \beta_1 = \beta_2 = 10^{-4}$	2.2E-3	0.3587	0.2376

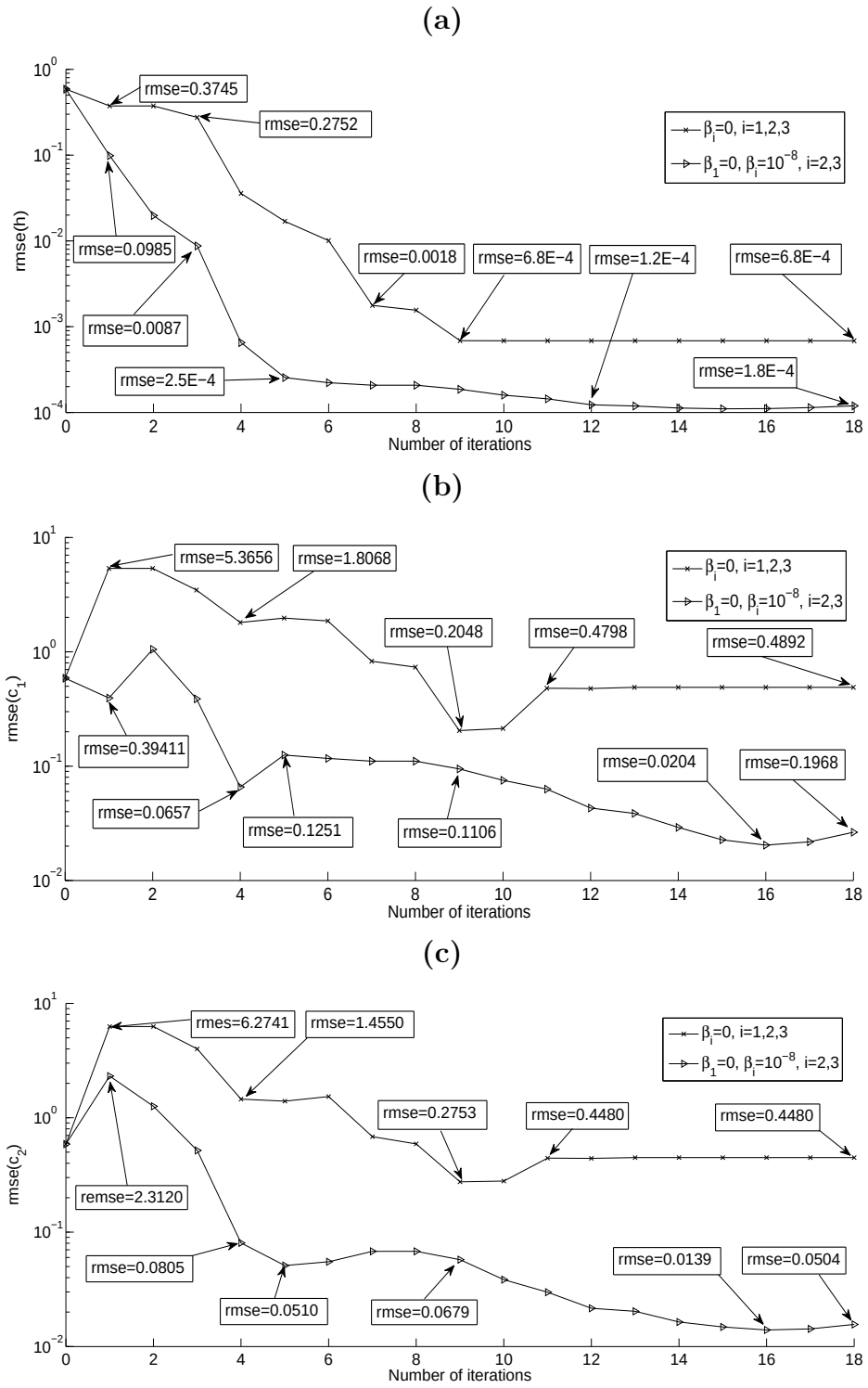

Figure 4.11: The $rmse$: (a) $rmse(h)$, (b) $rmse(c_1)$ and (c) $rmse(c_2)$, as functions of the number of iterations, no noise, with and without regularization, for Example 2.

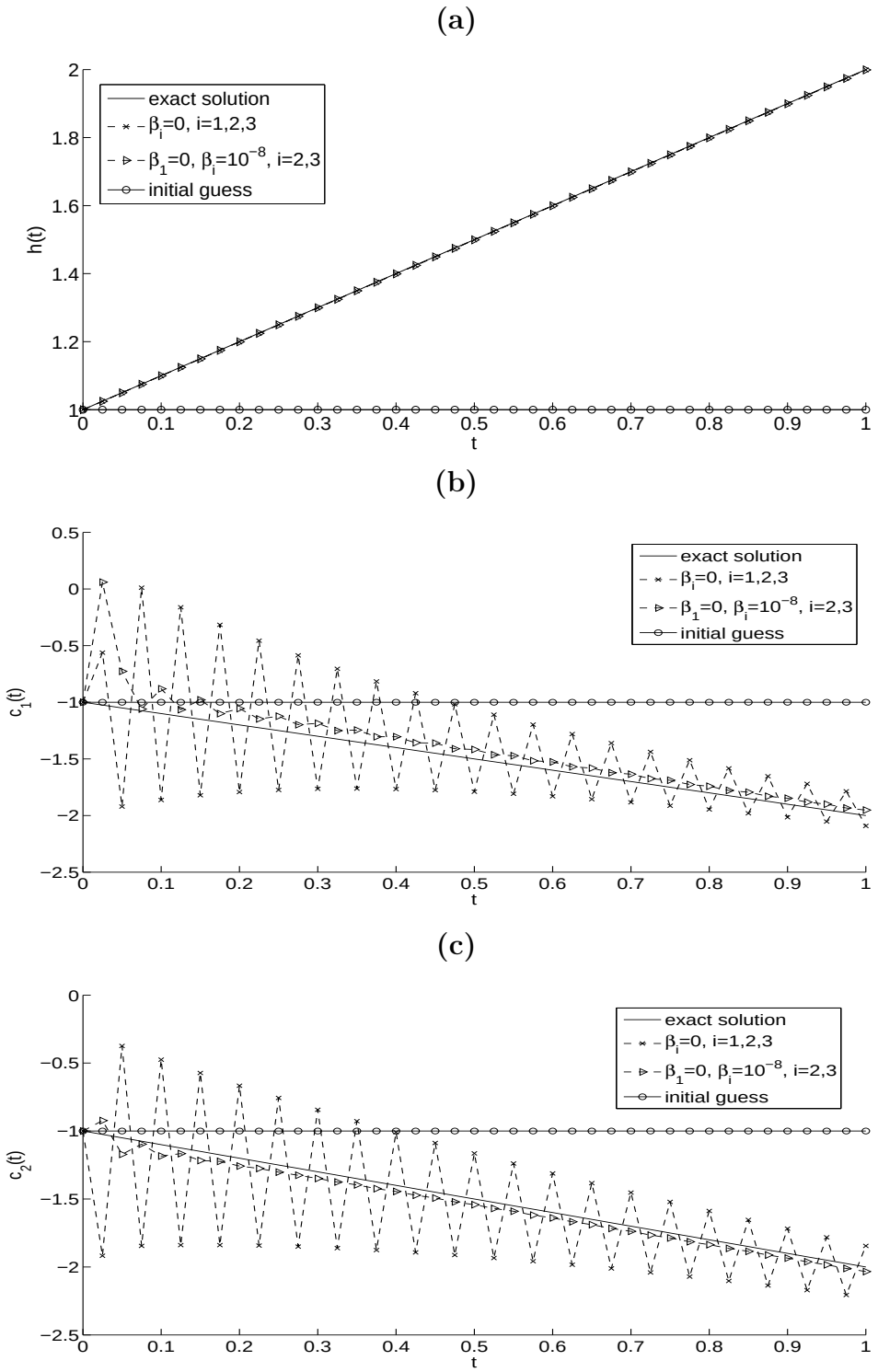

Figure 4.12: The exact (4.23) and numerical solutions for: (a) $h(t)$, (b) $c_1(t)$ and (c) $c_2(t)$, no noise, with and without regularization, for Example 2.

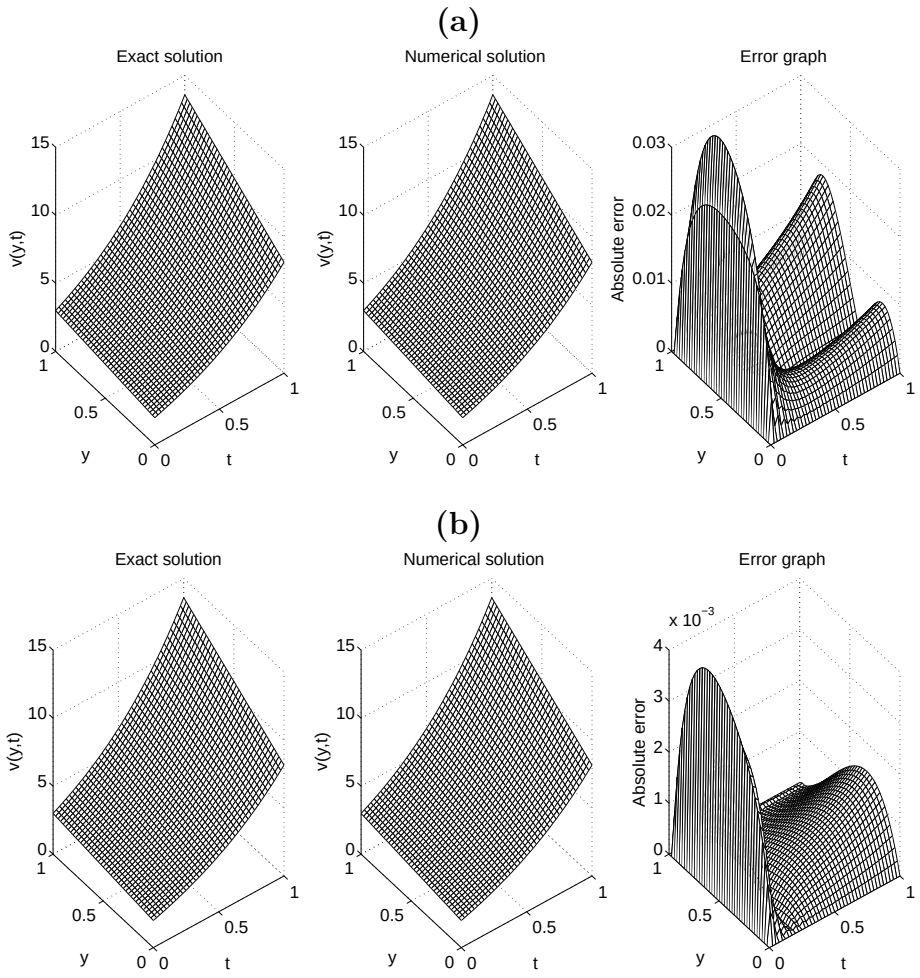

Figure 4.13: The exact (4.25) and numerical solutions for the transformed temperature $v(y,t)$, for Example 2, no noise, with (a) $\beta_i = 0, i = 1,2,3$ and (b) $\beta_1 = 0, \beta_i = 10^{-8}, i = 2,3$. The absolute error between them is also included.

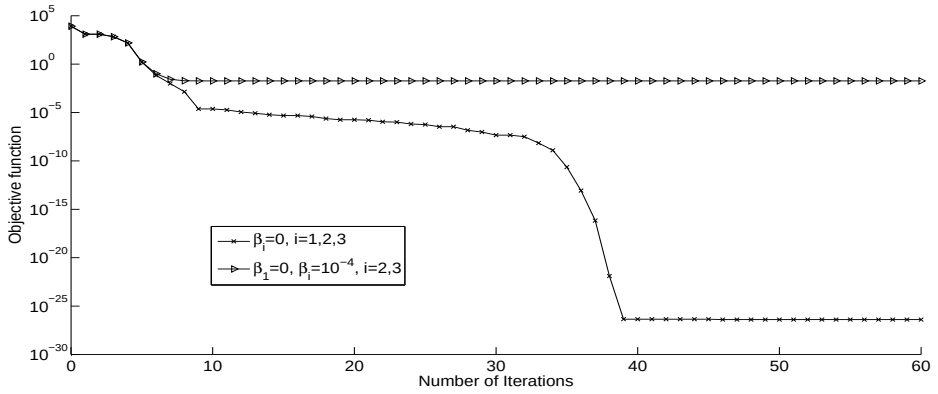

Figure 4.14: The objective function (4.18), as a function of a number of iterations, $p = 0.01\%$ noise, with and without regularization, for Example 2. Notice that the total amount of noise included in the input data when $p = 0.01\%$ is 0.0349.

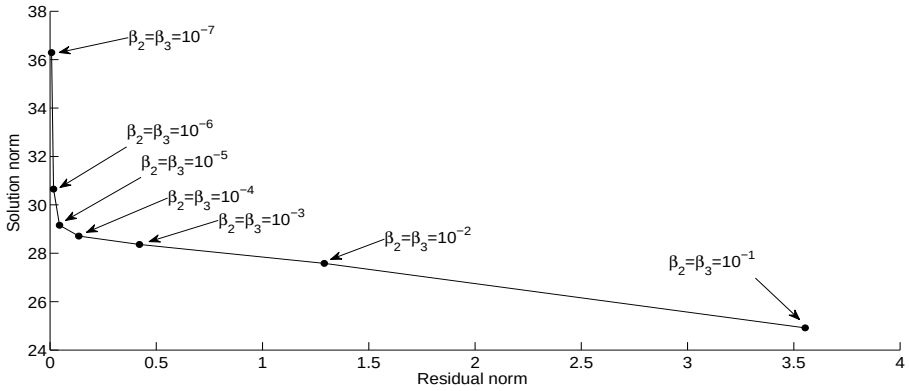

Figure 4.15: The residual norm (given by the square root of the first three terms in the right-hand side of (4.18)) versus the solution norm for various regularization parameters $\beta_2 = \beta_3 \in \{10^{-i} | i = \overline{1,7}\}$, for Example 2 with $p = 0.01\%$ noise.

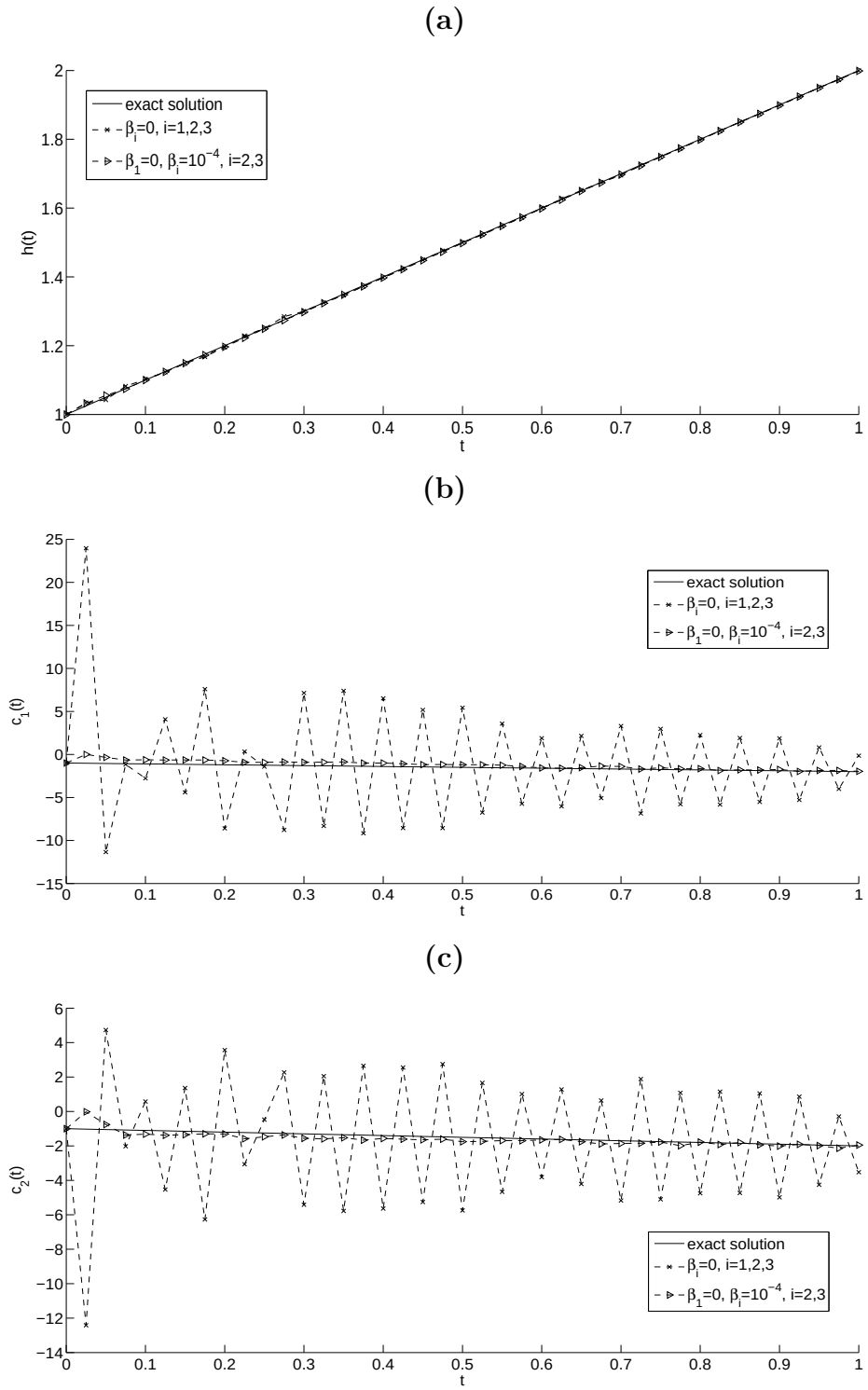

Figure 4.16: The exact (4.23) and numerical solutions for: (a) $h(t)$, (b) $c_1(t)$ and (c) $c_2(t)$, $p = 0.01\%$ noise, with and without regularization, for Example 2.

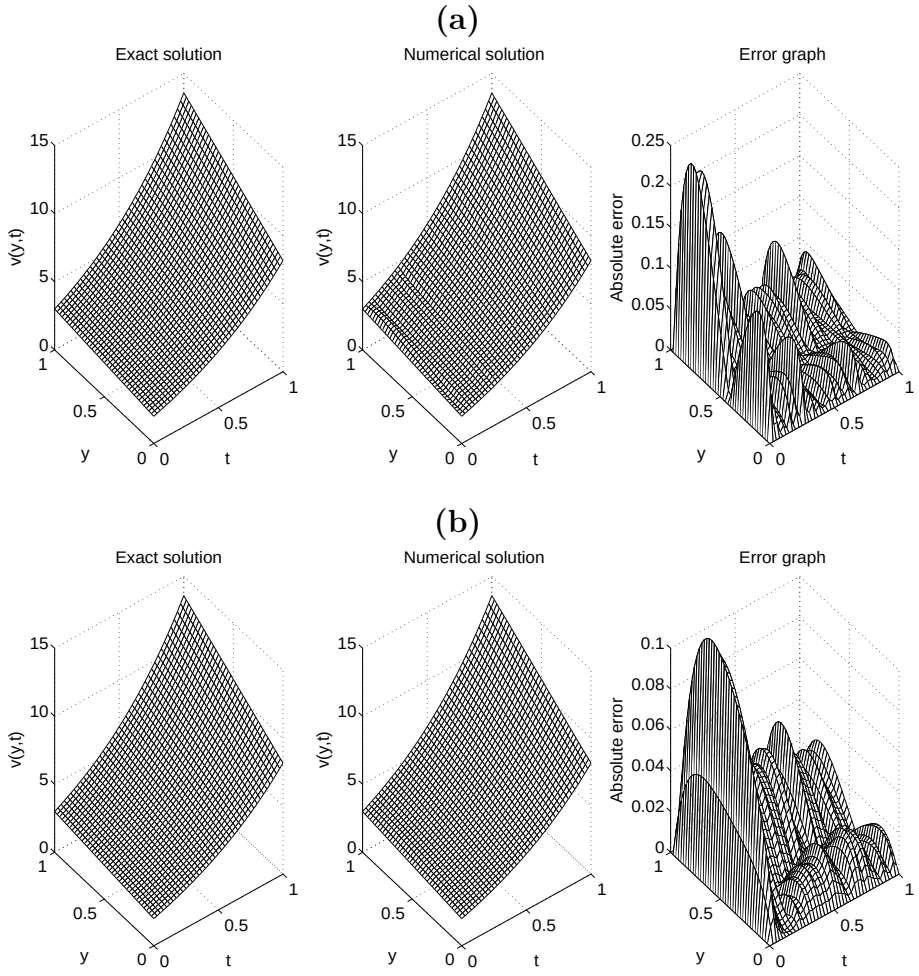

Figure 4.17: The exact and numerical solutions for the transformed temperature $v(y,t)$, for Example 2, $p = 0.01\%$ noise, with (a) $\beta_i = 0, i = 1,2,3$ and (b) $\beta_1 = 0, \beta_i = 10^{-4}, i = 2,3$. The absolute error between them is also included.

4.6 Conclusions

In this chapter, inverse nonlinear problems consisting of simultaneously identifying time-dependent reaction coefficients in the heat equation with a free boundary have been investigated. The direct solver based on the FDM with the Crank-Nicolson scheme has been employed. The inverse problem was solved using the MATLAB optimisation toolbox routine *lsqnonlin* for minimizing the nonlinear Tikhonov regularization functional. The accuracy and stability of the numerical results for the two inverse problems, for Examples 1 and 2, have been assessed. Based on the numerical results and discussion we can conclude that the Stefan condition (4.4) contains more information than the second-order heat moment condition (4.13). Although not illustrated, it is reported that similar conclusions have been obtained for many other numerical tests that we have investigated in-

cluding the recovery of non-smooth reaction coefficients. Extension to the case when both ends of the finite slab are moving, [119, 121], will be addressed in the next chapter.

Chapter 5

Determination of time-dependent coefficients and multiple free boundaries

5.1 Introduction

Free boundary problems involving Stefan condition have been considered to be one of the most important directions in the analysis of PDEs, with an abundance of applications to real world problems, including physics, chemistry, biology, [42], engineering, industry and other areas, [9, 26, 43]. For instance, during heat diffusion in melting ice, the boundary of the ice keeps on shifting, [69], and the latent heat is absorbed or released by the thermodynamic system without a change in temperature, [25]. In [24], the authors have discussed free boundary problems arising in two new scenarios, nonlocal diffusion and aggregation processes. The challenge of free boundary problems lies in the fact that the solution domain is unknown and has to be determined.

Determination of time-dependent coefficients problems involving free boundaries have been the point of interest of some recent works by Snitko [117, 118, 120]. In addition, in [96], the author investigated the parabolic heat equation with an unknown heat source and with a known moving boundary.

Inverse coefficient determination problems with one or several unknown coefficients play a substantial role in the theory and application of inverse problems. Using a simple change of variables, free boundary problems can be reduced to inverse coefficient problems in a fixed domain.

In recent papers, [57, 69] and the previous chapter the authors have investigated the determination of multiple time-dependent coefficients together with an unknown one side free boundary of the finite slab $0 < x < h(t)$. In this

chapter, we extend these analyses and investigate the determination of time-dependent coefficients together with two unknown free boundaries of the finite slab $h_1(t) < x < h_2(t)$. The inverse problems investigated in this chapter have already been proved to be locally uniquely solvable by Snitko [119, 121], but no reconstruction has been attempted, and it is the aim of this chapter to undertake the numerical solution of these problems.

The organization of the chapter is as follows. The mathematical statements of the inverse problems are described in Section 5.2. In Section 5.3, the solution of the direct problem based on the FDM with the Crank-Nicolson scheme is presented. Since the inverse problem is ill-posed (in the sense that the continuous dependence upon the input data is violated), the numerical method based on the FDM direct solver is combined with the Tikhonov regularization method, as described in Section 5.4. In Section 5.5, numerical results for a couple examples are presented and discussed. Finally, conclusions are highlighted in Section 5.6.

5.2 Statements of the inverse problem

In the moving domain $\Omega_T = \{(x,t)|\ h_1(t) < x < h_2(t),\ 0 < t < T\}$, see Figure 5.1, where $h_1(t) < h_2(t)$ are unknown free boundaries, with unknown temperature $u(x,t)$ and unknown time-dependent coefficients $b_1(t)$ and $b_2(t)$, we consider solving the one-dimensional time-dependent parabolic equation given by

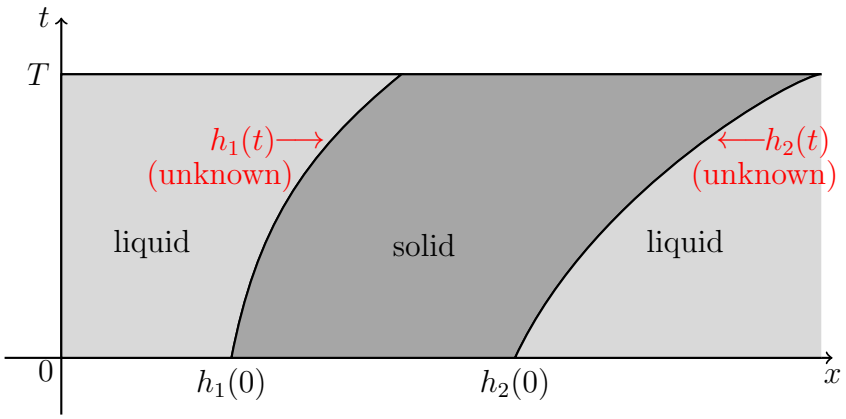

Figure 5.1: Sketch of the three-phase Stefan problem, with two unknown moving boundaries $h_1(t)$ and $h_2(t)$.

$$\frac{\partial u}{\partial t}(x,t) = a(x,t)\frac{\partial^2 u}{\partial x^2}(x,t) + (b_1(t)x + b_2(t))\frac{\partial u}{\partial x}(x,t) + c(x,t)u(x,t) + f(x,t), \quad (x,t) \in \Omega_T, \qquad (5.1)$$

where $a > 0$ is the given thermal diffusivity, f is a given heat source and c is a given reaction rate, subject to the initial condition

$$u(x,0) = \varphi(x), \quad x \in [h_1(0), h_2(0)], \tag{5.2}$$

where $h_1(0) = h_{01}$ and $h_2(0) = h_{02}$ are given numbers satisfying $h_{01} < h_{02}$, the Dirichlet boundary conditions

$$u(h_1(t),t) = \mu_1(t), \quad u(h_2(t),t) = \mu_2(t), \quad t \in [0,T], \tag{5.3}$$

and the over-determination conditions

$$h_1^{'}(t) - u_x(h_1(t),t) = \tilde{\mu_3}(t), \quad t \in [0,T], \tag{5.4}$$

$$h_2^{'}(t) + u_x(h_2(t),t) = \mu_3(t), \quad t \in [0,T], \tag{5.5}$$

$$\int_{h_1(t)}^{h_2(t)} u(x,t)dx = \mu_4(t), \quad t \in [0,T], \tag{5.6}$$

$$\int_{h_1(t)}^{h_2(t)} xu(x,t)dx = \mu_5(t), \quad t \in [0,T], \tag{5.7}$$

where $\varphi(x)$, $\tilde{\mu_3}(t)$, $\mu_i(t)$ for $i = \overline{1,5}$ are given functions satisfying compatibility conditions.

Note that the equations (5.4) and (5.5) represent Stefan conditions of melting between a solid and liquid. Also, equations (5.6) and (5.7) represents the mass (energy) and the first-order heat moment, respectively. The term $b_1(t)x + b_2(t)$ in (5.1) represents a convective fluid velocity which is linear in x with unknown time-dependent coefficients $b_1(t)$ and $b_2(t)$.

Introducing the new variable $y = \frac{x-h_1(t)}{h_2(t)-h_1(t)}$, we recast the problem (5.1)–(5.7) into the following inverse problem for the unknowns $(h_1(t),\ h_3(t),\ b_1(t),\ b_2(t), v(y,t))$, where $h_3(t) := h_2(t) - h_1(t)$ and $v(y,t) := u(yh_3(t) + h_1(t), t)$, see [119],

$$\begin{aligned}\frac{\partial v}{\partial t}(y,t) &= \frac{a(yh_3(t)+h_1(t),t)}{h_3^2(t)}\frac{\partial^2 v}{\partial y^2}(y,t)\\ &+\Big(\frac{b_1(t)(yh_3(t)+h_1(t)) + b_2(t)}{h_3(t)} + \frac{h_1'(t) + yh_3'(t)}{h_3(t)}\Big)\frac{\partial v}{\partial y}(y,t)\\ &+c(yh_3(t)+h_1(t),t)v(y,t) + f(yh_3(t)+h_1(t),t), \quad (y,t) \in Q_T,\end{aligned} \tag{5.8}$$

in the fixed domain $Q_T := \{(x,t)|\ 0 < y < 1, 0 < t < T\} = (0,1) \times (0,T)$,

$$v(y,0) = \varphi(yh_3(0) + h_1(0)), \quad y \in [0,1], \tag{5.9}$$

$$v(0,t)=\mu_1(t),\quad v(1,t)=\mu_2(t),\quad t\in[0,T], \tag{5.10}$$

$$h_1^{'}(t)-\frac{v_y(0,t)}{h_3(t)}=\tilde{\mu_3}(t),\quad t\in[0,T], \tag{5.11}$$

$$h_3^{'}(t)+\frac{v_y(0,t)+v_y(1,t)}{h_3(t)}+\tilde{\mu_3}(t)=\mu_3(t),\quad t\in[0,T], \tag{5.12}$$

$$h_3(t)\int_0^1 v(y,t)dy=\mu_4(t),\quad t\in[0,T], \tag{5.13}$$

$$h_3^2(t)\int_0^1 yv(y,t)dy+h_1(t)\mu_4(t)=\mu_5(t),\quad t\in[0,T]. \tag{5.14}$$

The sketch of the transformed inverse problem under investigation is shown in Figure 5.2.

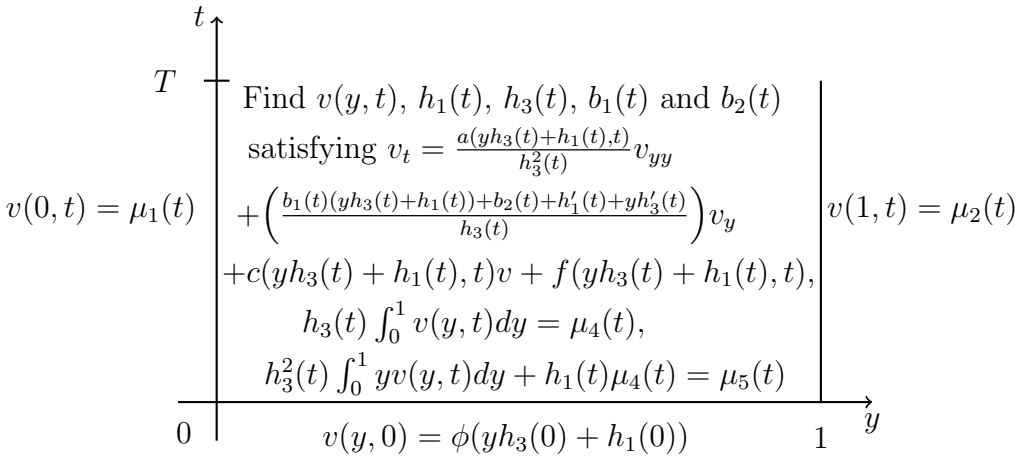

Figure 5.2: Sketch of the transformed inverse problem under investigation.

Definition 1. As a solution to the inverse problem (5.8)–(5.14), we consider the quintet $(h_1(t),h_3(t),b_1(t),b_2(t),v(y,t))\in(C^1[0,T])^2\times(C[0,T])^2\times C^{2,1}(\overline{Q_T})$, $h_3(t)>0$ for $t\in[0,T]$, that satisfies equations (5.8)–(5.14).

The local existence and uniqueness of the solution of problem (5.8)–(5.14) were established in [119] and read as follows.

Theorem 5.2.1. (Local existence of the solution) *Assume that the following*

conditions hold:

$$(A1)\quad a \in C^{1,0}(\mathbb{R}\times[0,T]),\ c,f \in C^{\alpha,0}(\mathbb{R}\times[0,T])\ for\ some\ \alpha\in(0,1),$$
$$\varphi \in C^2[h_{01},h_{02}],\ \mu_i \in C^1[0,T],\ i=1,2,4,5,\ \tilde{\mu_3},\mu_3 \in C[0,T];$$
$$(A2)\quad 0<a_0\le a(x,t)\le a_1,\ c(x,t)\le 0\ and\ f(x,t)\ge 0$$
$$for\ (x,t)\in\mathbb{R}\times[0,T],\ \varphi(x)\ge\varphi_0>0\ for\ x\in[h_{01},\infty),$$
$$\varphi'(x)>0\ for\ x\in[h_{01},h_{02}],\ \varphi'(x)-\varphi'(h_{02}+h_{01}-x)>0\ and$$
$$(h_{02}-x)\varphi'(h_{02}+h_{01}-x)-(x-h_{01})\varphi'(x)>0\ for\ x\in\Big[h_{01},\frac{h_{01}+h_{02}}{2}\Big),$$
$$\mu_i(t)>0, i=1,2,4,\ for\ t\in[0,T].$$

$(A3)$ *Compatibility conditions of the zero and first orders.*
Then, it is possible to indicate a time $T_0\in(0,T]$, *determined by the input data, such that there exists a (local) solution to problem (5.8)–(5.14) for* $(y,t)\in Q_{T_0}$.

Theorem 5.2.2. (Local uniqueness of the solution) *Assume that the following conditions are satisfied:*

$$a\in C^{2,0}(\mathbb{R}\times[0,T]),\ \varphi\in C^1[h_{01},h_{02}],\ c,f\in C^{1,0}(\mathbb{R}\times[0,T]),$$
$$a(x,t)>0\ for\ (x,t)\in\mathbb{R}\times[0,T],\varphi(x)\ge\varphi_0>0\ for\ x\in[h_{01},\infty),$$
$$\varphi'(x)-\varphi'(h_{02}+h_{01}-x)>0\ and\ (h_{02}-x)\varphi'(h_{02}+h_{01}-x)-(x-h_{01})\varphi'(x)>0$$
$$for\ x\in\Big[h_{01},\frac{h_{01}+h_{02}}{2}\Big),\ \mu_i(t)>0,\ i=1,2,4,\ for\ t\in[0,T].$$

Then, it is possible to indicate a time $T_1\in(0,T]$, *determined by the input data, such that problem (5.8)–(5.14) cannot have two different solutions for* $(y,t)\in Q_{T_1}$.

5.2.1 Related inverse problem statement

A related inverse problem has been considered in [121], where the Stefan conditions (5.4) and (5.5) (or (5.11) and (5.12)), were replaced by the second and third-order heat moment measurement

$$\int_{h_1(t)}^{h_2(t)} x^{i-4}u(x,t)dx=\mu_i(t),\quad i=6,7,\quad t\in[0,T], \tag{5.15}$$

or, in terms of change of variable $y=\frac{x-h_1(t)}{h_2(t)-h_1(t)}$,

$$h_3^3(t)\int_0^1 y^2v(y,t)dy+2h_1(t)\mu_5(t)-h_1^2(t)\mu_4(t)=\mu_6(t),\quad t\in[0,T], \tag{5.16}$$

$$h_3^4(t)\int_0^1 y^3 v(y,t)dy + 3h_1(t)\mu_6(t) - 3h_1^2(t)\mu_5(t) + h_1^3(t)\mu_4(t) = \mu_7(t), \quad t \in [0,T]. \quad (5.17)$$

The local existence and uniqueness to the inverse problem (5.8)–(5.10), (5.13), (5.14), (5.16) and (5.17), were established in [121] and read as follows.

Theorem 5.2.3. (Local existence of the solution) *Assume that conditions (A2) and (A3) of Theorem 5.2.1 are satisfied and that (A4) a, c, $f \in C^{1,0}(\mathbb{R}\times[0,T])$, $\varphi \in C^2[h_{01}, h_{02}]$, $\mu_i \in C^1[0,T], i = 1,2,4,5,6,7$. Then, there is a time $T_2 \in (0,T]$, determined by the input data, such that there exists a (local) solution to problem (5.8)–(5.10), (5.13), (5.14), (5.16) and (5.17) for $(y,t) \in Q_{T_2}$.*

Theorem 5.2.4. (Local uniqueness of the solution) *Assume that the conditions of Theorem 5.2.2 are satisfied. Then, there is a time $T_3 \in (0,T]$, determined by the input data, such that problem (5.8)–(5.10), (5.13), (5.14), (5.16) and (5.17) cannot have two different solutions for $(y,t) \in Q_{T_3}$.*

5.3 Numerical solution of direct problem

Consider the direct initial boundary value problem given by equations (5.8)–(5.10), where $h_1(t)$, $h_2(t)$, $b_1(t)$, $b_2(t)$, $a(x,t)$, $c(x,t)$, $f(x,t)$, $\varphi(x)$, $\mu_1(t)$ and $\mu_2(t)$ are known and the solution $v(y,t)$ is to be determined together with the quantities of interest $\tilde{\mu_3}(t)$, $\mu_i(t)$, $i = \overline{3,7}$. To achieve this, we use the FDM with the Crank-Nicolson scheme, [123], based on subdividing the solution $Q_T = (0,1)\times(0,T)$ into M and N subintervals of equal lengths Δy and Δt, where $\Delta y = 1/M$ and $\Delta t = T/N$, respectively. At the node (i,j) we denote $v(y_i,t_j) = v_{i,j}$, where $y_i = i\Delta y$, $t_j = j\Delta t$, $a(y_i,t_j) = a_{i,j}$, $c(y_i,t_j) = c_{i,j}$, $h_1(t_j) = h_{1_j}$, $h_3(t_j) = h_2(t_j) - h_1(t_j) = h_{3_j}$, $b_1(t_j) = b_{1_j}$, $b_2(t_j) = b_{2_j}$, and $f(y_i,t_j) = f_{i,j}$ for $i = \overline{0,M}$ and $j = \overline{0,N}$. Based on the FDM, equation (5.8) can be approximated as:

$$\begin{aligned} -A_{i,j+1}v_{i-1,j+1} + (1+B_{i,j+1})v_{i,j+1} - C_{i,j+1}v_{i+1,j+1} \\ = A_{i,j}v_{i-1,j} + (1-B_{i,j})v_{i,j} + C_{i,j}v_{i+1,j} + \frac{\Delta t}{2}(f_{i,j}+f_{i,j+1}), \\ \text{for } i = \overline{1,(M-1)}, \quad j = \overline{0,(N-1)}, \end{aligned} \quad (5.18)$$

where

$$A_{i,j} = \frac{(\Delta t)\zeta_{i,j}}{2(\Delta y)^2} - \frac{(\Delta t)\eta_{i,j}}{4(\Delta y)}, \quad B_{i,j} = \frac{(\Delta t)\zeta_{i,j}}{(\Delta y)^2} - \frac{(\Delta t)c_{i,j}}{2},$$
$$C_{i,j} = \frac{(\Delta t)\zeta_{i,j}}{2(\Delta y)^2} + \frac{(\Delta t)\eta_{i,j}}{4(\Delta y)}, \quad \zeta_{i,j} = \frac{a_{i,j}}{h_{3_j}^2},$$
$$\eta_{i,j} = \frac{b_{1_j}(y_i h_{3_j} + h_{1_j}) + b_{2_j} + h'_{1_j} + y_i h'_{3_j}}{h_{3_j}}. \tag{5.19}$$

The initial and boundary conditions in equations (5.9) and (5.10) are discretized as

$$v_{i,0} = \varphi(y_i h_{03} + h_{01}), \quad i = \overline{0, M}, \tag{5.20}$$

where $h_{03} = h_3(0)$,

$$v_{0,j} = \mu_1(t_j), \quad v_{M,j} = \mu_2(t_j), \quad j = \overline{0, N}. \tag{5.21}$$

At each time step t_{j+1}, for $j = \overline{0, (N-1)}$, using the Dirichlet boundary conditions (5.21), the difference equation (5.18) can be reformulated as a $(M-1)\times(M-1)$ system of linear equations of the form,

$$G\mathbf{v_{j+1}} = H\mathbf{v_j} + \mathbf{r}, \tag{5.22}$$

where $\mathbf{v_{j+1}} = (v_{1,j+1}, v_{2,j+1}, ..., v_{M-2,j+1}, v_{M-1,j+1})^{\mathrm{T}}$,

$$G = \begin{pmatrix} 1+B_{1,j+1} & -C_{1,j+1} & ... & 0 & 0 \\ -A_{2,j+1} & 1+B_{2,j+1} & ... & 0 & 0 \\ \vdots & \vdots & \ddots & \vdots & \vdots \\ 0 & 0 & ... & 1+B_{M-2,j+1} & -C_{M-2,j+1} \\ 0 & 0 & ... & -A_{M-1,j+1} & 1+B_{M-1,j+1} \end{pmatrix},$$

$$H = \begin{pmatrix} 1-B_{1,j} & C_{1,j} & ... & 0 & 0 \\ A_{2,j} & 1-B_{2,j} & ... & 0 & 0 \\ \vdots & \vdots & \ddots & \vdots & \vdots \\ 0 & 0 & ... & 1-B_{M-2,j} & C_{M-2,j} \\ 0 & 0 & ... & A_{M-1,j} & 1-B_{M-1,j} \end{pmatrix},$$

$$\mathbf{r} = \begin{pmatrix} A_{1,j}\mu_1(t_j) + A_{1,j+1}\mu_1(t_{j+1}) + \frac{\Delta t}{2}(f_{1,j} + f_{1,j+1}) \\ \frac{\Delta t}{2}(f_{2,j} + f_{2,j+1}) \\ \vdots \\ \frac{\Delta t}{2}(f_{M-2,j} + f_{M-2,j+1}) \\ C_{M-1,j}\mu_2(t_j) + C_{M-1,j+1}\mu_2(t_{j+1}) + \frac{\Delta t}{2}(f_{M-1,j} + f_{M-1,j+1}) \end{pmatrix}.$$

The expressions (5.11)–(5.14), (5.16) and (5.17) can be approximated using the following finite difference approximation formulae and trapezoidal rule for integrals:

$$\tilde{\mu_3}(t_j) = \frac{h_{1_j} - h_{1_{j-1}}}{\Delta t} - \frac{4v_{1,j} - v_{2,j} - 3v_{0,j}}{2(\Delta y)h_{3_j}}, \quad j = \overline{1, N}, \tag{5.23}$$

$$\mu_3(t_j) = \frac{h_{3_j} - h_{3_{j-1}}}{\Delta t} + \Big(\frac{4v_{1,j} - v_{2,j} - 3v_{0,j}}{2(\Delta y)h_{3_j}} - \frac{4v_{M-1,j} - v_{M-2,j} - 3v_{M,j}}{2(\Delta y)h_{3_j}}\Big) + \tilde{\mu_3}(t_j), \ j = \overline{1, N}, \tag{5.24}$$

$$\mu_{k+3}(t_j) = \frac{h_{3_j}^k}{2N}\Big(y_0^{k-1}v_{0,j} + y_M^{k-1}v_{M,j} + 2\sum_{i=1}^{M-1} y_i^{k-1}v_{i,j}\Big), \quad j = \overline{1, N}, \quad k = \overline{1, 4}. \tag{5.25}$$

5.4 Numerical solution of inverse problem

For the inverse problems described in Section 5.2, our aim is to obtain simultaneously stable reconstructions of the two unknown coefficients $b_1(t)$ and $b_2(t)$, together with the moving boundaries $h_1(t)$ and $h_3(t)$, and the transformed temperature $v(y, t)$, satisfying the equations (5.8)–(5.14) or, (5.8)–(5.10), (5.13), (5.14),

(5.16) and (5.17), by minimizing the nonlinear Tikhonov regularization function

$$
\begin{aligned}
F(\mathbf{h_1},\mathbf{h_3},\mathbf{b_1},\mathbf{b_2}) &= \sum_{j=1}^{N}\Big[h'_{1_j}-\frac{v_y(0,t_j)}{h_{3_j}}-\tilde{\mu_3}(t_j)\Big]^2\\
&+\sum_{j=1}^{N}\Big[h'_{3_j}+\frac{v_y(0,t_j)+v_y(1,t_j)}{h_{3_j}}+\tilde{\mu_3}(t_j)-\mu_3(t_j)\Big]^2\\
&+\sum_{j=1}^{N}\Big[h_{3_j}\int_0^1 v(y,t_j)dy-\mu_4(t_j)\Big]^2\\
&+\sum_{j=1}^{N}\Big[h_{3_j}^2\int_0^1 yv(y,t_j)dy+h_1(t_j)\mu_4(t_j)-\mu_5(t_j)\Big]^2\\
&+\beta_1\sum_{j=1}^{N}h_{1_j}^2+\beta_2\sum_{j=1}^{N}h_{3_j}^2+\beta_3\sum_{j=1}^{N}b_{1_j}^2+\beta_4\sum_{j=1}^{N}b_{2_j}^2, \qquad (5.26)
\end{aligned}
$$

or,

$$
\begin{aligned}
F_1(\mathbf{h_1},\mathbf{h_3},\mathbf{b_1},\mathbf{b_2}) &= \sum_{j=1}^{N}\Big[h_{3_j}\int_0^1 v(y,t_j)dy-\mu_4(t_j)\Big]^2\\
&+\sum_{j=1}^{N}\Big[h_{3_j}^2\int_0^1 yv(y,t_j)dy+h_1(t_j)\mu_4(t_j)-\mu_5(t_j)\Big]^2\\
&+\sum_{j=1}^{N}\Big[h_{3_j}^3\int_0^1 y^2v(y,t_j)dy+2h_1(t_j)\mu_5(t_j)-h_1^2(t_j)\mu_4(t_j)-\mu_6(t_j)\Big]^2\\
&+\sum_{j=1}^{N}\Big[h_{3_j}^4\int_0^1 y^3v(y,t_j)dy+3h_1(t_j)\mu_6(t_j)-3h_1^2(t_j)\mu_5(t_j)+h_1^3(t_j)\mu_4(t_j)\\
&\quad-\mu_7(t_j)\Big]^2+\beta_1\sum_{j=1}^{N}h_{1_j}^2+\beta_2\sum_{j=1}^{N}h_{3_j}^2+\beta_3\sum_{j=1}^{N}b_{1_j}^2+\beta_4\sum_{j=1}^{N}b_{2_j}^2, \qquad (5.27)
\end{aligned}
$$

respectively, where v solves (5.8)–(5.10) for given $(\mathbf{h_1},\mathbf{h_3},\mathbf{b_1},\mathbf{b_2})$, and $\beta_i \geq 0$ for $i=\overline{1,4}$ are regularization parameters to be prescribed. The minimization of F, or F_1, is performed using the MATLAB toolbox routine *lsqnonlin*, which does not require the user to supply the gradient of the objective function, [99]. This routine attempts to find the minimum of a sum of squares by starting from an arbitrary initial guesses, subject to the physical constraint $h_3(t)>0$. Thus, we take the lower and upper simple bounds for $h_3(t)$ to be 10^{-8} and 10^3, respectively, and the lower and upper bounds for the quantities $h_1(t)$, $b_1(t)$ and $b_2(t)$ to be -10^3 and 10^3, respectively. Furthermore, within *lsqnonlin*, we use the TRR algorithm [31], which is based on the interior-reflective Newton method. We also take the

parameters of the routine as follows:

- Maximum number of iterations, (MaxIter)= 10×(number of variables).
- Maximum number of objective function evaluations, (MaxFunEvals) = 10^5×(number of variables).
- Termination tolerance on the function value, (TolFun)= 10^{-20}.
- Solution tolerance, (XTol) = 10^{-20}.

In the expressions (5.19) and (5.26), we approximate the derivatives of $h_1(t)$ and $h_3(t)$ as

$$h'_{1_j} := h'_1(t_j) \approx \frac{h_1(t_j) - h_1(t_{j-1})}{\Delta t} = \frac{h_{1_j} - h_{1_{j-1}}}{\Delta t}, \quad j = \overline{1, N}, \tag{5.28}$$

$$h'_{3_j} := h'_3(t_j) \approx \frac{h_3(t_j) - h_3(t_{j-1})}{\Delta t} = \frac{h_{3_j} - h_{3_{j-1}}}{\Delta t}, \quad j = \overline{1, N}. \tag{5.29}$$

The measured data are (5.4)–(5.7) and (5.15). In order to model the errors in this data, we replace $\tilde{\mu_3}(t_j)$ and $\mu_{k+2}(t_j)$, $k = \overline{1, 5}$, in equations (5.11)–(5.14) or, (5.16) and (5.17) by $\tilde{\mu_3}^{\epsilon}$ and $\mu_{k+2}^{\epsilon k}(t_j)$, respectively, as

$$\tilde{\mu_3}^{\epsilon}(t_j) = \tilde{\mu_3}(t_j) + \epsilon_j, \quad \mu_{k+2}^{\epsilon k}(t_j) = \mu_{k+2}(t_j) + \epsilon k_j, \quad k = \overline{1, 5}, \quad j = \overline{1, N}, \tag{5.30}$$

where ϵ_j, ϵk_j are random variables generated from a Gaussian normal distribution with mean zero and standard deviations σ, σ_k given by

$$\sigma = p \times \max_{t \in [0,T]} |\tilde{\mu_3}(t)|, \quad \sigma_k = p \times \max_{t \in [0,T]} |\mu_{k+2}(t)|, \quad k = \overline{1, 5}, \tag{5.31}$$

where p represents the percentage of noise.

5.5 Numerical results and discussion

In this section, we present a couple of benchmark numerical test examples to illustrate the accuracy and stability of the numerical methods based on the FDM with Crank-Nicolson scheme described in Section 5.3 combined with the minimization of the objective function F, or F_1 described in Section 5.4. Furthermore, we add noise to the input measurement data (5.11)–(5.14), (5.16) and (5.17) to simulate the real situation of measurement noisy data, by using equations (5.30) and

(5.31). To quantify the accuracy of the approximate solution, we employ the root mean squares error (rmse) defined by

$$\text{rmse}(h_1) = \left[\frac{T}{N}\sum_{j=1}^{N}\Big(h_1^{Numerical}(t_j) - h_1^{Exact}(t_j)\Big)^2\right]^{1/2}, \tag{5.32}$$

and similar expressions exist for $h_3(t)$, $b_1(t)$ and $b_2(t)$. For simplicity, we take $T = 1$ in all examples.

5.5.1 Example 1 (for inverse problem I)

We consider the first inverse problem given by (5.1)–(5.7) with unknown coefficients $h_1(t)$, $h_2(t)$, $b_1(t)$ and $b_2(t)$, and solve this with the following input data:

$$\begin{aligned} a(x,t) = \frac{1}{100}(1+t) + x, \quad c(x,t) = -1 - x - t,\\ \varphi(x) = \pi + \tan^{-1}(x), \quad \mu_1(t) = (1+t)\Big(\pi + \tan^{-1}\Big(\frac{5+t}{10}\Big)\Big),\\ \mu_2(t) = (1+t)\Big(\pi + \tan^{-1}\Big(\frac{15+2t}{10}\Big)\Big),\\ f(x,t) = \pi + \frac{(1+t)x(1+t+100x)}{50\,(1+x^2)^2} - \frac{t(1+t)(1+x)}{1+x^2}\\ + \tan^{-1}(x) + (1+t)(1+t+x)(\pi + \tan^{-1}(x)), \end{aligned} \tag{5.33}$$

$$\tilde{\mu_3}(t) = \frac{1}{10} - \frac{1+t}{1+\left(\frac{1}{2}+\frac{t}{10}\right)^2}, \quad \mu_3(t) = \frac{1}{5} + \frac{1+t}{1+\left(\frac{3}{2}+\frac{t}{5}\right)^2}, \tag{5.34}$$

$$\begin{aligned} \mu_4(t) = \frac{1}{10}(1+t)\Big[10\pi + \pi t + (15+2t)\tan^{-1}\Big(\frac{15+2t}{10}\Big)\\ -(5+t)\tan^{-1}\Big(\frac{5+t}{10}\Big) + 5\ln\Big(\frac{125+t(10+t)}{325+4t(15+t)}\Big)\Big], \end{aligned} \tag{5.35}$$

$$\begin{aligned} \mu_5(t) = \frac{1}{200}(1+t)\Big[(10+t)\Big(-10+\pi(20+3t)\Big)\\ +\Big(325+4t(15+t)\Big)\tan^{-1}\Big(\frac{15+2t}{10}\Big)\\ -\Big(125+t(10+t)\Big)\tan^{-1}\Big(\frac{5+t}{10}\Big)\Big]. \end{aligned} \tag{5.36}$$

Remark that conditions of Theorems 5.2.1 and 5.2.2 are satisfied and therefore, the local existence and uniqueness of the solution are guaranteed. In fact, one can easily check that the analytical solution of the transformed inverse problem

(5.8)–(5.14) is given by

$$v(y,t) = u(yh_3(t) + h_1(t), t) = (1+t)\Big(\pi + \tan^{-1}\Big(\frac{1}{10}(5+t+10y+ty)\Big)\Big), \quad (5.37)$$

$$h_1(t) = \frac{1}{2} + \frac{t}{10}, \quad h_2(t) = \frac{3}{2} + \frac{t}{5}, \quad b_1(t) = t, \quad b_2(t) = t. \quad (5.38)$$

Also,

$$u(x,t) = (1+t)\Big(\pi + \tan^{-1}(x)\Big). \quad (5.39)$$

In the direct problem given by (5.8)–(5.10) and (5.38), the numerical results for the interior transformed temperature $v(y,t)$ have been obtained in excellent agreement with the analytical solution (5.37) and therefore, they are not presented. Apart from the interior transformed temperature $v(y,t)$, other outputs of interest are the overdetermination data (5.4)–(5.7), which analytically are given by (5.34)–(5.36). Table 5.1 shows that the analytical and numerical solutions for these quantities obtained with various mesh sizes $M = N \in \{10, 20, 40\}$ are in very good agreement.

Table 5.1: The analytical and numerical solutions for $\tilde{\mu_3}(t)$, $\mu_k(t)$, $k = \overline{3,7}$, with $M = N \in \{10, 20, 40\}$, for the direct problem.

t	0.1	0.2	0.3	...	0.8	0.9	1	
$\tilde{\mu_3}(t)$	-0.7732	-0.8444	-0.9147	...	-1.2451	-1.3072	-1.3679	$M = N = 10$
	-0.7731	-0.8447	-0.9150	...	-1.2466	-1.3090	-1.3701	$M = N = 20$
	-0.7730	-0.8446	-0.9149	...	-1.2469	-1.3093	-1.3705	$M = N = 40$
	-0.7729	-0.8446	-0.9149	...	-1.2469	-1.3094	-1.3706	exact
$\mu_3(t)$	0.5320	0.5551	0.5779	...	0.6778	0.6955	0.7124	$M = N = 10$
	0.5322	0.5559	0.5786	...	0.6791	0.6969	0.7140	$M = N = 20$
	0.5323	0.5559	0.5786	...	0.6793	0.6971	0.7141	$M = N = 40$
	0.5323	0.5559	0.5786	...	0.6793	0.6971	0.7141	exact
$\mu_4(t)$	4.3474	4.7984	5.2587	...	7.7009	8.2176	8.7436	$M = N = 10$
	4.3478	4.7988	5.2592	...	7.7018	8.2185	8.7446	$M = N = 20$
	4.3479	4.7990	5.2594	...	7.7020	8.2187	8.7448	$M = N = 40$
	4.3479	4.7990	5.2594	...	7.7021	8.2188	8.7449	exact
$\mu_5(t)$	4.4615	4.9966	5.5550	...	8.7139	9.4220	10.1566	$M = N = 10$
	4.4610	4.9960	5.5544	...	8.7130	9.4211	10.1556	$M = N = 20$
	4.4608	4.9958	5.5542	...	8.7128	9.4208	10.1553	$M = N = 40$
	4.4608	4.9958	5.5541	...	8.7127	9.4208	10.1552	exact
$\mu_6(t)$	4.9522	5.6234	6.3379	...	10.6167	11.6254	12.6891	$M = N = 10$
	4.9461	5.6166	6.3303	...	10.6044	11.6121	12.6746	$M = N = 20$
	4.9446	5.6149	6.3284	...	10.6014	11.6087	12.6710	$M = N = 40$
	4.9441	5.6143	6.3277	...	10.6004	11.6076	12.6698	exact
$\mu_7(t)$	5.8339	6.7142	7.6683	...	13.6917	15.1780	16.7692	$M = N = 10$
	5.8248	6.7039	7.6567	...	13.6721	15.1565	16.7457	$M = N = 20$
	5.8226	6.7013	7.6538	...	13.6672	15.1512	16.7399	$M = N = 40$
	5.8218	6.7005	7.6528	...	13.6656	15.1494	16.7379	exact

In the inverse problem (5.8)–(5.14), we take the initial guesses for the vectors $\mathbf{h_1}$, $\mathbf{h_3}$, $\mathbf{b_1}$ and $\mathbf{b_2}$ as follows:

$$h^0_{1_j} = h_{01} = 0.5,\ h^0_{3_j} = h_{02} - h_{01} = 1,\ b^0_{1_j} = b_1(0) = 0,\ b^0_{2_j} = b_2(0) = 0,$$
$$j = \overline{1,N},\ (5.40)$$

where the values of $b_1(0)$ and $b_2(0)$ have been obtained exactly using the compatibility of (5.1)–(5.7).

We start the investigation for reconstructing the time-dependent unknowns coefficients $h_1(t)$, $h_3(t)$, $b_1(t)$ and $b_2(t)$, when there is no noise in the input data (5.11)–(5.14), i.e. $p = 0$ in (5.31). The objective function F, as a function of the number of iterations, is plotted (curve $-\Box-$) in Figures 5.3 and 5.4, for no noise, without and with regularization, respectively. From these figures, it can be seen that a rapid monotonic decreasing convergence to a very low value of $O(10^{-24})$ is achieved in about 16 iterations in the case of no regularization, i.e. $\beta_i = 0$, $i = \overline{1,4}$, and of $O(10^{-6})$ in the case of regularization with $\beta_1 = \beta_2 = 0$,

$\beta_3 = \beta_4 = 10^{-7}$.

The analytical (5.37) and numerical solutions for the transformed temperature $v(y,t)$, with no noise, with and without regularizarion are shown in Figure 5.5. From this figure, it can be noticed that the inverse problem is stable and accurate in the transformed temperature $v(y,t)$. The $rmse$ values for the unknowns coefficients $h_1(t)$, $h_3(t)$, $b_1(t)$ and $b_2(t)$ are presented in Figure 5.6 with and without regularization, versus the number of iterations. It can be seen that the $rmse$ values settle rapidly to stationary values after 5 to 6 iterations. It can also be observed that $rmse(h_1)$ and $rmse(h_3)$ values are much lower than the $rmse(b_1)$ and $rmse(b_2)$, pointing out that the free boundaries $h_1(t)$ and $h_3(t)$ are recovered more accurately than the coefficients $b_1(t)$ and $b_2(t)$.

The numerical results presented in Figure 5.7 show that although the retrieval of free boundaries $h_1(t)$ and $h_3(t)$, see Figures 5.7(a) and 5.7(b), are very accurate, some slight instability starts to manifest in the unregularization solutions for the coefficients $b_1(t)$ and $b_2(t)$, see Figures 5.7(c) and 5.7(d), respectively. Thus, some slight regularization with, $\beta_1 = \beta_2 = 0$, $\beta_3 = \beta_4 = 10^{-7}$, is applied in order to obtain stable and accurate solutions for the coefficients $b_1(t)$ and $b_2(t)$, see Figures 5.9(c) and 5.9(d). As the numerical results for the free boundaries h_1 and h_3 have been found stable, in the remaining of the chapter we take $\beta_1 = \beta_2 = 0$ and vary only the regularization parameter $\beta_3 = \beta_4 > 0$.

Next, we investigate the stability of the numerical solution with respect to various levels of $p \in \{0.01\%, 0.1\%\}$ noise in (5.31) included in the input data $\tilde{\mu_3}(t)$, $\mu_3(t)$, $\mu_4(t)$ and $\mu_5(t)$. From the previous discussion, we anticipate that regularization is required in order to obtain stable and accurate solutions because the inverse problem is ill-posed. The L-curve, [48], for the choice of the regularization parameter is shown in Figure 5.8, by plotting the solution norm $\sqrt{||\mathbf{h_1}||^2+||\mathbf{h_3}||^2+||\mathbf{b_1}||^2+||\mathbf{b_1}||^2}$, as a function of the residual norm given by square root of the sum of first four terms in the rigth-hand side of equation (5.26). Form this figure, it can be observed that regularization parameters near the "corner" of the L-curve are $\beta_3 = \beta_4 \in \{10^{-5}, 10^{-4}\}$ for $p = 0.01\%$ noise, and $\beta_3 = \beta_4 \in \{10^{-5}, 10^{-4}, 10^{-3}\}$ for $p = 0.1\%$.

The decreasing monotonic convergence of the objective function F, as a function of the number of iterations, without and with regularization are shown in Figures 5.3 and 5.4, respectively. In case of no regularization, Figure 5.3 shows that convergence is more rapidly achieved as the amount of noise p decreases. In order to stabilise the coefficients $b_1(t)$ and $b_2(t)$, we employ regularization with $\beta_3 = \beta_4 = 10^{-4}$ (suggested by the L-curve in Figure 5.8(a)), obtaining $rmse(b_1) = 0.0469$ and $rmse(b_2) = 0.0526$ for $p = 0.01\%$ noise, and

with $\beta_3 = \beta_4 = 10^{-3}$ (suggested by the L-curve in Figure 5.8(b)), obtaining $rmse(b_1) = 0.0999$ and $rmse(b_2) = 0.1018$ for $p = 0.1\%$ noise. Numerical results are shown in Figure 5.9. For more, information about the $rmse$ values for various levels of noise and with and without regularization, see Table 5.2.

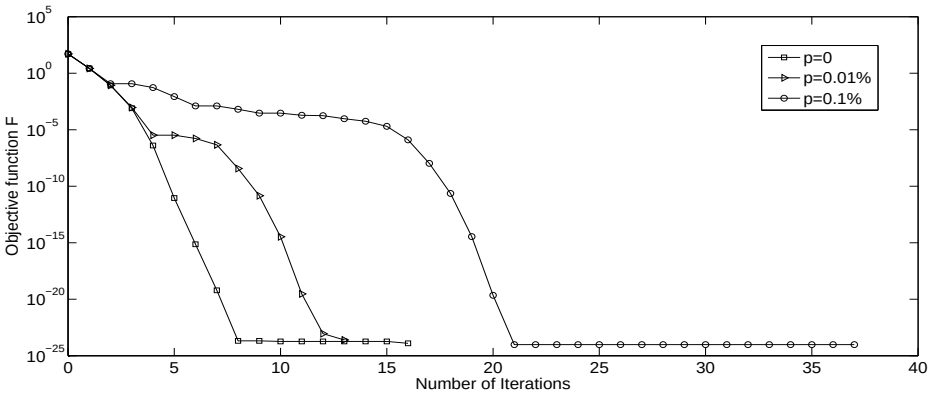

Figure 5.3: The objective function F, as a function of the number of iterations, for $p \in \{0, 0.01\%, 0.1\%\}$ noise, no regularization, for Example 1.

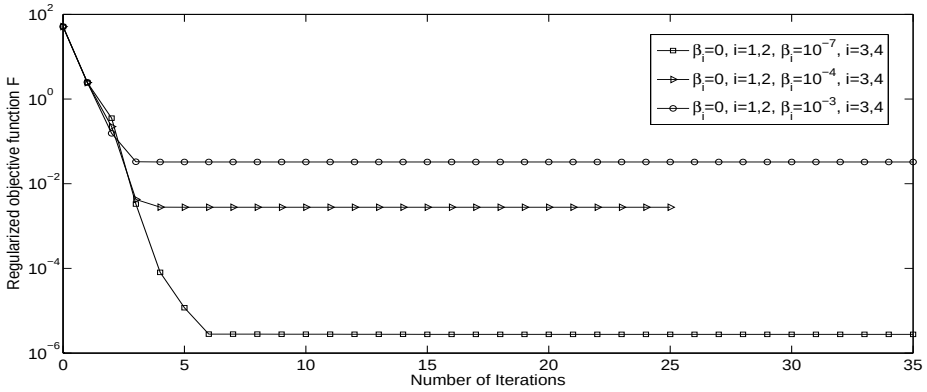

Figure 5.4: The regularized objective function F, as a function of the number of iterations, for noise $p = 0$ $(-\square-)$, $p = 0.01\%$ $(-\triangleright-)$ and $p = 0.1\%$ $(-\circ-)$, with regularization, for Example 1.

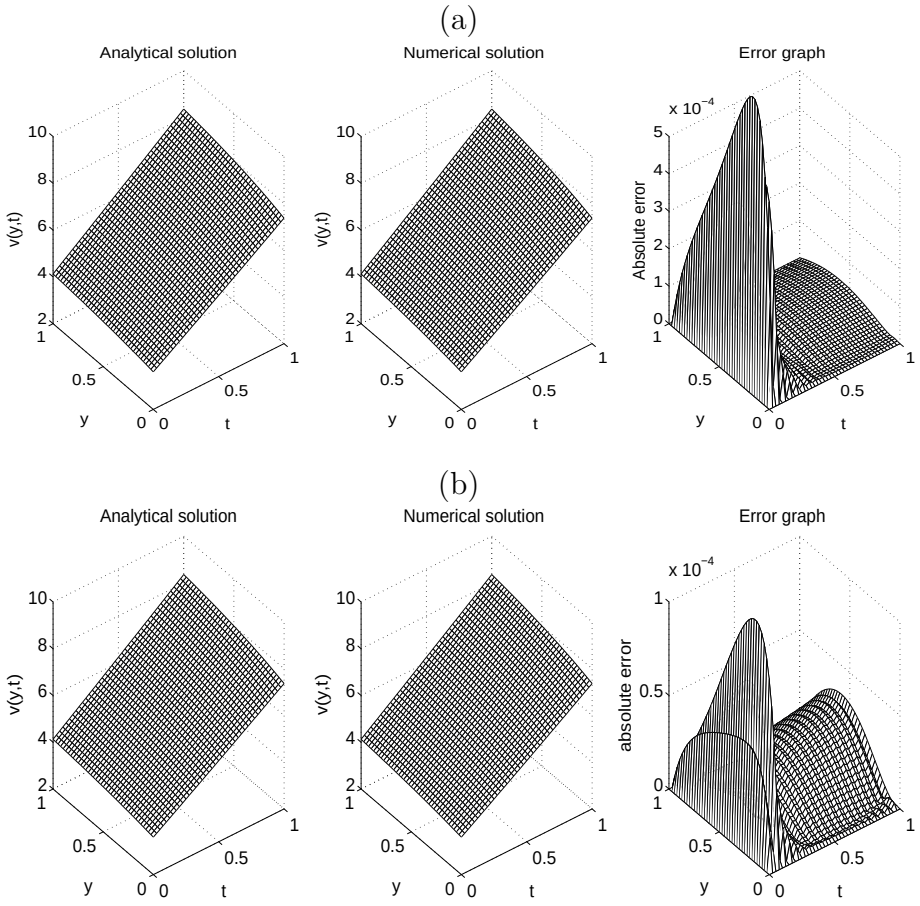

Figure 5.5: The analytical (5.37) and numerical solutions for the transformed temperature $v(y,t)$, for Example 1, no noise, with $\beta_1 = \beta_2 = 0$ and: (a) $\beta_3 = \beta_4 = 0$ and (b) $\beta_3 = \beta_4 = 10^{-7}$. The absolute error between them is also included.

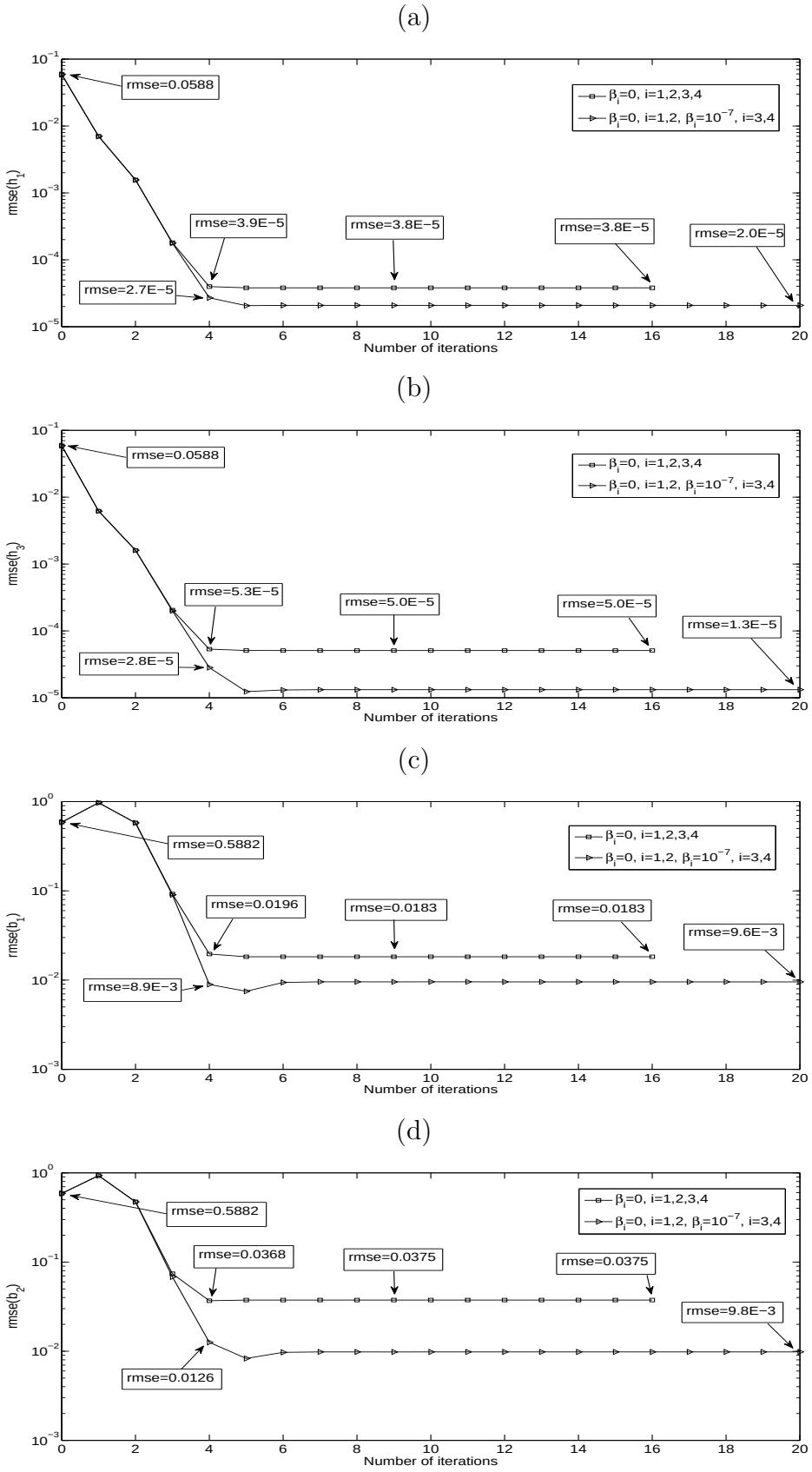

Figure 5.6: The *rmse* values: (a) $h_1(t)$, (b) $h_3(t)$, (c) $b_1(t)$ and (d) $b_2(t)$, as functions of the number of iterations, no noise, with and without regularization, for Example 1.

(a)

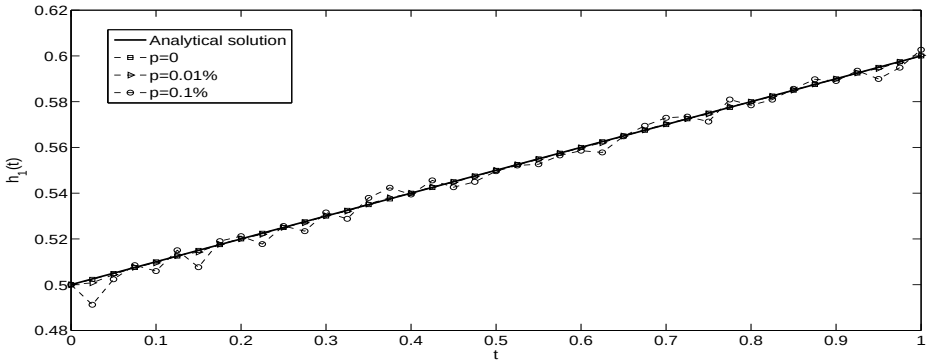

(b)

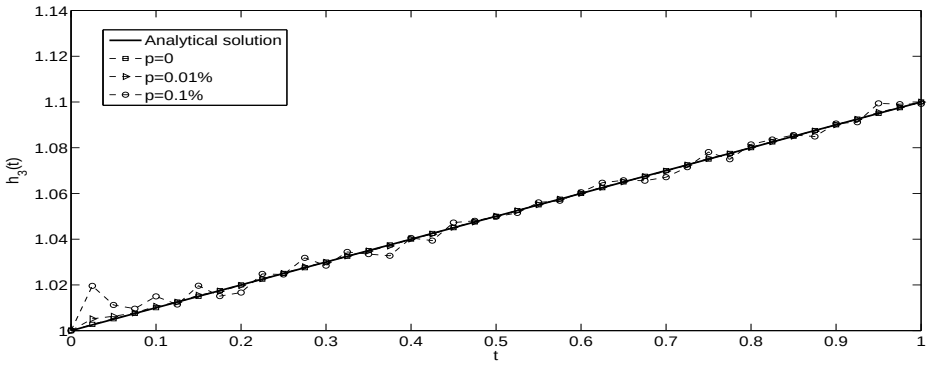

(c)

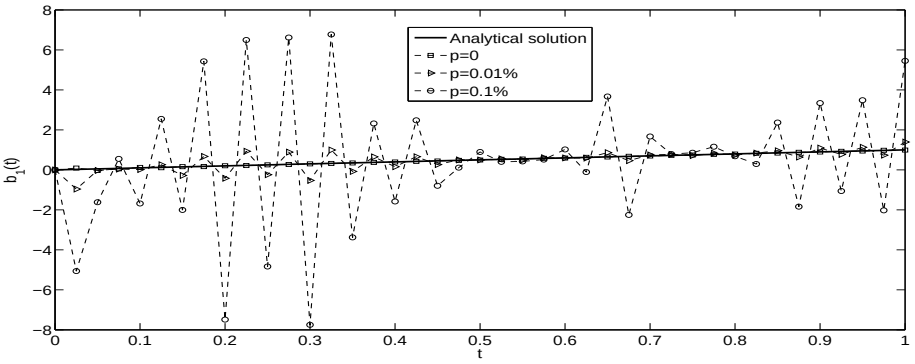

(d)

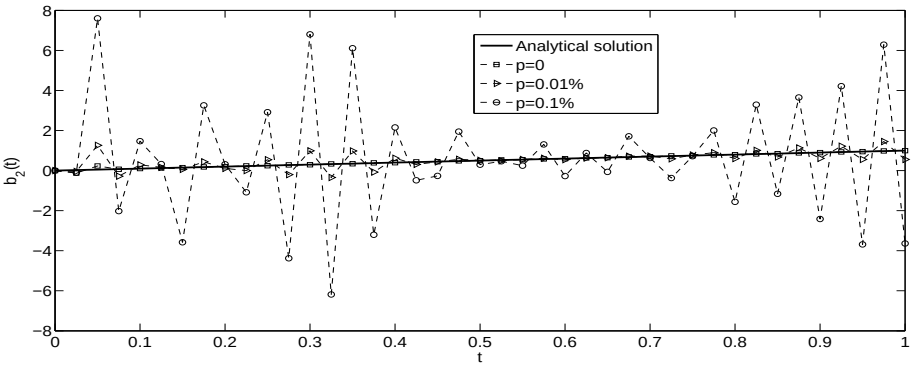

Figure 5.7: The analytical (5.38) and numerical solutions for: (a) $h_1(t)$, (b) $h_3(t)$, (c) $b_1(t)$ and (d) $b_2(t)$, for $p \in \{0, 0.01\%, 0.1\%\}$ noise, no regularization, for Example 1.

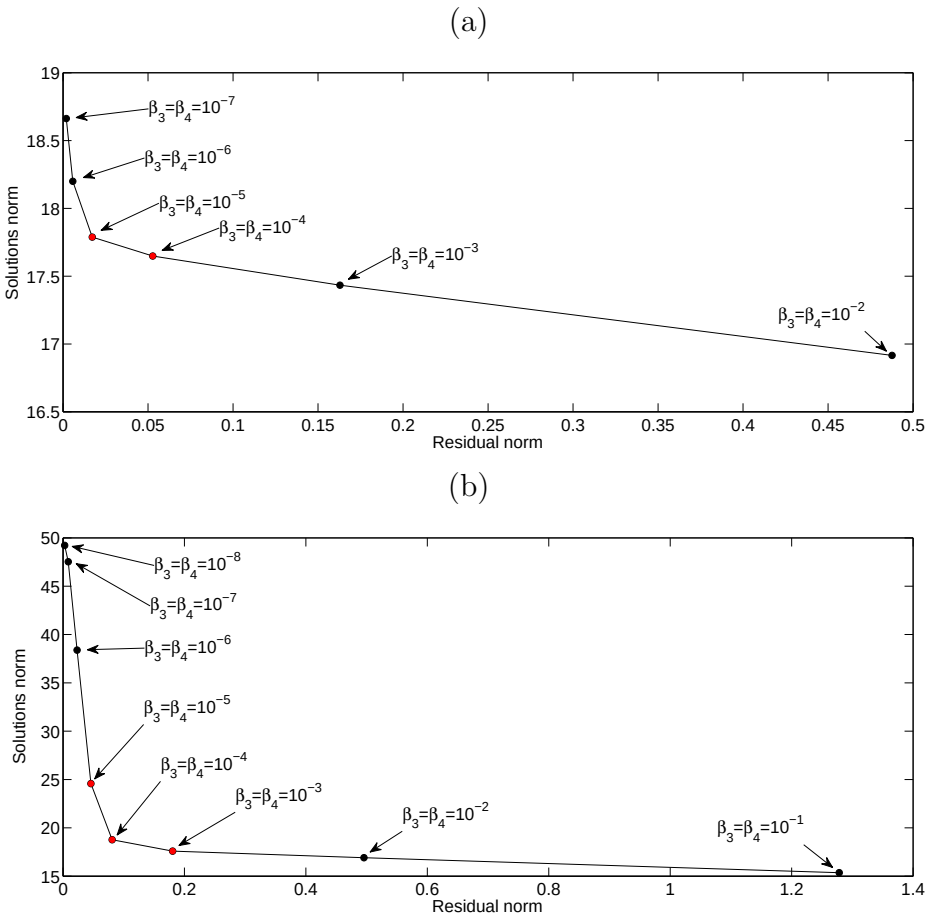

Figure 5.8: The residual norm versus the solution norm for various regularization parameters, for Example 1, with (a) $p = 0.01\%$ and (b) $p = 0.1\%$ noise.

(a)

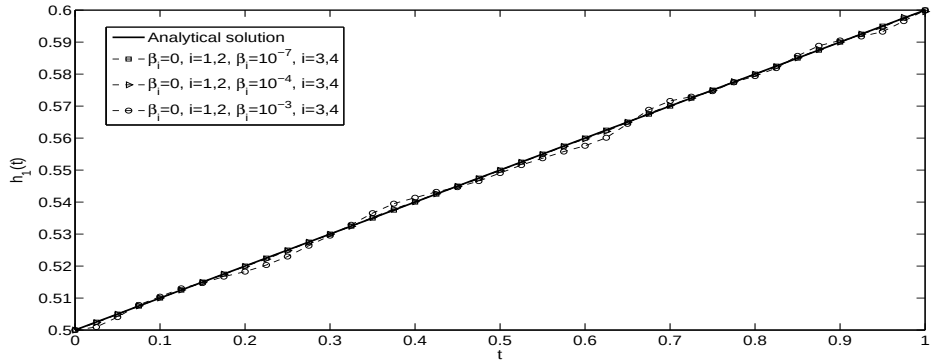

(b)

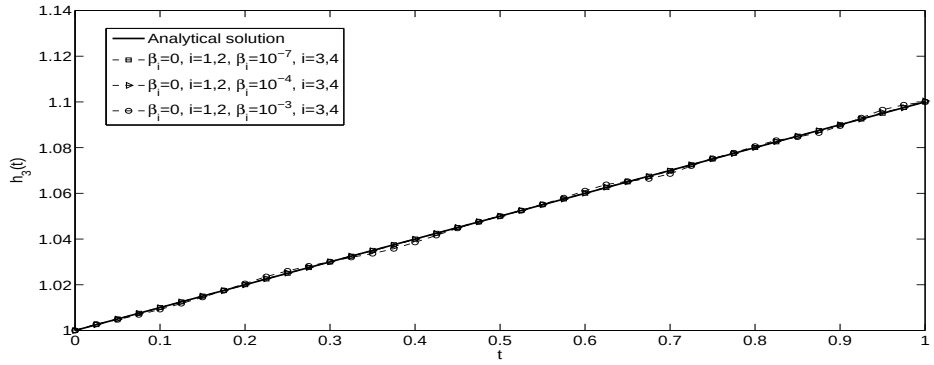

(c)

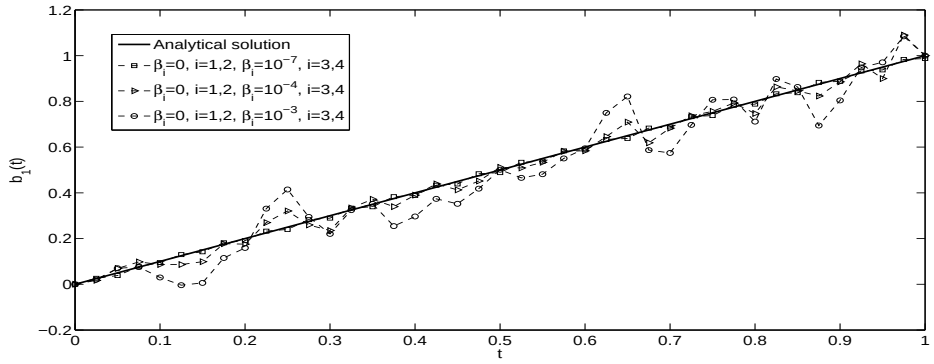

(d)

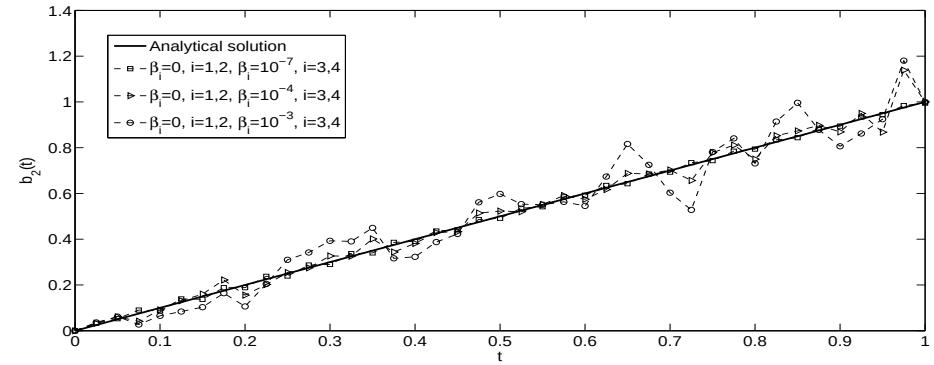

Figure 5.9: The analytical (5.38) and numerical solutions for: (a) $h_1(t)$, (b) $h_3(t)$, (c) $b_1(t)$ and (d) $b_2(t)$, for noise $p = 0$ $(-\square-)$, $p = 0.01\%$ $(-\triangleright-)$ and $p = 0.1\%$ $(-\circ-)$, with regularization, for Example 1.

Table 5.2: The $rmse$ values for $p \in \{0, 0.01\%, 0.1\%\}$ noise, with and without regularization, for Example 1.

p	Regularization	$rmse(h_1)$	$rmse(h_3)$	$rmse(b_1)$	$rmse(b_2)$
0	$\beta_i = 0, i = \overline{1,4}$	3.8E-5	5.0E-5	0.0183	0.0375
	$\beta_3 = \beta_4 = 10^{-8}$	2.0E-5	1.3E-5	9.5E-3	9.9E-3
	$\beta_3 = \beta_4 = 10^{-7}$	**2.0E-5**	**1.3E-5**	**9.6E-3**	**9.8E-3**
	$\beta_3 = \beta_4 = 10^{-6}$	2.0E-5	1.1E-5	0.0107	0.0101
	$\beta_3 = \beta_4 = 10^{-5}$	2.8E-5	1.6E-5	0.0195	0.0164
0.01%	$\beta_i = 0, i = \overline{1,4}$	4.0E-4	5.2E-4	0.3523	0.3406
	$\beta_3 = \beta_4 = 10^{-8}$	3.6E-4	4.2E-4	2.1264	2.1329
	$\beta_3 = \beta_4 = 10^{-7}$	3.4E-4	3.8E-4	0.3124	0.3030
	$\beta_3 = \beta_4 = 10^{-6}$	3.0E-4	2.8E-4	0.2043	0.2311
	$\beta_3 = \beta_4 = 10^{-5}$	2.3E-4	1.6E-4	0.0799	0.1099
	$\beta_3 = \beta_4 = 10^{-4}$	**1.9E-4**	**1.3E-4**	**0.0469**	**0.0526**
	$\beta_3 = \beta_4 = 10^{-3}$	7.1E-4	5.0E-4	0.0931	0.0822
	$\beta_3 = \beta_4 = 10^{-2}$	3.5E-3	2.6E-3	0.1896	0.1610
	$\beta_3 = \beta_4 = 10^{-1}$	0.0183	0.0112	0.3260	0.2793
0.1%	$\beta_i = 0, i = \overline{1,4}$	3.4E-3	3.7E-3	3.3290	3.0690
	$\beta_3 = \beta_4 = 10^{-8}$	3.5E-3	4.2E-3	3.0069	3.0316
	$\beta_3 = \beta_4 = 10^{-7}$	3.5E-3	4.4E-3	2.8401	2.9265
	$\beta_3 = \beta_4 = 10^{-6}$	3.2E-3	3.5E-3	1.7770	2.2791
	$\beta_3 = \beta_4 = 10^{-5}$	2.4E-3	1.8E-3	0.8622	1.0312
	$\beta_3 = \beta_4 = 10^{-4}$	1.7E-3	1.2E-3	0.3243	0.3048
	$\beta_3 = \beta_4 = 10^{-3}$	**1.3E-3**	**9.5E-4**	**0.0999**	**0.1018**
	$\beta_3 = \beta_4 = 10^{-2}$	3.6E-3	2.8E-3	0.1799	0.1542
	$\beta_3 = \beta_4 = 10^{-1}$	0.0154	0.0115	0.3251	0.2791

5.5.2 Example 2 (for inverse problem II)

In this example, we consider the second inverse problem given by equations (5.1)–(5.3), (5.6), (5.7) and (5.15), with the same input data (5.33) and (5.35)–(5.39) as in Example 1, except that the data $\tilde{\mu_3}(t)$ and $\mu_3(t)$ given by equations (5.4) and (5.5) are replaced by the second and third-order heat moment $\mu_6(t)$ and $\mu_7(t)$ given by equations (5.16) and (5.17) as

$$\mu_6(t) = \frac{1+t}{3000}\Big(-1000 + 3250\pi - 250t + 1275\pi t - 15t^2 + 165\pi t^2 + 7\pi t^3 + (15+2t)^3 \tan^{-1}\Big(\frac{15+2t}{10}\Big) - (5+t)^3 \tan^{-1}\Big(\frac{5+t}{10}\Big) + 500 \ln\Big(\frac{325+60t+4t^2}{125+10t+t^2}\Big)\Big), \tag{5.41}$$

$$\mu_7(t) = \frac{1+t}{120000}\Big(5(10+t)(3\pi(20+3t)(50+t(14+t)) - 2(25 \\ +t(95+7t))) + 3(5+2t)(25+2t)(325+4t(15+t))\tan^{-1}\Big(\frac{15+2t}{10}\Big) \\ -3(-5+t)(15+t)(125+t(10+t))\tan^{-1}\Big(\frac{5+t}{10}\Big)\Big). \quad (5.42)$$

Table 5.1 shows that the analytical ((5.41) and (5.42)) and numerical solutions for $\mu_6(t)$ and $\mu_7(t)$ obtained with various mesh sizes $M = N \in \{10, 20, 40\}$ are in very good agreement.

One can remark that the conditions of Theorems 5.2.3 and 5.2.4 are satisfied and therefore, the local existence and uniqueness of the solution are guaranteed. The initial guesses for the vectors $\mathbf{h_1}$, $\mathbf{h_3}$, $\mathbf{b_1}$ and $\mathbf{b_2}$ are given by (5.40), the same as in Example 1. Note that the values of $b_1(0)$ and $b_2(0)$ can be determined using the compatibility of input data in (5.1)–(5.7), see [56, 119, 121].

As we did in Example 1, we start the investigation with the case of exact input data (5.13), (5.14), (5.16) and (5.17), i.e. $p = 0$ in (5.30). The objective function F_1, as a function of the number of iterations without and with regularization is plotted in Figure 5.10. From this figure, it can be seen that a monotonic convergence is rapidly achieved in a few iterations. The objective function F_1 decreases and takes a very low stationary value of $O(10^{-27})$ in about 19 iterations when we do not employ any regularization, i.e. $\beta_i = 0$, $i = \overline{1,4}$, and of $O(10^{-5})$ in the case of regularization with $\beta_1 = \beta_2 = 0$, $\beta_3 = \beta_4 = 10^{-6}$. The numerical reconstruction results for the unknown coefficients are illustrated in Figure 5.11. From Figures 5.11(a) and 5.11(b) it can be noticed that very accurate recoveries for the free boundaries $h_1(t)$ and $h_3(t)$ are obtained. With no regularization, the numerical results for the coefficients $b_1(t)$ and $b_2(t)$ presented in Figures 5.11(c) and 5.11(d) are quite inaccurate with the values of $rmse(b_1) = 0.3001$ and $rmse(b_2) = 1.4094$, respectively. However, when we apply the regularization with $\beta_1 = \beta_2 = 0$, $\beta_3 = \beta_4 = 10^{-6}$ to F_1, we obtain more accurate reconstructions for $b_1(t)$ and $b_2(t)$, with $rmse(b_1)$ and $rmse(b_2)$ values decreasing to 0.0589 and 0.0498, respectively.

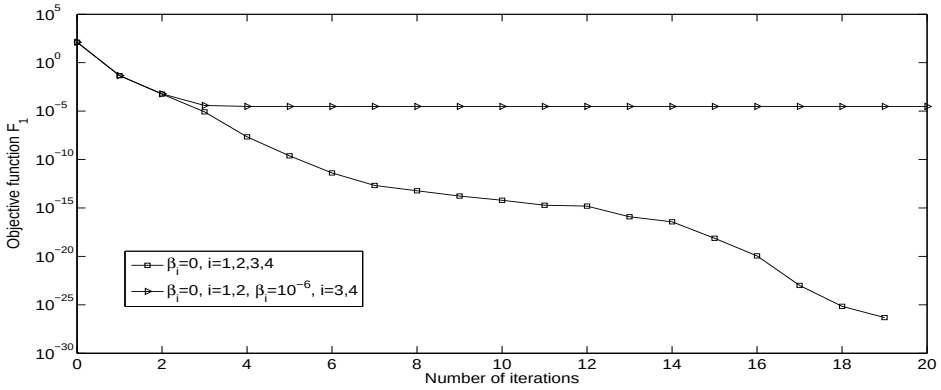

Figure 5.10: The objective function F_1, as a function of the number of iterations, no noise, with and without regularization, for Example 2.

(a)

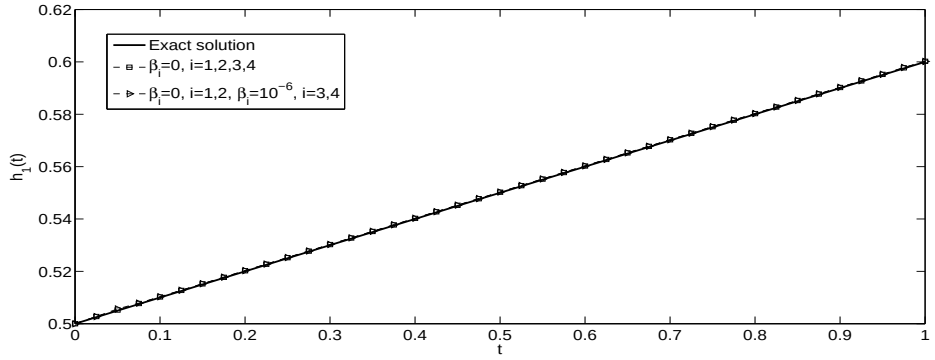

(b)

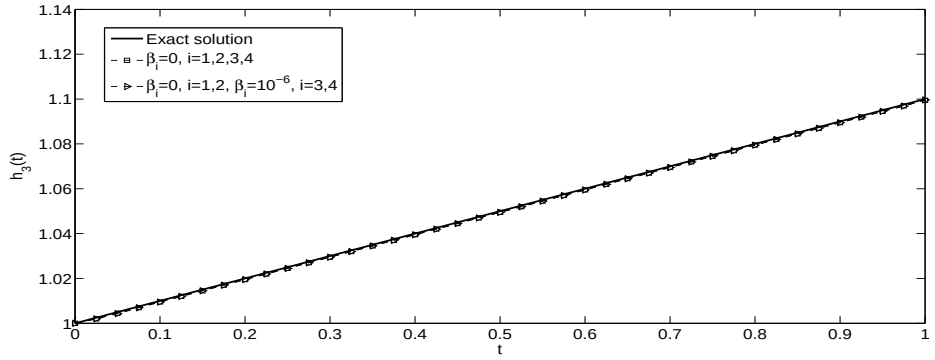

(c)

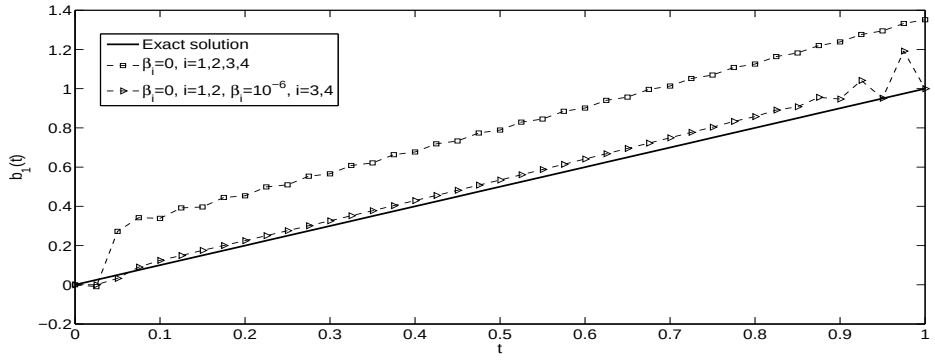

(d)

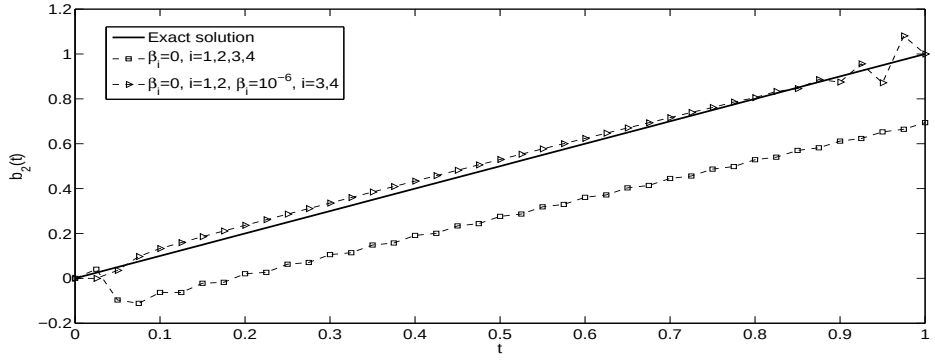

Figure 5.11: The analytical (5.38) and numerical solutions for: (a) $h_1(t)$, (b) $h_3(t)$, (c) $b_1(t)$ and (d) $b_2(t)$, no noise, with and without regularization, for Example 2.

Next, we consider the case of noisy data (5.13), (5.14), (5.16) and (5.17) perturbed by $p = 0.01\%$ noise, as in (5.31). We have also investigated higher amounts of noise p in (5.31), but the results obtained were less accurate and therefore, they are not presented. The investigation of the inversion of noisy data performed in this subsection, when compared with that of Example 1, indicates that the second inverse problem (5.1)–(5.3), (5.6), (5.7), (5.16) and (5.17) is more ill-posed than the first inverse problem (5.1)–(5.7).

The objective function F_1, as a function of the number of iterations, is shown in Figure 5.12. From this figure, it can be seen that in the case of no regularization, i.e. $\beta_i = 0, i = \overline{1,4}$, a slow convergence is recorded and, in fact, the process of minimization of the routine *lsqnonlin* is stopped when the prescribed maximum number of 400 iterations is reached. The corresponding numerical results for the unknown coefficients are presented in Figure 5.13. From Figures 5.13(a) and 5.13(b) it can be seen that stable and accurate numerical results are obtained for the free boundaries $h_1(t)$ and $h_3(t)$. However, from Figures 5.13(c) and 5.13(d) one can observe that unstable (highly oscillatory) and very inaccurate solution for $b_1(t)$ and $b_2(t)$ are obtained with $rmse(b_1) = 48.1$ and $rmse(b_1) = 49.8$. This is expected since the problem under investigation is ill-posed and small errors in the input data (5.13), (5.14), (5.16) and (5.17) lead to a drastic amount of error in the output coefficients $b_1(t)$ and $b_2(t)$. Therefore, regularization is required in order to restore the stability of the solution in the coefficients $b_1(t)$ and $b_2(t)$.

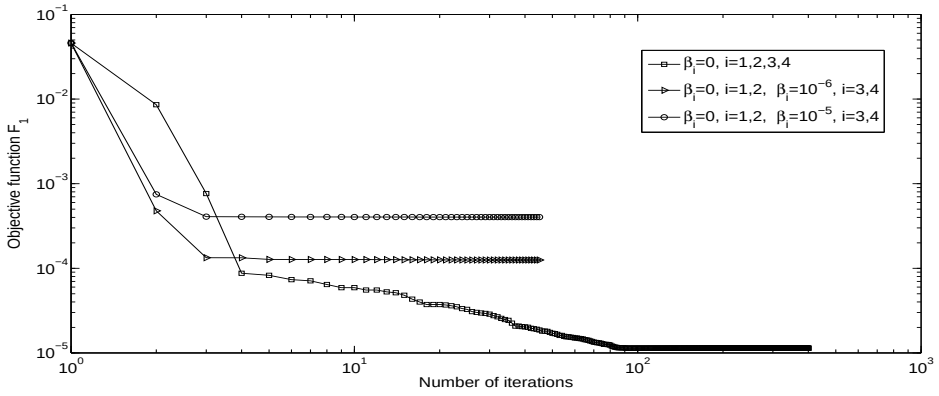

Figure 5.12: The objective function F_1, as a function of the number of iterations, for $p = 0.01\%$ noise, with and without regularization, for Example 2.

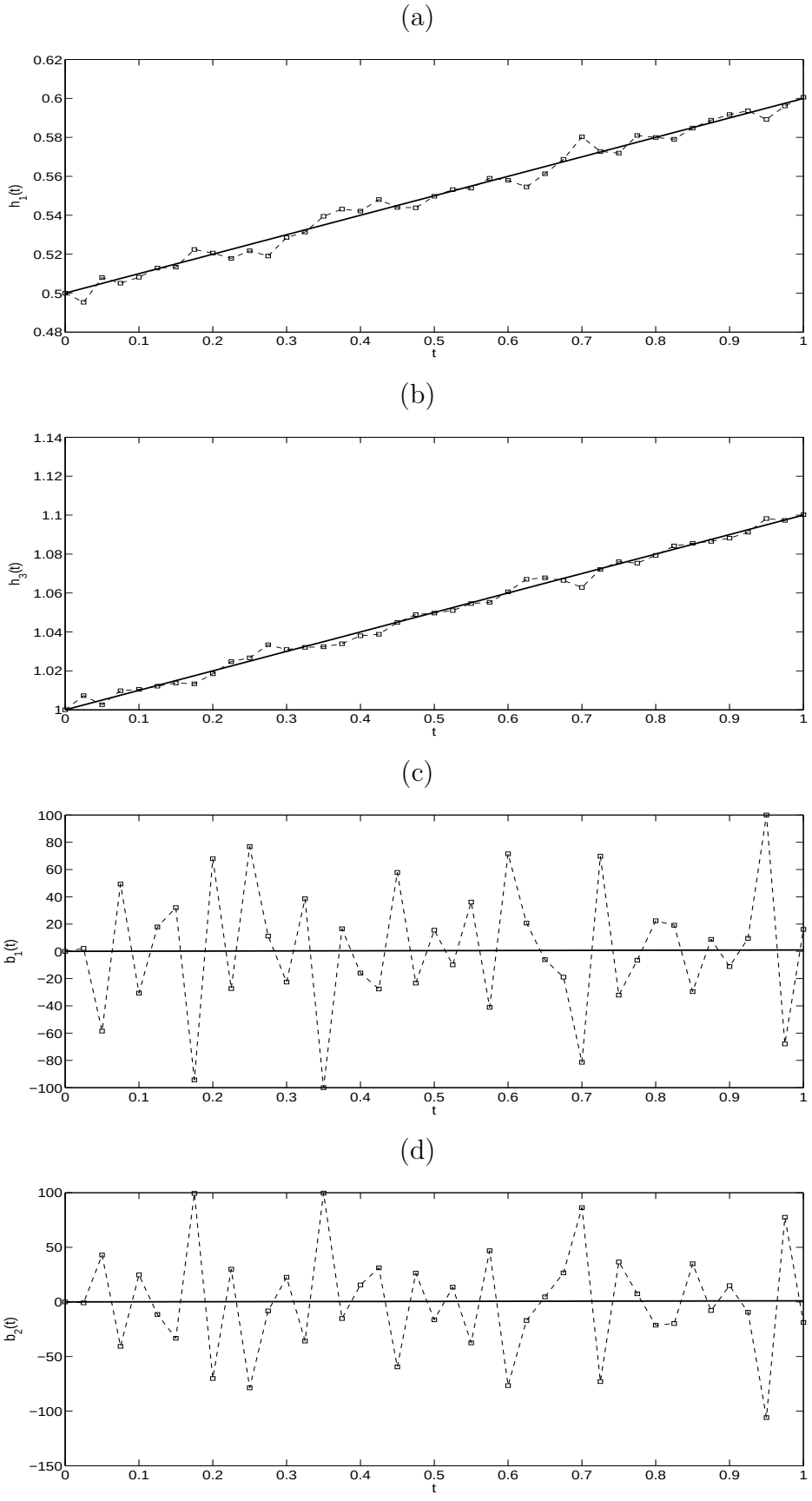

Figure 5.13: The analytical (—) and numerical solutions (−□−) for: (a) $h_1(t)$, (b) $h_3(t)$, (c) $b_1(t)$ and (d) $b_2(t)$, for $p = 0.01\%$ noise, without regularization, for Example 2.

The L-curve, [48], for the choice of the regularization parameters is shown in Figure 5.14, by plotting the solution norm, as a function of the residual norm. From this figure, it can be observed that regularization parameters near the "corner" of the L-curve are $\beta_3 = \beta_4 \in \{10^{-6}, 10^{-5}\}$. The regularized decreasing monotonic convergence of the objective function F_1, as a function of the number of iterations, is shown in Figure 5.12. To stabilise the coefficients $b_1(t)$ and $b_2(t)$, we employ regularization with $\beta_3 = \beta_4 \in \{10^{-6}, 10^{-5}\}$ (suggested by the L-curve in Figure 5.14), obtaining $rmse(b_1) \in \{0.3062, 0.1594\}$ and $rmse(b_2) \in \{0.2920, 0.1590\}$, see Figures 5.15(c) and 5.15(d), for these coefficients. Furthermore, from Table 5.3 it can be seen that the computational time is reduced from 32 hours to 3 hours by the inclusion of regularization in F_1. For more, information about the $rmse$ values for $p = 0.01\%$ noise, with and without regularization, see Table 5.4.

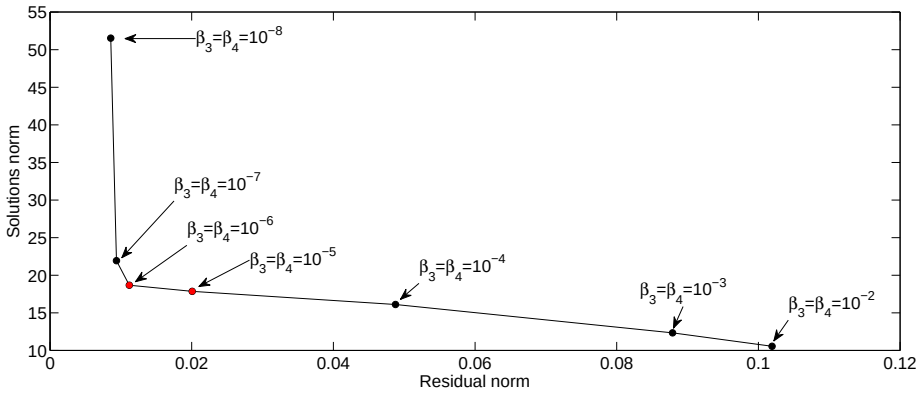

Figure 5.14: The residual norm versus the solution norm for various regularization parameters, for Example 2, with $p = 0.01\%$ noise.

Table 5.3: The $rmse$ values and computational time with $p = 0.01\%$ noise, for Example 2.

$\beta_i = 0, i = 1, 2$	$\beta_i = 0, i = 3, 4$	$\beta_i = 10^{-6}, i = 3, 4$	$\beta_i = 10^{-5}, i = 3, 4$
$rmse(h_1)$	3.9E-3	1.6E-3	1.4E-3
$rmse(h_3)$	2.6E-3	1.4E-3	1.1E-3
$rmse(b_1)$	48.1629	0.3062	0.1594
$rmse(b_2)$	49.8146	0.2920	0.1590
Computational time	32 hours	3 hours	3 hours

(a)

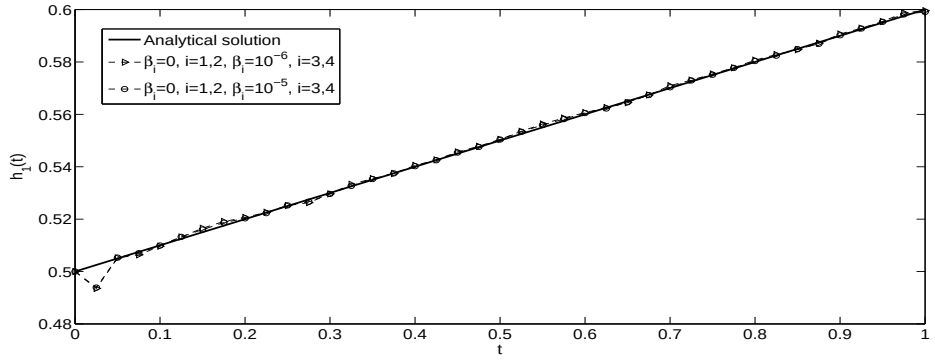

(b)

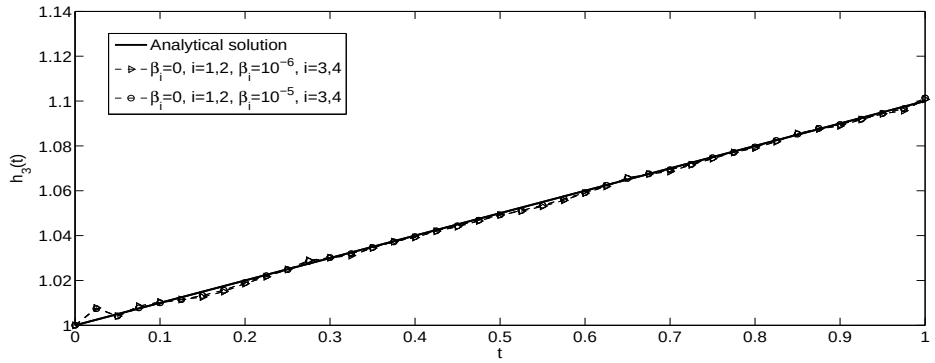

(c)

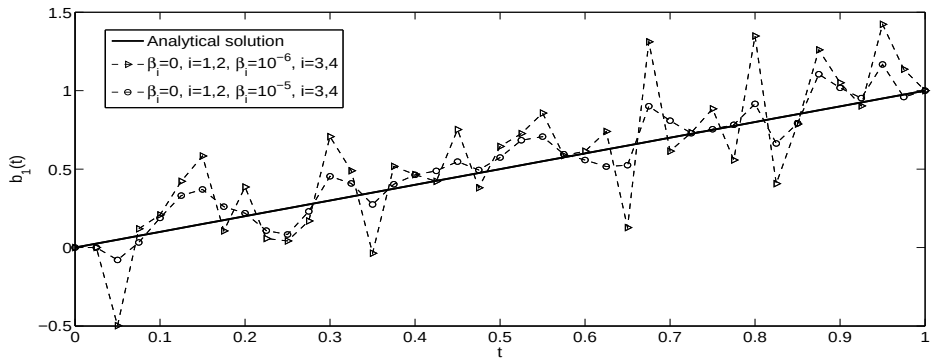

(d)

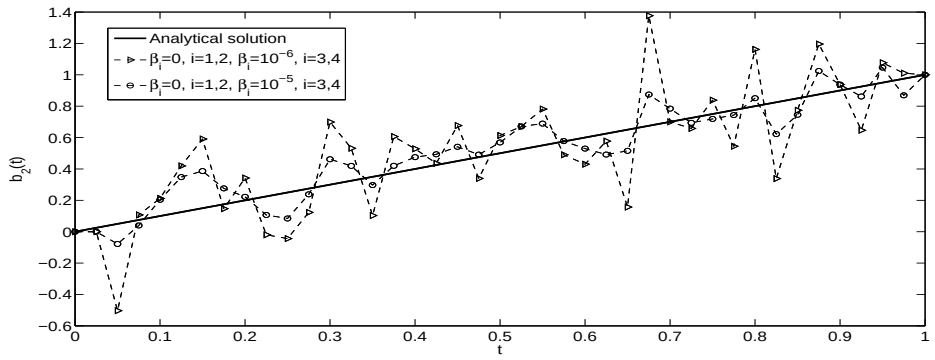

Figure 5.15: The analytical (5.38) and numerical solutions for: (a) $h_1(t)$, (b) $h_3(t)$, (c) $b_1(t)$ and (d) $b_2(t)$, for $p = 0.01\%$ noise, with regularization, for Example 2.

Table 5.4: The *rmse* values for $p \in \{0, 0.01\%\}$ noise, with and without regularization, for Example 2.

p	Regularization	$rmse(h_1)$	$rmse(h_3)$	$rmse(b_1)$	$rmse(b_2)$
0	$\beta_i = 0, i = \overline{1,4}$	2.3E-4	5.2E-4	0.3001	1.4094
	$\beta_3 = \beta_4 = 10^{-8}$	2.8E-4	5.5E-4	0.1284	0.0729
	$\beta_3 = \beta_4 = 10^{-7}$	3.0E-4	5.6E-4	0.0620	0.0339
	$\beta_3 = \beta_4 = 10^{-6}$	**3.0E-4**	**5.4E-4**	**0.0589**	**0.0498**
	$\beta_3 = \beta_4 = 10^{-5}$	3.5E-4	4.2E-4	0.0739	0.0779
0.01%	$\beta_i = 0, i = \overline{1,4}$	3.9E-3	2.6E-3	48.1629	49.8146
	$\beta_3 = \beta_4 = 10^{-8}$	1.4E-3	1.4E-3	3.1935	3.2308
	$\beta_3 = \beta_4 = 10^{-7}$	1.5E-3	1.4E-3	0.7338	0.6982
	$\beta_3 = \beta_4 = 10^{-6}$	1.6E-3	1.4E-3	0.3062	0.2920
	$\beta_3 = \beta_4 = 10^{-5}$	**1.4E-3**	**1.1E-3**	**0.1594**	**0.1590**
	$\beta_3 = \beta_4 = 10^{-4}$	1.8E-3	1.9E-3	0.1632	0.1810
	$\beta_3 = \beta_4 = 10^{-3}$	5.0E-3	6.6E-3	0.4278	0.4377
	$\beta_3 = \beta_4 = 10^{-2}$	6.7E-3	8.9E-3	0.5657	0.5673
	$\beta_3 = \beta_4 = 10^{-1}$	6.9E-3	9.2E-3	0.5860	0.5858

5.6 Conclusions

A simultaneous determination of time-dependent coefficients and multiple free boundaries in the heat equation has been numerically investigated for the first time. The free boundary problems have been reduced to inverse coefficient problems in a fixed domain. The numerical solution of the direct problem based on the FDM with the Crank-Nicolson scheme has been employed. The inverse problem has been solved using the MATLAB optimisation toolbox routine *lsqnonlin* for minimizing the objective function F, or F_1. The Tikhonov regularization has been employed in order to obtain stable and accurate results because the inverse problem is ill-posed and very sensitive to noise. The numerical results have been presented and discussed for the two inverse problems, showing that accurate and stable approximate solutions have been achieved. Based on the numerical results and discussion we can conclude that the Stefan conditions (5.4) and (5.5) contain more information than the heat moments of several orders (5.16) and (5.17). Therefore, the second inverse problem (5.1)–(5.3), (5.6), (5.7), (5.16) and (5.17) is more ill-posed than the first inverse problem (5.1)–(5.7). Although not illustrated, similar conclusions have been obtained for other numerical tests concerning the recovery of non-smooth coefficients with multiple unknown free boundaries.

Chapter 6

Determination of time-dependent coefficients for degenerate parabolic PDEs

6.1 Introduction

In the previous chapters, inverse problems concerned with simultaneously determining several time-dependent coefficients for non-degenerate (regular) parabolic PDEs, with fixed or even moving boundaries, have been investigated. On the other hand, only a few papers were concerned with degenerate parabolic PDEs, [53, 54, 70, 71, 80, 116, 133]. These studies are theoretical and they are important because they establish sufficient conditions for the unique solvability of the time-dependent coefficient identification problems. However, no numerical reconstruction has been attempted and it is the purpose of this chapter to numerically recover the unknown coefficients in a stable and accurate manner. Therefore, in this chapter inverse problems concerned with determining the time-dependent thermal diffusivity and convection coefficients for a (weakly) degenerate parabolic heat equation, together with the temperature from over-determination data is, for the first time, numerically solved. It is supposed that the thermal diffusivity coefficient vanishes at the initial moment of time. Here, we investigate the case of weakly degeneration where the degeneracy is given by a time-dependent power law t^{α} with $\alpha \in (0,1)$, though stronger degeneracies with $\alpha \geq 1$ can also be addressed.

The structure of the chapter is as follows. The mathematical formulations of the inverse problems are described in Section 6.2. In Section 6.3, the numerical solution of the direct problem is based on FDM with the Crank-Nicolson scheme, used as direct solver for these problems. The Tikhonov regularization method is

described in Section 6.4. Numerical results for a few examples are presented and discussed in Section 6.5. Finally, conclusions are presented in Section 6.6.

6.2 Mathematical formulations of the inverse problems

We consider the convection-diffusion equation in a finite slab of length $l > 0$ over a time duration $T > 0$ satisfying the parabolic PDE

$$\frac{\partial u}{\partial t}(x,t) = a(t)\frac{\partial^2 u}{\partial x^2}(x,t) + b(t)\frac{\partial u}{\partial x}(x,t) + f(x,t), \\ (x,t) \in Q_T := (0,l) \times (0,T), \tag{6.1}$$

where u is the unknown temperature, f is a given heat source, and a and b are time-dependent thermal diffusivity and convection coefficients, respectively, which may be known or unknown. For simplicity, we have assumed that no reaction term $c(x,t)u(x,t)$ is present in (6.1). Furthermore, we assume that the PDE (6.1) is weakly degenerate and becomes non-uniformly parabolic, with a belonging to the admissible class

$$\mathcal{A}_\alpha := \Big\{ a \in C[0,T] \Big| \; a(t) > 0 \text{ for } t \in (0,T], \text{ and there exists the finite } \lim_{t \searrow 0} \frac{a(t)}{t^\alpha} > 0 \Big\}, \tag{6.2}$$

where $\alpha \in (0,1)$ is the given degree of weakly power law degeneration. The case $\alpha \geq 1$ corresponding to strong degeneration will be investigated in the future. Equation (6.1) is subjected to the initial condition

$$u(x,0) = \varphi(x), \quad x \in [0,l], \tag{6.3}$$

and the Dirichlet boundary conditions

$$u(0,t) = \mu_1(t), \quad u(l,t) = \mu_2(t), \quad t \in [0,T]. \tag{6.4}$$

We next formulate three inverse problems with respect to whether the coefficients $a(t)$ and/or $b(t)$ are known or unknown and state sufficient conditions for the uniqueness of solution. Denote $\mathcal{E} := C^{2,1}(Q_T) \cap C^{1,0}(\overline{Q_T})$.

6.2.1 Inverse Problem 1 (IP1)

We consider the inverse problem of determining the pair $(a(t), u(x,t)) \in \mathcal{A}_\alpha \times \mathcal{E}$ satisfying (6.1), (6.3), (6.4) and the additional heat flux measurement

$$a(t)\frac{\partial u}{\partial x}(0,t) = q_0(t), \quad t \in [0,T]. \tag{6.5}$$

We state the following uniqueness theorem, which is accommodated from [80, 116].

Theorem 6.2.1. *Assume that the following conditions are satisfied:*

(A) $\varphi \in C^2[0,l],\ \mu_1, \mu_2 \in C^1[0,T],\ b \in C[0,T],\ f \in C^{1,0}(\overline{Q_T})$;

(B) $q_0(t) \neq 0$ *for* $t \in (0,T]$ *and there exists the finite* $\lim\limits_{t \searrow 0} \dfrac{q_0(t)}{t^\alpha} \neq 0$.

Then, the IP1 given by equations (6.1), (6.3)–(6.5) cannot have more than one solution $(a(t), u(x,t)) \in \mathcal{A}_\alpha \times \mathcal{E}$.

A two-dimensional variant of the IP1 has been considered theoretically in [133], but its numerical simulation in the context of our investigation is deferred to a future work.

6.2.2 Inverse Problem 2 (IP2)

We consider the inverse problem of determining the pair $(b(t), u(x,t)) \in C[0,T] \times \mathcal{E}$ satisfying (6.1), (6.3), (6.4) and the additional mass integral measurement

$$\int_0^l u(x,t)dx = \mu_4(t), \quad t \in [0,T]. \tag{6.6}$$

We state the following uniqueness theorem, which is accommodated from [53].

Theorem 6.2.2. *Assume that the following conditions are satisfied:*

(C) $\varphi \in C^1[0,l],\ \mu_1, \mu_2 \in C^1[0,T],\ f \in C^{1,0}(\overline{Q_T})$;

(D) $\mu_1(t) - \mu_2(t) \neq 0$ *for* $t \in [0,T]$.

Then, the IP2 given by equations (6.1), (6.3), (6.4) and (6.6) cannot have more than one solution $(b(t), u(x,t)) \in C[0,T] \times \mathcal{E}$.

6.2.3 Inverse Problem 3 (IP3)

We consider the inverse problem of determining the triplet $(a(t), b(t), u(x,t)) \in \mathcal{A}_\alpha \times C[0,T] \times \mathcal{E}$ satisfying (6.1), (6.3), (6.4) and the additional measurements (6.5) and (6.6). We state the following uniqueness theorem, which is accommodated from [70].

Theorem 6.2.3. *Let the assumptions* (B) *and* (D) *hold and assume also that the following condition is satisfied:*

$$(E) \quad \varphi \in C^3[0,l],\ \mu_1, \mu_2 \in C^1[0,T],\ f \in C^{1,0}(\overline{Q_T}).$$

Then, the IP3 given by equations (6.1), (6.3)–(6.6) cannot have more than one solution $(a(t), b(t), u(x,t)) \in \mathcal{A}_\alpha \times C[0,T] \times \mathcal{E}$.

The proofs of uniqueness Theorems 1–3 given in [53, 70, 80, 116] rely on Green's functions and the theory of Volterra integral equations of the second kind.

6.3 Numerical solution for the direct problem

The direct initial boundary value problem is given by equations (6.1), (6.3) and (6.4), where $a(t) \in \mathcal{A}_\alpha$, $b(t) \in C[0,T]$, $\mu_1(t) \in C^1[0,T]$, $\mu_2(t) \in C^1[0,T]$, $\varphi \in C^2[0,l]$ and $f(x,t) \in C^{1,0}(\overline{Q_T})$ are known, and the solution $u(x,t)$ is to be determined together with the quantities of interest $q_0(t)$ and $\mu_4(t)$. To achieve this, we use the FDM with the Crank-Nicolson scheme, based on subdividing the solution domain $Q_T = (0,l) \times (0,T)$ into M and N subintervals of equal step lengths Δx and Δt, where $\Delta x = l/M$ and $\Delta t = T/N$, respectively. At the node (i,j) we denote $u(x_i, t_j) = u_{i,j}$, where $x_i = i\Delta x$, $t_j = j\Delta t$, $a(t_j) = a_j$, $b(t_j) = b_j$, and $f(x_i, t_j) = f_{i,j}$ for $i = \overline{0, M}$ and $j = \overline{0, N}$. The initial and boundary conditions in equations (6.3) and (6.4) are discretized as

$$u_{i,0} = \varphi(x_i), \quad i = \overline{0, M}, \quad u_{0,j} = \mu_1(t_j), \quad u_{M,j} = \mu_2(t_j), \quad j = \overline{0, N}. \tag{6.7}$$

The expressions in equations (6.5) and (6.6) are calculated using the following second-order finite difference approximation formula and trapezoidal rule for integrals:

$$q_0(t_j) = \Big(\frac{4u_{1,j} - u_{2,j} - 3u_{0,j}}{2(\Delta x)}\Big) a_j, \quad j = \overline{1, N}. \tag{6.8}$$

$$\mu_4(t_j) = \frac{l}{2N}\Big(u_{0,j} + u_{M,j} + 2\sum_{i=1}^{M-1} u_{i,j}\Big), \quad j = \overline{1,N}. \tag{6.9}$$

Using the Crank-Nicolson scheme, we approximate (6.1) by

$$\frac{u_{i,j+1} - u_{i,j}}{\Delta t} = \frac{1}{2}(G_{i,j} + G_{i,j+1}), \quad i = \overline{1,(M-1)},\ j = \overline{0,(N-1)}, \tag{6.10}$$

where

$$G_{i,j} = a_j \frac{u_{i+1,j} - 2u_{i,j} + u_{i-1,j}}{(\Delta x)^2} + b_j \frac{u_{i+1,j} - u_{i-1,j}}{2(\Delta x)} + f_{i,j}, \\ i = \overline{1,(M-1)}, \quad j = \overline{1,N}. \tag{6.11}$$

Because of the degeneracy at the initial time $t = 0$, for $j = 0$,

$$G_{i,0} = f_{i,0} + b_0\varphi'(x_i) + \Psi(x_i), \quad i = \overline{1,(M-1)}, \tag{6.12}$$

where the function

$$\Psi(x) := \lim_{t \searrow 0} a(t)\frac{\partial^2 u}{\partial x^2}(x,t). \tag{6.13}$$

To estimate the function $\Psi(x)$ in (6.13), we proceed as in [58, 116], as follows. From [116], we know that

$$\begin{aligned} \frac{\partial^2 u}{\partial x^2}(x,t) &= \int_0^l \mathcal{G}(x,t;\xi,0)\varphi''(\xi)d\xi \\ &+ \int_0^t \left[\frac{\partial \mathcal{G}}{\partial \xi}(x,t;0,\tau)\Big(\mu_1'(\tau) - f(0,\tau) - b(\tau)\frac{\partial u}{\partial \xi}(0,\tau)\Big)\right. \\ &\left. - \frac{\partial \mathcal{G}}{\partial \xi}(x,t;l,\tau)\Big(\mu_2'(\tau) - f(l,\tau) - b(\tau)\frac{\partial u}{\partial \xi}(l,\tau)\Big)\right]d\tau \\ &- \int_0^t \int_0^l \frac{\partial \mathcal{G}}{\partial \xi}(x,t;\xi,\tau)\Big(\frac{\partial f}{\partial \xi}(\xi,\tau) + b(\tau)\frac{\partial^2 u}{\partial \xi^2}(\xi,\tau)\Big)d\xi d\tau, \quad (x,t) \in Q_T, \end{aligned} \tag{6.14}$$

where

$$\mathcal{G}(x,t;\xi,\tau) = \frac{H(t-\tau)}{2\sqrt{\pi(\theta(t) - \theta(\tau))}} \sum_{n=-\infty}^{\infty} \left[\exp\left(-\frac{(x - \xi + 2nl)^2}{4(\theta(t) - \theta(\tau))}\right)\right. \\ \left. - \exp\left(-\frac{(x + \xi + 2nl)^2}{4(\theta(t) - \theta(\tau))}\right)\right] \tag{6.15}$$

is the Green function for the equation $u_t = a(t)u_{xx}$ with Dirichlet boundary conditions, H is the Heaviside function and $\theta(t) = \int_0^t a(\tau)d\tau$. From [80], we also

know that when $b \equiv 0$, then (6.14) simplifies as

$$\frac{\partial^2 u}{\partial x^2}(x,t) = \int_0^l \mathcal{G}(x,t;\xi,0)\varphi''(\xi)d\xi + \int_0^t \left[\frac{\partial \mathcal{G}}{\partial \xi}(x,t;0,\tau)\Big(\mu_1'(\tau) - f(0,\tau)\Big) - \frac{\partial \mathcal{G}}{\partial \xi}(x,t;l,\tau)\Big(\mu_2'(\tau) - f(l,\tau)\Big)\right]d\tau - \int_0^t \int_0^l \frac{\partial \mathcal{G}}{\partial \xi}(x,t;\xi,\tau)\frac{\partial f}{\partial \xi}(\xi,\tau)d\xi d\tau, \quad (x,t) \in Q_T, \tag{6.16}$$

and we have the estimates

$$\Big|\int_0^l \mathcal{G}(x,t;\xi,0)\varphi''(\xi)d\xi\Big| \leq ||\varphi''||_{L^\infty(0,l)}, \tag{6.17}$$

$$\Big|\int_0^t \int_0^l \frac{\partial \mathcal{G}}{\partial \xi}(x,t;\xi,\tau)\frac{\partial f}{\partial \xi}(\xi,\tau)d\xi d\tau\Big| \leq C_0 t^{(1-\alpha)/2}, \tag{6.18}$$

$$\Big|\int_0^t \frac{\partial \mathcal{G}}{\partial \xi}(x,t;0,\tau)\Big(\mu_1'(\tau) - f(0,\tau)\Big)d\tau\Big| \leq \frac{C_1}{t^\alpha}, \tag{6.19}$$

$$\Big|\int_0^t \frac{\partial \mathcal{G}}{\partial \xi}(x,t;l,\tau)\Big(\mu_2'(\tau) - f(l,\tau)\Big)d\tau\Big| \leq \frac{C_2}{t^\alpha}, \tag{6.20}$$

for some positive constants C_0, C_1 and C_2.

Away from $t = 0$ the heat equation (6.1) is non-degenerate and it can be approximated as usual using the Crank-Nicolson FDM, as follows:

$$\begin{aligned} &-A_{j+1}u_{i-1,j+1} + (1 + B_{j+1})u_{i,j+1} - C_{j+1}u_{i+1,j+1} \\ &\quad = A_j u_{i-1,j} + (1 - B_j)u_{i,j} + C_j u_{i+1,j} + \frac{\Delta t}{2}(f_{i,j} + f_{i,j+1}), \end{aligned} \tag{6.21}$$

for $i = \overline{1,(M-1)}$, $j = \overline{1,(N-1)}$, where

$$A_j = \frac{(\Delta t)a_j}{2(\Delta x)^2} - \frac{(\Delta t)b_j}{4(\Delta x)}, \quad B_j = \frac{(\Delta t)a_j}{(\Delta x)^2}, \quad C_j = \frac{(\Delta t)a_j}{2(\Delta x)^2} + \frac{(\Delta t)b_j}{4(\Delta x)}. \tag{6.22}$$

At each time step t_{j+1}, for $j = \overline{1,(N-1)}$, using the Dirichlet boundary conditions (6.7), the difference equation (6.21) can be reformulated as a $(M-1) \times (M-1)$ system of linear equations

$$G\mathbf{u} = \mathbf{k}, \tag{6.23}$$

where $\mathbf{u} = (u_{1,j+1}, u_{2,j+1}, ..., u_{M-2,j+1}, u_{M-1,j+1})^{\mathrm{T}}$, $\quad \mathbf{k} = (k_1, k_2, ..., k_{M-1})^{\mathrm{T}}$,

$$G = \begin{pmatrix} 1+B_{j+1} & -C_{j+1} & 0 & ... & 0 & 0 & 0 \\ -A_{j+1} & 1+B_{j+1} & -C_{j+1} & ... & 0 & 0 & 0 \\ \vdots & \vdots & \vdots & \ddots & \vdots & \vdots & \vdots \\ 0 & 0 & 0 & ... & -A_{j+1} & 1+B_{j+1} & -C_{j+1} \\ 0 & 0 & 0 & ... & 0 & -A_{j+1} & 1+B_{j+1} \end{pmatrix},$$

$$k_1 = A_j\mu_1(t_j) + (1-B_j)u_{1,j} + C_j u_{2,j} + A_{j+1}\mu_1(t_{j+1}) + \frac{\Delta t}{2}(f_{1,j+1} + f_{1,j}),$$

$$k_i = A_j u_{i-1,j} + (1-B_j)u_{i,j} + C_j u_{i+1,j} + \frac{\Delta t}{2}(f_{i,j+1} + f_{i,j}),\ i = \overline{2,(M-2)},$$

$$k_{M-1} = A_j u_{M-2,j} + (1-B_j)u_{M-1,j} + C_j\mu_2(t_j) + C_{j+1}\mu_2(t_{j+1}) + \frac{\Delta t}{2}(f_{M-1,j+1} + f_{M-1,j}).$$

6.4 Numerical solution for the inverse problems

We wish to obtain stable reconstructions of the unknown coefficients $a(t)$ and/or $b(t)$ together with the temperature $u(x,t)$, by minimizing the nonlinear Tikhonov regularization function

$$F_1(\mathbf{a}) = \sum_{j=1}^{N} \Big[a_j u_x(0,t_j) - q_0(t_j)\Big]^2 + \beta \sum_{j=1}^{N} a_j^2, \tag{6.24}$$

or,

$$F_2(\mathbf{b}) = \sum_{j=1}^{N} \Big[\int_0^l u(x,t_j)dx - \mu_4(t_j)\Big]^2 + \beta \sum_{j=1}^{N} b_j^2, \tag{6.25}$$

or,

$$F_3(\mathbf{a},\mathbf{b}) = \sum_{j=1}^{N} \Big[a_j u_x(0,t_j) - q_0(t_j)\Big]^2 + \sum_{j=1}^{N} \Big[\int_0^l u(x,t_j)dx - \mu_4(t_j)\Big]^2 + \beta\Big(\sum_{j=1}^{N} a_j^2 + \sum_{j=1}^{N} b_j^2\Big), \tag{6.26}$$

respectively, where u solves (6.1), (6.3) and (6.4) for given $\mathbf{a}$ and $\mathbf{b}$, and $\beta \geq 0$ is regularization parameter to be prescribed. The minimization of F_1, or F_2, or F_3, is performed using the MATLAB toolbox routine *lsqnonlin*. In the numerical computation, we take the parameters of the routine as follows.

- Maximum number of iterations, (MaxIter) = 400.
- Maximum number of objective function evaluations, (MaxFunEvals) = $10^5\times$(number of variables).
- Termination tolerance on the function value, (TolFun) = 10^{-20}.
- Solution Tolerance, (SolTol) = 10^{-20}.

The IP1, IP2 and IP3 are solved subject to both exact and noisy measurements (6.5) and (6.6). The noisy data are numerically simulated as follows:

$$q_0^{\epsilon 1}(t_j) = q_0(t_j) + \epsilon 1_j, \quad \mu_4^{\epsilon 2}(t_j) = \mu_4(t_j) + \epsilon 2_j, \quad j = \overline{1, N}, \tag{6.27}$$

where $\epsilon 1_j$ and $\epsilon 2_j$ are random variables generated from a Gaussian normal distribution with mean zero and standard deviations $\sigma 1$ and $\sigma 2$ given by

$$\sigma 1 = p \times \max_{t\in[0,T]} |q_0(t)|, \quad \sigma 2 = p \times \max_{t\in[0,T]} |\mu_4(t)|, \tag{6.28}$$

where p represents the percentage of noise. We use the MATLAB function *normrnd* to generate the random variables $\underline{\epsilon 1} = (\epsilon 1_j)_{j=\overline{1,N}}$ and $\underline{\epsilon 2} = (\epsilon 2_j)_{j=\overline{1,N}}$ as follows:

$$\underline{\epsilon 1} = normrnd(0, \sigma 1, N), \quad \underline{\epsilon 2} = normrnd(0, \sigma 2, N). \tag{6.29}$$

6.5 Numerical results and discussion

In this section, we present examples for IP1, IP2 and IP3 in order to test the accuracy and stability of the numerical methods introduced in Section 6.3 based on the FDM, described in Section 6.3, combined with the minimization of the objective function F_1, or F_2, or F_3, described in Section 6.4. Furthermore, we add noise to the input data (6.5) and (6.6) to simulate the real situation of noisy measurements, by using equations (6.27)–(6.29). To assess the accuracy of the approximate solutions, we introduce the root mean square errors (rmse) defined as follows:

$$rmse(a) = \left[\frac{T}{N}\sum_{j=1}^{N}\left(a^{Numerical}(t_j) - a^{Exact}(t_j)\right)^2\right]^{1/2}, \tag{6.30}$$

$$rmse(b) = \left[\frac{T}{N}\sum_{j=1}^{N}\left(b^{Numerical}(t_j) - b^{Exact}(t_j)\right)^2\right]^{1/2}. \tag{6.31}$$

For simplicity, we take $l = T = 1$ in all examples. We take the lower and upper simple bounds for $a(t)$ to be 0 and 10^2, and for $b(t)$ to be -10^2 and 10^2, respectively. These bounds allow a wide search range for the unknowns. In the FDM, we take $M = N = 40$. We also take $\alpha = 0.5$ as a typical degree of weak power law degeneracy in (6.2).

6.5.1 Example 1 (for IP1) - Finding $a(t)$ when $b(t)$ is known

Consider the IP1 given by equations (6.1), (6.3)–(6.5) with unknown thermal diffusivity $a(t)$, and input data

$$\varphi(x) = x^3 + x,\ \mu_1(t) = 0,\ \mu_2(t) = 2e^t,\quad f(x,t) = xe^t(1 - t^{1/2} + x^2), \tag{6.32}$$

$$b(t) = 0, \tag{6.33}$$

$$q_0(t) = t^{1/2}e^t/6. \tag{6.34}$$

One can observe that the assumptions (A) and (B) of Theorem 6.2.1 are satisfied and thus the solution of IP1 is unique, if it exists. It can easily be checked by direct substitution that the analytical solution for the temperature $u(x,t)$ is

$$u(x,t) = (x^3 + x)e^t, \quad (x,t) \in \overline{Q_T} \tag{6.35}$$

and for the thermal diffusivity $a(t)$ is

$$a(t) = t^{1/2}/6, \quad t \in [0,1]. \tag{6.36}$$

We take the inital guess for $a(t)$ as $a^0(t) = t/6$ for $t \in (0,1]$, knowing that since $a \in \mathcal{A}_\alpha$ we must have $a(0) = 0$.

Before we attempt any finite-difference numerics it is important to calculate the function $\Psi(x)$ given by equation (6.13) since its value is needed in initiating the FDM time-marching procedure in equation (6.12). With the data (6.32) and (6.33) and using (6.2), equation (6.13) yield that, [59],

$$\Psi(x) = -\lim_{t\searrow 0} a(t)\int_0^t \frac{\partial \mathcal{G}}{\partial \xi}(x,t;1,\tau)e^\tau \tau^{1/2}d\tau = 0. \tag{6.37}$$

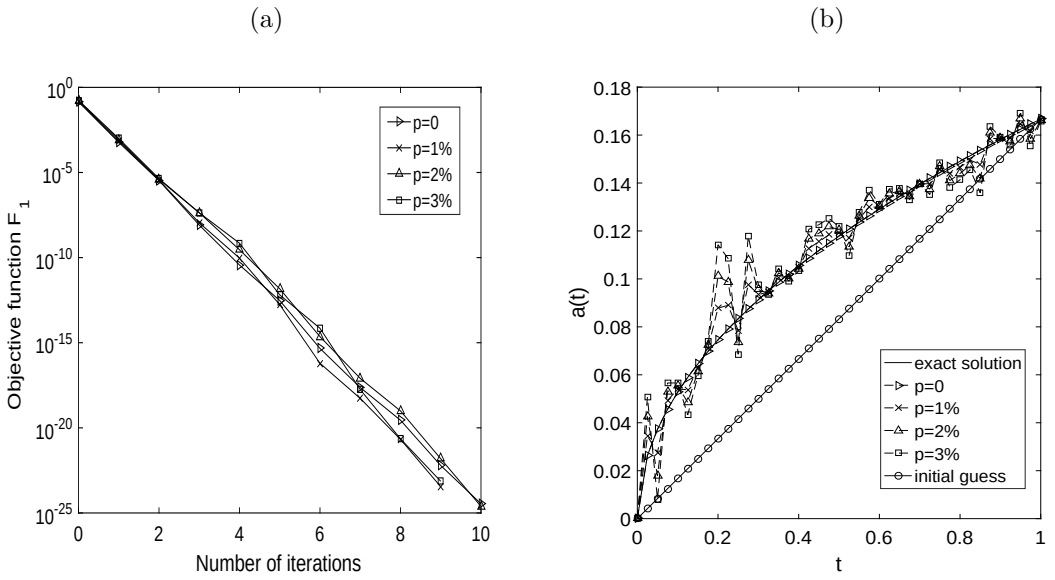

Figure 6.1: (a) The unregularized objective function F_1, as a function of the number of iterations, and (b) the solution for the thermal diffusivity $a(t)$, for Example 1.

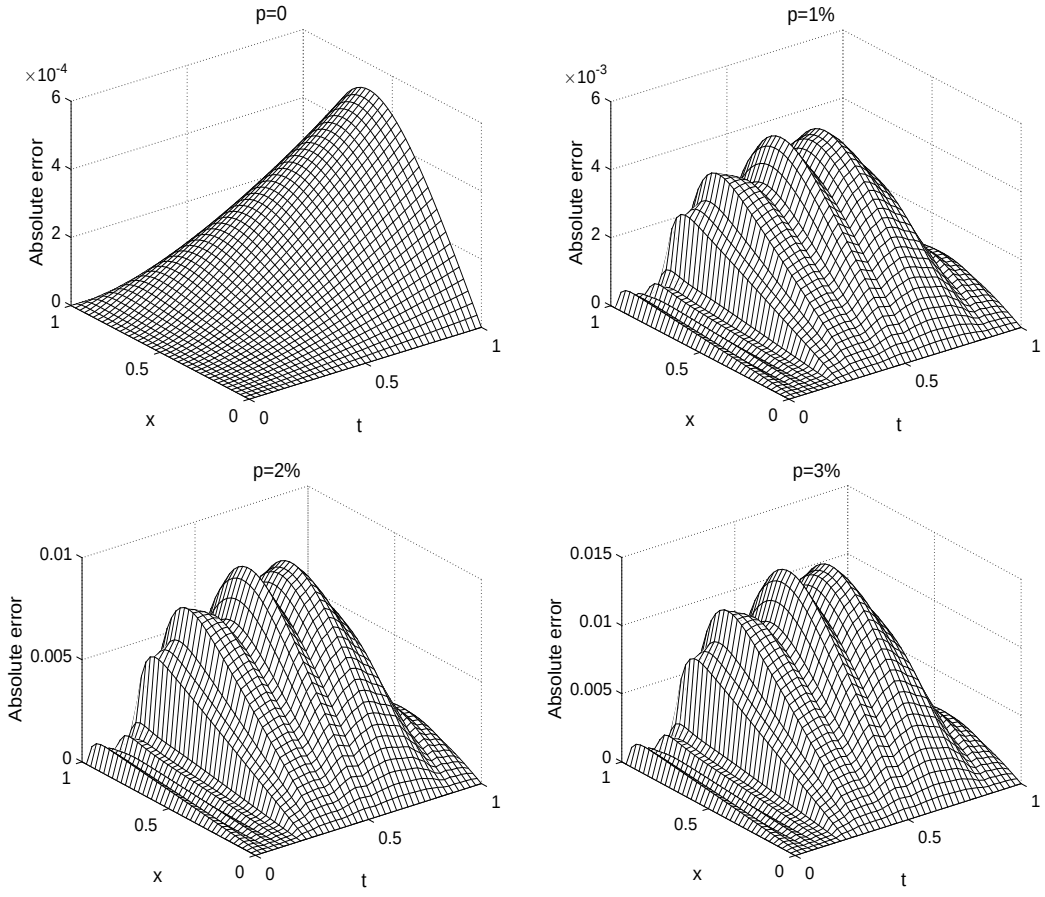

Figure 6.2: The absolute error between the exact (6.35) and numerical solutions for the temperature $u(x,t)$, for Example 1, with $p \in \{0,1,2,3\}\%$ noise.

We attempt to recover the unknown thermal diffusivity $a(t)$ and the tempera-

ture $u(x,t)$ for exact input data, i.e. $p = 0$ in (6.26), as well as for $p \in \{1,2,3\}\%$ noisy data. The unregularized objective function F_1 given by (6.24) with $\beta = 0$, as a function of the number of iterations, is plotted in Figure 6.1(a). From this figure, it can be seen that the objective function F_1 is rapidly decreasing to a very low value of $O(10^{-25})$ in about 10 iterations (in less than 3 minutes CPU time). The related numerical results for the thermal diffusivity $a(t)$ are presented in Figure 6.1(b). From this figure it can be seen that there is good agreement between the numerical results and the analytical solution (6.36) for exact data, i.e. $p = 0$, and consistent with the errors in the input data for $p > 0$. The numerical solution for the thermal diffusivity converges to the analytical solution (6.36), as the percentage of noise p decreases, with $rmse(a) \in \{0.0001, 0.0044, 0.0088, 0.0132\}$ for $p \in \{0,1,2,3\}\%$, respectively.

Finally, Figure 6.2 shows the absolute error between the exact solution (6.35) and the numerical solutions for the temperature $u(x,t)$ for various amounts of noise $p \in \{0,1,2,3\}\%$. From this figure it can be seen that the numerical solution is stable and furthermore, its accuracy improves as the noise level p decreases.

6.5.2 Example 2 (for IP2) - Finding $b(t)$ when $a(t)$ is known

Consider the IP2 given by equations (6.1), (6.3), (6.4) and (6.6) with unknown covection coefficient $b(t)$, and input data (6.32), (6.36) and

$$\mu_4(t) = 3e^t/4. \tag{6.38}$$

One can remark that the assumptions (C) and (D) of Theorem 6.2.2 are satisfied and thus the solution of IP2 is unique, if it exists. In fact, the analytical solution for the unknown convection coefficient $b(t)$ is given by (6.33) and for the temperature $u(x,t)$ by (6.35). Although the analytical solution (6.33) for $b(t)$ is trivial, the numerical $rmse(b)$ given by (6.31) can still be calculated and is meaningful.

We take the initial guess for $b(t)$ as $b^0(t) = t(1-t)$ for $t \in (0,1]$, knowing that from (6.1) and (6.13) we have that $b(0) = (\mu_1'(0) - \Psi(0) - f(0,0))/\varphi'(0)$. This parabolic initial guess is sufficiently far from the analytical solution (6.33).

We consider first the case where there is no noise (i.e. $p = 0$) included in the input data $\mu_4(t)$ in (6.38). The objective function F_2, as a function of the number of iterations is displayed in Figure 6.3(a). From this figure, it can be seen that the decreasing convergence of the objective function F_2 is very fast and is achieved in 5 iterations (in 2 minutes CPU time) to reach a stationary value of $O(10^{-29})$. The corresponding numerical results of the time-dependent convection coefficient $b(t)$ are depicted in Figure 6.3(b) and accurate results of $O(10^{-4})$ error

can be observed.

Next, we investigate the stability of the IP2 with respect to noise. We include $p = 1\%$ noise to the data (6.38) simulated numerically, via equation (6.27) for $\mu_4(t)$. The $rmse$ values (6.31) versus the number for the unknown convection coefficient $b(t)$ are presented in Figure 6.4 with and without regularization, versus the number of iterations. It can be seen that the $rmse$ values settle rapidly to a stationary value $O(10^{-3})$ after 2 to 3 iterations when regularization is included, but in case of no regularization they increase with the number of iterations, as expected since the unregularized solution is unstable. In Figure 6.5 and Table 6.1 we present the unknown convection coefficient $b(t)$ and the $rmes(b)$ given by equation (6.31), the number of iterations and computational time. It can be seen that the numerical results for the convection coefficient are unstable (highly oscillating and unbounded), see Figure 6.5(a), if no regularization, i.e. $\beta = 0$, is employed, or even if β is too small such as 10^{-3}. Clearly, one can observe the effect of the regularization parameter $\beta > 0$ in decreasing the oscillatory unstable behaviour of the convection coefficient $b(t)$. Overall, the numerical results obtained with $\beta \in \{1, 2\}$ seem stable and accurate, see Figure 6.5(b) and Table 6.1.

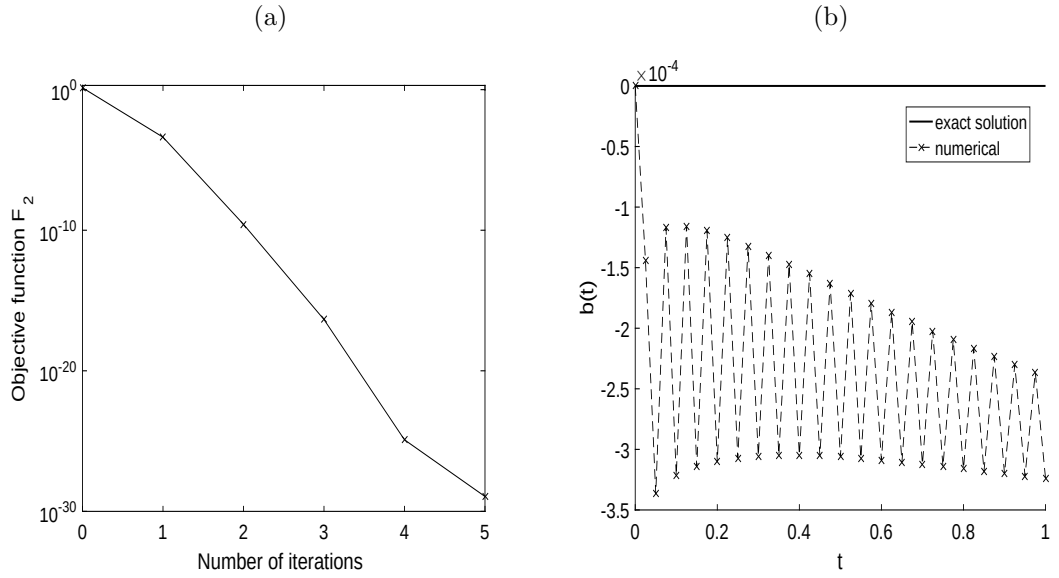

Figure 6.3: (a) The objective function F_2, as a function of the number of iterations, and (b) the solution for the convection coefficient $b(t)$, for Example 2, with no noise and no regularization.

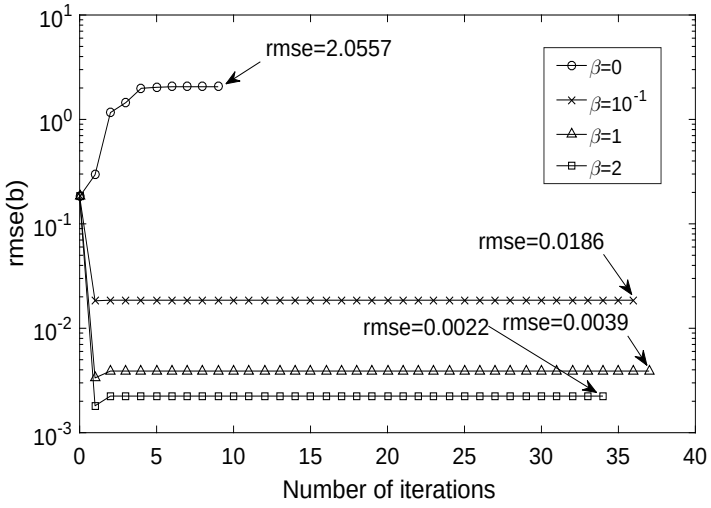

Figure 6.4: The *rmse* values for the convection coefficient $b(t)$, as functions of the number of iterations, for Example 2 with $p = 1\%$ noise, with and without regularization.

(a) (b)

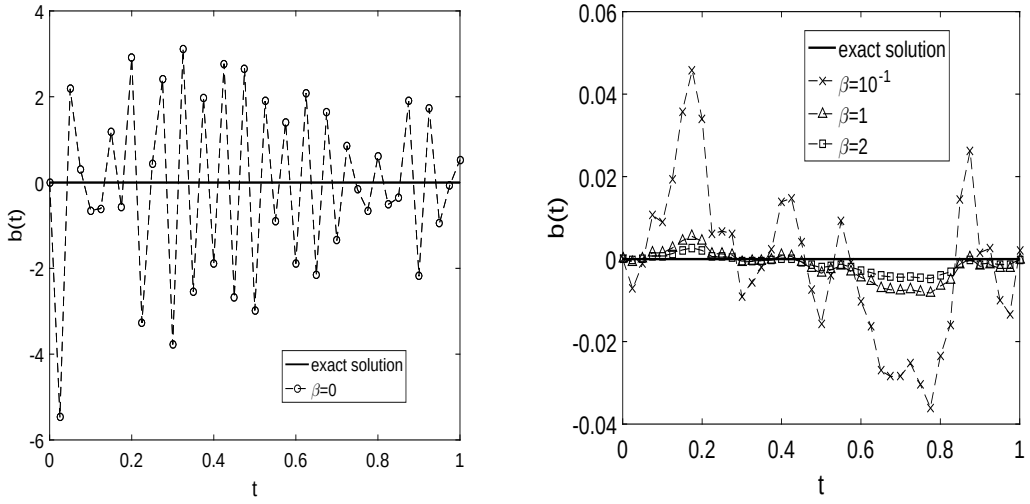

Figure 6.5: The exact (6.33) and numerical solutions for the convection coefficient $b(t)$, for $p = 1\%$ noise, (a) without regularization and (b) with regularization, for Example 2.

Table 6.1: The $rmse(b)$ values, number of iterations and computational time for $p \in \{0, 1\%\}$ noise, with and without regularization, for Example 2.

p	β	$rmse(b)$	Iter	Time
0	0	2.5E-4	5	2 mins
1%	0	2.0557	9	3 mins
	10^{-3}	0.3269	37	9 mins
	10^{-2}	0.0812	34	7 mins
	10^{-1}	0.0186	36	8 mins
	1	0.0039	37	9 mins
	2	0.0022	34	7 mins

6.5.3 Example 3 (for IP3) - Finding $a(t)$ and $b(t)$ together

Consider the IP3 given by equations (6.1), (6.3)–(6.6) with unknown coefficients $a(t)$ and $b(t)$, and input data (6.32), (6.34) and (6.38). One can observe that the assumptions (B), (D) and (E) of Theorem 6.2.3 are satisfied and thus the solution of IP3 is unique. The analytical solution for the triplet $(u(x,t), a(t), b(t))$ is given by equations (6.35), (6.36) and (6.33), respectively.

We start first with the case of exact data, i.e. $p = 0$. Figure 6.6 illustrates the exact and numerical coefficients $a(t)$ and $b(t)$ plotted after 6 iterations of minimization of the objective function F_3 in (6.26) without regularization, i.e. $\beta = 0$. Frome this figure, it can be seen that a very good agreement between the numerical and analytical solutions are obtained with $rmse(a) = 2.8E-4$ and $rmse(b) = 7.0E-4$.

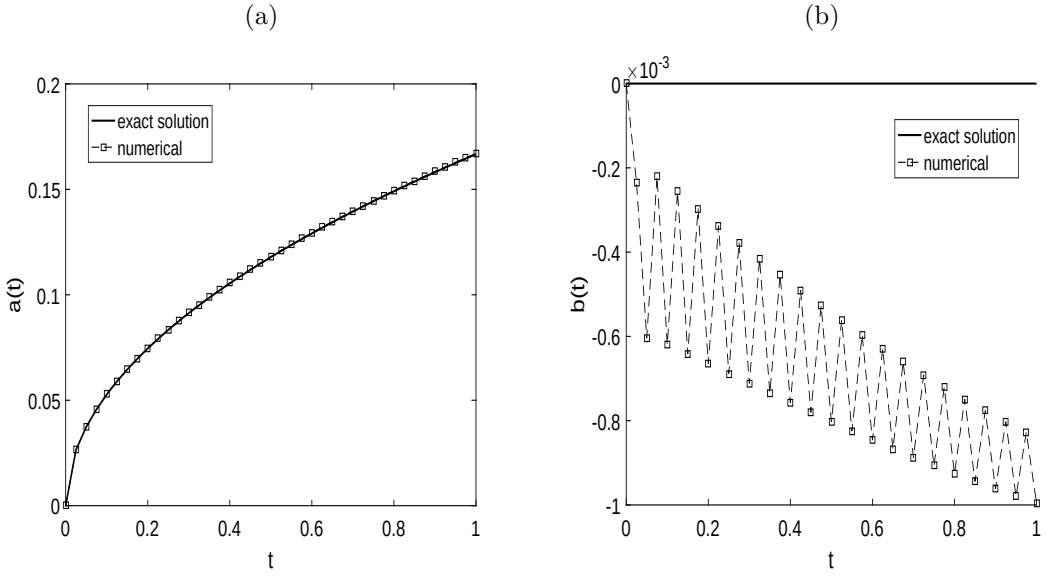

Figure 6.6: The exact ((6.36) and (6.33)) and numerical solutions for: (a) the thermal diffusivity $a(t)$ and (b) the convection coefficient $b(t)$, for Example 3, with no noise and no regularization.

We next include $p = 1\%$ in the input data (6.34) and (6.38). From the previous IP2 analysis, we anticipate that regularization is needed in order to achieve stable and accurate results. The numerical results for the thermal diffusivity $a(t)$ and the convection coefficient $b(t)$ for $p = 1\%$ noise are presented in Figure 6.7. From this figure it can be seen that stable and reasonable accurate numerical results are obtained for $\beta \in \{10^{-2}, 10^{-1}\}$.

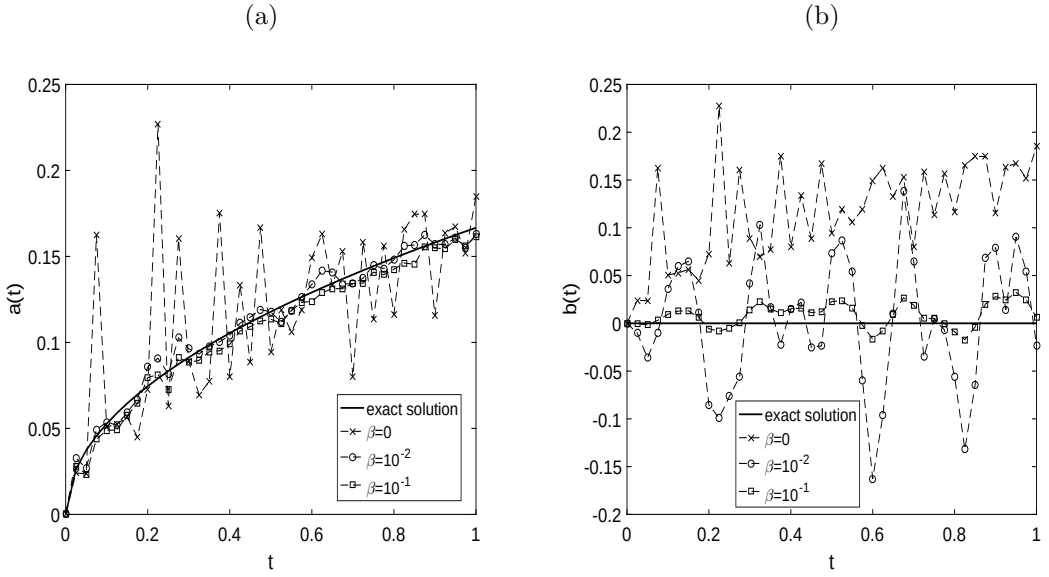

Figure 6.7: The exact ((6.36) and (6.33)) and numerical solutions for: (a) the thermal diffusivity $a(t)$ and (b) the convection coefficient $b(t)$, with $p = 1\%$ noise for Example 3, with and without regularization.

6.6 Conclusions

This chapter has presented the determination of time-dependent thermal diffusivity coefficient and/or the convection coefficient for a weakly degenerate heat equation from heat flux and/or mass/energy measurement/specification/ overdetermination. Three coefficient identification problems (termed IP1, IP2 and IP3) have been investigated. The uniqueness of solution holds under easy verifiable sufficient conditions on the input data, as proven in the previous theoretical literature [53, 70, 80, 116] but without numerical realisation. We stress that when solving parabolic PDEs which are degenerate at the initial time $t = 0$, the numerical challenge is how to calculate the function $\Psi(x)$ in (6.13) in order to initiate, via (6.12), the time marching FDM process. The resulting inverse problems have been reformulated as constrained regularized minimization problems which were solved using the MATLAB optimization toolbox routine *lsqnonlin*. The nonlinear Tikhonov regularization has been employed in order to obtain stable and

accurate results because the inverse problems under investigation are ill-posed and sensitive to noise. The numerically obtained results are stable and accurate. The main difficulty in regularization when we solve the IP2 or IP3 is how to choose an appropriate regularization parameter β which compromises between accuracy and stability. However, one can use techniques such as the L-curve method [48] or Morozov's discrepancy principle [100] to find such a parameter, but in our work we have used trial and error. As mentioned in [35], the regularization parameter β is selected based on experience by first choosing a small value and gradually increasing it until any numerical oscillations in the unknown coefficients disappear.

The reconstruction of time-dependent thermal diffusivity and convection coefficients for a weakly degenerate heat equation with free boundary, [75], will be investigated in a future work.

Chapter 7

Determination of an additive time- and space-dependent heat source coefficient

7.1 Introduction

Inverse problems for the parabolic heat equation consisting of determining the unknown radiative/absorption/perfusion coefficient depending on both time and space have recently received some attention, [31, 36, 115]. The knowledge of this physical property is important in understanding the heat transfer in biological tissue, [128]. Its direct measurement is not available in the general case when it depends on both space and time. However, it can be inferred by inverse methods based on the measurement of the interior temperature, as considered in [130]. On the other hand, this formulation means that infinitely many intrusive temperature measurements with thermocouples embedded inside the material are necessary at all space points and for all times. A possible alternative to this general inverse modelling is to restrict the generality of the coefficient by seeking it as a sum of a function dependent of time and one dependent of space. This additive class in which the admissible coefficient is sought allows to formulate an inverse problem for which the measurement of the temperature in time at a single fixed space point together with measurement in space at a fixed time are sufficient to ensure that the identification is possible. A similar approach has previously been investigated in related problems concerned with the identification of an additive heat source, [49, 52]. However, the inverse heat source problem is linear whilst the coefficient identification problem investigated in this chapter is nonlinear and this significantly complicates its study.

The chapter is structured as follows: In Section 7.2, the mathematical formu-

lation of the inverse problem is given. In Section 7.3, the numerical solution of the direct problem based on the FDM with a Crank-Nicolson scheme is briefly introduced. In Section 7.4, the numerical approach to solve the inverse problem based on a minimization algorithm is given. Numerical results are presented and discussed in Section 7.5. Finally, conclusions are stated in Section 7.6.

7.2 Mathematical formulation

Fix the parameters $L > 0$ and $T > 0$ representing the length of a finite slab and the time duration, respectively. Denote by $Q_T = \{(x,t)|\ 0 < x < L, 0 < t < T\}$ the solution domain. In the context of bio-heat transfer, [91] or heat transfer of fins used in condensers and evaporators, [98], we consider the parabolic heat equation

$$\frac{\partial u}{\partial t}(x,t) = \frac{\partial^2 u}{\partial x^2}(x,t) + (f(t) + g(x))u(x,t), \quad (x,t) \in Q_T, \tag{7.1}$$

where $f(t)$ and $g(x)$ are coefficient functions to be identified together with the temperature $u(x,t)$. In (7.1), the term $q(x,t) := f(t)+g(x)$ represents a radiative or perfusion coefficient. Previous studies, e.g. [127, 129], considered the cases $g = 0$ or $f = 0$, so in that respect, our identification of an additive coefficient $q(x,t) = f(t) + g(x)$ with unknown functions f and g, is a generalization. At the other extreme, when $q(x,t)$ does not separate its identification requires the measurment of $u(x,t)$ at all points inside the solution domain Q_T, [36, 37, 130], which may be impractical.

Equation (7.1) has to be solved subject to the initial condition

$$u(x,0) = \phi(x), \quad 0 \le x \le L, \tag{7.2}$$

the homogeneous Neumann boundary conditions

$$\frac{\partial u}{\partial x}(0,t) = \frac{\partial u}{\partial x}(L,t) = 0, \quad 0 \le t \le T, \tag{7.3}$$

and the additional temperature measurements

$$u(X_0,t) = \beta(t), \quad 0 \le t \le T, \tag{7.4}$$

at a fixed space location $0 < X_0 < L$, and

$$u(x,T) = \psi(x), \quad 0 \le x \le L, \tag{7.5}$$

at the final time $t = T$. The sketch of the inverse problem under investigation is shown in Figure 7.1.

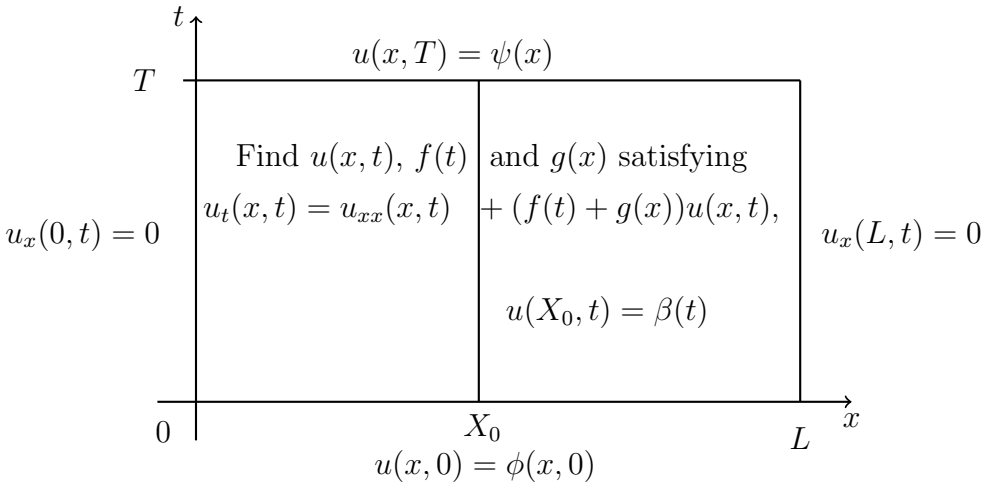

Figure 7.1: Sketch of the inverse problem under investigation.

The conditions (7.3) express that the ends $\{0, L\}$ of the finite slab $(0, L)$ are insulated. In order to avoid non-uniqueness reproduced by the trivial identity $f(t) + g(x) = (f(t) + c) + (g(x) - c)$, where c is an arbitrary non-zero constant, we take a fixing condition, say at $x = X_1$ fixed in $(0, L)$, assuming that

$$g(X_1) = \alpha \tag{7.6}$$

is given. Alternatively, one could have a fixing condition on f instead of (7.6). In the above equations, the functions ϕ, β, ψ and the constant α are given, whilst the triplet of functions $f(t), g(x)$ and $u(x, t)$ are unknown. Further, assume that the conditions (7.2)–(7.5) are compatible, i.e.

$$\phi'(0) = \phi'(L) = \psi'(0) = \psi'(L) = 0, \quad \beta(0) = \phi(X_0), \quad \beta(T) = \psi(X_0). \tag{7.7}$$

The existence and uniqueness of a classical solution to the inverse problem (7.1)–(7.7) were established in [115]. Without going into too much detail, it is useful to state the unique solvability of the inverse problem (7.1)–(7.7) in a particular case, as follows, [60, 115].

Proposition 1. *Suppose*

$$0 < \phi \in C^4[0, L], \quad 0 < \psi \in C^4[0, L], \quad 0 < \beta \in C^1[0, T] \tag{7.8}$$

and assume that

$$\psi(x) = c\phi(x),\ x \in [0, L], \tag{7.9}$$

where $c = \beta(T)/\beta(0)$. *Then the inverse problem* (7.1)-(7.7) *has a unique solution* $(u, f, g) \in (C^2(Q_T) \cap C^1(\overline{Q_T})) \times C^1[0, T] \times C^1[0, L]$ *which is explicitly given by*

$$u(x,t) = \frac{\beta(t)}{\beta(0)}\phi(x), \quad (x,t) \in \overline{Q_T}, \tag{7.10}$$

$$f(t) = \frac{\beta'(t)}{\beta(t)} - \alpha - \frac{\phi''(X_1)}{\phi(X_1)}, \quad t \in [0, T], \tag{7.11}$$

$$g(x) = -\frac{\phi''(x)}{\phi(x)} + \alpha + \frac{\phi''(X_1)}{\phi(X_1)}, \quad x \in [0, L]. \tag{7.12}$$

This proposition is useful because it indicates how to construct analytical solutions of the inverse problem (7.1)–(7.7) for which numerical methods can be assessed, see later on Examples 1 and 2 in Section 7.5. In addition, the explicit formulas (7.11) and (7.12) contain derivatives of the measured data which is numerically unstable. That is, although the inverse problem (7.1)–(7.7) is uniquely solvable it is still ill-posed since small errors in the input measured data (7.4) and (7.5) cause large error in the output solution for f and g. Therefore, in the numerical computation the main focus is on the development of stable nonlinear optimization algorithms, [113], as will be described in Section 7.4. But before we do that, in the next section we briefly describe the FDM employed for discretising the direct problem.

7.3 Numerical solution of the direct problem

In this section, we consider the direct initial boundary value problem given by equations (7.1)–(7.3) when f and g are given. We use the FDM with a Crank-Nicholson scheme. The discrete form of the direct problem is as follows. We denote $u(x_i, t_j) = u_{i,j}, f(t_j) = f_j$ and $g(x_i) = g_i$, where $x_i = i\Delta x, t_j = j\Delta t$ for $i = \overline{0, M}, j = \overline{0, N}$, and $\Delta x = \frac{L}{M},\ \Delta t = \frac{T}{N}$.

Considering the general partial differential equation

$$u_t = G(x, t, u, u_{xx}), \tag{7.13}$$

the Crank-Nicolson method, [123], discretises (7.13), (7.2) and (7.3) as

$$\frac{u_{i,j+1}-u_{i,j}}{\Delta t}=\frac{1}{2}(G_{i,j}+G_{i,j+1}),\qquad i=\overline{1,(M-1)},\ j=\overline{0,(N-1)}, \tag{7.14}$$

$$u_{i,0}=\phi(x_i),\quad i=\overline{0,M}, \tag{7.15}$$

$$\frac{u_{1,j}-u_{-1,j}}{2(\Delta x)}=\frac{u_{M+1,j}-u_{M-1,j}}{2(\Delta x)}=0,\quad j=\overline{1,N}, \tag{7.16}$$

where

$$\begin{aligned} G_{i,j}&=G\Big(x_i,t_j,u_{i,j},\frac{u_{i+1,j}-2u_{i,j}+u_{i-1,j}}{(\Delta x)^2}\Big),\\ G_{i,j+1}&=G\Big(x_i,t_{j+1},u_{i,j+1},\frac{u_{i+1,j+1}-2u_{i,j+1}+u_{i-1,j+1}}{(\Delta x)^2}\Big),\\ &\qquad i=\overline{0,M},\quad j=\overline{0,(N-1)} \end{aligned} \tag{7.17}$$

and $u_{-1,j}$ and $u_{M+1,j}$ for $j=\overline{1,N}$ are fictitious values at points located outside the computational domain.

For our problem, equation (7.1) is of the form (7.13) and the above discretisation then renders the following discrete form of (7.1):

$$\begin{aligned} &-Au_{i-1,j+1}+(1+B_{i,j+1})u_{i,j+1}-Au_{i+1,j+1}\\ &\qquad=Au_{i-1,j}+(1-B_{i,j})u_{i,j}+Au_{i+1,j}, \end{aligned} \tag{7.18}$$

for $i=\overline{0,M}$, $j=\overline{0,(N-1)}$, where $A=\dfrac{(\Delta t)}{2(\Delta x)^2}$, $B_{i,j}=\dfrac{(\Delta t)}{(\Delta x)^2}-\dfrac{(\Delta t)}{2}(f_j+g_i)$.

At each time step t_{j+1}, for $j=\overline{0,(N-1)}$, using the homogeneous Neumann boundary conditions (7.16), the above difference equation can be reformulated as an $M\times M$ system of linear equations of the form,

$$L\mathbf{u_{j+1}}=E\mathbf{u_j}, \tag{7.19}$$

where $\mathbf{u_{j+1}}=(u_{0,j+1},u_{1,j+1},...,u_{M,j+1})^{\mathrm{T}}$,

$$L=\begin{pmatrix} 1+B_{0,j+1} & -2A & 0 & ... & 0 & 0 & 0\\ -A & 1+B_{1,j+1} & -A & ... & 0 & 0 & 0\\ \vdots & \vdots & \vdots & \ddots & \vdots & \vdots & \vdots\\ 0 & 0 & 0 & ... & -A & 1+B_{M-1,j+1} & -A\\ 0 & 0 & 0 & ... & 0 & -2A & 1+B_{M,j+1} \end{pmatrix},$$

and

$$E = \begin{pmatrix} 1-B_{0,j} & 2A & 0 & ... & 0 & 0 & 0 \\ A & 1-B_{1,j} & A & ... & 0 & 0 & 0 \\ \vdots & \vdots & \vdots & \ddots & \vdots & \vdots & \vdots \\ 0 & 0 & 0 & ... & A & 1-B_{M-1,j} & A \\ 0 & 0 & 0 & ... & 0 & 2A & 1-B_{M,j} \end{pmatrix}.$$

The grid convergence of the above FDM is considered next for solving the direct Neumann problem (7.1)–(7.3) with $T = L = 1$, and input data

$$\phi(x) = u(x,0) = x^2(x-1)^2 + 1, \tag{7.20}$$

$$f(t) = \frac{1}{1+t}, \quad g(x) = \frac{-2+12x-12x^2}{1+x^2-2x^3+x^4}. \tag{7.21}$$

The analytical solution for the temperature is given by

$$u(x,t) = \Big(x^2(x-1)^2 + 1\Big)(1+t). \tag{7.22}$$

Figure 7.2 shows the surface plots of the analytical solution (7.22) in comparison with the numerical FDM solutions obtained with various $M = N \in \{10, 20, 40\}$. The absolute errors between those solutions are also included and it can be seen that these errors decrease as the FDM grid becomes finer.

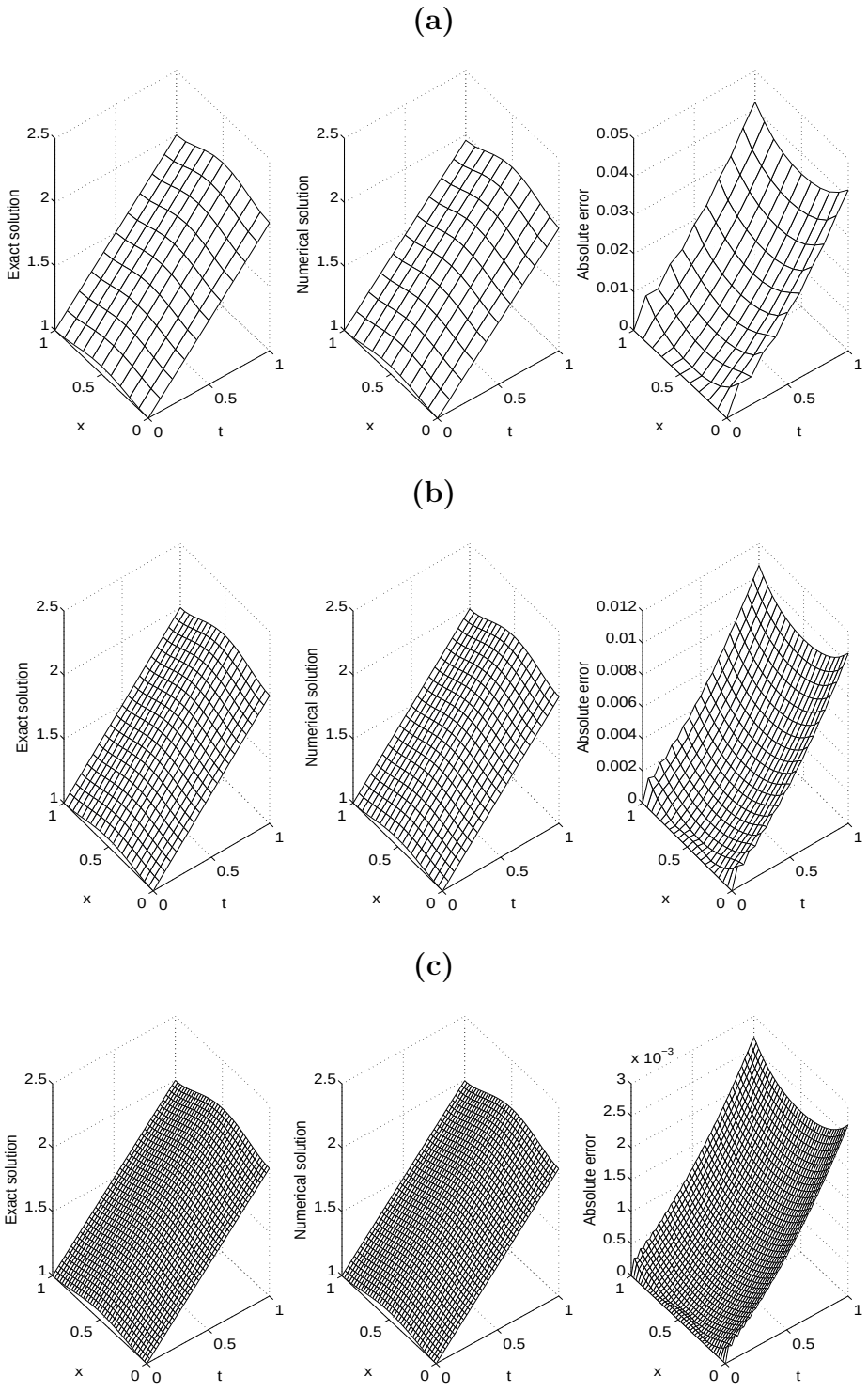

Figure 7.2: The exact (7.22) and numerical solutions for the temperature $u(x,t)$, with various mesh sizes (a) $M = N = 10$, (b) $M = N = 20$, and (c) $M = N = 40$, for the direct problem. The absolute error between them is also included.

The numerical solutions for the interior temperatures (7.4) and (7.5) are com-

pared in Figure 7.3 with the exact solutions given by

$$\beta(t) = u(X_0, t) = \frac{17}{16}(1+t), \quad \psi(x) = u(x, T) = 2\Big(x^2(x-1)^2 + 1\Big), \\ T = 1, \quad X_0 = \frac{1}{2}. \quad (7.23)$$

From Figure 7.3 it can be seen that the numerical solutions converge to the corresponding exact solutions (7.23), as the FDM grid becomes finer. In fact, the root mean square errors (rmse) defined by

$$rmse(\beta) = \sqrt{\frac{1}{N}\sum_{j=1}^{N}\Big(\beta^{numerical}(t_j) - \beta^{exact}(t_j)\Big)^2}, \quad (7.24)$$

$$rmse(\psi) = \sqrt{\frac{1}{M}\sum_{i=1}^{M}\Big(\psi^{numerical}(x_i) - \psi^{exact}(x_i)\Big)^2}, \quad (7.25)$$

indicated in Table 7.1, show more clearly their decreases as the grid size becomes smaller.

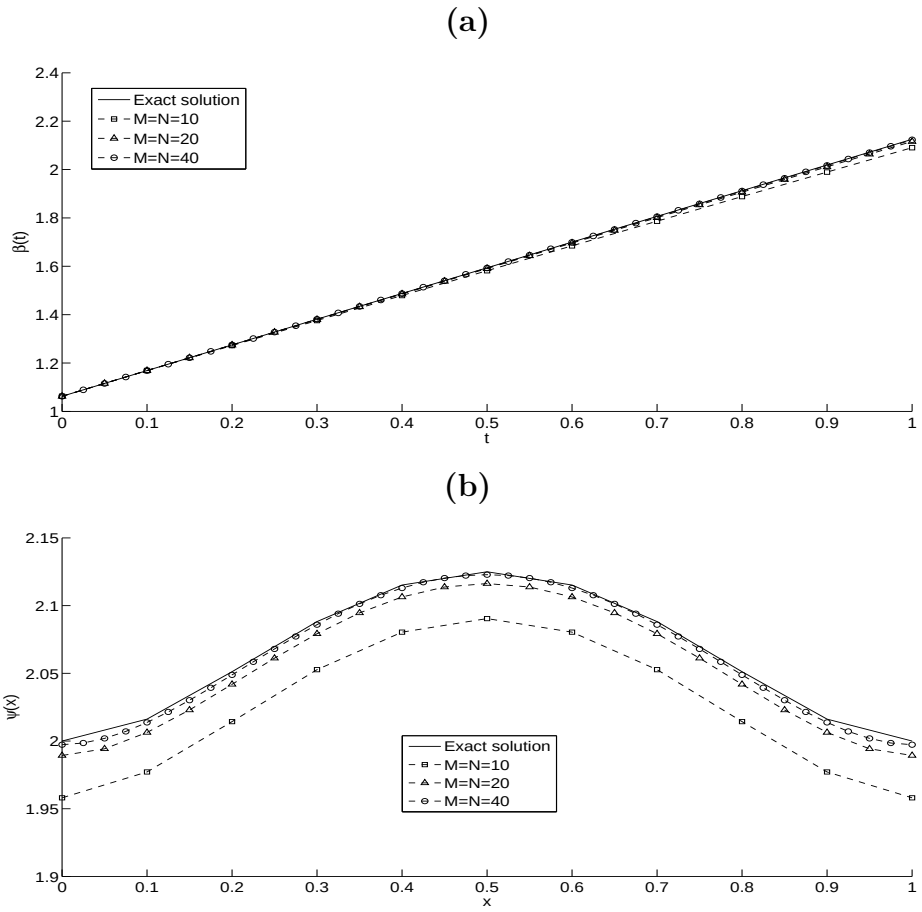

Figure 7.3: The exact and numerical solutions for: (a) $\beta(t)$ and (b) $\psi(x)$, various mesh sizes $M = N \in \{10, 20, 40\}$, for the direct problem.

Table 7.1: The $(rmse)$ given by equations (7.24) and (7.25) for $\beta(t)$ and $\psi(x)$, with various mesh sizes $M = N \in \{10, 20, 40\}$, for the direct problem.

$M = N$	10	20	40
$rmse(\beta)$	0.0179	0.0044	0.0011
$rmse(\psi)$	0.0374	0.0094	0.0024

7.4 Numerical approach for the inverse problem

In this section, we wish to obtain simultaneously the unknown functions $f(t)$ and $g(x)$ in the inverse problem (7.1)–(7.7) reformulated as minimizing the regularized objective function

$$\mathbb{F}(f,g) = \|u(x,T) - \psi(x)\|^2 + \|u(X_0,t) - \beta(t)\|^2 + \beta_1\|f(t)\|^2 + \beta_2\|g(x)\|^2 + (g(X_1) - \alpha)^2, \tag{7.26}$$

where u solves (7.1)–(7.3) for given f and g, $\beta_1 \geq 0$ and $\beta_2 \geq 0$ are regularization parameters, and the norm is usually the L^2-norm. Assuming, for convenience, that we take $X_0 \in (0, L)$ such that there exists $i_0 \in \{1, ..., M\}$ for which $X_0 = x_{i_0}$, in discrete form (7.26) becomes

$$\mathbb{F}(\mathbf{f}, \mathbf{g}) = \sum_{\substack{i=1 \\ i \neq i_0}}^{M} \Big[u(x_i, T) - \psi(x_i)\Big]^2 + \sum_{j=1}^{N} \Big[u(X_0, t_j) - \beta(t_j)\Big]^2 + (g(X_1) - \alpha)^2 + \beta_1 \sum_{j=1}^{N} f_j^2 + \beta_2 \sum_{i=1}^{M} g_i^2. \tag{7.27}$$

The value for $i = i_0$ in the first sum has been excluded in order to avoid duplicating the compatibility condition (in (7.7)) $u(X_0, T) = u(x_{i_0}, T) = \beta(T) = \beta(t_N) = \psi(x_{i_0}) = \psi(X_0)$. The minimization of (7.27) is performed using the MATLAB toolbox routine *lsqnonlin*. We have compiled this routine with the following parameters:

- Algorithm = TRR, [31].
- Maximum number of iterations, (MaxIter) = 400.
- Maximum number of objective function evaluations, (MaxFunEvals) = $10^2 \times$(number of variables).
- Termination tolerance on the function value, (TolFun) = 10^{-20}.
- x Tolerance, (xTol) = 10^{-20}.
- The lower and upper simple bounds are -10^3 and 10^3 for $\mathbf{f}$ and $\mathbf{g}$.

The inverse problem under investigation is solved subject to both exact and noisy data which are numerically simulated as

$$\beta^{\epsilon 1}(t_j) = \beta(t_j) + \epsilon 1_j, \quad j = \overline{1, N}, \tag{7.28}$$

$$\psi^{\epsilon 2}(x_i) = \psi(x_i) + \epsilon 2_i, \quad i = \overline{1, M}, \quad i \neq i_0, \tag{7.29}$$

where $\epsilon 1_j$ and $\epsilon 2_i$ are random variables generated from normal distributions with mean zero and standard deviations $\sigma 1$ and $\sigma 2$ given by

$$\sigma 1 = p \times \max_{t \in [0,T]} |\beta(t)|, \quad \sigma 2 = p \times \max_{x \in [0,L]} |\psi(x)|, \tag{7.30}$$

where p represents the percentage of noise. We use the MATLAB function *normrnd* to generate the random variables $\underline{\epsilon 1} = (\epsilon 1_j)_{j=\overline{1,N}}$ and $\underline{\epsilon 2} = (\epsilon 2_i)_{i=\overline{1,(M-1)}}$

given by

$$\underline{\epsilon 1} = normrnd(0, \sigma 1, N), \quad \underline{\epsilon 2} = normrnd(0, \sigma 2, M-1). \tag{7.31}$$

7.5 Numerical results and discussion

In this section, we present examples in order to test the accuracy and stability of the numerical methods introduced in Sections 7.3 and 7.4, respectively. The root mean square errors (rmse) are used to evaluate the accuracy of the numerical results and are defined by

$$rmse(f) = \sqrt{\frac{1}{N}\sum_{j=1}^{N}\left(f^{numerical}(t_j) - f^{exact}(t_j)\right)^2}, \tag{7.32}$$

$$rmse(g) = \sqrt{\frac{1}{M}\sum_{i=1}^{M}\left(g^{numerical}(x_i) - g^{exact}(x_i)\right)^2}. \tag{7.33}$$

In all examples we take, for simplicity, $T = 1$, $L = 1$ and $X_0 = X_1 = L/2 = 0.5$. Consequently, $i_0 = M/2$ in (7.27). In all the inverse calculations we take $M = N = 40$.

7.5.1 Example 1

We solve the inverse problem (7.1)–(7.7) with unknown coefficients $f(t)$ and $g(x)$ and the input data (7.20), (7.23) and $\alpha = g(0.5) = 16/17$. From this data one can observe that the conditions of Proposition 1 of Section 7.2 are satisfied and hence the inverse problem has a unique solution given by (7.10)–(7.12) which yield the expressions (7.21) and (7.22). We take the initial guess as

$$f^0(t) = 1 - \frac{t}{2}, \quad g^0(x) = \begin{cases} -2 + \frac{100}{17}x, & 0 \le x \le 0.5, \\ \frac{66}{17} - \frac{100}{17}x, & 0.5 < x \le 1, \end{cases} \tag{7.34}$$

which are straight lines passing through $f(0) = 1$, $f(1) = 1/2$, and $g(0) = -2$, $g(0.5) = 16/17$, $g(1) = -2$.

Considering no noise in the measurement data (7.4) and (7.5), the unregularized objective function (7.27), i.e. $\beta_1 = \beta_2 = 0$, as a function of a number of iterations plotted in Figure 7.4, shows a rapid decrease to a low value of $O(10^{-29})$ in 19 iterations. Figure 7.5 shows the exact and numerical solutions of the functions $f(t)$ and $g(x)$, respectively. From this figure it can be seen that very accurate

numerical solutions are obtained.

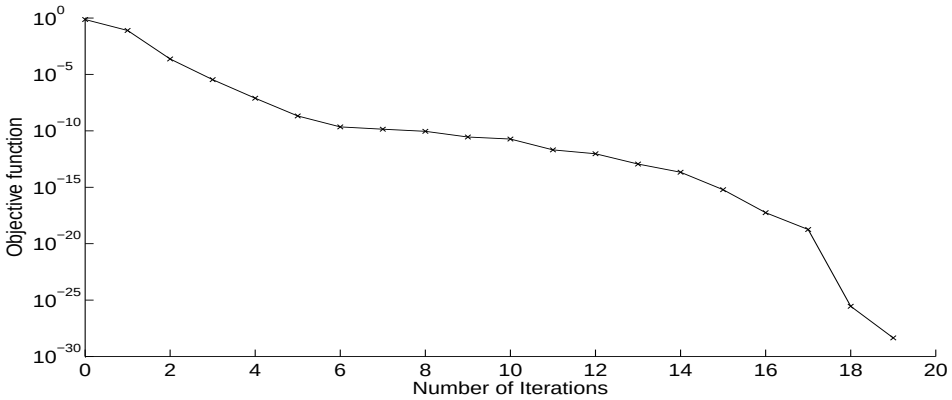

Figure 7.4: Objective function (7.27) for Example 1 with no noise and no regularization.

Next, we add a small amount of $p = 0.01\%$ noise to the measured data (7.4) and (7.5). For higher amounts of noise the numerical results were less accurate and therefore they are not presented. The point to stress here is that since the inverse problem is ill-posed then we expect that regularization is needed in order to achieve stable and accurate results. The monotonic decreasing convergence of the objective function (7.27), as a function of the number of iterations, is shown in Figure 7.6 with and without regularization. Figure 7.7 shows the graphs of the recovered functions. From Figure 7.7 it can be seen that, as expected, when $\beta_1 = \beta_2 = 0$ we obtain unstable and inaccurate solutions because the problem is ill-posed and very sensitive to noise. Thus regularization is needed in order to stabilise the solutions. We selected by trial and error the regularization parameters $\beta_1 = 10^{-9}$ and $\beta_2 = 10^{-7}$ which give stable and reasonablly accurate solutions for the functions $f(t)$ and $g(x)$. For more elaborate choices of multiple regularization parameters, see [7, 41].

The related numerical results for the temperature $u(x,t)$ with $p = 0.01\%$ noise, and with and without regularization, are presented in Figure 7.8 showing good agreement with the exact solution (7.22).

Other details about the number of iterations, the number of function evaluations, the value of the objective function (7.27) at the final iteration, the $rmse(f)$ and $rmse(g)$ in (7.32) and (7.33), respectively, and the computational time are given in Table 7.2. Overall, from this table as well as from Figures 7.4-7.8 it can be seen that accurate and stable numerical results are rapidly achieved by the MATLAB toolbox iterative routine *lsqnonlin* minimizing the objective function (7.27).

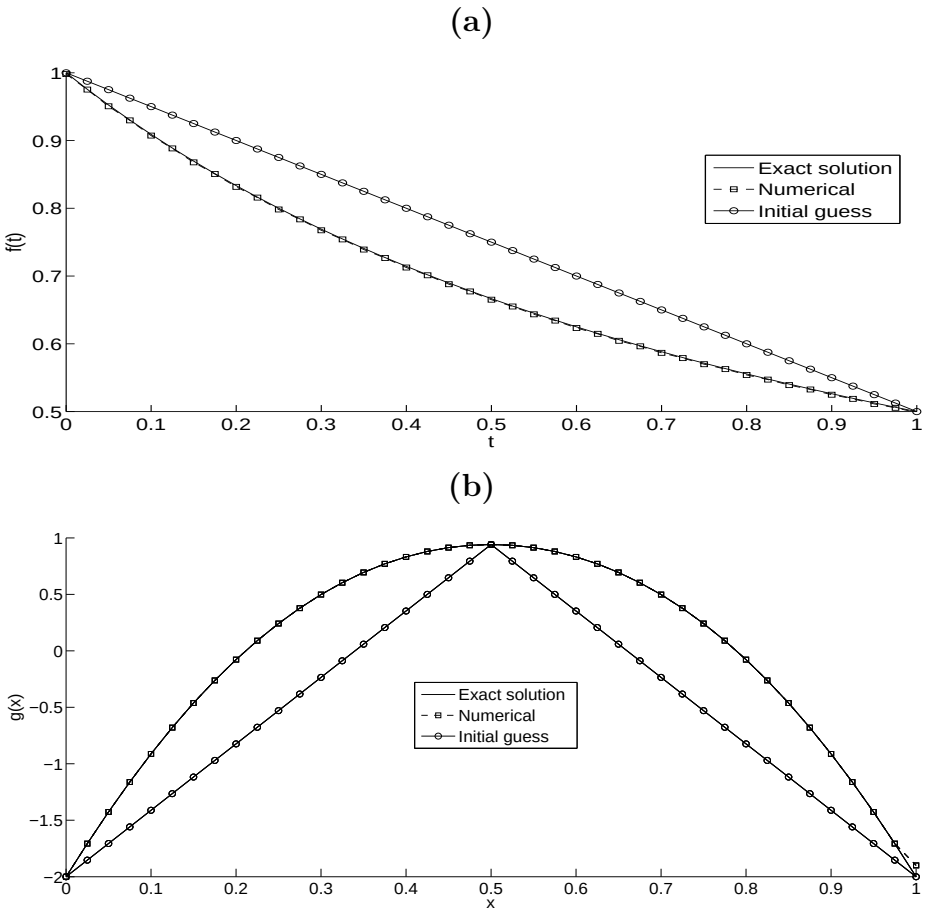

Figure 7.5: (a) Coefficient $f(t)$ and (b) coefficient $g(x)$, for Example 1 with no noise and no regularization.

Table 7.2: Number of iterations, number of function evaluations, value of the objective function (7.27) at final iteration, $rmse(f)$ and $rmse(g)$, and computational time, for Example 1.

Numerical outputs	$p = 0$ ($\beta_1 = \beta_2 = 0$)	$p = 0.01\%$ ($\beta_1 = \beta_2 = 0$)	$p = 0.01\%$ ($\beta_1 = 10^{-9}$, $\beta_2 = 10^{-7}$)
No. of iterations	19	36	46
No. of function evaluations	1660	3071	3901
Value of objective function (7.27) at final iteration	4.4E-29	6.5E-11	3.2E-6
$rmse(f)$	0.0013	0.1454	0.1024
$rmse(g)$	0.0156	0.6698	0.1634
Computational time (sec)	163	306	386

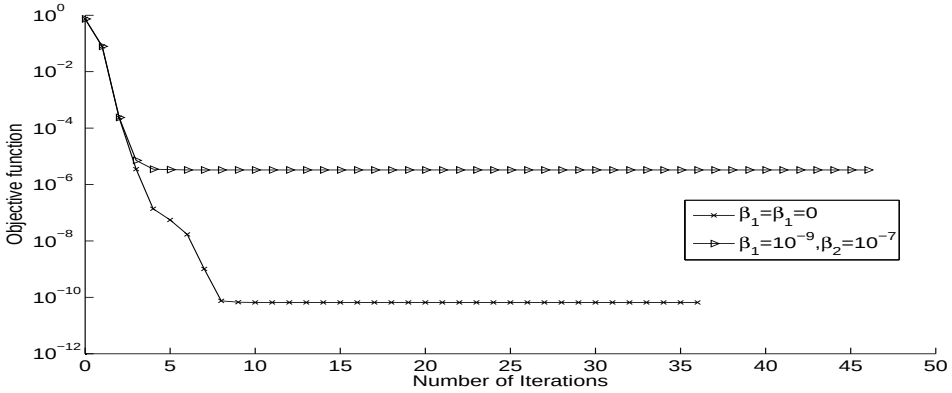

Figure 7.6: Objective function (7.27), for Example 1 with $p = 0.01\%$ noise, with and without regularization.

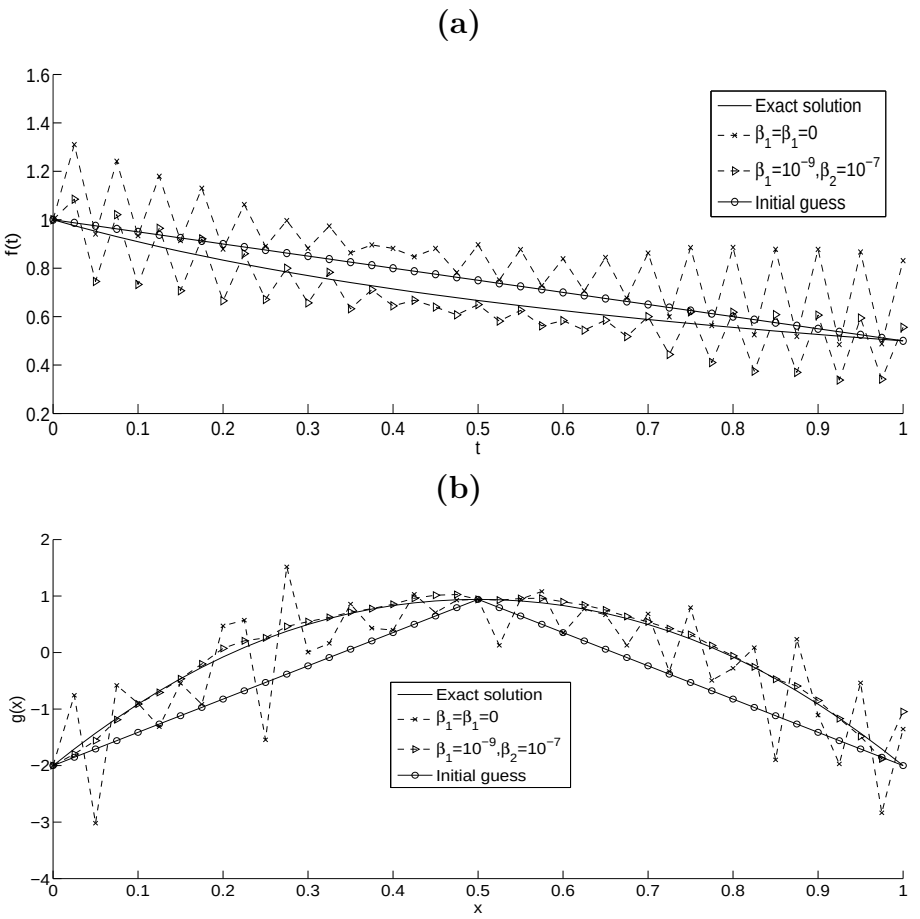

Figure 7.7: (a) Coefficient $f(t)$ and (b) coefficient $g(x)$, for Example 1 with $p = 0.01\%$ noise, with and without regularization.

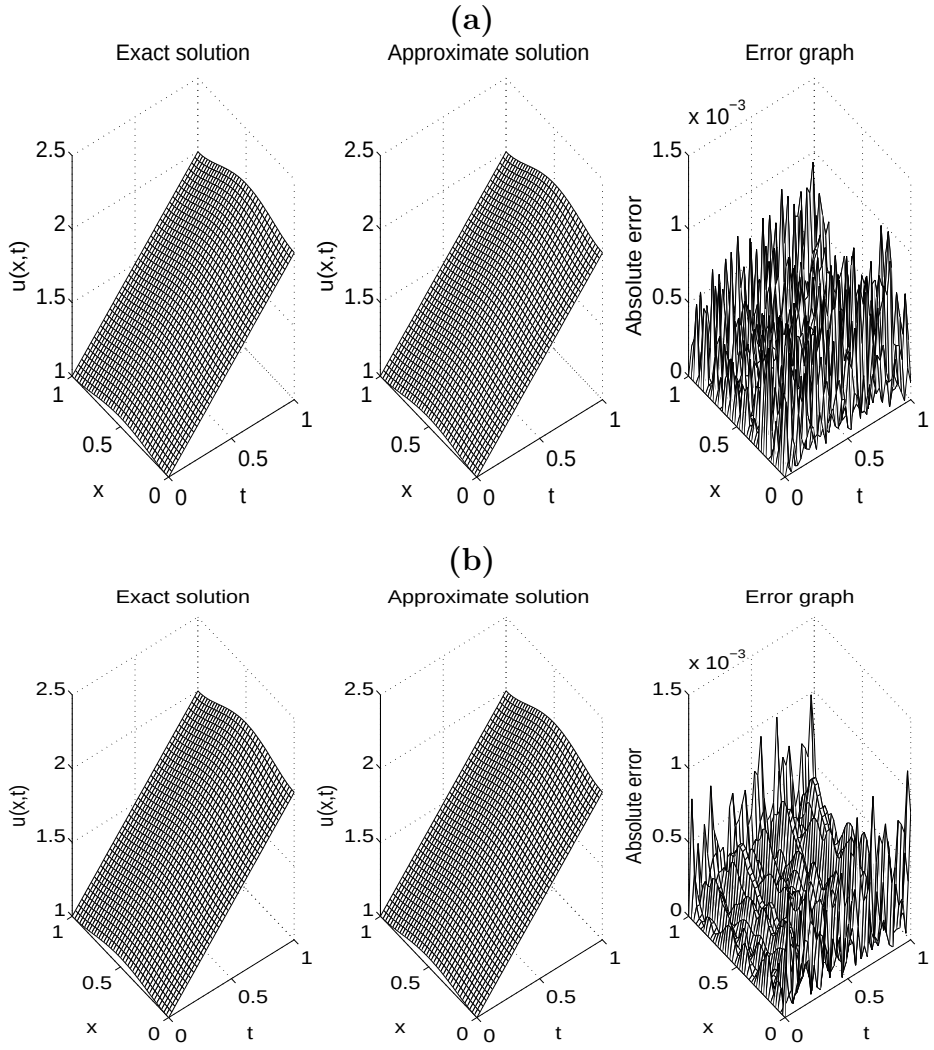

Figure 7.8: The exact and approximate solutions for the temperatures $u(x,t)$, for Example 1, with (a) $\beta_1 = \beta_2 = 0$ and (b) $\beta_1 = 10^{-9}$, $\beta_2 = 10^{-7}$, for $p = 0.01\%$ noise. The absolute error between them is also included.

7.5.2 Example 2

Consider the inverse problem (7.1)–(7.7) with the input data

$$\phi(x) = u(x,0) = 2 + \cos(\pi x), \tag{7.35}$$

$$\beta(t) = u(0.5,t) = 2e^{\frac{t^2}{1+t}}, \quad \psi(x) = u(x,1) = \sqrt{e}(2+\cos(\pi x)),$$
$$\alpha = g(0.5) = 0. \tag{7.36}$$

As in Example 1, the conditions of Proposition 1 are satisfied and the unique solution of the inverse problem (7.1)–(7.7) is given by (7.10)–(7.12) which yield

$$f(t) = \frac{t(t+2)}{(t+1)^2}, \quad g(x) = \frac{\pi^2 \cos(\pi x)}{2 + \cos(\pi x)}, \tag{7.37}$$

$$u(x,t) = e^{\frac{t^2}{1+t}} \Big(2 + \cos(\pi x)\Big). \tag{7.38}$$

We take the initial guess as

$$f^0(t) = 0, \quad g^0(x) = \begin{cases} \frac{\pi^2}{3} - \frac{2\pi^2}{3}x, & 0 \le x \le 0.5, \\ \pi^2 - 2\pi^2 x, & 0.5 < x \le 1. \end{cases} \tag{7.39}$$

Analogous quantities and conclusions to Figures 7.4–7.7 and Table 7.2 of Example 1 are presented and obtained in Figures 7.9–7.12 and Table 7.3 of Example 2.

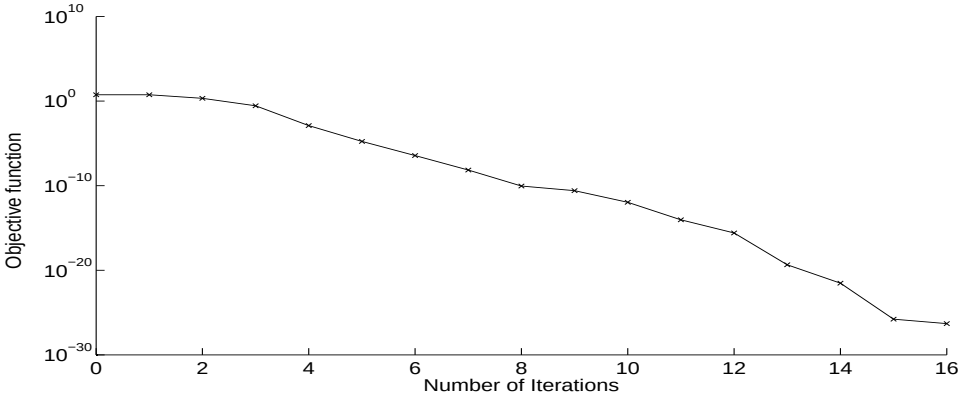

Figure 7.9: Objective function (7.27), for Example 2 with no noise and no regularization.

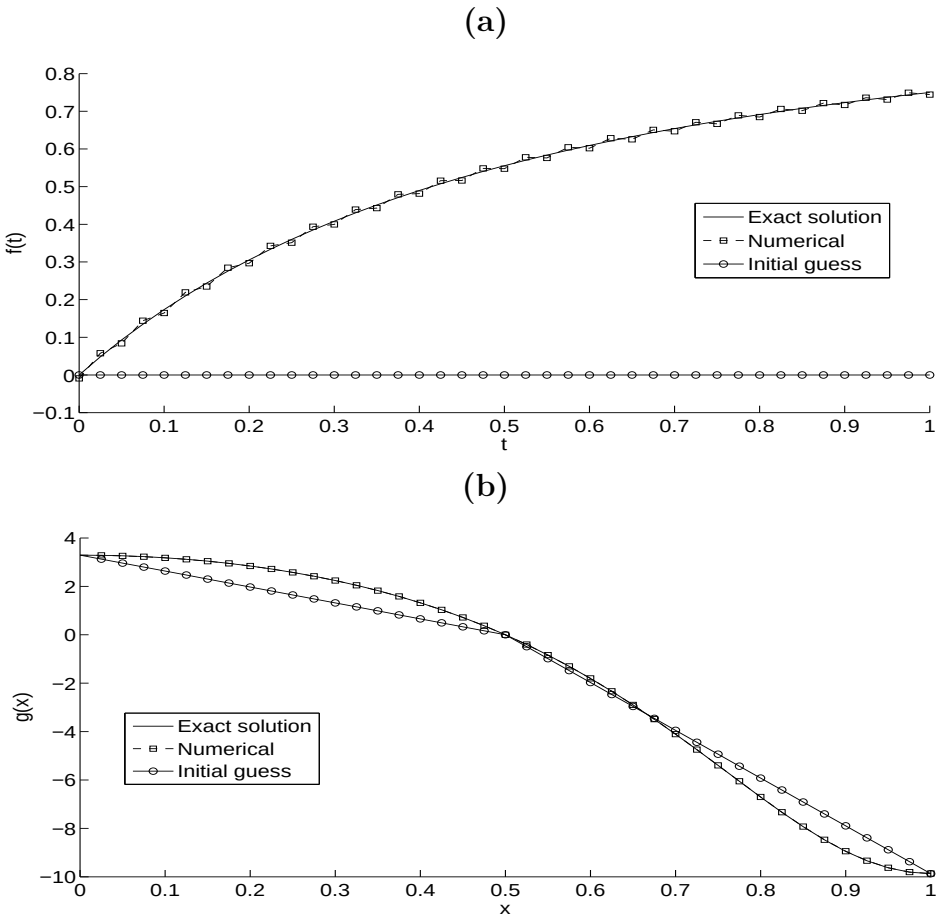

Figure 7.10: (a) Coefficient $f(t)$ and (b) coefficient $g(x)$, for Example 2 with no noise and no regularization.

Table 7.3: Number of iterations, number of function evaluations, value of the objective function (7.27) at final iteration, $rmse(f)$ and $rmse(g)$, and computational time, for Example 2.

Numerical outputs	$p = 0$ ($\beta_1 = \beta_2 = 0$)	$p = 0.01\%$ ($\beta_1 = \beta_2 = 0$)	$p = 0.01\%$ ($\beta_1 = 10^{-12}$, $\beta_2 = 10^{-11}$)
No. of iterations	16	39	52
No. of function evaluations	1411	3320	3416
Value of objective function (7.27) at final iteration	4.9E-27	1.5E-10	1.2E-8
$rmse(f)$	0.0077	0.1462	0.1084
$rmse(g)$	0.0025	1.2917	1.2847
Computational time (mins)	2	5	7

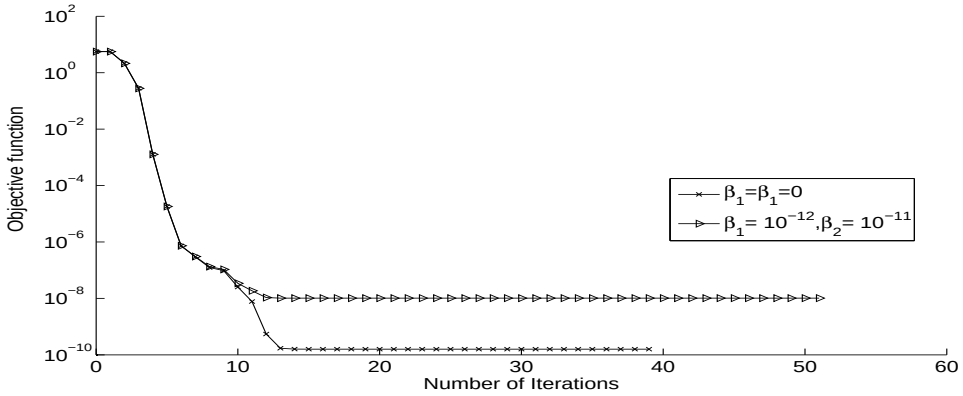

Figure 7.11: Objective function (7.27), for Example 2 with $p = 0.01\%$ noise, with and without regularization.

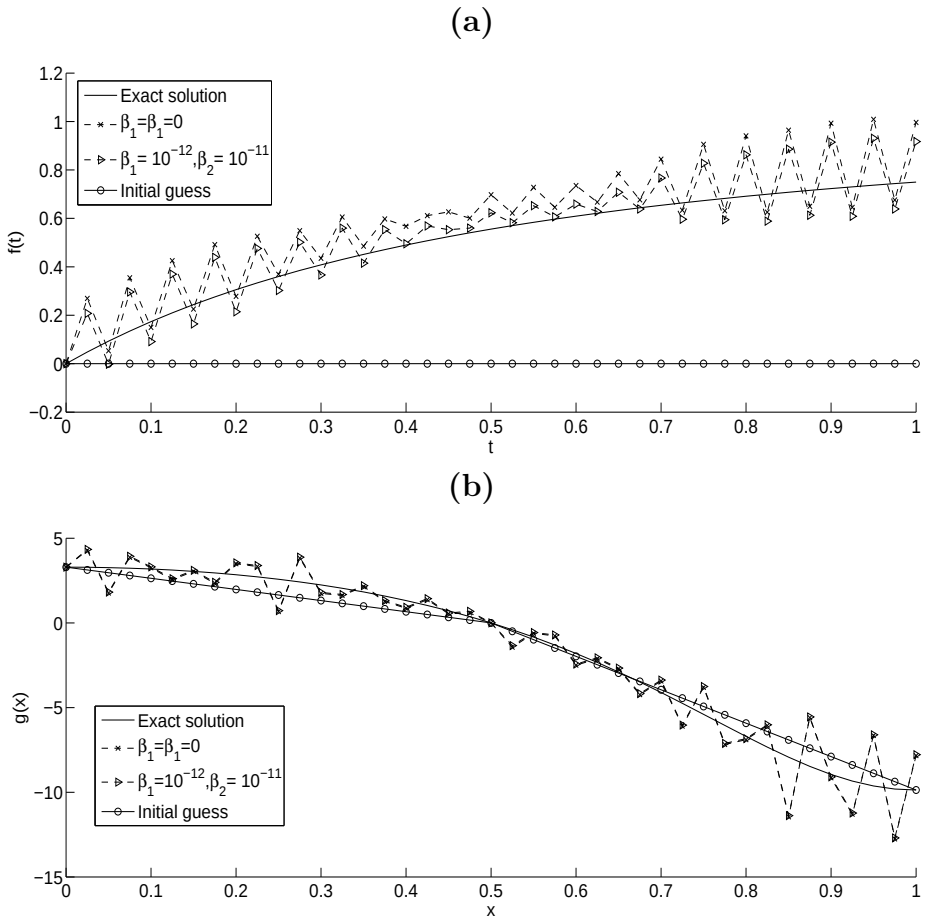

Figure 7.12: (a) Coefficient $f(t)$ and (b) coefficient $g(x)$, for Example 2 with $p = 0.01\%$ noise, with and without regularization.

7.5.3 Example 3

The previous examples possessed an analytical solution available for the triplet $(u(x,t), f(t), g(x))$. In this section, we investigate an example for which an an-

alytical solution for $u(x,t)$ is not available. We take the initial condition (7.2) given by

$$u(x,0)=\phi(x)=\begin{cases}1, & 0\le x<1/4,\\ \frac{5}{4}-x, & 1/4<x\le 1/2,\\ x+\frac{1}{4}, & 1/2<x\le 3/4,\\ 1, & 3/4<x\le 1,\end{cases} \tag{7.40}$$

which represents a non-smooth function. In the absence of an analytical solution for $u(x,t)$ being available we generate the input data (7.4) and (7.5) numerically by solving first the direct problem given by (7.1)–(7.3) with $\phi(x)$ given by (7.40), and the known functions

$$f(t)=1+t, \quad g(x)=1+x, \tag{7.41}$$

using the FDM described in Section 7.3.

The numerical results for $\beta(t)$ and $\psi(x)$ in equations (7.4) and (7.5), respectivly, are shown in Figure 7.13, for various $M=N\in\{20,40,80\}$. From this figure, it can be seen that the numerical solution is convergent as the FDM mesh size decreases.

The example considered in this subsection violates the sufficient conditions of uniqueness of solution of Proposition 1 and [115] and therefore, it is a severe test for our method of regularization.

In order to avoid committing an inverse crime the mesh that is used for numerically simulating the measured data (7.4) and (7.5) by solving the direct problem is taken to be more dense than the one used for the solution of the inverse problem, [84]. Consequently, in the inverse problem we use the FDM with $M=N=40$ and half of the data for β and ψ obtained from solving the direct problem with $M=N=80$. We also take the initial guess as

$$f^0(t)=1, \quad g^0(x)=1. \tag{7.42}$$

The objective function (7.27) with no noise and no regularization, as a function of the number of iterations, is plotted in Figure 7.14. From this figure it can be seen that a rapid monotonic decreasing convergence to a low value of $O(10^{-28})$ is achieved in about 12 iterations.

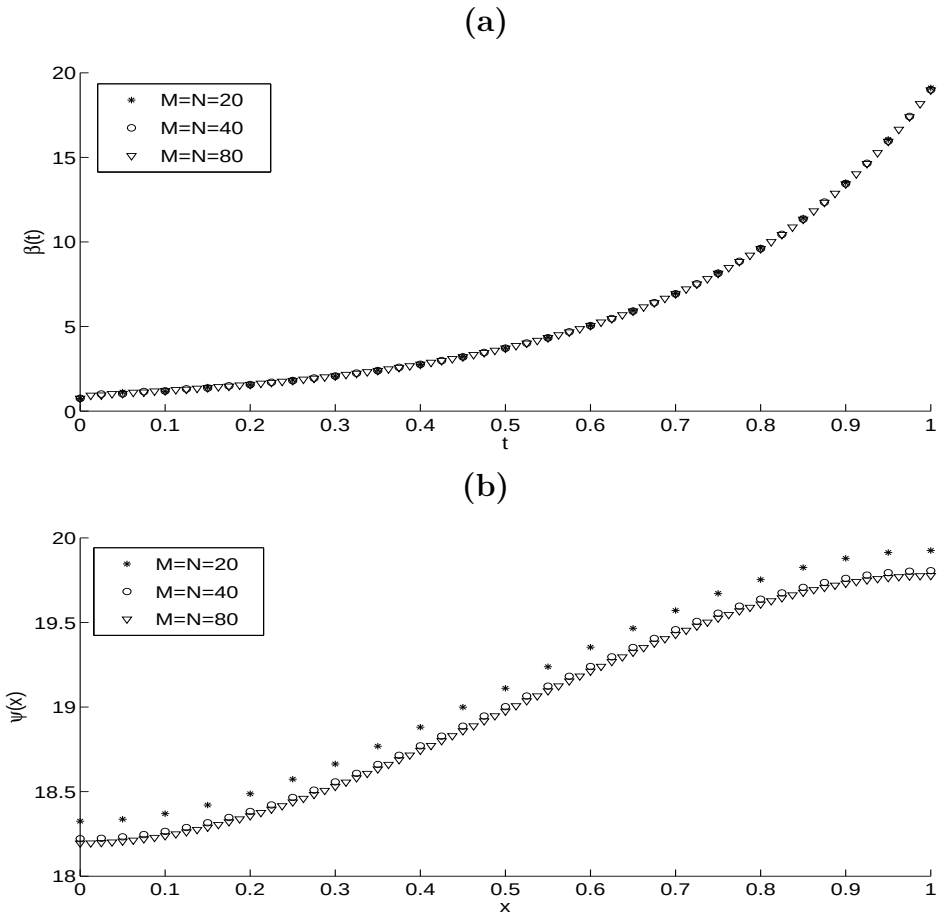

Figure 7.13: The numerically convergent solutions for (a) $\beta(t)$ and (b) $\psi(x)$, for Example 3 with various mesh sizes $M = N \in \{20, 40, 80\}$ for the direct problem.

Figure 7.15 shows the exact and numerical solution of the unknown coefficients $f(t)$ and $g(x)$, and one can see that stable and accurate solutions are obtained.

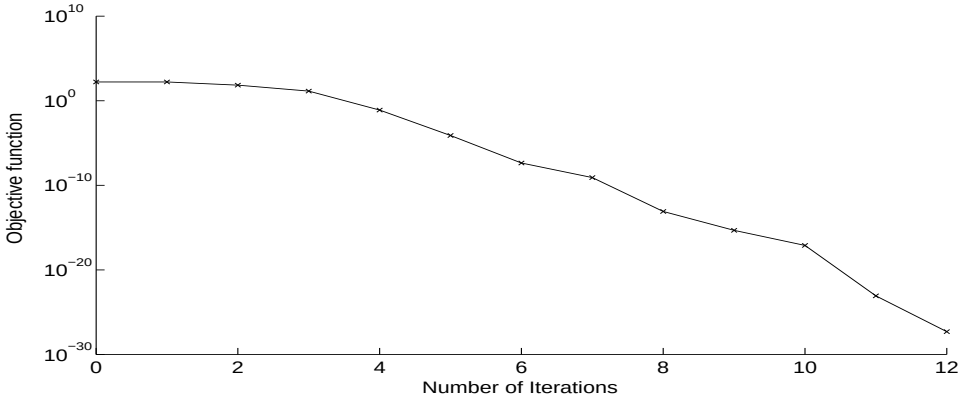

Figure 7.14: Objective function (7.27), for Example 3 with no noise and no regularization.

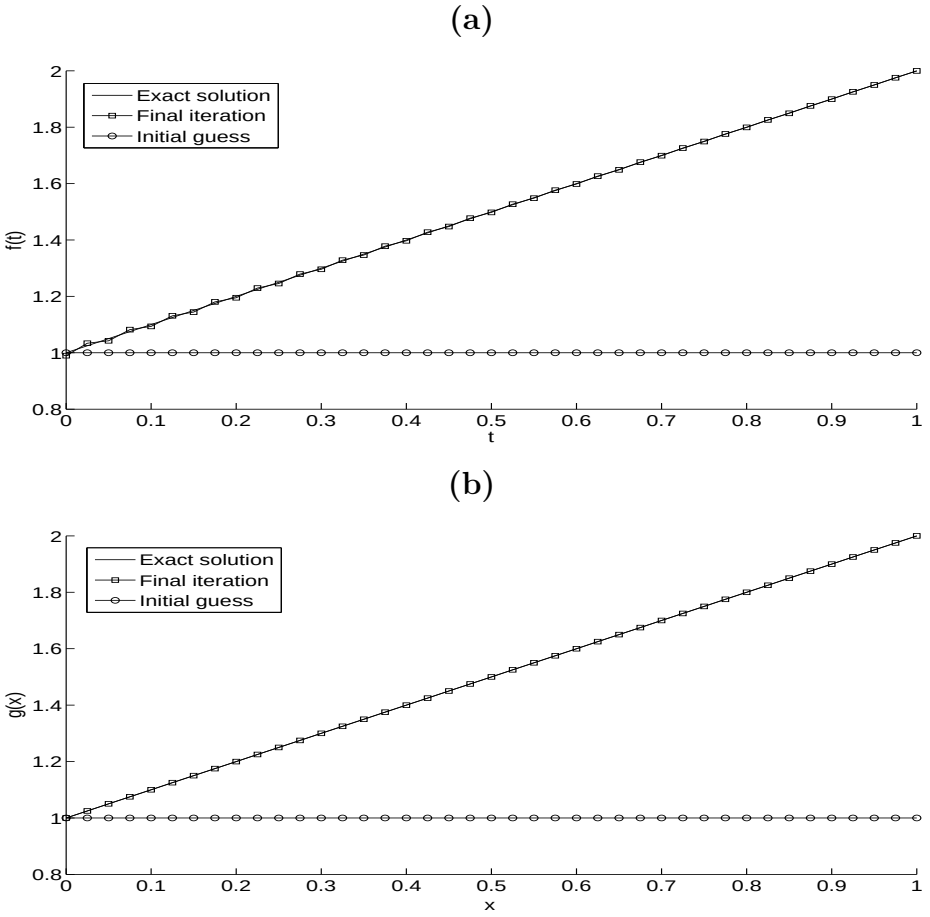

Figure 7.15: (a) Coefficient $f(t)$ and (b) coefficient $g(x)$, for Example 3 with no noise and no regularization.

Next, we add $p \in \{0.01, 0.1, 1\}\%$ noise to the measured data (7.4) and (7.5). The numerical results without regularization have been found unstable and therefore they are not presented. The regularized objective function (7.27), as a function of the number of iterations, is shown in Figure 7.16. Figure 7.17 presents the graphs of the recovered functions. From this figure one can observe that stabilised solutions are obtained by employing regularization.

Finally, details about the number of iterations, the $rmse(f)$ and $rmse(g)$ in (7.32) and (7.33), respectively, and the computational time, are given in Table 7.4 for various values of the regularization parameters $\beta_1 = \beta_2$. For $p = 1\%$ noise and no regularization the computational time and the number of iterations increase drastically and the $rmse(f)$ and $rmse(g)$ become very large, which is expected due to the instability of the inverse and ill-posed problem. However, as previously obtained from Figure 7.17, it can be seen that accurate and stable numerical results are achieved if regularization is employed.

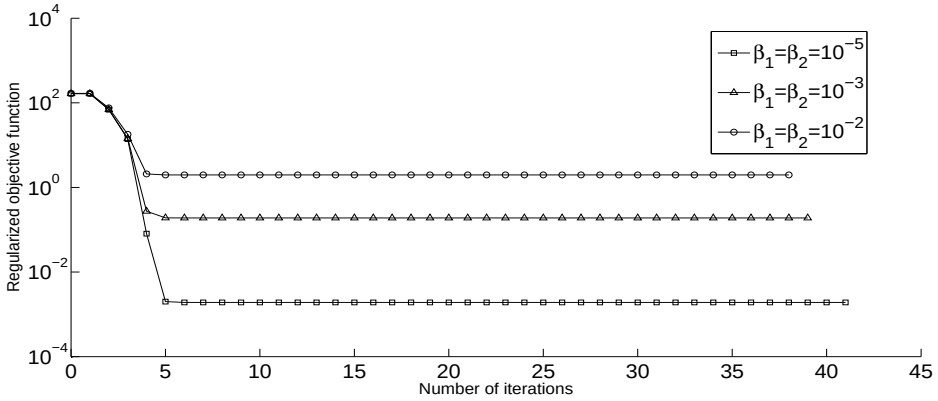

Figure 7.16: Objective function (7.27), for Example 3 with noise $p = 0.01\%$ $(-\square-)$, $p = 0.1\%$ $(-\triangle-)$ and $p = 1\%$ $(-\circ-)$, with regularization.

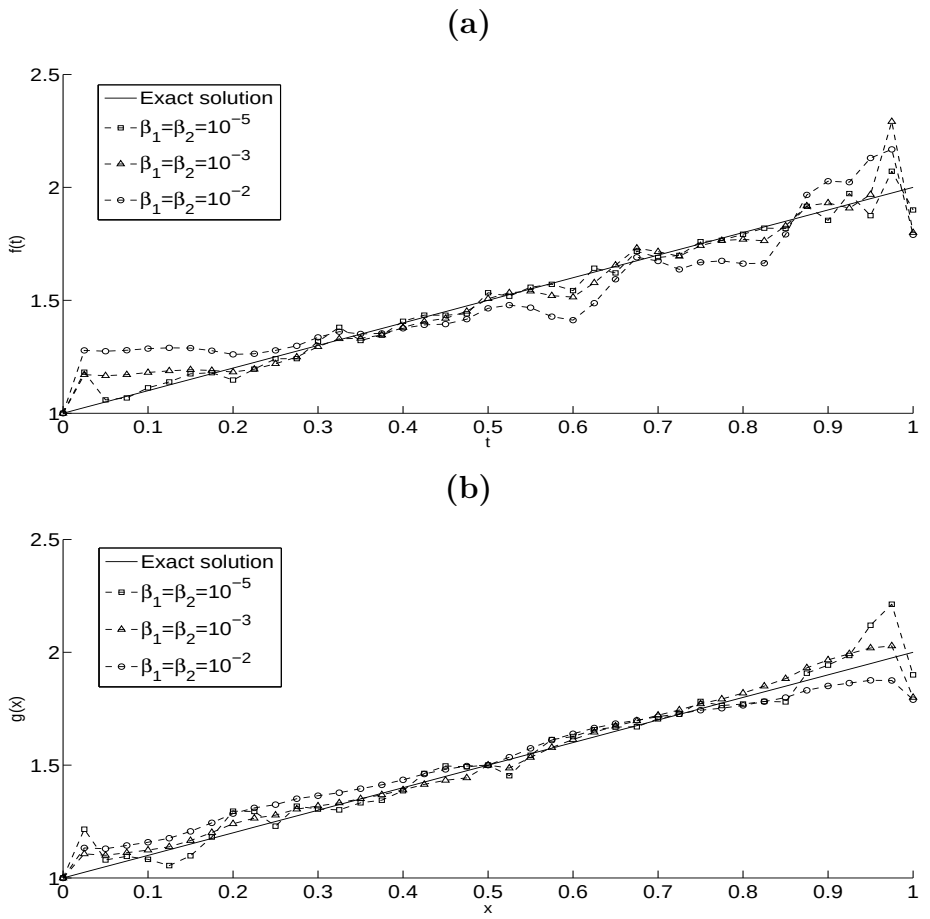

Figure 7.17: (a) Coefficient $f(t)$ and (b) coefficient $g(x)$, for Example 3 with noise $p = 0.01\%$ $(-\square-)$, $p = 0.1\%$ $(-\triangle-)$ and $p = 1\%$ $(-\circ-)$, with regularization.

Table 7.4: Number of iterations, computational time, and $rmse$ values for $p \in \{0.01, 0.1, 1\}\%$ noise, with and without regularization, for Example 3.

p	Regularization	$rmse(f)$	$rmse(g)$	Iter	Time
0.01%	$\beta_1 = \beta_2 = 0$	0.3373	0.5775	18	3 mins
	$\beta_1 = \beta_2 = 10^{-5}$	0.0406	0.0658	42	4 mins
	$\beta_1 = \beta_2 = 10^{-4}$	0.0525	0.0448	41	5 mins
	$\beta_1 = \beta_2 = 10^{-3}$	0.0613	0.0403	38	6 mins
	$\beta_1 = \beta_2 = 10^{-2}$	0.0899	0.0494	41	5 mins
	$\beta_1 = \beta_2 = 10^{-1}$	0.1831	0.1180	41	5 mins
0.1%	$\beta_1 = \beta_2 = 0$	3.3704	5.7759	47	8 mins
	$\beta_1 = \beta_2 = 10^{-5}$	0.2458	0.3619	47	8 mins
	$\beta_1 = \beta_2 = 10^{-4}$	0.1018	0.0895	39	6 mins
	$\beta_1 = \beta_2 = 10^{-3}$	0.0678	0.0335	39	6 mins
	$\beta_1 = \beta_2 = 10^{-2}$	0.0909	0.0466	50	9 mins
	$\beta_1 = \beta_2 = 10^{-1}$	0.1830	0.1197	50	9 mins
1%	$\beta_1 = \beta_2 = 0$	35.9469	53.9733	401	1 hour
	$\beta_1 = \beta_2 = 10^{-5}$	2.5250	3.5760	50	9 mins
	$\beta_1 = \beta_2 = 10^{-4}$	0.9086	0.7765	47	8 mins
	$\beta_1 = \beta_2 = 10^{-3}$	0.2720	0.1581	50	9 mins
	$\beta_1 = \beta_2 = 10^{-2}$	0.1139	0.0527	38	6 mins
	$\beta_1 = \beta_2 = 10^{-1}$	0.1820	0.1366	50	9 mins

7.6 Conclusions

This chapter has presented the determination of an additive time and space-dependent perfusion coefficient from data measurements in the one-dimensional parabolic heat equation. The direct solver based on a Crank-Nicolson finite difference scheme was employed. The resulting inverse problem has been reformulated as a constrained regularized minimization problem which was solved using the MATLAB optimization toolbox routine *lsqnonlin*. The numerically obtained results are stable and accurate.

Except for Section 2.6, all the inverses investigated so far considered one-dimensional space-dependent situations. In the next two chapters we consider two-dimensional problems.

Chapter 8

Determination of a time-dependent free boundary in a two-dimensional parabolic problem

8.1 Introduction

Free boundary problems for parabolic equations play a very important role in many branches of physics, engineering, chemistry, biology and other areas, see [9, 26, 43] to mention only a few. For instance, simultaneous determination of time-dependent coefficients and multiple free boundaries were recently investigated in [61], whilst in [68], free boundary problems with nonlinear diffusion were considered. The numerical solution for inverse free boundary and Stefan problems, based on the method of fundamental solutions, was obtained in [51, 81]. The heat equation with an unknown time-dependent thermal diffusivity or heat source in a domain with a free boundary was also investigated in [67] and [96], respectively. In [69], the authors investigated the determination of multiple time-dependent coefficients together with an unknown free boundary. In [24], the authors discussed free boundary problems arising in two new scenarios, nonlocal diffusion and aggregation processes.

The challenge of free boundary problems lies in the fact that the solution domain is unknown and has to be determined. However, only a few papers are concerned with time-dependent free boundary for parabolic equations in two-dimensions or more, [2, 4, 73]. In this chapter, the inverse problem concerned with determining the time-dependent free boundary together with the temper-

ature from over-determination mass (average temperature) data, whose unique local solvability was previously established in [73], is for the first time numerically investigated.

The organization of the chapter is as follows. The two-dimensional inverse time-dependent free boundary problem for the heat equation is formulated in Section 8.2. In Section 8.3, an alternating direction explicit (ADE) finite-difference method (FDM) is described. In Section 8.4, the numerical approach based on the minimization of the nonlinear least-squares objective function is introduced. Numerical results are presented and discussed in Section 8.5. Finally, conclusions are highlighted in Section 8.6.

8.2 Mathematical formulation

In the moving domain $\Omega_T := \{(y_1, y_2, t) |\ 0 < y_1 < h,\ 0 < y_2 < g(t)\Psi(y_1),\ 0 < t < T\}$, with a free boundary of unknown intensity $g = g(t) > 0$, but with known space variation $\Psi(y_1) > 0$, we consider the two-dimensional parabolic equation

$$u_t = \Delta u + b_1(y_1, y_2, t)u_{y_1} + b_2(y_1, y_2, t)u_{y_2} + c(y_1, y_2, t)u + f(y_1, y_2, t), \quad (y_1, y_2, t) \in \Omega_T, \tag{8.1}$$

for the unknown dependent variable $u(y_1, y_2, t)$, herein called temperature, given the known convection coefficients b_1 and b_2, reaction coefficient c and heat source f. Equation (8.1) has to be solved subject to the initial condition

$$u(y_1, y_2, 0) = \varphi(y_1, y_2), \quad 0 \le y_1 \le h, \quad 0 \le y_2 \le g(0)\Psi(y_1), \tag{8.2}$$

the Dirichlet boundary conditions

$$\begin{cases} u(0, y_2, t) = \mu_{11}(y_2, t), \quad 0 \le y_2 \le \Psi(0)g(t), \quad 0 \le t \le T, \\ u(h, y_2, t) = \mu_{12}(y_2, t), \quad 0 \le y_2 \le \Psi(h)g(t), \quad 0 \le t \le T, \\ u(y_1, 0, t) = \mu_{21}(y_1, t), \quad 0 \le y_1 \le h, \quad 0 \le t \le T, \\ u(y_1, \Psi(y_1)g(t), t) = \mu_{22}(y_1, t), \quad 0 \le y_1 \le h, \quad 0 \le t \le T, \end{cases} \tag{8.3}$$

and the additional mass/energy specification

$$\int_0^h dy_1 \int_0^{g(t)\Psi(y_1)} u(y_1, y_2, t) dy_2 = \mu_5(t), \quad 0 \le t \le T. \tag{8.4}$$

Of course, the additional condition (8.4) giving the mass/energy of the heat conducting system [21, 22] is measured in practice, and is needed in order to supply

for the missing information represented by the unknown function $g(t)$. Alternative additional information to (8.4) such as an internal temperature measurement

$$u(y_1^0, y_2^0, t) = \mu_5^0(t), \quad 0 \le t \le T, \tag{8.5}$$

at a fixed interior point (y_1^0, y_2^0) with $0 < y_1^0 < h$, $0 < y_2^0 < g(t)\Psi(y_1)$, or a heat flux measurement

$$\frac{\partial u}{\partial n}(y_1^1, y_2^1, t) = q(y_1^1, y_2^1, t), \tag{8.6}$$

at a point (y_1^1, y_2^1, t) on the boundary $S_T := \{0\} \times \{(y_2, t)|\ 0 \le y_2 \le \Psi(0)g(t), t \in (0, T]\} \cup \{h\} \times \{(y_2, t)|\ 0 \le y_2 \le \Psi(h)g(t), t \in (0, T]\} \cup [0, h] \times (\{0\} \cup \{(y_1, y_2, t)|\ y_1 \in [0, h],\ y_2 = \Psi(y_1)g(t), t \in (0, T]\})$ can also be considered. In (8.6), n denotes the outward unit normal to the boundary S_T.

The local existence and uniqueness of solution of the inverse problem (8.1)–(8.4) were established in [73] and read as stated in the following two theorems.

Theorem 8.2.1. *Consider the following conditions:*

$(A1)$ $\varphi \in C([0, h] \times [0, \infty))$, $\mu_{11}, \mu_{12} \in C([0, \infty) \times [0, T])$, $\mu_{21}, \mu_{22} \in C([0, h] \times [0, T])$, $\mu_5 \in C^1[0, T]$, $b_k, c, f \in C([0, h] \times [0, \infty) \times [0, T])$, $k = 1, 2$;

$(A2)$ $\varphi(y_1, y_2) \ge \varphi_0 > 0$, $(y_1, y_2) \in [0, h] \times [0, \infty)$, $\min\{\mu_{11}(y_2, t), \mu_{12}(y_2, t\} \ge \mu_{i0} > 0$, $i = 1, 2$, $(y_2, t) \in [0, \infty) \times [0, T]$, $\min\{\mu_{21}(y_1, t), \mu_{22}(y_1, t)\} > 0$, $(y_1, t) \in [0, h] \times [0, T]$, $\mu_5(t) > 0$, $t \in [0, T]$, $f(y_1, y_2, t) \ge 0$, $(y_1, y_2, t) \in [0, h] \times [0, \infty) \times [0, T]$, $\Psi(y_1) > 0$, $y_1 \in [0, h]$;

$(A3)$ $\mu_{11} \in C^{2,1}([0, K_1\Psi(0)] \times [0, T])$, $\mu_{12} \in C^{2,1}([0, K_1\Psi(h)] \times [0, T])$, $\mu_{21}, \mu_{22} \in C^{2,1}([0, h] \times [0, T])$, $b_1, b_2, c, f \in C^{1,0}(\overline{Q})$, *where*
$Q := \{(y_1, y_2, t) : 0 < y_1 < h, 0 < y_2 < K_1\Psi(y_1), 0 < t < T\}$,
$\varphi \in C^2(\overline{D_0})$, *where* $D_0 := \{(y_1, y_2) : 0 < y_1 < h, 0 < y_2 < g(0)\Psi(y_1)\}$,
$\Psi \in C^2[0, h]$, $\lim\limits_{y_1 \to 0} \Psi'(y_1) = +\infty$, $\lim\limits_{y_1 \to h} \Psi'(y_1) = -\infty$;

(A4) conditions of consistency of order zero [90] between the initial condition (8.2) and the Dirichlet boundary conditions (8.3);

$(A5)$ $\varphi \in C([0,h]\times[0,\infty))$, $\mu_{11},\mu_{12} \in C([0,\infty)\times[0,T])$, $\mu_{21},\mu_{22} \in C([0,h]\times[0,T])$, $\mu_5 \in C^1[0,T]$, $b_k, c, f \in C^{1,0}([0,h]\times[0,\infty)\times[0,T])$, $k=1,2$, $\Psi \in C^1[0,T]$.

If $(A1)$–$(A3)$ *are satisfied then there exists a number* $T_0 \in (0,T]$*, which is determined by input data, such that the problem (8.1)–(8.4) has a solution* $(g(t), u(y_1,y_2,t)) \in C^1[0,T_0]\times\left(C^{2,1}(\Omega_{T_0})\cap C^{1,0}(\overline{\Omega_{T_0}})\right) =: A_{T_0}$ *with* $g(t)>0$ *for* $t\in[0,T_0]$.

If $(A2)$, $(A4)$ *and* $(A5)$ *are satisfied the same existence result holds in the set* $(g(t),u(y_1,y_2,t)) \in C^1[0,T_0]\times(C^{2,1}(\Omega_{T_0})\cap C\left(\overline{\Omega_{T_0)}}\right))$ *with* $g(t)>0$ *for* $t\in[0,T_0]$.

In $(A3)$*, the positive constant* K_1 *represents an upper bound for the function* $g(t)$ *for* $t\in[0,T]$*, which is obtained from (8.4) and the max-min principle for the function* u*, which under assumptions* $(A1)$ *and* $(A2)$*, yields, [73],*

$$u(y_1,y_2,t) \geq M_0 > 0, \quad (y_1,y_2,t) \in \overline{\Omega_T} \tag{8.7}$$

for some positive constant M_0*. Thus, we can take*

$$K_1 = \max_{0\leq t\leq T}|\mu_5(t)|/(M_0 h(\min_{0\leq y_1\leq h}\Psi(y_1))).$$

Note also that under assumptions $(A1)$ and $(A2)$, equation (8.4) applied at $t=0$ yields the value of $g(0)$ as the unique positive solution of the nonlinear equation

$$\int_0^h dy_1 \int_0^{g(0)\Psi(y_1)} \varphi(y_1,y_2)dy_2 = \mu_5(0). \tag{8.8}$$

Theorem 8.2.2. *Let the following conditions be fulfilled:*

$(A6)$ $b_i, c, f \in C^{1,0}([0,h]\times[0,\infty)\times[0,T])$, $\mu_{11},\mu_{12} \in C^{3,1}([0,\infty)\times[0,T])$, $i=1,2$, $0<\Psi\in C^2[0,h]$, $\int_0^h \Psi(y_1)\mu_{22}(y_1,t)dy_1 \neq 0$ *for* $t\in[0,T]$;

$(A7)$ $\varphi(y_1,y_2)\geq\varphi_0>0$, $(y_1,y_2)\in[0,h]\times[0,\infty)$.

Then, if $C^1[0,T]\ni\mu_5(t)\neq 0$ *for* $t\in[0,T]$*, the inverse problem (8.1)–(8.4) cannot have more than one solution* $(g(t),u(y_1,y_2,t))$ *in the class* A_T*, with* $g(t)>0$ *for*

$t \in [0, T]$.

The following theorem establishes the stability of the inverse problem (8.1)–(8.4) under small perturbations in the measured additional mass/energy data (8.4), see [58] for the proof.

Theorem 8.2.3. *Assume that* $(A6)$ *and* $(A7)$ *are satisfied. Let* $\mu_5(t) \neq 0$ *and* $\mu_5^\epsilon(t)$ *for* $t \in [0, T]$*, be two given data (8.4) in* $C^1[0, T]$ *satisfying*

$$||\mu_5 - \mu_5^\epsilon||_{C^1[0,T]} \leq \varepsilon \tag{8.9}$$

for some non-negative constant ε*. Then, if it exists, the unique solution* $(g(t), u(y_1, y_2, t)) \in A_T$ *with* $g(t) > 0$ *for* $t \in [0, T]$*, of the inverse problem (8.1)–(8.4) under the perturbation* $\mu_5^\epsilon(t)$ *of* $\mu_5(t)$ *in (8.4), satisfying (8.9), is stable for small* $\varepsilon > 0$*.*

Remark 1. The stability Theorem 8.2.3 obviously implies, by taking $\varepsilon = 0$, the uniqueness Theorem 8.2.2. Theorem 8.2.3 ensures the stability in case the data (8.4) is smooth of class $C^1[0, T]$. However, the presence of the derivative $(\mu_5^\varepsilon)'(t)$ of the 'noisy' non-smooth function $\mu_5^\varepsilon(t)$, coming from measurement, in (8.7) highlights the practical ill-posedness of the inverse free surface problem under investigation.

8.3 Numerical discretisation of the direct problem

For the numerical discretization in a fixed domain it is useful to employ further the change of variables $x_1 = y_1$, $x_2 = y_2/(g(t)\Psi(y_1))$, see [73], to transform the problem (8.1)–(8.4) to the following inverse problem for the time-dependent free boundary intensity function $g(t)$ and the new 'temperature' function $v(x_1, x_2, t) := u(x_1, x_2 g(t)\Psi(x_1), t)$:

$$\begin{aligned} v_t = v_{x_1x_1} + \frac{1}{g^2(t)\Psi^2(x_1)} v_{x_2x_2} + b_1(x_1, x_2 g(t)\Psi(x_1), t) v_{x_1} \\ + \left(\frac{b_2(x_1, x_2 g(t)\Psi(x_1), t) + x_2 g'(t)\Psi(x_1)}{g(t)\Psi(x_1)} \right) v_{x_2} + c(x_1, x_2 g(t)\Psi(x_1), t) v \\ + f(x_1, x_2 g(t)\Psi(x_1), t), \quad (x_1, x_2, t) \in \Omega \times (0, T), \end{aligned} \tag{8.10}$$

$$v(x_1, x_2, 0) = \varphi(x_1, x_2 g(0)\Psi(x_1)), \quad (x_1, x_2) \in \overline{\Omega}, \tag{8.11}$$

$$v(0,x_2,t)=\mu_{11}(x_2g(t)\Psi(0),t),\quad v(h,x_2,t)=\mu_{12}(x_2g(t)\Psi(h),t),\\ (x_2,t)\in[0,1]\times[0,T],\tag{8.12}$$

$$v(x_1,0,t)=\mu_{21}(x_1,t),\quad v(x_1,1,t)=\mu_{22}(x_1,t),\ (x_1,t)\in[0,h]\times[0,T],\tag{8.13}$$

$$g(t)\iint\limits_{\Omega}\Psi(x_1)v(x_1,x_2,t)dx_1dx_2=\mu_5(t),\quad t\in[0,T],\tag{8.14}$$

where $\Omega=(0,h)\times(0,1)$.

We consider in this section, the direct initial boundary value problem given by equations (8.10)–(8.13), where the functions g, Ψ, b_1, b_2, c, f, φ and $\mu_{i,j}$ for $i,j=1,2$, are known and the solution $v(x_1,x_2,t)$ is to be determined. We subdivide the solution domain $\Omega\times(0,T)$ into M_1, M_2 and N uniform subintervals of equal lengths Δx_1, Δx_2 and Δt, where $\Delta x_1=h/M_1$, $\Delta x_2=1/M_2$, and $\Delta t=T/N$, respectively. At the node (i,j,n), we denote $v^n_{i,j}:=v(x_{1i},x_{2j},t_n)$, where $x_{1i}=i\Delta x_1$, $x_{2j}=j\Delta x_2$, $t_n=n\Delta t$, $g_n:=g(t_n)$, $\Psi_i:=\Psi(x_{1i})$, $b^n_{1_{i,j}}:=b_1(x_{1i},x_{2j}g_n\Psi_i,t_n)$, $b^n_{2_{i,j}}:=b_1(x_{1i},x_{2j}g_n\Psi_i,t_n)$, $c^n_{i,j}:=c(x_{1i},x_{2j}g_n\Psi_i,t_n)$ and $f^n_{i,j}:=f(x_{1i},x_{2j}g_n\Psi_i,t_n)$ for $i=\overline{0,M_1}$, $j=\overline{0,M_2}$ and $n=\overline{0,N}$.

8.3.1 Alternating direction explicit (ADE) method

Alternating direction explicit (ADE) methods not only provide computational simplicity, but also possess the advantage of the implicit methods in that no severe limitation is imposed on the time step. Based on the method described in [5, 6, 106], in this section an unconditionally stable numerical procedure for solving nonlinear the two-dimensional parabolic heat equation (8.10) with initial and boundary conditions (8.11)–(8.13) will be described.

Let $\tilde v^n_{i,j}$ and $\tilde u^n_{i,j}$ satisfy the following equations which are multilevel finite difference discretisations of equation (8.10):

$$\frac{\tilde v^{n+1}_{i,j}-\tilde v^n_{i,j}}{\Delta t}=\frac{\tilde v^n_{i+1,j}-\tilde v^n_{i,j}-\tilde v^{n+1}_{i,j}+\tilde v^{n+1}_{i-1,j}}{(\Delta x_1)^2}\\ +\frac{1}{g_n^2\Psi_i^2}\Big(\frac{\tilde v^n_{i,j+1}-\tilde v^n_{i,j}-\tilde v^{n+1}_{i,j}+\tilde v^{n+1}_{i,j-1}}{(\Delta x_2)^2}\Big)+b^n_{1_{i,j}}\Big(\frac{\tilde v^n_{i+1,j}-\tilde v^{n+1}_{i-1,j}}{2(\Delta x_1)}\Big)\\ +\Big(\frac{b^n_{2_{i,j}}+x_{2j}g_n'\Psi_i}{g_n\Psi_i}\Big)\Big(\frac{\tilde v^n_{i,j+1}-\tilde v^{n+1}_{i,j-1}}{2(\Delta x_2)}\Big)+c^n_{i,j}\Big(\frac{\tilde v^{n+1}_{i,j}+\tilde v^n_{i,j}}{2}\Big)\\ +\frac{1}{2}\Big(f^{n+1}_{i,j}+f^n_{i,j}\Big),\ i=\overline{1,M_1-1},\ j=\overline{1,M_2-1},\ n=\overline{0,N-1},\tag{8.15}$$

$$\frac{\tilde{u}_{i,j}^{n+1}-\tilde{u}_{i,j}^{n}}{\Delta t}=\frac{\tilde{u}_{i+1,j}^{n+1}-\tilde{u}_{i,j}^{n+1}-\tilde{u}_{i,j}^{n}+\tilde{u}_{i-1,j}^{n}}{(\Delta x_1)^2}$$
$$+\frac{1}{g_n^2\Psi_i^2}\Big(\frac{\tilde{u}_{i,j+1}^{n+1}-\tilde{u}_{i,j}^{n+1}-\tilde{u}_{i,j}^{n}+\tilde{u}_{i,j-1}^{n}}{(\Delta x_2)^2}\Big)+b_{1_{i,j}}^{n}\Big(\frac{\tilde{u}_{i+1,j}^{n+1}-\tilde{u}_{i-1,j}^{n}}{2(\Delta x_1)}\Big)$$
$$+\Big(\frac{b_{2_{i,j}}^{n}+x_{2j}g_n'\Psi_i}{g_n\Psi_i}\Big)\Big(\frac{\tilde{u}_{i,j+1}^{n+1}-\tilde{u}_{i,j-1}^{n}}{2(\Delta x_2)}\Big)+c_{i,j}^{n}\Big(\frac{\tilde{u}_{i,j}^{n}+\tilde{u}_{i,j}^{n+1}}{2}\Big)$$
$$+\frac{1}{2}\Big(f_{i,j}^{n+1}+f_{i,j}^{n}\Big),\ i=\overline{M_1-1,1},\ j=\overline{M_2-1,1},\ n=\overline{0,N-1}. \tag{8.16}$$

Furthermore, let the $\tilde{v}_{i,j}^{n}$ and $\tilde{u}_{i,j}^{n}$ also satisfy the initial and boundary conditions (8.11)–(8.13), namely

$$\tilde{v}_{i,j}^{0}=\tilde{u}_{i,j}^{0}=\varphi(x_{1i},x_{2j}),\quad i=\overline{0,M_1},\quad j=\overline{0,M_2}, \tag{8.17}$$

$$\tilde{v}_{0,j}^{n}=\tilde{u}_{0,j}^{n}=\mu_{11}(x_{2j}g_n\Psi(0),t_n),\quad \tilde{v}_{M_1,j}^{n}=\tilde{u}_{M_1,j}^{n}=\mu_{12}(x_{2j}g_n\Psi(h),t_n),$$
$$j=\overline{0,M_2},\quad n=\overline{1,N}, \tag{8.18}$$

$$\tilde{v}_{i,0}^{n}=\tilde{u}_{i,0}^{n}=\mu_{21}(x_{1i},t_n),\quad \tilde{v}_{i,M_2}^{n}=\tilde{u}_{i,M_2}^{n}=\mu_{22}(x_{1i},t_n),\quad i=\overline{0,M_1},$$
$$n=\overline{1,N}. \tag{8.19}$$

In expressions (8.15) and (8.16), the derivative of g is approximated as

$$g_n':=g'(t_n)\approx\frac{g(t_n)-g(t_{n-1})}{\Delta t}=\frac{g_n-g_{n-1}}{\Delta t},\quad n=\overline{1,N}. \tag{8.20}$$

Equations (8.15) and (8.16) are rearranged in order to obtain explicit expressions for $\tilde{v}_{i,j}^{n+1}$ and $\tilde{u}_{i,j}^{n+1}$. They, respectively, become

$$\tilde{v}_{i,j}^{n+1}=A_{i,j}^{n}\tilde{v}_{i,j}^{n}+B_{i,j}^{n}(\tilde{v}_{i+1,j}^{n}+\tilde{v}_{i-1,j}^{n+1})+C_{i,j}^{n}(\tilde{v}_{i,j+1}^{n}+\tilde{v}_{i,j-1}^{n+1})$$
$$+D_{i,j}^{n}(\tilde{v}_{i+1,j}^{n}-\tilde{v}_{i-1,j}^{n+1})+E_{i,j}^{n}(\tilde{v}_{i,j+1}^{n}-\tilde{v}_{i,j-1}^{n+1})+G_{i,j}^{*},$$
$$i=\overline{1,M_1-1},\quad j=\overline{1,M_2-1},\quad n=\overline{0,N-1}, \tag{8.21}$$

$$\tilde{u}_{i,j}^{n+1}=A_{i,j}^{n}\tilde{u}_{i,j}^{n}+B_{i,j}^{n}(\tilde{u}_{i+1,j}^{n+1}+\tilde{u}_{i-1,j}^{n})+C_{i,j}^{n}(\tilde{u}_{i,j+1}^{n+1}+\tilde{u}_{i,j-1}^{n})$$
$$+D_{i,j}^{n}(\tilde{u}_{i+1,j}^{n+1}-\tilde{u}_{i-1,j}^{n})+E_{i,j}^{n}(\tilde{u}_{i,j+1}^{n+1}-\tilde{u}_{i,j-1}^{n})+G_{i,j}^{*},$$
$$i=\overline{M_1-1,1},\quad j=\overline{M_2-1,1},\quad n=\overline{0,N-1}, \tag{8.22}$$

where

$$A^n_{i,j} = \frac{1-\lambda^n_{i,j}}{1+\lambda^n_{i,j}}, \quad B^n_{i,j} = \frac{\Delta t}{(\Delta x_1)^2(1+\lambda^n_{i,j})},$$
$$C^n_{i,j} = \frac{\Delta t}{g_n^2\Psi_i^2(\Delta x_2)^2(1+\lambda^n_{i,j})}, \; D^n_{i,j} = \frac{(\Delta t)b^n_{1_{i,j}}}{2\Delta x_1(1+\lambda^n_{i,j})},$$
$$E^n_{i,j} = \frac{\Delta t}{2\Delta x_2}\left(\frac{b^n_{2_{i,j}} + x_{2j}g_n'\Psi_i}{g_n\Psi_i(1+\lambda^n_{i,j})}\right), \; G^*_{i,j} = \frac{\Delta t}{2(1+\lambda^n_{i,j})}\Big(f^{n+1}_{i,j} + f^n_{i,j}\Big),$$
$$\lambda^n_{i,j} = \Delta t\left(\frac{1}{(\Delta x_1)^2} + \frac{1}{g_n^2\Psi_i^2(\Delta x_2)^2} - \frac{c^n_{i,j}}{2}\right). \tag{8.23}$$

From (8.21) and (8.17)–(8.19) for $\tilde{v}$, $\tilde{v}^{n+1}_{i,j}$ can be computed explicitly. In this case, calculations proceed from the grid point close to the boundaries $x_1 = 0$ and $x_2 = 0$, as i, j increasing. The needed values such as $\tilde{v}^{n+1}_{i-1,j}$, $\tilde{v}^{n+1}_{i,j-1}$, $\tilde{v}^n_{i,j}$, $\tilde{v}^n_{i+1,j}$ and $\tilde{v}^n_{i,j+1}$ will be known from initial and boundary conditions (8.17)–(8.19). Similarly, $\tilde{u}^{n+1}_{i,j}$ can be calculated explicitly from (8.22) and (8.17)–(8.19) for $\tilde{u}$, beginning at the boundaries $x_1 = 1$ and $x_2 = 1$ and marching in a sequence of decreasing i and j, i.e. $i = M_1 - 1, M_1 - 2, ..., 1$, $j = M_2 - 1, M_2 - 2, ..., 1$. These values are then substituted into the simple arithmetic mean approximation

$$v^{n+1}_{i,j} = \frac{\tilde{v}^{n+1}_{i,j} + \tilde{u}^{n+1}_{i,j}}{2} \tag{8.24}$$

to obtain the solution $v^{n+1}_{i,j}$. This procedure is unconditionally stable, as both equations (8.21) and (8.22) are unconditionally stable, but the time increment Δt cannot be taken indefinitely large. It has been noticed in [5] that if the time increment is taken very large, the solution obtained will be stable but may not describe the actual physical problem. This behavior is common to all unconditionally stable explicit or semi-implicit methods.

The double integral in (8.14) is approximated using the trapezoidal rule

[34, 44], as follows:

$$\int_0^h \int_0^1 \Psi(x_1)v(x_1,x_2,t)dx_2dx_1 = \frac{1}{4M_1M_2}\Bigg[\Psi(0)v(0,0,t_n) + \Psi(h)v(h,0,t_n) + \Psi(0)v(0,1,t_n) + \Psi(h)v(h,1,t_n) + 2\sum_{i=1}^{M_1-1}\Psi(x_{1i})v(x_{1i},0,t_n) + 2\sum_{i=1}^{M_1-1}\Psi(x_{1i})v(x_{1i},1,t_n) + 2\sum_{j=1}^{M_2-1}\Psi(0)v(0,x_{2j},t_n) + 2\sum_{j=1}^{M_2-1}\Psi(h)v(h,x_{2j},t_n) + 4\sum_{j=1}^{M_2-1}\sum_{i=1}^{M_1-1}\Psi(x_{1i})v(x_{1i},x_{2j},t_n)\Bigg], \quad n=\overline{1,N}. \tag{8.25}$$

8.4 Numerical solution of inverse problem

In this section, we aim to obtain stable reconstructions for time-dependent intensity $g(t)$ of the the free boundary and the transformed temperature $v(x_1,x_2,t)$, satisfing equations (8.10)–(8.14). The inverse problem can be formulated as a nonlinear least-squares minimization of the objective function

$$F(g) := \left\| g(t)\int_0^h\int_0^1 \Psi(x_1)v(x_1,x_2,t;g)dx_2dx_1 - \mu_5(t)\right\|^2_{L^2[0,T]} \tag{8.26}$$

or, in discretizations form,

$$F(\underline{g}) = \sum_{n=1}^{N}\left[g_n\int_0^h\int_0^1 \Psi(x_1)v(x_1,x_2,t_n;\underline{g})dx_2dx_1 - \mu_5(t_n)\right]^2, \tag{8.27}$$

where $\underline{g}=(g_n)_{n=\overline{1,N}}$ and $v(x_1,x_2,t;g)$ solves (8.10)–(8.13) for given g. The minimization of the objective function (8.27) is performed using the MATLAB toolbox routine *lsqnonlin*.

In the numerical computation, we take the parameters of the routine as follows:

- Maximum number of iterations, (MaxIter) = 400.
- Maximum number of objective function evaluations, (MaxFunEvals) = 10^5.
- Termination tolerance on the function value, (TolFun) = 10^{-20}.
- Solution tolerance value, (xTol) = 10^{-20}.

8.5 Numerical results and discussion

In this section, we present a test example in order to illustrate the accuracy and stability of the ADE numerical procedure introduced earlier in Section 8.3 combined with the minimization of the least-squares functional (8.27), as described in Section 8.4. We employ the root mean square errors (rmse), in order to assess the accuracy of the numerical results, defined as

$$rmse(g) = \left[\frac{T}{N}\sum_{n=1}^{N}\Big(g_n - g^{Exact}(t_n)\Big)^2\right]^{1/2}. \tag{8.28}$$

For simplicity, we take $h = T = 1$. The lower bounds and upper bounds for the coefficient $g(t)$ are taken as 10^{-9} and 10^2, respectively. The initial guesses for $g(t)$ is taken as the value of $g(0)$, which is obtainable from (8.14).

The inverse problem given by equations (8.10)–(8.14) is solved subject to both exact and noisy data. The noisy data in (8.14) is numerically simulated as

$$\mu_5^{\epsilon}(t_n) = \mu_5(t_n) + \epsilon_n, \quad n = \overline{1, N}, \tag{8.29}$$

where ϵ_n are random variables generated from a Gaussian normal distribution with mean zero and standard deviation $\sigma = p \times \max_{t\in[0,1]}|\mu_5(t)|$, where p represents the percentage of noise. We use the MATLAB function *normrnd* to generate the random variables $\underline{\epsilon} = (\epsilon_n)_{n=\overline{1,N}} := normrnd(0, \sigma, N)$.

We consider the inverse problem (8.1)–(8.4) with the following input data:

$$\begin{aligned}
&\Psi(y_1) = 1,\ b_1(y_1, y_2, t) = \frac{1}{2}(y_1 + y_2 + t),\ b_2(y_1, y_2, t) = \frac{1}{2}(y_1 + y_2 + t),\\
&c(y_1, y_2, t) = \frac{1}{2}(y_1 + y_2 + t),\ \varphi(y_1, y_2) = 3 - (-1 + 2y_1)^2 - (-1 + y_2)^2,\\
&\mu_{11}(y_2, t) = 2 + t - (-1 + y_2)^2,\ \mu_{12}(y_2, t) = 2 + t - (-1 + y_2)^2,\\
&\mu_{21}(y_1, t) = 2 + t - (-1 + 2y_1)^2,\ \mu_{22}(y_1, t) = \frac{1}{9}(14 + 13t - t^2 + 36y_1\\
&-36y_1^2) - (-1 + 2y_1)^2,\ f(y_1, y_2, t) = 11 + 2(-1 + 2y_1)(t + y_1 + y_2)\\
&+(-1 + y_2)(t + y_1 + y_2) - \frac{1}{2}(t + y_1 + y_2)(1 + t + 4y_1 - 4y_1^2 + 2y_2 - y_2^2),
\end{aligned} \tag{8.30}$$

$$\mu_5(t) = \frac{1}{81}(1 + t)(53 + 34t - t^2). \tag{8.31}$$

Remark that conditions of Theorem 8.2.2 are satisfied and therefore, the uniqueness of the solution is guaranteed. In fact, one can easily check that the analytical

solution of the transformed inverse problem (8.10)–(8.14) is given by

$$v(x_1, x_2, t) = u(x_1, x_2 g(t)\Psi(x_1), t) = 3 + t - (1 - 2x_1)^2 - \frac{1}{9}(-3 + x_2 + t x_2)^2, \tag{8.32}$$

and

$$g(t) = \frac{1}{3}(1 + t). \tag{8.33}$$

Also,

$$u(y_1, y_2, t) = 3 + t - (-1 + 2y_1)^2 - (-1 + y_2)^2. \tag{8.34}$$

First, we assess the accuracy of the direct problem given by equations (8.1)–(8.3) (or (8.10)–(8.13)) with the input data (8.30) when $g(t)$ is known and given by (8.33). The numerical results for the interior transformed temperature $v(x_1, x_2, t)$ have been obtained in excellent agreement with the analytical solution (8.32) and therefore they are not presented. Apart from the interior temperature, other output of interest is the data (8.4) (or (8.14)), which analytically is given by (8.31). Table 8.1 shows that the analytical and numerical solutions for this quantity obtained with various numbers of space grids $M_1 = M_2 \in \{5, 10, 20\}$ and with various numbers of time steps $N \in \{20, 40, 80\}$ are in very good agreement. Also, the root mean square errors $rmse$ defined by

$$rmse(\mu_5) = \left[\frac{1}{N} \sum_{n=1}^{N} \left(\mu_5^{Numerical}(t_n) - \mu_5^{Exact}(t_n) \right)^2 \right]^{1/2}, \tag{8.35}$$

indicated in Table 8.1, show more clearly the convergence of the numerical ADE solution to the analytical solution (8.31).

Table 8.1: The exact (8.31) and numerical solutions for $\mu_5(t)$, with various $M_1 = M_2 \in \{5, 10, 20\}$ and $N \in \{20, 40, 80\}$, for the direct problem. The $rmse$ values (8.35) are also included.

$M_1 = M_2$	N	$t = 0.1$	$t = 0.2$	$t = 0.3$	...	$t = 0.9$	$rmse$
5	20	0.7554	0.8741	1.0006	...	1.9232	0.0148
	40	0.7556	0.8741	1.0007	...	1.9233	0.0147
	80	0.7556	0.8742	1.0007	...	1.9234	0.0146
10	20	0.7629	0.8823	1.0096	...	1.9369	0.0039
	40	0.7631	0.8825	1.0098	...	1.9372	0.0038
	80	0.7632	0.8825	1.0098	...	1.9373	0.0037
20	20	0.7648	0.8841	1.0116	...	1.9398	0.0015
	40	0.7649	0.8845	1.0120	...	1.9405	0.0011
	80	0.7651	0.8846	1.0121	...	1.9408	0.0009
exact		0.7658	0.8853	1.0129	...	1.9420	0

Next we investigate the inverse problem. We fix $M_1 = M_2 = 10$ and $N = 40$ and we start the investigation for determining the unknown time-dependent intensity $g(t)$ and the transformed temperature $v(x_1, x_2, t)$ for $p \in \{0, 1, 2, 3\}\%$ noise in the measured data (8.29). Although not illustrated, it is reported that a rapid monotonic decreasing convergence of the objective function (8.27) to a very small minimum value of $O(10^{-28})$ is achieved in about 7 iterations. Figure 8.1 shows the absolute error between the exact solution (8.32) and the numerical solutions for the transformed temperature $v(x_1, x_2, t)$. From this figure it can be seen that the accuracy of the numerical solution for the transformed temperature $v(x_1, x_2, t)$ improves, as the noise level p decreases.

The numerical results for $g(t)$ are shown in Figure 8.2. For more clarity, we also report that the $rmse(g)$ values (8.28) are $0.0014, 0.0127, 0.0250$ and 0.0373 for $p \in \{0, 1, 2, 3\}\%$ noise, respectively. As expected, for exact data, i.e. $p = 0$, the unique solution (8.33), which is guaranteed from Theorem 8.2.2, is retrieved very accurately. As noise p is included in the input data (8.29), Figure 8.2 shows that the numerical results are reasonably accurate but start to build up oscillations as the amount of noise p increases. This is expected since the inverse problem under investigation is ill-posed. In order to restore stability we penalise the least-squares function (8.26) by adding a first-order smoothing term $\lambda||g'(t)||^2_{L^2[0,T]}$ to it since the theory requires $g \in C^1[0, T]$, where $\lambda > 0$ is a regularization parameter to be prescribed. Then, in discretised form this first-order Tikhonov functional recasts as

$$F_\lambda(\underline{g}) = F(\underline{g}) + \lambda \sum_{n=1}^{N} \left(\frac{g_n - g_{n-1}}{\Delta t} \right)^2. \tag{8.36}$$

For $p = 5\%$ noise, Figure 8.3 shows the analytical solution (8.33) in comparison with the numerical solutions obtained by minimizing the objective functional (8.36) for various regularization parameters. The $rmse(g)$ values are 0.0618, 0.0440, 0.0292 and 0.0322 for $\lambda \in \{0, 10^{-3}, 10^{-2}, 10^{-1}\}$, respectively. From Figure 8.3 it can be seen that the numerical unregularized solution obtained with $\lambda = 0$ manifests instability, however, inclusion of regularization with $\lambda = 10^{-2}$ to 10^{-1} provides a stable solution which is consistent in accuracy with the $p = 5\%$ noise with which the input data (8.29) has been contaminated. The last remaining thing to do is to provide some reasoning on how to choose the regularization parameter $\lambda > 0$ in the functional (8.36). One possible argument for this choice is given by the L-curve plotted in Figure 8.4. For various values of the regularization parameter λ, for the obtained minimizer $\underline{g}_\lambda$ of (8.36), we plot the derivative norm $||\underline{g}'_\lambda|| = \sqrt{\sum_{n=1}^{N} \left(\frac{g_n - g_{n-1}}{\Delta t}\right)^2}$ versus the residual norm $\sqrt{F(\underline{g}_\lambda)}$. The corner of the L-curve around $\lambda = 10^{-2}$, illustrated in Figure 8.4, is taken as a good choice for the regularization parameter λ compromising/balancing the fit of data (residual comparable to the amount of noise included) with the stability of solution (bounded derivative solution norm).

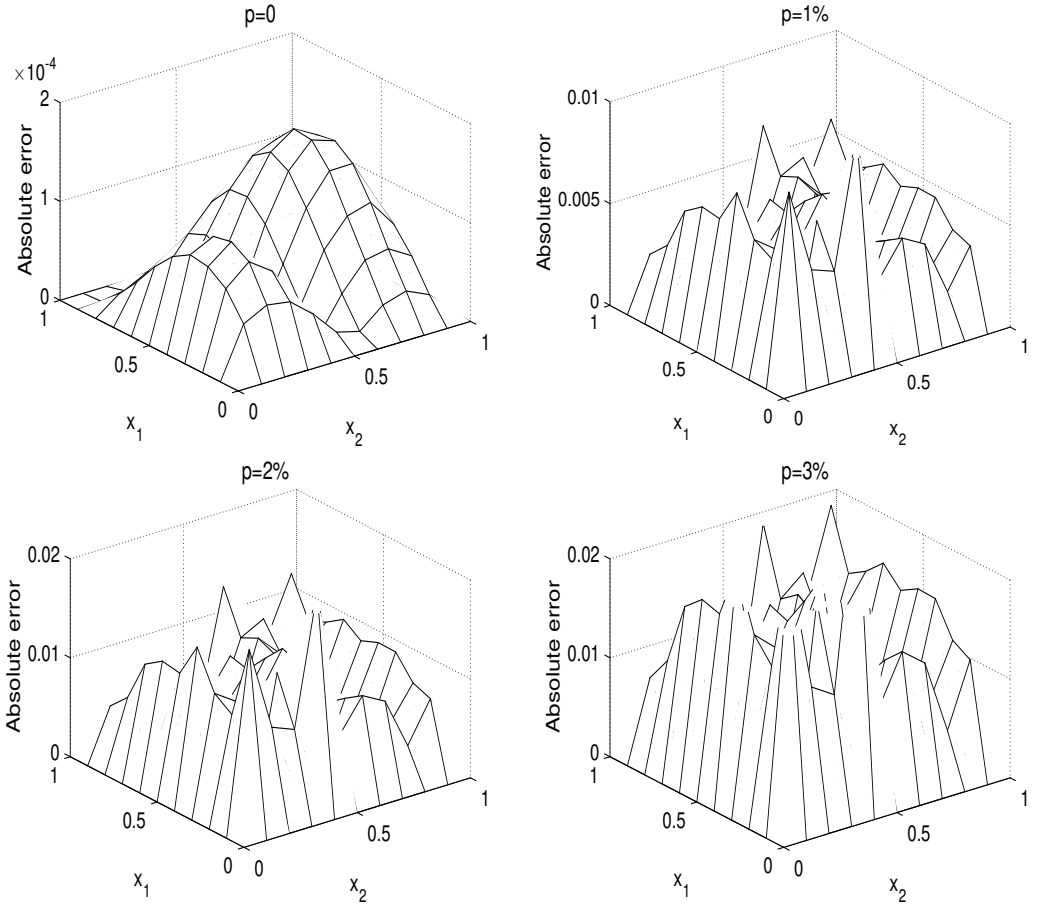

Figure 8.1: The absolute error between the analytical (8.32) and numerical solutions for the transformed temperature $v(x_1, x_2, 1)$, for $p \in \{0, 1, 2, 3\}\%$ noise, without regularization.

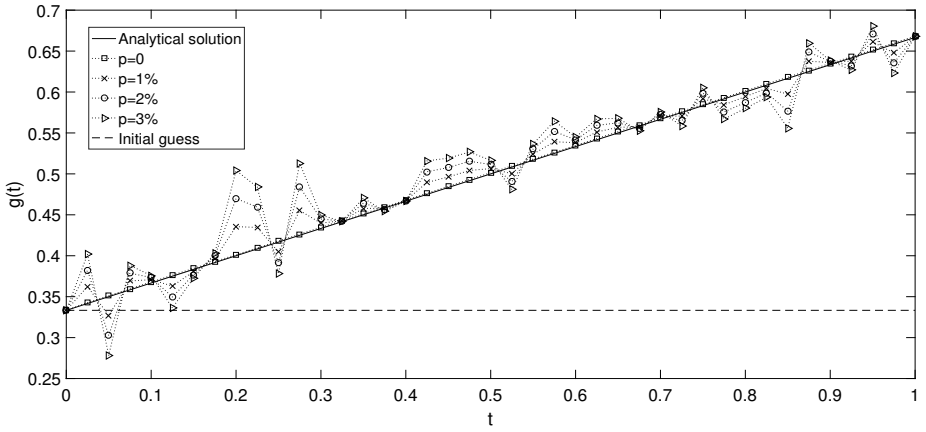

Figure 8.2: The analytical (8.33) and numerical solutions for the intensity $g(t)$ of the free boundary, for $p \in \{0, 1, 2, 3\}\%$ noise, without regularization.

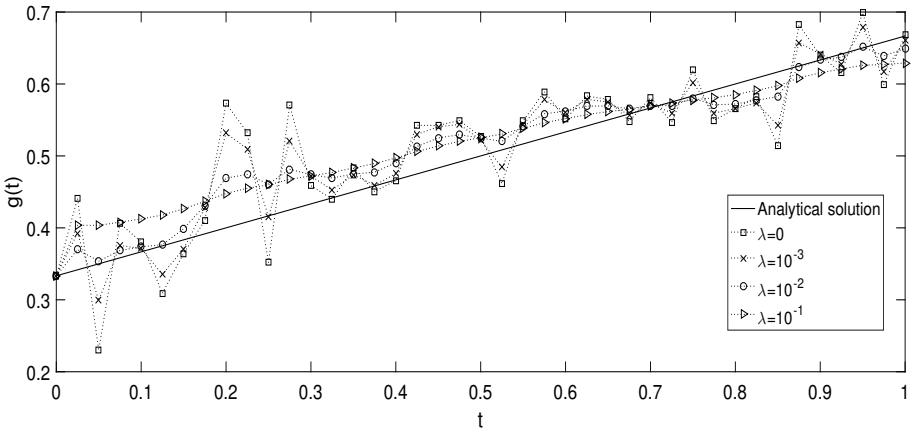

Figure 8.3: The analytical (8.33) and numerical solutions for the intensity $g(t)$ of the free boundary, for $p = 5\%$ noise, with various regularization parameters $\lambda \in \{0, 10^{-3}, 10^{-2}, 10^{-1}\}$.

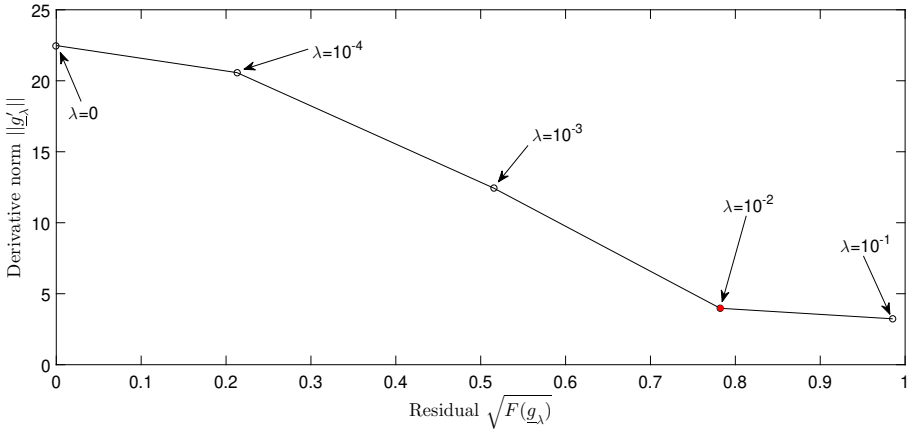

Figure 8.4: The derivative norm $||g'_\lambda||$ versus the residual norm $\sqrt{F(g_\lambda)}$ for the L-curve with various regularization parameters, $p = 5\%$ noise.

8.6 Conclusions

This chapter has presented the determination of a time-dependent intensity of a free boundary and the temperature in a two-dimensional parabolic problem from mass (energy) measurement. This nonlinear inverse problem has been shown to be (locally) well-posed and a stability theorem has been stated. The free boundary problem has been transformed to a fixed domain, and the direct solver based on ADE finite difference scheme has been employed. The inverse problem has been solved using the MATLAB optimisation toolbox routine *lsqnonlin* for minimizing the least-squares objective function further penalised with first-order regularization when noisy data have been inverted. Numerical results have been presented

and discussed, showing that accurate and stable approximate solutions have been obtained. Extension to three-dimensions is, in principle, straightforward.

Chapter 9

Reconstruction of an orthotropic thermal conductivity

9.1 Introduction

The reconstruction of coefficients in the parabolic heat equation, [74], has been the focus of attention in several fields, e.g. finance, groundwater flow, oil recovery, and heat transfer. In particular, the identification of coefficients in two-dimensional heat conduction problems has received significant attention from many researchers [28, 29, 76, 137]. Most of these studies relate to isotropic materials. However, it has been found that factors such as manufacturing and curing processes have impact on the material properties of a structure, often introducing extra variations, including anisotropy, [55], which are difficult to measure directly.

The estimation of thermal properties for multi-dimensional inhomogeneous and anisotropic media is quite limited in the literature, see e.g. [14, 87]. Such a coefficient problem presents several difficulties because it is inverse, nonlinear and ill-posed.

At steady-state, the study on the determination of the diffusivity/conductivity of a layered and orthotropic medium has been addressed in [3, 14]. At the same time, the general case of identification of an anisotropic spacewise dependent conductivity in the elliptic Laplace-Beltrami equation was thoroughly investigated in [132]. However, in the time-dependent case the scenario has received very limited attention from researchers. Here, we only highlight the nonlinear identification of a temperature-dependent orthotropic material, [114], the recovery of the leading coefficients of a heterogeneous orthotropic medium, [63, 64], and the space-dependent anisotropic case addressed in [87].

The organization of the chapter is as follows. The two-dimensional inverse

problem is formulated in Section 9.2. In Section 9.3, the alternating direction explicit (ADE) finite-difference method (FDM) is described. In Section 9.4, the numerical approach based on the minimization of the nonlinear least-squares objective function is introduced. Numerical results are presented and discussed in Section 9.5. Finally, conclusions are presented in Section 9.6.

9.2 Statement of the inverse problem

Consider the inverse problem of finding the orthotropic thermal conductivity component $a(y,t) > 0$ in the two-dimensional parabolic heat equation

$$\frac{\partial u}{\partial t}(x,y,t) = a(y,t)\frac{\partial^2 u}{\partial x^2}(x,y,t) + \frac{\partial^2 u}{\partial y^2}(x,y,t) + f(x,y,t), \quad (x,y,t) \in Q_T, \tag{9.1}$$

where f is given heat source, along with the unknown temperature $u(x,y,t)$ in the domain $Q_T = \{(x,y,t) : 0 < x < h, 0 < y < l, 0 < t < T\}$, subject to the initial condition

$$u(x,y,0) = \varphi(x,y), \quad (x,y) \in [0,h] \times [0,l], \tag{9.2}$$

the Dirichlet boundary conditions

$$u(0,y,t) = \mu_{11}(y,t), \quad u(h,y,t) = \mu_{12}(y,t), \quad (y,t) \in [0,l] \times [0,T], \tag{9.3}$$

$$u(x,0,t) = \mu_{21}(x,t), \quad u(x,l,t) = \mu_{22}(x,t), \quad (x,t) \in [0,h] \times [0,T], \tag{9.4}$$

and the heat flux over-specification

$$a(y,t)\frac{\partial u}{\partial x}(0,y,t) = \kappa(y,t), \quad (y,t) \in [0,l] \times [0,T], \tag{9.5}$$

where φ, μ_{1i}, μ_{2i} for $i = 1,2$ are given functions satisfying compatibility conditions.

The local existence and uniqueness of solution of the inverse problem (9.1)–(9.5) were established in [76] and read as stated in the following two theorems.

Theorem 9.2.1. *Suppose that the following assumptions are satisfied:*

(A1) $\varphi \in C^2(\overline{D})$, *where* $D := \{(x,y) : 0 < x < h, 0 < y < l\}$,
$\mu_{1i} \in C^{2,1}([0,l] \times [0,T])$, $\mu_{2i} \in C^{2,1}([0,h] \times [0,T])$, $i = 1,2$,
$\kappa \in C^{\gamma,0}([0,l] \times [0,T])$, $f \in C^{1+\gamma,\gamma,0}(\overline{Q_T})$ *for some* $\gamma \in (0,1)$;

(A2) $\varphi_x(x,y) > 0,\ (x,y) \in \overline{D},\ \mu_{11_t}(y,t) - \mu_{11_{yy}}(y,t) - f(0,y,t) \le 0,$
$\mu_{12_t}(y,t) - \mu_{12_{yy}}(y,t) - f(h,y,t) \ge 0,\ \kappa(y,t) > 0,\ (y,t) \in [0,l] \times [0,T],$
$\mu_{2i_x}(x,t) > 0,\ i = 1,2,\ (x,t) \in [0,h] \times [0,T],\ f_x(x,y,t) \ge 0,\ (x,y,t) \in \overline{Q_T}$;

(A3) *conditions of compatibility of order zero [90] between the initial condition (9.2) and the Dirichlet boundary conditions (9.3) and (9.4).*

Then, there exists $T_0 \in (0,T]$*, which is determined by the input data, such that the problem (9.1)–(9.5) has a solution* $(a(y,t), u(x,y,t)) \in C^{\gamma,0}([0,l] \times [0,T_0]) \times C^{2,1}(\overline{Q_{T_0}})$*, with* $a(y,t) > 0$ *for* $(y,t) \in [0,l] \times [0,T_0]$.

We remark that a formal elimination of $a(y,t)$ in (9.5) and substitution into (9.1) result in the nonlinear partial differential equation

$$u_t(x,y,t) = \frac{\kappa(y,t)}{u_x(0,y,t)} u_{xx}(x,y,t) + u_{yy}(x,y,t) + f(x,y,t), \quad (x,y,t) \in Q_T \tag{9.6}$$

to be solved for the temperature $u(x,y,t)$ subject to the initial and boundary conditions (9.2)–(9.4). Also, at the initial time $t = 0$ the value of the principal direction component is known and it can easily be obtained form the over-specification condition (9.5) as follows:

$$a(y,0) = \frac{\kappa(y,0)}{\varphi_x(0,y)}, \quad y \in [0,l]. \tag{9.7}$$

Theorem 9.2.2. *Suppose that the condition* $C^{\gamma,0}([0,l] \times [0,T]) \ni \kappa(y,t) \neq 0$*, is satisfied. Then, the inverse problem (9.1)–(9.5) cannot have more than one solution in the class* $(a(y,t), u(x,y,t)) \in C^{\gamma,0}([0,l] \times [0,T]) \times C^{2,1}(\overline{Q_T})$*, with* $a(y,t) > 0$ *for* $(y,t) \in [0,l] \times [0,T]$ *for some* $\gamma \in (0,1)$.

9.3 Numerical solution of the direct problem

In this section, we consider the direct initial boundary value problem (9.1)–(9.5), where $a(y,t)$, $f(x,y,t)$, $\varphi(x,y)$, $\kappa(y,t)$, $\mu_{1i}(y,t)$ and $\mu_{2i}(x,t)$ for $i = 1,2$, are known and the solution $u(x,y,t)$ is to be determined. To achieve this, we use the alternating direction explicit (ADE) finite-difference method (FDM) which is unconditionally stable, as described in the next subsection.

We subdivide the solution domain Q_T into M_1, M_2 and N subintervals of equal step lengths Δx, Δy, and uniform time step Δt, where $\Delta x = h/M_1$, $\Delta y = l/M_2$, and $\Delta t = T/N$, respectively. At the node (i,j,n), we denote $u^n_{i,j} := u(x_i, y_j, t_n)$,

where $x_i = i\Delta x$, $y_j = j\Delta y$, $t_n = n\Delta t$, $a_{j,n} := a(y_j, t_n)$ and $f^n_{i,j} := f(x_i, y_j, t_n)$ for $i = \overline{0, M_1}$, $j = \overline{0, M_2}$, $n = \overline{0, N}$.

9.3.1 Alternating direction explicit finite difference method (ADE-FDM)

As previously described in subsection 8.3.1, the ADE-FDM makes use of two approximations that are implemented for computations proceeding in alternating directions, e.g., from left to right and from right to left, with each approximation being explicit in its respective direction of computation [5, 6, 23]. This numerical scheme possesses the advantage of the implicit methods, i.e., no severe limitation in the size of the time increment. Also, the ADE-FDM has another advantage, namely, that is unconditionally stable. For solving the direct problem (9.1)–(9.4) the ADE-FDM is as follows.

Let $\tilde{u}^n_{i,j}$ and $\tilde{v}^n_{i,j}$ be the solutions of the following equations which are multilevel finite difference discretization of equation (9.1):

$$\frac{\tilde{u}^{n+1}_{i,j} - \tilde{u}^n_{i,j}}{\Delta t} = a_{j,n}\Big(\frac{\tilde{u}^n_{i+1,j} - \tilde{u}^n_{i,j} - \tilde{u}^{n+1}_{i,j} + \tilde{u}^{n+1}_{i-1,j}}{(\Delta x)^2}\Big) + \Big(\frac{\tilde{u}^n_{i,j+1} - \tilde{u}^n_{i,j} - \tilde{u}^{n+1}_{i,j} + \tilde{u}^{n+1}_{i,j-1}}{(\Delta y)^2}\Big) + \frac{1}{2}(f^{n+1}_{i,j} + f^n_{i,j}),$$
$$i = \overline{1, M_1 - 1}, \quad j = \overline{1, M_2 - 1}, \quad n = \overline{0, N - 1}, \tag{9.8}$$

$$\frac{\tilde{v}^{n+1}_{i,j} - \tilde{v}^n_{i,j}}{\Delta t} = a_{j,n}\Big(\frac{\tilde{v}^{n+1}_{i+1,j} - \tilde{v}^{n+1}_{i,j} - \tilde{v}^n_{i,j} + \tilde{v}^n_{i-1,j}}{(\Delta x)^2}\Big) + \Big(\frac{\tilde{v}^{n+1}_{i,j+1} - \tilde{v}^{n+1}_{i,j} - \tilde{v}^n_{i,j} + \tilde{v}^n_{i,j-1}}{(\Delta y)^2}\Big) + \frac{1}{2}(f^{n+1}_{i,j} + f^n_{i,j}),$$
$$i = \overline{M_1 - 1, 1}, \quad j = \overline{M_2 - 1, 1}, \quad n = \overline{0, N - 1}. \tag{9.9}$$

Furthermore, let the $\tilde{u}^n_{i,j}$ and $\tilde{v}^n_{i,j}$ also satisfy the initial and boundary conditions (9.2)–(9.4), namely,

$$\tilde{u}^0_{i,j} = \tilde{v}^0_{i,j} = \varphi(x_i, y_j), \quad i = \overline{0, M_1}, \quad j = \overline{0, M_2}, \tag{9.10}$$

$$\tilde{u}^n_{0,j} = \tilde{v}^n_{0,j} = \mu_{11}(y_j, t_n), \quad \tilde{u}^n_{M_1,j} = \tilde{v}^n_{M_1,j} = \mu_{12}(y_j, t_n), \quad j = \overline{0, M_2}, \quad n = \overline{1, N}, \tag{9.11}$$

$$\tilde{u}^n_{i,0} = \tilde{v}^n_{i,0} = \mu_{21}(x_i, t_n), \quad \tilde{u}^n_{i,M_2} = \tilde{v}^n_{i,M_2} = \mu_{22}(x_i, t_n), \quad i = \overline{0, M_1}, \\ n = \overline{1, N}. \tag{9.12}$$

Rearranging the terms in (9.8) and (9.9), we obtain the explicit calculations of $\tilde{u}^{n+1}_{i,j}$ and $\tilde{v}^{n+1}_{i,j}$ as follows:

$$\tilde{u}^{n+1}_{i,j} = A_{j,n}\tilde{u}^n_{i,j} + B_{j,n}(\tilde{u}^n_{i+1,j} + \tilde{u}^{n+1}_{i-1,j}) + C_{j,n}(\tilde{u}^n_{i,j+1} + \tilde{u}^{n+1}_{i,j-1}) + D^*_{i,j}, \\ i = \overline{1, M_1 - 1}, \quad j = \overline{1, M_2 - 1}, \quad n = \overline{0, N - 1}, \tag{9.13}$$

$$\tilde{v}^{n+1}_{i,j} = A_{j,n}\tilde{v}^n_{i,j} + B_{j,n}(\tilde{v}^{n+1}_{i+1,j} + \tilde{v}^n_{i-1,j}) + C_{j,n}(\tilde{v}^{n+1}_{i,j+1} + \tilde{v}^n_{i,j-1}) + D^*_{i,j}, \\ i = \overline{M_1 - 1, 1}, \quad j = \overline{M_2 - 1, 1}, \quad n = \overline{0, N - 1}, \tag{9.14}$$

where

$$A_{j,n} = \frac{1 - \lambda_{j,n}}{1 + \lambda_{j,n}}, \quad B_{j,n} = \frac{(\Delta t)a_{j,n}}{(\Delta x)^2(1 + \lambda_{j,n})}, \quad C_{j,n} = \frac{(\Delta t)}{(\Delta y)^2(1 + \lambda_{j,n})}, \\ D^*_{i,j} = \frac{\Delta t}{2(1 + \lambda_{j,n})}\left(f^{n+1}_{i,j} + f^n_{i,j}\right), \quad \lambda_{j,n} = \frac{(\Delta t)a_{j,n}}{(\Delta x)^2} + \frac{\Delta t}{(\Delta y)^2}. \tag{9.15}$$

From (9.13) and (9.10)–(9.12) for $\tilde{u}$, $\tilde{u}^{n+1}_{i,j}$ can be computed explicitly. In this case, calculations proceed from the grid point close to the boundaries $x = 0$ and $y = 0$, as i, j are increasing. The needed values such as $\tilde{u}^{n+1}_{i-1,j}$, $\tilde{u}^n_{i,j}$ and $\tilde{u}^n_{i+1,j}$ will be known from initial and boundary conditions (9.10)–(9.12). Similarly, $\tilde{v}^{n+1}_{i,j}$ can be calculated explicitly from (9.14) and (9.10)–(9.12) for $\tilde{v}$, beginning at the boundaries $x = 1$ and $y = 1$ and marching in a sequence of decreasing i and j, i.e. $i = M_1 - 1, M_1 - 2, ..., 1$, $j = M_2 - 1, M_2 - 2, ..., 1$. These values are then substituted into the simple arithmetic mean approximation

$$u^{n+1}_{i,j} = \frac{\tilde{u}^{n+1}_{i,j} + \tilde{v}^{n+1}_{i,j}}{2}. \tag{9.16}$$

to obtain the solution $u^{n+1}_{i,j}$. This procedure is unconditionally stable, as both equations (9.13) and (9.14) are unconditionally stable. The heat flux (9.5) can be calculated using the FDM approximation

$$\kappa(y_j, t_n) = a_{j,n}\left(\frac{4u(1, y_j, t_n) - u(2, y_j, t_n) - 3\mu_{11}(y_j, t_n)}{2\Delta x}\right), \\ j = \overline{1, M_2 - 1}, \quad n = \overline{1, N}. \tag{9.17}$$

9.4 Numerical solution of the inverse problem

In this section, our aim is to obtain a stable reconstruction of the orthotropic thermal conductivity component $a(y,t) > 0$ together with the temperature $u(x,y,t)$, satisfing equations (9.1)–(9.5). The inverse problem can be formulated as a nonlinear least-squares minimization of the least-squares objective function given by

$$F(a) = \Big\| a(y,t)u_x(0,y,t) - \kappa(y,t) \Big\|^2, \tag{9.18}$$

or, in discretised form

$$F(\mathbf{a}) = \sum_{n=1}^{N} \sum_{j=0}^{M_2} \Big[a_{j,n} u_x(0,y_j,t_n) - \kappa(y_j,t_n) \Big]^2, \tag{9.19}$$

where $u(x,y,t)$ solves (9.1)–(9.4) for given $\mathbf{a}$. The minimization of the objective function (9.19) is performed using the MATLAB toolbox routine *lsqnonlin*. Since the MATLAB routine *lsqnonlin* accepts only a vector of unknowns we make the matrice a be a long vector by renumbering its components.

In the numerical computation, we take the parameters of the routine, as follows.

- Maximum number of iterations, (MaxIter) = 400.
- Maximum number of objective function evaluations, (MaxFunEvals) = 10^5.
- Termination tolerance on the function value, (TolFun) = 10^{-20}.
- Solution tolerance value, (xTol) = 10^{-20}.

The inverse problem given by (9.1)–(9.5) is solved subject to both exact and noisy heat flux data (9.5). The noisy data are numerically simulated, as follows:

$$\kappa^{\epsilon}(y_j,t_n) = \kappa(y_j,t_n) + \epsilon_{j,n}, \quad j = \overline{0,M_2}, \quad n = \overline{1,N}, \tag{9.20}$$

where $\epsilon_{j,n}$ are random variables generated from a Gaussian normal distribution with mean zero and standard deviation σ

$$\sigma = p \times \max_{(y,t)\in[0,h]\times[0,T]} |\kappa(y,t)|, \tag{9.21}$$

where p represents the percentage of noise. We use the MATLAB function *normrnd* to generate the random variables $\underline{\boldsymbol{\epsilon}} = (\epsilon_{j,n})_{j=\overline{0,M_2},n=\overline{1,N}}$, as follows:

$$\underline{\boldsymbol{\epsilon}} = normrnd(0,\sigma,M_2+1,N). \tag{9.22}$$

In the case of noisy data (9.20), we replace $\kappa(y_j, t_n)$ by $\kappa^\epsilon(y_j, t_n)$ in (9.19).

9.5 Numerical results and discussion

In this section, we present numerical results for the recovery of the orthotropic thermal conductivity $a(y,t)$ together with the temperature $u(x,y,t)$, in order to illustrate the accuracy and stability of the numerical methods based on the ADE-FDM, as described in Section 9.3, combined with the minimization of the objective function (9.19), as described in Section 9.4. Furthermore, we add noise to the input measurement data (9.5) to simulate the real situation of measurement noisy data, by using equations (9.20)–(9.22). We employ the root mean square errors ($rmse$), in order to quantify the accuracy of the approximate solutions, defined by

$$rmse(a) = \left[\frac{1}{N(M_2+1)}\sum_{n=1}^{N}\sum_{j=0}^{M_2}\left(a^{Numerical}(y_j,t_n) - a^{Exact}(y_j,t_n)\right)^2\right]^{1/2}. \quad (9.23)$$

For simplicity, we take $h = l = T = 1$. We take the lower and upper simple bounds for $a(y,t)$ to be 10^{-4} and 10^2, respectively. These bounds allow a wide search range for the unknown positive orthotropic thermal conductivity component $a(y,t)$.

Consider the inverse problem (9.1)–(9.5) with unknown orthotropic thermal conductivity $a(y,t)$ and solve this inverse problem with the input data φ, μ_{1i} and μ_{1i}, $i = 1, 2$, given by

$$\begin{aligned} \varphi(y,x) = u(x,y,0) = x - y, \quad f(x,y,t) &= \frac{1}{5}e^{t/5}(x-y), \\ \mu_{11}(y,t) = u(0,y,t) = -e^{t/5}y, \quad \mu_{12}(y,t) &= u(1,y,t) = e^{t/5}(1-y), \\ \mu_{21}(x,t) = u(x,0,t) = e^{t/5}x, \quad \mu_{22}(x,t) &= u(x,1,t) = e^{t/5}(x-1), \end{aligned} \quad (9.24)$$

$$\kappa(y,t) = a(y,t)u_x(0,y,t) = \frac{1}{100}e^{t/5}(1+t+y). \quad (9.25)$$

Remark that the conditions of Theorems 9.2.1 and 9.2.2 are satisfied and therefore, the local solvability of the solution is guaranteed. In fact, it can easily be checked by direct substitution that the analytical solutions $u(x,y,t)$ and $a(y,t)$ are given by

$$u(x,y,t) = e^{t/5}(x-y), \quad (x,y,t) \in \overline{Q_T}, \quad (9.26)$$

$$a(y,t) = \frac{y+t+1}{100}, \quad (y,t) \in [0,1] \times [0,1]. \tag{9.27}$$

We assess the accuracy of the direct problem given by equations (9.1)–(9.4) with the input data (9.24) when $a(y,t)$ is known and given by (9.27). Figures 9.1 and 9.2 shows the absolute error between the exact solutions (9.26) and (9.25) and the numerical solutions for the temperature $u(x,y,t)$ and the heat flux quantity of interest $\kappa(y,x)$. From these figures, it can be seen that the accuracy of the numerical solution for the temperature $u(x,y,t)$ and heat flux $\kappa(y,x)$ are improving, as the time steps $\Delta t = T/N$ decreases. The root mean square error $rmse(\kappa)$ defined by

$$rmse(\kappa) = \left[\frac{1}{N(M_2+1)} \sum_{n=1}^{N} \sum_{j=0}^{M_2} \left(\kappa^{Numerical}(y_j,t_n) - \kappa^{Exact}(y_j,t_n) \right)^2 \right]^{1/2}, \tag{9.28}$$

indicated in Table 9.1, shows more clearly the convergence of the numerical ADE-FDM solution to the exact heat flux (9.25).

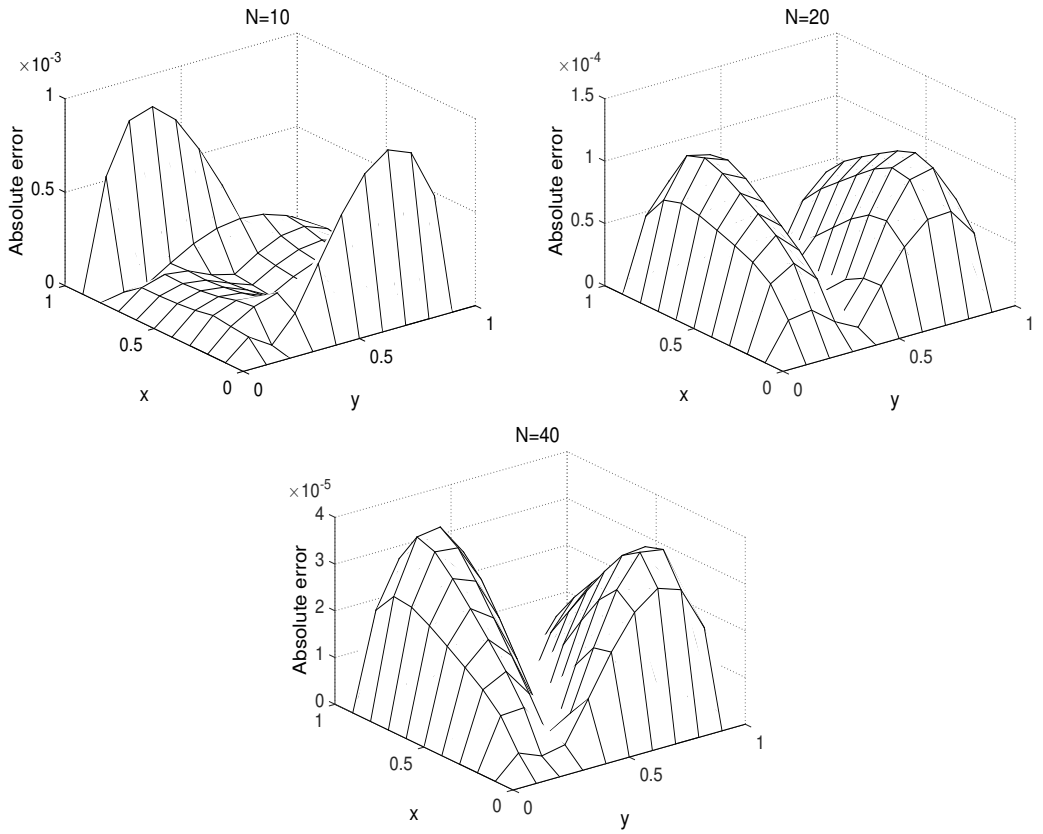

Figure 9.1: The absolute errors between the exact (9.26) and numerical solutions for the temperature $u(x,y,1)$, with $M_1 = M_2 = 10$ and various $N \in \{10, 20, 40\}$, for the direct problem.

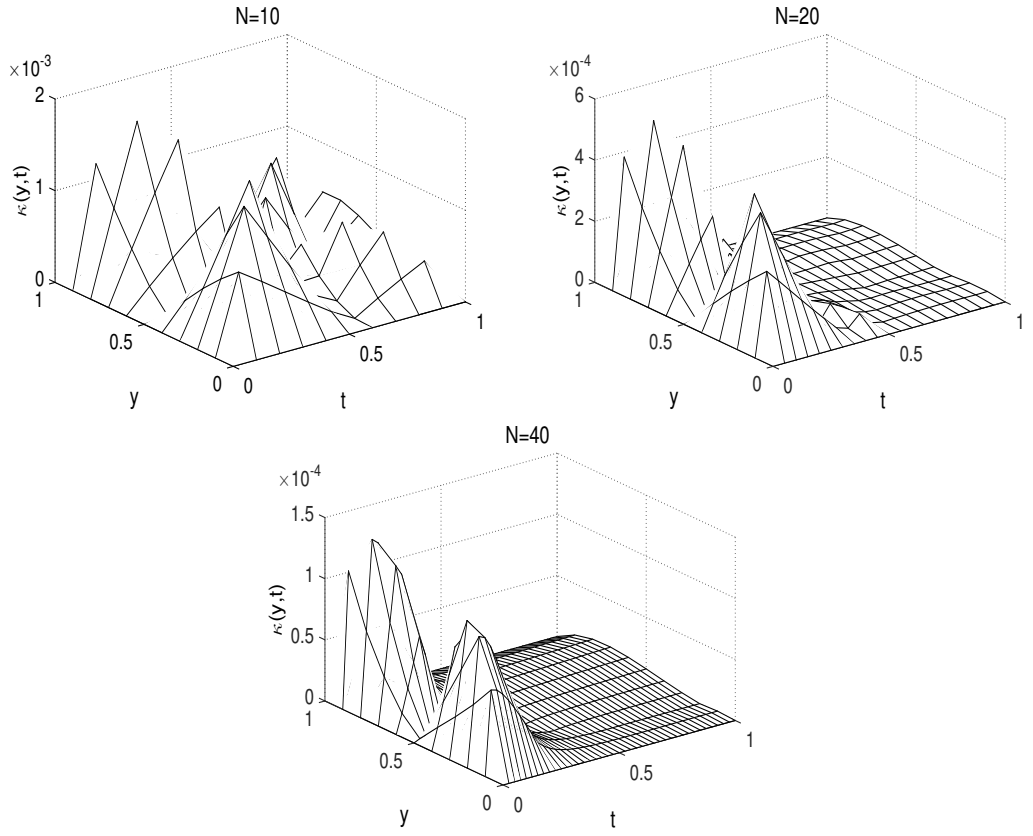

Figure 9.2: The absolute errors between the exact (9.25) and numerical solutions for the heat flux $\kappa(y,t)$, with $M_1 = M_2 = 10$ and various $N \in \{10, 20, 40\}$, for the direct problem.

Table 9.1: The exact (9.25) and numerical solutions for $\kappa(y,t)$, with $M_1 = M_2 = 10$ and various $N \in \{10, 20, 40\}$, for the direct problem. The $rmse(\kappa)$ values (9.28) are also included.

		$N = 10$	$N = 20$	$N = 40$	
y	t	$\kappa(y,t)$	$\kappa(y,t)$	$\kappa(y,t)$	Exact
0.1	0.1	0.0128	0.0120	0.0122	0.0122
0.2	0.2	0.0131	0.0143	0.0145	0.0145
0.3	0.3	0.0154	0.0169	0.0169	0.0169
0.4	0.4	0.0183	0.0195	0.0195	0.0194
0.5	0.5	0.0218	0.0221	0.0221	0.0221
0.6	0.6	0.0239	0.0248	0.0248	0.0248
0.7	0.7	0.0265	0.0276	0.0276	0.0276
0.8	0.8	0.0295	0.0305	0.0305	0.0305
0.9	0.9	0.0329	0.0335	0.0335	0.0335
$rmse(\kappa)$		5.8E-4	1.2E-4	2.9E-5	0

Now, we investigate the inverse problem. We take $M_1 = M_2 = 10$ and $N = 20$ and we start our investigation for reconstructing the unknown orthotropic thermal conductivity $a(y,t)$ and the temperature $u(x,y,t)$ for exact and noisy measured

input data (9.20), i.e., for the cases $p \in \{0, 1, 3, 5\}\%$ of noise. The initial guess for $a(y, t)$ has been taken as

$$a^0(y, t) = a(y, 0) = \frac{y + 1}{100}, \quad y \in [0, 1]. \tag{9.29}$$

Note that the value of $a(y, 0)$ is available from (9.7). The objective function (9.19), as a function of the number of iterations, is plotted in Figure 9.3. From this figure, it can be seen that a monotonic decreasing convergence is achieved in about 7 to 8 iterations to reach a very low prescribed tolerance of $O(10^{-28})$. The numerically obtained results for $a(y, t)$ are illustrated in Figure 9.4 and summarised in Table 9.2. From this figure and table, it can be seen that as the percentage of noise p decreases from 5% to 3% to 1% and then to zero the numerically obtained results becomes more stable and accurate.

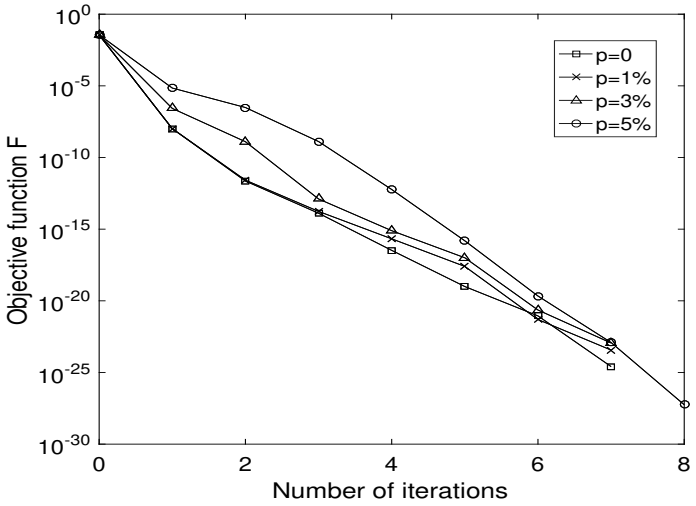

Figure 9.3: The objective function (9.19), as a function of the number of iterations, for various noise levels $p \in \{0, 1, 3, 5\}\%$.

Table 9.2: The number of iterations, the value of the objective function (9.19) at final iteration, the $rmse(a)$ values (9.23) and the computational time, for various noise levels $p \in \{0, 1, 3, 5\}\%$.

Numerical outputs	$p = 0$	$p = 1\%$	$p = 3\%$	$p = 5\%$
Number of iterations	7	7	7	8
Minimum value of (9.19)	2.5E-25	3.6E-24	1.1E-23	5.6E-28
$rmse(a)$	1.2E-4	3.6E-4	1.0E-3	1.7E-3
Computational time	19 mins	19 mins	19 mins	22 mins

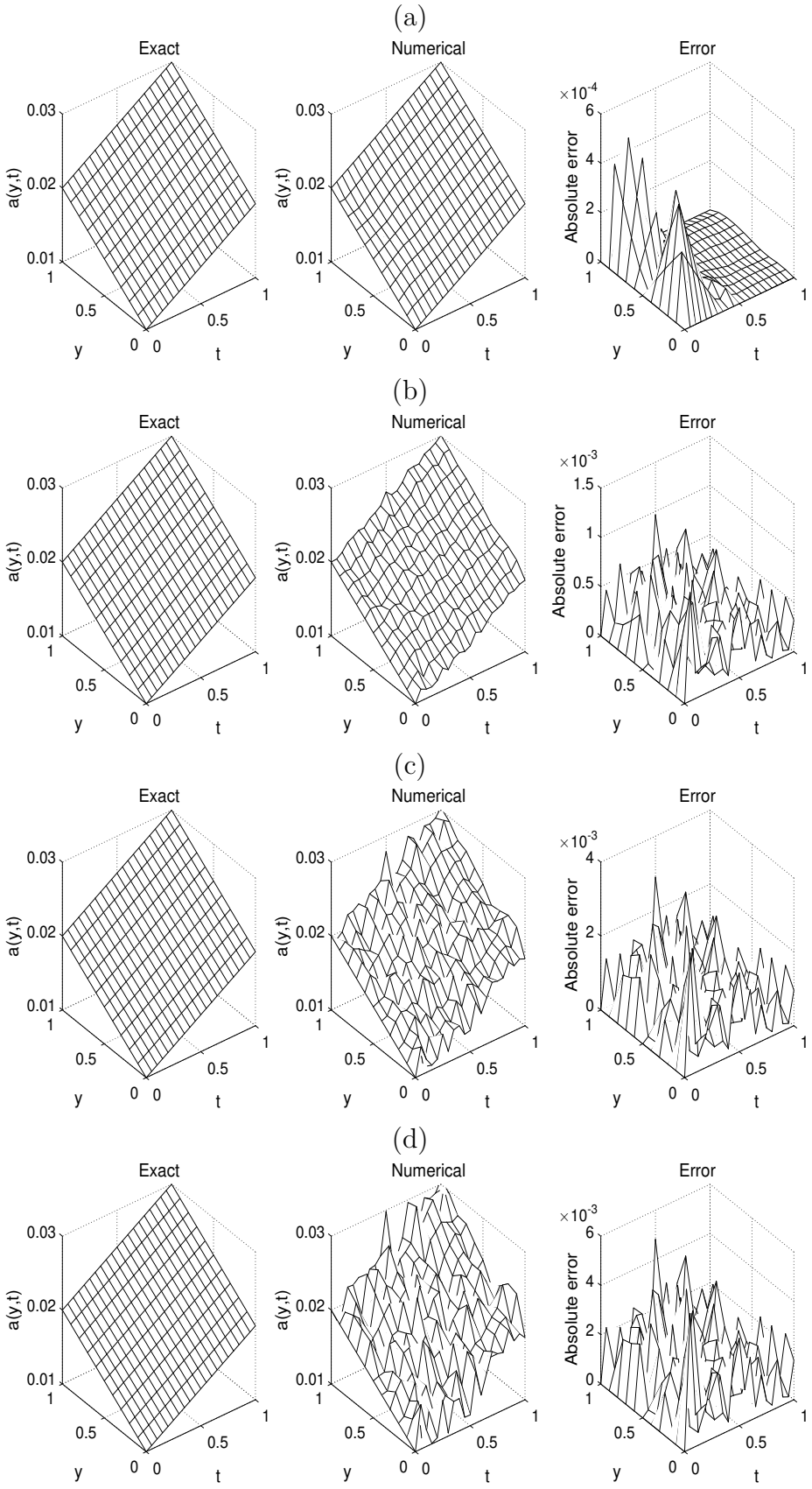

Figure 9.4: The exact (9.27) and numerical solutions for the orthotropic thermal conductivity component $a(y,t)$, for various noise levels: (a) $p = 0$, (b) $p = 1\%$, (c) $p = 3\%$ and (d) $p = 5\%$ noise. The absolute error between them is also included.

9.6 Conclusions

In this chapter, the inverse problem involving the reconstruction of an orthotropic thermal conductivity component $a(y,t)$ and the temperature $u(x,y,t)$ in the two-dimensional parabolic heat equation (9.1) from the heat flux over-specification (9.5) has been investigated. Sufficient conditions which ensure a unique solvability of solution are provided [76]. The direct solver based on the ADE-FDM has been employed. The inverse problem solution based on a nonlinear least-squares minimization problem using the MATLAB optimisation toolbox routine *lsqnonlin* has been developed. Numerical results presented and discussed for both exact and noisy data show that accurate and stable solutions have been obtained. The reconstruction of both components of the orthotropic thermal conductivity in the two-dimensional parabolic heat equation from nonlocal over-determination heat flux specifications is currently ongoing research.

Chapter 10

General conclusions and future work

10.1 Conclusions

The aim of this thesis was to solve several types of inverse coefficient identification problems in the parabolic heat equation. Specifically, the problems of coefficient identification in fixed or moving domains for a single as well as multiple unknowns have been investigated. Every inverse problem has practical physical applications in a real-life scenario. Examples of such scenarios include determination of an unknown free boundary of melting-freezing processes and identification of thermal properties of a given material.

Many physical contexts can be modeled by partial differential equations. If every required input data is known, then, in general, the solution can be uniquely obtained and used in the prediction of the system's output behaviour under various conditions. However, if part of the required data is not available, then it is impossible to apply such a model in these physical contexts. Such a situation is what is referred to as an inverse problem. The application of inverse problems is of utmost importance in instances where the immediate measurement of appropriate parameters is not possible, such as when the rapidity of the process as well as the unknown material or hostile environment are not accessible.

Inverse coefficient identification problems consist of one or more coefficients which are unknown along with the primary dependent variable. Thus, one needs more information to get the unspecified coefficients. The additional information is normally given as measured over-specified data containing random noise. These inverse problems are solved based on several types of over-determination conditions, including heat momentum of the first, second and third order, Stefan condition, the heat flux, nonlocal observation, general integral type over-

determination, mass/energy specification, additional temperature measurement, and Cauchy data. In a case where the underlying problem is ill-posed, the random noise in these measurements brings about considerable oscillations and uncontrolled behavior in the output solution, which makes the inverse problem difficult to solve using traditional numerical approaches.

In this thesis, the inverse problems are reduced to nonlinear constrained minimization problems by incorporating penalty terms to stabilize the solution. Several approaches are used to select the regulation parameter, e.g. the L-curve method, [48]. This method is actually a plot for many positive regularization parameters of the norm of the regularised solution versus the corresponding residual norm. If such a curve has an L-shape then one can choose the regularization parameter at the 'corner' of it. Simple trial and error can also be used according to experience by first selecting a small value and consistently raising it till all the numerical oscillations in the unknown coefficients are eliminated. More rigorously, the regularization parameter is selected by the discrepancy principle technique which has been adopted in Section 1.6.3.

For every inverse problem considered in the thesis, the stability and accuracy of the numerical results were carefully tested for several mesh sizes and noise levels incorporated into the input data to simulate the case of real measured data. Additionally, for every problem, the FDM direct solver has been used in the process of minimizing the least-squares functional linked with the gap between the measured and the computed data. Moreover, an alternating direction explicit scheme has been used in two-dimensions. The entire iterative process of minimization has been carried out using the *lsqnonlin* routine from the MATLAB optimization toolbox, which enables one to impose simple constraints on every unknown coefficient. Also, the user does not need to supply the gradient of the minimizing functional.

The Tikhonov regularization approach is only applied where necessary. This method modifies the residual functional by adding a penalty condition to make the solution stable. Whenever the Tikhonov regularization approach is applied, each nonlinear inverse problem has been recast into a nonlinear constrained minimization problem subject to bounds on the variables. The choice of the regularization parameters has been clearly explained throughout the thesis. The stability of the numerical solutions has been evaluated by including random noise in the input data. Every numerical solution has been compared with its known analytical solution where available. Otherwise, the numerical solution is compared with the matching direct problem numerical solution.

Overall, the numerical results obtained by using the methods established in

this thesis, i.e. the FDM with a Crank-Nicolson or ADE or FTCS combined with the minimization of the nonlinear Tikhonov regularization functional using the MATLAB optimization toolbox routine *lsqnonlin* and the L-curve, the discrepancy principle, or trial and error technique for choosing the regularization parameter, illustrate that accurate and stable solutions can be obtained for reconstructing one or more unknown, mainly, time-dependent coefficients in parabolic PDEs. Moreover, in all the inverse and ill-posed problems considered in this thesis, the numerical results were thoroughly investigated with various mesh sizes and up to 5% noise added to the input data, which is a realistic amount of noise in practical measurement. We have also perturbed the input data with larger amounts of noise than 5%, but the results obtained were less accurate and therefore they were not presented. For more details about other types of regularization, see Section 10.2. In summary, all numerical results with/without noise contamination have been found to be accurate and stable.

In addition, since the FDM with a Crank-Nicolson or ADE or FTCS is applied to solve the PDEs, which may limit the applications of the nonlinear least-squares optimization solver proposed in this thesis, the FEM or FVM could be a good method to solve the PDEs in irregular domains. Also, since we have depended on the initial guess, only local solutions may be obtained. For a global minimizer to nonlinear optimization problems as described in Section 1.8, whose convergence to a better approximation of the true solution is independent of the initial guess is deferred to a future work.

In the remainder of this section we summarize in more detail the conclusions that we have drawn from the inverse problems analysed in each chapter.

In Chapter 1, a general introduction to direct and inverse problems has been presented. General description for the inverse Stefan problem has been given in Section 1.5 followed by the stability analysis for the inverse problems under investigation based on Tikhonov's regularization method with appropriate choice of regularization parameters, e.g. the L-curve method, the discrepancy principle criterion and trial and error technique in order to achieve a stable and accurate solution. A quick overview of numerical methods for discretising and solving PDE's has been provided. Moreover, a brief description of MATLAB optimization toolbox routine has been explained along with some commands followed by a description of the TRR algorithm. Finally, the purpose and outline of the thesis was highlighted in Section 1.9.

In Chapter 2, an inverse problem which requires determining the time-dependent thermal conductivity and the transient temperature satisfying the one-dimensional parabolic heat equation with initial data, Dirichlet boundary conditions, and the

heat flux as an overdetermination condition has been investigated. The inverse problem is recast as a nonlinear least-squares minimization subject to a physical positivity bound on the unknown thermal conductivity. Numerically, this is effectively solved using the *lsqnonlin* routine from the MATLAB toolbox. Numerical results indicate that accurate and reasonably stable solutions have been obtained. This problem seems rather stable and hence, in general, no regularization was found necessary to be employed. An extension to a two-dimensional coefficient identification problem, which is a variant of the one-dimensional problem, has been discussed in Section 2.6. For this newly formulated problem the use of regularization is necessary in order to ensure that a numerically stable solution is obtained.

In Chapter 3, a couple of inverse problems which require the simultaneous reconstruction of time-dependent thermal conductivity, convection or absorption coefficients from the measurements of the heat moments in the one-dimensional parabolic heat equation governing transient heat and bio-heat thermal processes have been investigated. The measurement of the heat moments formulates a less stable inverse problem than the measurement of the heat fluxes. The IP2 seems more ill-posed that the IP1 and regularization was needed in order to obtain a stable solution. The choice of the regularization parameter was discussed based on the L-curve method, the discrepancy principle and a trial and error technique. Numerical results illustrated for several benchmarks test examples show that an accurate and stable solution has been obtained.

Chapter 4 focused on the simultaneous identification of time-dependent reaction coefficients along with the temperature and a free boundary, whilst Chapter 5 was concerned with two-phase inverse Stefan coefficient identification problems with multiple free boundaries. In these chapters, numerical investigations for the recovery of multiple time-dependent coefficients entering the parabolic heat equation with a free boundary subject to a heat flux, specification of the energy, a Stefan condition, and several-orders heat moment measurements have been considered. The moving boundary(ies) value problem(s) was/were first transformed, by a simple change of variables, to a problem formulated in a fixed domain. In Chapter 4, the Stefan condition was replaced by a second-order heat moment specification, whilst in Chapter 5 the Stefan conditions were replaced by the second and third-order heat moment measurement. Therefore, the second inverse problem is more ill-posed than the first one. These inverse problems have been solved using the MATLAB optimisation toolbox routine *lsqnonlin* for minimizing the objective function. It is interesting to remark that, based on the comparison between Examples 1 and 2, the Stefan condition contains more information

than the second or third-order heat moment. Notably, Tikhonov's regularization method, apart from restoring the stability of the numerical solution, also reduces the computational time. The regularization parameter has been chosen based on the L-curve criterion for both inverse problems. Numerical results presented and discussed for several test examples show that accurate and stable numerical solutions have been achieved.

In Chapter 6, three novel inverse problems of determining the time-dependent thermal diffusivity coefficient for degenerate parabolic PDEs, which vanishes at the initial time, the convection coefficient and the temperature for a one-dimensional parabolic equation, from some additional information about the process (the so-called overdetermination conditions) have, for the first time, been investigated. The IP1 was found to be well-posed, whilst the IP2 and IP3 were found to be ill-posed and sensitive to noise. The resulting inverse problems have been reformulated as constrained regularized minimization problems which were solved using the MATLAB optimization toolbox routine *lsqnonlin*. Nonlinear Tikhonov regularization has been employed in order to obtain stable and accurate results. The numerical results illustrated for three test examples showed that an accurate and stable solution has been obtained.

In Chapter 7, the inverse problem concerning the determination of an additive time and space-dependent heat source coefficient from additional temperature measurements in the one-dimensional parabolic heat equation has been considered. The uniqueness of solution of the inverse coefficient problem is briefly discussed in a particular case. However, the problem is still ill-posed since small errors in the input data cause large errors in the output solution. The resulting inverse problem has been reformulated as a constrained regularized minimization problem which was solved using the MATLAB optimization toolbox routine *lsqnonlin*. Numerical results presented for three examples show the efficiency of the computational method and the accuracy and stability of the numerical solution even in the presence of noise in the input data.

In Chapter 8, an inverse problem concerning the determination of the time-dependent intensity of a free boundary and the temperature in a two-dimensional parabolic problem in a rectangular domain has been, for the first time, numerically investigated. The measurement which is sufficient to provide a unique solution was given by energy/mass of the heat conducting system. A stability theorem was stated. The free boundary problem has been transformed to a fixed domain. The ADE-FDM has been employed as a direct solver, whilst the inverse solver based on a nonlinear least-squares minimization has been efficiently implemented using the MATLAB optimization toolbox routine *lsqnonlin* further

penalised with the first-order regularization when noisy data have been inverted. Numerical results presented and discussed showed that accurate and stable numerical solutions have been obtained.

Finally, in Chapter 9, the inverse problem concerning the reconstruction of an orthotropic thermal conductivity and the temperature in the two-dimensional parabolic heat equation in a rectangular domain from the heat flux overspecification has been investigated. The overdetermination condition which ensures a unique solvability of the solution is given by the specification of the heat flux. The same numerical method as in Chapter 8 has produced accurate and stable numerical reconstruction of the orthotropic conductivity component.

10.2 Future work

The numerical results presented in this thesis confirm the fact that efficient approaches can be developed for solving more complicated coefficient identification problems, inverse initial value problems or inverse geometric problems. As far as these features are concerned, one can point out the following possible future work:

(i) Extend and develop the numerical FDM implementation to three-dimensional problems;

(ii) Extend the analysis to determine coefficients that depend both on space and time;

(iii) Chapter 6 details the numerical results concerning the identification of the time-dependent thermal diffusivity for degenerate parabolic PDEs in one-dimensions. It would be interesting to study the degenerate inverse problem in two-dimensions, see [133]. Also, it is possible to extend this study to strong degenerate parabolic PDEs in the case where $\alpha \geq 1$;

(iv) It is also proposed in Chapter 6 to extend the determination of time-dependent thermal diffusivity and convection coefficients for degenerate PDEs with free boundary, [75];

(v) Use the FEM or FVM combined with nonlinear least-squares minimization to reconstruct unknown coefficients in nonlinear inverse problems for irregular solution domains;

(vi) Develop a global convergent method, [112], independent of the initial guess;

(vii) Apply the models in this thesis to real world problems concerned with material characterisation and thermal property identification. It would be interesting to apply our methods to data from:

(a) Computer simulations that had more of the physics and used a different numerical technique, e.g. finite elements;

(b) Experimental data obtained from sensor measurements.

(viii) For problems with larger noise, e.g. $p > 5\%$ to look at global optimization schemes, e.g. Monte Carlo Multi Chain methods, to see if one can get better results. Also, try other types of regularization, e.g. total variation penalty term or the Landweber method.

Bibliography

[1] Akhundov, A.Ya. (1983) An inverse problem for linear parabolic equations, *Doklady Akademii Nauk AzSSR*, 39(5):3-6.

[2] Barans'ka, I.E. (2007) Inverse problem in a domain with free boundary for the two-dimensional parabolic equation, *Mat. Met. Fiz.-Mekh. Polya*, **50**, No. 2, 17–28.

[3] Barans'ka, I.E. (2008) The inverse problem in a domain with free bound for an anisotropic equation of parabolic type, *Naykovy Visnyk Chernivetskogo Universytetu Matematyka*, **374**, 13-28.

[4] Barans'ka, I.E. and Ivanchov, M.I. (2007) Inverse problem for a two-dimensional heat-conduction equation in a domain with free boundary, *Ukr. Mat. Visn.*, **4**, 457–484.

[5] Barakat, H.Z. and Clark, A.J. (1966) On the solution of the diffusion equations by numerical methods, *Journal of Heat Transfer*, **88**, 421–427.

[6] Barakat, Z., Ehrhardt, M. and Gunther, M. (2015) Alternating direction explicit methods for convection diffusion equations, *Acta Mathematica Universitatis Comenianae*, **84**, 309–325.

[7] Belge, M., Kilmer, M. and Miller, E. (2002) Efficient determination of multiple regularization parameters in a generalized L-curve framework, *Inverse Problems*, **18**, 1161–1183.

[8] Branch, M.A., Coleman, T.F. and Li, Y. (1999) A subspace, interior, and conjugate gradient method for large-scale bound-constrained minimization problems, *SIAM Journal on Scientific Computing*, **21**, 1-23.

[9] Broadbridge, P., Tritscher, P. and Avagliano, A. (1993) Free boundary problems with nonlinear diffusion, *Mathematical and Computer Modelling*, **18**, 15–34.

[10] Brown, R.F. (1993) *A Topological Introduction to Nonlinear Analysis*, Basel, Switzerland: Birkhäuser, Kassel.

[11] Borukhov, V.T. and Kostyukova, O.I. (2013) Identification of time-dependent coefficients of heat transfer by the methods of suboptimal stage-by-stage optimation, *International Journal of Heat and Mass Transfer*, **59**, 286–294.

[12] Cannon, J.R. (1963) Determination of an unknown coefficient in a parabolic differential equation, *Duke Mathematical Journal,* **30**, 313–323.

[13] Cannon, J.R. (1984) *The One-dimensional Heat Equation*, Addison-Wesley, Menlo Park, California.

[14] Cannon, J.R. and Jones Jr., B. F. (1963) Determination of the diffusivity of an anisotropic medium, *International Journal of Engineering Science*, **1**, 457-460.

[15] Cannon, J.R. and Rundell, W. (1991) Recovering a time dependent coefficient in a parabolic differential equation, *Journal of Mathematical Analysis and Applications*, 160(2):572-582.

[16] Cannon, J.R., Lin, Y. and Wang, S. (1991) Determination of a control parameter in a parabolic partial differential equation, *Journal of the Australian Mathematical Society, Series B,* **33**, 149–163.

[17] Cannon, J.R. and DuChateau, P. (1973) Determination of unknown physical properties in heat conduction problems, *International Journal of Engineering Science*, 11(7):783-794.

[18] Cannon, J.R. and DuChateau, P. (1973) Determining unknown coefficients in a nonlinear heat conduction problem, *SIAM Journal on Applied Mathematics*, 24(3):298-314.

[19] Cannon, J.R. and Primicerio, M. (1971) A two phase Stefan problem: regularity of the free boundary, *Annali di Matematica Pura ed Applicata*, **88**, 217-228.

[20] Cannon, J.R. and Primicerio, M. (1971) A two phase Stefan problem with flux boundary conditions, *Annali di Matematica Pura ed Applicata*, **88**, 193–205.

[21] Cannon, J.R. and van der Hoek, J. (1982) The one phase Stefan problem subject to the specification of energy, *Journal of Mathematical Analysis and Applications*, **86**, 281–291.

[22] Cannon, J.R. and van der Hoek, J. (1986) Diffusion subject to the specification of mass, *Journal of Mathematical Analysis and Applications*, **115**, 517–529.

[23] Campbell, L.J. and Yin, B. (2007) On the stability of alternating-direction explicit methods for advection-diffusion equations, *Numerical Methods Partial Differential Equations*, **23**, 1429–1444.

[24] Carrillo, J.A. and Vázquez, J.L. (2015) Some free boundary problems involving nonlocal diffusion and aggregation, *Philosophical Transactions of the Royal Society A*, **373**, 26261360.

[25] Caplan, M.E., Giri, A. and Hopkins, P.E. (2014) Analytical model for the effects of wetting on thermal boundary conductance across solid/classical liquid interfaces, *The Journal of Chemical Physics*, **140**, 154701.

[26] Chen, G.Q. and Feldman, M. (2015) Free boundary problems in shock reflection/diffraction and related transonic flow problems, *Philosophical Transactions of the Royal Society A*, **373**, 20140276.

[27] Crank, J. (1984) *Free and Moving Boundary Problems*, Clarendon Press, Oxford.

[28] Coles, C. and Murio, D.A. (2000) Identification of parameters in the 2-D IHCP, *Computers and Mathematics with Applications*, **40**, 939-956.

[29] Coles, C. and Murio, D.A. (2001) Simultaneous space diffusivity and source term reconstruction in 2D IHCP, *Computers and Mathematics with Applications*, **42**, 1549-1564.

[30] Coleman, T.F. and Li, Y. (1994) On the convergence of interior-reflective newton methods for nonlinear minimization subject to bounds, *Mathematical Programming*, 67(1–3):189-224.

[31] Coleman, T.F. and Li, Y. (1996) An interior trust region approach for nonlinear minimization subject to bounds, *SIAM Journal on Optimization*, **6**, 418–445.

[32] Coleman, T.F. and Verma, A. (2001) A preconditioned conjugate gradient approach to linear equality constrained minimization, *Computational Optimization and Applications*, **20**, 61–72.

[33] Conti, R. and Ruberti, A. (1973) *5th Conference on Optimization Techniques, Part I,* (Series: I.F.I.P. TC7 Optimization Conference), 565 pages, Berlin: Springer.

[34] Dehghan, M. (2001) Determination of a control parameter in the two-dimensional diffusion equation, *Applied Numerical Mathematics*, **37**, 489-502.

[35] Dennis, B.H., Dulikravich, G.S. and Yoshimura, S. (2004) A finite element formulation for the determination of unknown boundary conditions for three-dimensional steady thermoelastic problems, *Journal of Heat Transfer*, 126(1), 110–118.

[36] Deng, Z.C., Yang, L., Yu, J.N. and Luo, G.W. (2010) Identifying the radiative coefficient of an evolutional type heat conduction equation by optimization method, *Journal of Mathematical Analysis and Applications,* **362**, 210–223.

[37] Deng, Z.C., Yu, J.N. and Yang, L. (2008) Optimization method for an evolutional type inverse heat conduction problem, *Journal of Physics A: Mathematical and Theoretical,* **41**, 035201, (20 pp).

[38] DuChateau, P. and Zachmann, D. (1989) *Applied Partial Differential Equations*, Harper & Row, New York.

[39] Engl, H.W. and Kugler, P. (2005) Nonlinear inverse problems: theoretical aspects and some industrial applications, In *Multidisciplinary Methods for Analysis Optimization and Control of Complex Systems,* (eds. V. Capasso and J. Priaux), volume 6 of Mathematics in Industry, 3-47. Springer, Berlin.

[40] Engl, H.W., Hanke, M. and Neubauer, A. (1996) *Regularization of Inverse Problems*, Dordrecht, Kluwer.

[41] Fornasier, M., Naumova, V. and Pereverzyev, S.V. (2014) Parameter choice strategies for multipenalty regularization, *SIAM Journal on Numerical Analysis*, **52**, 1770–1794.

[42] Friedman, A. (2015) Free boundary problems in biology, *Philosophical Transactions of the Royal Society A*, **373**, 20140368.

[43] Friedman, A. (2000) Free boundary problems in science and technology, *Notices of the American Mathematical Society*, **47**, 854-861.

[44] Gerald, C.F. and Wheatley, P.O. (1994) *Applied Numerical Analysis*, 5th Edition, Addison-Wesley, Reading, MA.

[45] Goldman, N.L. (1997) *Inverse Stefan Problems*, Springer Science & Business Media, Berlin.

[46] Hadamard, J. (2003) *Lectures on Cauchy's Problem in Linear Partial Differential Equations*, Yale University Press, New Haven.

[47] Hansen, P.C. (2001) *The L-curve and its use in the numerical treatment of inverse problems*, in Computational Inverse Problems in Electrocardiology, (ed. P. Johnston), WIT Press, Southampton, 119–142.

[48] Hansen, P.C. (1992) Analysis of discrete ill-posed problems by means of the L-curve. *SIAM Review,* **34**, 561–580.

[49] Hazanee, A. and Lesnic, D. (2013) Reconstruction of an additive space- and time- dependent heat source, *European Journal of Computational Mechanics*, **22**, 304–329.

[50] Hinestroza, D., Peralta, J. and Olivar, L.E. (2013) Regularization algorithm within two parameters for the identification of the heat conduction coefficient in the parabolic equation, *Mathematical and Computer Modelling,* 57(7):1990-1998.

[51] Hon, Y.C. and Li, M. (2008) A computational method for inverse free boundary determination problem, *International Journal for Numerical Methods in Engineering*, **73** (9):1291-1309.

[52] Hao Dinh Nho, Thanh Phan Xuan, Lesnic, D. and Ivanchov, M. (2014) Determination of a source in the heat equation from integral observations, *Journal of Computational and Applied Mathematics*, **264**, 82–98.

[53] Hryntsiv, N. (2009) Determination of the coefficient of the first derivative in a parabolic equation with degeneration, *Visnyk Lviv Univ., Ser. Mekh. Mat.*, **71**, 78-87.

[54] Hryntsiv, N. (2011) Non-local inverse problems for a weakly degenerate parabolic equation, *Journal of National Univ. Lviv Politechnika. Physical and Math. Sciences*, **696**, 32–39.

[55] Huang, L., Sun, X., Liu, Y. and Cen, Z. (2004) Parameter identification for two-dimensional orthotropic material bodies by the boundary element method, *Eng. Anal. Boundary Elements*, **28**, 109-121.

[56] Huntul, M.J. and Lesnic, D. (2017) Determination of time-dependent coefficients and multiple free boundaries, *Eurasian Journal of Mathematical and Computer Applications*, **5**, 15–43.

[57] Huntul, M.J. and Lesnic, D. (2018) Time-dependent reaction coefficient identification problems with a free boundary, *International Journal of Applied and Computational Mathematics*, submitted.

[58] Huntul, M.J. and Lesnic, D. (2018) Determination of a time-dependent free boundary in a two-dimensional parabolic problem, *International Journal of Applied and Computational Mathematics*, submitted.

[59] Huntul, M.J. and Lesnic, D. (2018) Determination of time-dependent coefficients for a weakly degenerate heat equation, *Siberian Journal of Numerical Mathematics*, submitted.

[60] Huntul, M.J., Lesnic, D. and Johansson, B.T. (2018) Determination of an additive time- and space-dependent coefficient in the heat equation, *International Journal of Numerical Methods for Heat and Fluid Flow*, 28(6), 1352–1373.

[61] Huntul, M.J., Lesnic, D. and Hussein, M.S. (2017) Reconstruction of time-dependent coefficients from heat moments, *Applied Mathematics and Computation*, **301**, 233–253.

[62] Hussein, M.S, Lesnic, D. and Ivanchov, M.I. (2014) Simultaneous determination of time-dependent coefficients in the heat equation, *Computers and Mathematics with Applications*, **67**, 1065–1091.

[63] Hussein, M.S., Lesnic, D. and Ivanchov, M.I. (2017) Identification of a heterogeneous orthotropic conductivity in a rectangular domain, *International Journal of Novel Ideas*, **1**, 1-11.

[64] Hussein, M.S., Kinash, N., Lesnic, D. and Ivanchov, M. (2016) Retrieving the time-dependent thermal conductivity of an orthotropic rectangular conductor, *Applicable Analysis*, **96**, 1–15.

[65] Hussein, M.S. and Lesnic, D. (2016) Simultaneous determination of time and space-dependent coefficients in a parabolic equation, *Communications in Nonlinear Science and Numerical Simulations,* **33**, 194–217.

[66] Hussein, M.S., Lesnic, D. and Ismailov, M.I. (2016) An inverse problem of finding the time-dependent diffusion coefficient from an integral condition, *Mathematical Methods in the Applied Sciences*, **39**, 963–980.

[67] Hussein, M.S. and Lesnic, D. (2014) Determination of a time-dependent thermal diffusivity and free boundary in heat conduction, *International Communications in Heat and Mass Transfer*, **53**, 154–163.

[68] Hussein, M.S., Lesnic, D. and Ivanchov, M. (2013) Free boundary determination in nonlinear diffusion, *East Asian Journal on Applied Mathematics*, **3**, 295–310.

[69] Hussein, M.S., Lesnic, D., Ivanchov, M.I. and Snitko, H.A. (2016) Multiple time-dependent identification thermal problems with a free boundary, *Applied Numerical Mathematics*, **99**, 42–50.

[70] Huzyk, N. (2014) Inverse problem of determining the coefficients in a degenerate parabolic equation, *Electronic Journal of Differential Equations*, **172**, 1–11.

[71] Huzyk, N.M. (2016) Determination of the lower coefficient in a parabolic equation with strong degeneration, *Ukrainian Mathematical Journal*, **68**, 1049–1061.

[72] Ivanchov, M.I. (1998) On determination of a time-dependent leading coefficient in a parabolic equation, *Siberian Mathematical Journal*, **39**, 465–475.

[73] Ivanchov, M.I. (2012) A problem with free boundary for a two-dimensional parabolic equation, *Journal of Mathematical Sciences*, **183**, 17–28.

[74] Ivanchov, M. (2003) *Inverse Problems for Equations of Parabolic Type*, VNTL Publishers, Lviv, Ukraine.

[75] Ivanchov, M.I. and Hryntsiv, N. (2010) Inverse problem for a weakly degenerate parabolic equation in a domain with free boundary, *Journal of Mathematical Sciences*, **167**, 16-29.

[76] Ivanchov, M.I and Kinash, N.E. (2018) Inverse problem for the heat-conduction equation in a rectangular domain, *Ukrainian Mathematical Journal*, **69**, 1865-1876.

[77] Ivanchov, N.I. (1994) On the inverse problem of simultaneous determination of thermal conductivity and specific heat capacity, *Siberian Mathematical Journal*, 35(3):547-555.

[78] Ivanchov, M.I. and Pabyrivs'ka, N.V. (2001) Simultaneous determination of two coefficients of a parabolic equation in the case of nonlocal and integral conditions, *Ukrainian Mathematical Journal*, **53**, 674–684.

[79] Ivanchov, N.I. and Pabyrivs'ka, N.V. (2002) On determination of two time-dependent coefficients in a parabolic equation, *Siberian Mathematical Journal*, **43**, 323–329.

[80] Ivanchov, M.I. and Saldina, N.V. (2005) Inverse problem for the heat equation with degeneration, *Ukrainian Mathematical Journal*, **57**, 1825–1835.

[81] Johansson, B.T., Lesnic, D. and Reeve, T. (2011) A method of fundamental solutions for the one-dimensional inverse Stefan problem, *Applied Mathematical Modelling*, **35**(9):4367-4378.

[82] Jones, B.F., Jr. (1962) The determination of a coefficient in a parabolic differential equation, Part I. Existence and uniqueness, *Journal of Mathematical Mechanics,* **11**, 907–918.

[83] Jones, B.F., Jr. (1963) Various methods for finding unknown coefficients in parabolic differential equations, *Communications on Pure and Applied Mathematics,* **16**, 33–44.

[84] Kaipio, J. and Somersalo, E. (2007) Statistical inverse problems: discretization, model reduction and inverse crimes, *Journal of Computational and Applied Mathematics*, **198**, 493–504.

[85] Kirsch, A. (2011) *An Introduction to the Mathematical Theory of Inverse Problems*, volume 120. Springer Science & Business Media, New York.

[86] Kinash, N.Ye. (2018) A nonlocal inverse problem for the two-dimensional heat-conduction equation, *Journal of Mathematical Sciences*, **231**, 558-571.

[87] Knowles, I. and Yan, A. (2002) The recovery of an anisotropic conductivity in groundwater modelling, *Applicable Analysis*, **81**, 1347-1365.

[88] Kress, R. (1989) *Linear Integral Equations*, Springer Verlag, New York.

[89] Lamé, G. and Clapeyron, B.P. (1831) Mémoire sur la solidification par refroidissement d'un globe liquide, *Annales de Chimie et de Physique*, **47**, 250–256.

[90] Ladyzhenskaya, O.A., Solonnikov, V.A. and Uraltseva, N.N. (1968) *Linear and Quasilinear Equations of Parabolic Type*, American Mathematical Society, Providence, Rhode Island, USA.

[91] Lesnic, D. and Trucu, D. (2010) The identification of blood perfusion coefficient in bio-heat transfer, *Inverse Problems, Design and Optimization Symposim (IPDO-2010)*, Joao Pessoa, Brazil, CD-ROM, pp. 277-284.

[92] Lesnic, D., Elliott, L. and Ingham, D.B. (1997) The solution of an inverse heat conduction problem subject to the specification of energies, *International Journal of Heat and Mass Transfer*, 41(1):25-32.

[93] Lesnic, D., Yousefi, S.A. and Ivanchov, M. (2013) Determination of a timedependent diffusivity from nonlocal conditions, *Journal of Applied Mathematics and Computing*, 41(1-2):301-320.

[94] LeVeque, R.J. (2002) *Finite Volume Methods for Hyperbolic Problems*, volume 31. Cambridge University Press.

[95] Lu, S. and Pereverzev, S.V. (2011) Multi-parameter regularization and its numerical realization, *Numerische Mathematik*, **118**, 1–31.

[96] Malyshev, I.G. (1975) Inverse problems for the heat-conduction equation in a domain with a moving boundary, *Ukrainian Mathematical Journal*, **27**, 568–572.

[97] Martin, C. (1987) Principles of boundary element methods, *Computer Physics Reports*, **6**, 243–274.

[98] Marin, L., Elliott, L., Heggs, P.J., Ingham, D.B., Lesnic, D. and Wen, X. (2004) Analysis of polygonal fins using the boundary element method, *Applied Thermal Engineering*, **24**, 1321–1339.

[99] Mathworks (2016) Documentation optimization toolbox-least squares algorithms, www.mathworks.com.

[100] Morozov, V.A. (1966) On the solution of functional equations by the method of regularization, *Soviet Mathematics Doklady*, **7**, 414-417.

[101] Morton, K.W. and Mayers, D.F. (2005) *Numerical Solution of Partial Differential Equations: An Introduction*, Cambridge University Press.

[102] Moré, J.J. and Sorensen, D.C. (1983) Computing a trust region step, *SIAM Journal on Scientific and Statistical Computing*, **4**, 553–572.

[103] Muzylev, N.V. (1980) Uniqueness theorems for some converse problems of heat conduction, *USSR Computational Mathematics and Mathematical Physics*, 20(2):120-134.

[104] Muzylev, N.V. (1983) On the uniqueness of the simultaneous determination of thermal conductivity and volume heat capacity, *USSR Computational Mathematics and Mathematical Physics*, 23(1):69-73.

[105] Mugnolo, D. and Nicaise, S. (2015) The heat equation under conditions on the moments in higher dimensions, *Mathematische Nachrichten*, **288**, 295–308.

[106] Ozisik, M.N. (1994) *Finite Difference Methods in Heat Transfer*, Boca Raton, FL: CRC Press.

[107] Pabyrivs'ka, N. (2000) Integral conditions in an inverse problem for a parabolic equation, *Visnyk Lviv Univ. Ser. Mech. - Math.*, **56**, 142–149.

[108] Petrov, Yu.P. and Sizikov, V.S. (2005) *Well-posed, Ill-posed and Intermediate Problems*, VSP, The Netherlands.

[109] Pilant, M.S. and Rundell, W. (1990) Undetermined coefficient problems for quasilinear parabolic equations, In: *Inverse Problems in Partial Differential Equations,* (eds. D.L. Colton, R.E. Ewing and W. Rundell), pp. 165-185, SIAM, Philadelphia.

[110] Prilepko, A.I., Orlovsky, D.G. and Vasin, I.A. (2000) *Methods for Solving Inverse Problems in Mathematical Physics*, M. Dekker, New York.

[111] Reddy, J.N. (1993) *An Introduction to the Finite Element Method*, McGraw-Hill, New York.

[112] Rhoden, A., Patong, N., Liu, Y., Su, J. and Liu, H. (2013) A globally convergent numerical method for coefficient inverse problems with time-dependent data, In: *Applied Inverse Problems*, (ed. L. Beilina), Volume 48 of Springer Proceedings in Mathematics & Statistics, pp. 105-128, Springer, New York.

[113] Samarskii, A.A. and Vabishchevich, P.N. (2007) *Numerical Methods for Solving Inverse Problems of Mathematical Physics*, De Gruyter, Berlin.

[114] Sawaf, B., Ozisik, M.N. and Jarny, Y. (1995) An inverse analysis to estimate linearly temperature dependent thermal conductivity components and heat capacity of an orthotropic medium, *International Journal of Heat and Mass Transfer*, **38**, 3005-3010.

[115] Savateev, E.G. (1995) On the problem of identification of a coefficient in a parabolic equation. *Siberian Mathematical Journal,* **36**, 177–185.

[116] Saldina, N. (2005) Inverse problem for a parabolic equation with degeneration, *Visnyk Lviv Univ., Ser. Mekh. Mat.*, **64**, 245-257, (in Ukrainian).

[117] Snitko, H.A. (2010) Coefficient inverse problem for a parabolic equation in a domain with free boundary, *Journal of Mathematical Science*, **167**, 30–46.

[118] Snitko, H.A. (2012) Inverse problem for determination of time-dependent coefficients of a parabolic equation in a free-boundary domain, *Journal of Mathematical Science*, **181**, 350–365.

[119] Snitko, H.A. (2014) On a coefficient inverse problem for a parabolic equation in a domain with free boundary, *Journal of Mathematical Sciences*, **200**, 374–388.

[120] Snitko, H.A. (2014) Inverse problem of finding time-dependent functions in the minor coefficient of a parabolic equation in the domain with free boundary, *Journal of Mathematical Science*, **203**, 40–54.

[121] Snitko, H.A. (2014) Determination of the lowest coefficient for a one-dimensional parabolic equation in a domain with free boundary, *Ukrainian Mathematical Journal*, **65**, 1698–1719.

[122] Shiping, Z. and Minggen, C. (2009) A new algorithm for determining the leading coefficient in the parabolic equation, *World Academy of Science, Engineering and Technology*, 31:508-512.

[123] Smith, G.D. (1985) *Numerical Solution of Partial Differential Equations: Finite Difference Methods*, Clarendon Press, Oxford, Third edition.

[124] Soboleva, O.V. and Brizitskii, R.V. (2016) Numerical study of the inverse problem for the diffusion-reaction equation using optimization methods, *IOP Conference Series: Materials Science and Engineering*, **124**, 012096 (5 pp).

[125] Tikhonov, A.N. (1943) On the stability of inverse problems, *Doklady Akademii Nauk SSSR*, 39:195-198.

[126] Thomee, V. (2001) From finite differences to finite elements: a short history of numerical analysis of partial differential equations, *Journal of Computational and Applied Mathematics*, **128**, 1–54.

[127] Trucu, D., Ingham, D.B. and Lesnic, D. (2008) Inverse time-dependent perfusion coefficient identification, *Journal of Physics: Conference Series: 4th AIP Internatinal Conference and the 1st Congress of the IPIA*, **124**, 012050, (28 pages).

[128] Trucu, D. (2009) *Inverse Problems for Blood Perfusion Identification*, PhD Thesis, University of Leeds.

[129] Trucu, D., Ingham, D.B. and Lesnic, D. (2010) Space-dependent perfusion coefficient identification in the transient bio-heat equation *Journal of Engineering Mathematics*, **67**, 307–315.

[130] Trucu, D., Ingham, D.B. and Lesnic, D. (2011) Reconstruction of the space- and time-dependent blood perfusion coefficient in bio-heat transfer, *Heat Transfer Engineering,* **32**, 800–810.

[131] Twomey, S. (1963) On the numerical solution of Fredholm integral equations of first kind by inversion of the linear system produced by quadrature, *Journal of the Association for Computing Machinery*, **10**, 97–101.

[132] Uhlmann, G. (1999) Developments in inverse problems since Calderón's foundational paper, In: *Harmonic Analysis and Partial Differential Equations*, University of Chicago Press, Chicago, IL, USA, pp.295-345.

[133] Vlasov, V. (2014) An inverse problem for a weakly degenerate parabolic equation in a rectangular domain, In: *ICIPE2014 - 8th International Conference on Inverse Problems in Engineering*, May 12-15, 2014, Poland, (eds. I. Szczygiel, A.J. Nowak and M. Rojczyk), pp. 423–432.

[134] Vogel, C.R. (1996) Non-convergence of the L-curve regularization parameter selection method, *Inverse Problems*, **12**, 535–547.

[135] Wang, Y., Yang, C. and Yagola, A. (2011) *Optimization and Regularization for Computational Inverse Problems and Applications*, Springer-Verlag, Berlin.

[136] Wang, P. and Zheng, K. (2002) Determination of an unknown coefficient in a nonlinear heat equation, *Journal of Mathematical Analysis and Applications*, 271(2):525-533.

[137] Yi, Z. and Murio, D.A. (2004) Identification of source terms in 2-D IHCP, *Computers and Mathematics with Applications*, **47**, 1517-1533.

[138] Yousefi, S.A., Lesnic, D. and Barikbin, Z. (2012) Satisfier function in Ritz-Galerkin method for the identification of a time-dependent diffusivity, *Journal of Inverse and Ill-Posed Problems*, **20**, 701–722.